DEPARTMENT OF CHEMISTRY
UNIVERSITY COLLEGE
CORK

INVOLVEMENT OF INCIPIENT HYDROUS OXIDE SPECIES IN ELECTROCATALYSIS AT SOME METAL ELECTRODE SURFACES

A thesis presented for the Ph.D. Degree
of the National University of Ireland

by

William Anthony O'Leary B.Sc.

- August 1989 -

TO MY PARENTS

Declan and Eileen

AND TO

Jane

FOR ALL YOUR SUPPORT

ABSTRACT

In this thesis a novel theory of electrocatalysis at metal (especially noble metal)/solution interfaces was developed based on the assumption of metal adatom/incipient hydrous oxide cyclic redox transitions. Adatoms are considered as metastable, low coverage species that oxidise in-situ at potentials of often significantly cathodic to the regular metal/metal oxide transition. Because the adatom coverage is so low the electrochemical or spectroscopic response for oxidation is frequently overlooked; however, the product of such oxidation, referred to here as incipient hydrous oxide seems to be the important mediator in a wide variety of electrocatalytically demanding oxidation processes. Conversely, electrocatalytically demanding reductions apparently occur only at adatom sites at the metal/solution interface - such reactions generally occur only at potentials below, i.e. more cathodic than, the adatom/hydrous oxide transition.

It was established that while silver in base oxidises in a regular manner (forming initially OH_{ads} species) at potentials above 1.0 V (RHE), there is a minor redox transition at much lower potentials, ca. 0.35 V (RHE). The latter process is assumed to an adatom/hydrous oxide transition and the low coverage Ag(1) hydrous oxide (or hydroxide) species was shown to trigger or mediate the oxidation of aldehydes, e.g. HCHO. The results of a study of this system were shown to be in good agreement with a kinetic model based on the above assumptions; the similarity between this type of behaviour and enzyme-catalysed processes - both systems involve interfacial active sites - was pointed out. Similar behaviour was established for gold where both Au(1) and Au(111) hydrous oxide mediators were shown to be the effective oxidants for different organic species.

One of the most active electrocatalytic materials known at the present time is platinum. While the classical view of this high activity is based on the concept of activated chemisorption (and the important role of the latter is not discounted here) a vital role is attributed to the adatom/hydrous oxide transition. It was suggested that the well known intermediate (or anomalous) peak in the hydrogen region of the cyclic voltammogram for platinum region

is in fact due to an adatom/hydrous oxide transition. Using potential stepping procedures to minimise the effect of deactivating (CO_{ads}) species, it was shown that the onset (anodic sweep) and termination (cathodic sweep) potential for the oxidation of a wide variety of organics coincided with the potential for the intermediate peak. The converse was also shown to apply; sluggish reduction reactions, that involve interaction with metal adatoms, occur at significant rates only in the region below the hydrous oxide/adatom transition.

ACKNOWLEDGEMENTS

Firstly, I would like to thank Prof. L.D. Burke for all his help and guidance throughout the course of this thesis.

Also, thanks to the 'lads' of 320 including Vincent, Mick, Con, David, John, Sally, Timmy, Kieran, Janusz, James, Joe and Brian, it wouldn't have been the same without you. And my classmates especially Marguerite and Elizabeth, Anita, Mary C., Mary K., Paul, Martha, Brian, Noreen G., Noreen Mc and all fellow postgrads who made my stay memorable.

Thanks to the Administrative Staff, Mary O'Neill and Eileen O'Callaghan but mainly Karen Whelan and Majella O'Sullivan for their patience and 'pressure' not to mention typing skills. Also, to the Technical Staff, Mick O'Shea, Derry Kearney, Johnny Ryan, Ollie Nash, Tony Hogan, John Caffrey and all the rest.

Thanks to my proofreaders Jane, Declan, Timmy, Paula and Harold.

The members of U.C.C. Hockey Club deserve a special mention especially Kevin (Tulip), Eamonn (Stan), Shelly, Jim and Edith for keeping me in a suitable alcoholic haze when needed (and sometimes not!).

My family cannot be thanked enough. Declan and Eileen I don't think I will ever be able to repay for all their support and never losing faith in me. Richard, Hilary (Big Sis.), Paula (from afar) and Declan Jr. (my best buddy) for everything.

Last, but definitely not least, thanks to Jane for helping me make the decision to undertake this thesis and then putting up with everything which that decision entailed. Thanks for always being there.

William Anthony O'Leary

WILLIAM ANTHONY O'LEARY

AUGUST, 1989

CONTENTS

CHAPTER 5: PLATINUM

CHAPTER 1

Introduction

Electrochemistry is an area of major research at the present time largely in connection with the development of new and more efficient energy transfer and storage systems and to conserve existing resources generally. Topics of immediate interest include battery and fuel cell development, corrosion and waste treatment. The topic is becoming more interdisciplinary with the increasing need to understand more fully the structures and products formed in the interphasial region between a solid and an electrolytic solution.

The present thesis outlines the interaction of reactive molecules with some noble metal electrodes in aqueous solution under potentiostatic and potentiodynamic conditions and gives a novel description of the implications of the results in terms of our understanding of electrocatalysis.

However, before discussing the nature of this phenomena in greater detail, a survey of the properties of electrochemical interphases, the kinetics of charge transfer at same, and a review of the field of electrocatalysis to date will be presented.

1.1. ELECTRODE-SOLUTION INTERPHASE

The interphase [1] is that region at the phase boundary where variations in chemical and electrical forces give rise to adsorption, dipole orientation and charge separation effects, with the result that properties, especially on the solution side of the boundary, differ appreciably from those in the bulk. However, the determination of the absolute potential difference across a single interphase is not experimentally possible. This is due to the properties of the measuring instrument - the use of which results in the creation of an extra interphase between the solution and the instrument in question. Therefore, only the potential difference across a pair of interphases may be measured. By using a non-polarisable (reversible) interphase as the second interphase changes in potential difference for the interphase under investigation may be measured.

There are a number of different types of potentials encountered in electrochemical systems:

(i) The Galvani (Inner) Potential (Φ) [2]: - This is the energy required to overcome electrical forces in transporting unit positive charge from infinity in a vacuum to the point in question. Implicit in this definition is an attempt to separate chemical and electrical effects.

(ii) The Volta (Outer) Potential (ψ) [2]: - This is the work involved in transporting unit positive charge from infinity in a vacuum to a point close to the surface of the phase but just outside the range of chemical forces (ca. 10^{-6} cm from the surface).

(iii) Surface Potential (χ) [3]: - This is the difference in electrical potential between the interior and exterior of a phase. It is the work done in carrying positive charge across dipolar layers in the interphase.

$$\chi = \Phi - \psi \qquad (1:1:1)$$

(iv) Chemical Potential (μ) [4]: - This is the work associated with the transportation of a mole of component i from the dilute gas state at infinity into the phase of the mixture in question, all species being neutral.

$$\mu_i = \left(\frac{\delta G}{\delta n_i}\right)_{T,P,n_j} \qquad (1:1:2)$$

where G is the free energy at constant pressure, n_i is the number of moles of i in the phase and n_j is the number of moles of any other components in the phase. However, chemical and electrical effects in reality cannot be separated [5,6]. Hence,

(v) The Electrochemical Potential ($\bar{\mu}$):- This is the total work done, both electrical and chemical, in taking a mole of species i from infinity in a vacuum to a point deep within the bulk of a charged phase.

$$\bar{\mu} = \mu + z_i F\Phi \qquad (1:1:3)$$

where z_i is the charge, in electron units, of the species i and F is the Faraday constant.

By replacing the vacuum with another phase, e.g. an electrolyte, the interphase forms an electric double layer. The potential across this double layer will be $\Delta\Phi$, the Galvani potential difference.

1.2. METAL-SOLUTION INTERPHASE

The metal-solution interphase has been more thoroughly investigated than any other and has been comprehensively reviewed [7-10]. Due to the high electronic conductivity of metals, virtually no space charge develops within the metal at the interphase. Consequently, the interphase region largely encompasses the solution phase close to the metal surface.

The experimental investigation of this region has tended to concentrate on the electrocapillary method [11] which involves the determination of the metal/solution interphasial tension, γ, as a function of solution composition and potential. The ease in determining the interphasial tension of liquids, together with the homogeneity, reproducibility and high polarisability of a mercury surface has placed the mercury/solution interphase in a unique position in this area of research.

Employing thermodynamic arguments associated with the Gibbs-Duhem equation, and allowing for the free energy associated with the formation of the interphase, Lippmann [12] showed that the excess charge density on the metal, q_m, at constant temperature (T), pressure (P) and electrolyte concentration (μ_i) is given by the expression

$$q_m = -\left(\frac{\delta\gamma}{\delta E}\right)_{T,P,\mu_i} \qquad (1:2:1)$$

Experimentally derived electrocapillary curves of interphasial tension against potential tend to be of parabolic form (Fig. 1.1(a)); the potential at the maximum where $q_m = 0$ is known as the potential of zero charge (pzc). At this point the Volta potential difference across the interphase is zero ($\Delta\psi = 0$) and therefore

$$\Delta\Phi_{pzc} = \Delta\chi_{pzc} \qquad (1:2:2)$$

The decrease in interphasial tension on either side of the electrocapillary maximum is attributed to mutual repulsion between adsorbed ions following increasing adsorption as the potential departs from the pzc value. This decrease tends to be more enhanced under anodic conditions where anions are usually adsorbed more strongly due to a combination of both electrostatic and covalent forces. In general, ions tend to be specifically adsorbed if they are bereft at the point of contact of a primary hydration sheath; for ions of a given type, e.g. halides, adsorption increases with increasing radius.

Differentiation of the Lippmann equation with respect to potential yields an expression for the differential capacity, C, of the interphase,

$$C = \left(\frac{\delta q_m}{\delta E}\right)_{P,T,\mu_i} = -\left(\frac{\delta^2\gamma}{\delta E^2}\right)_{P,T,\mu_i} \qquad (1:2:3)$$

Plots of capacity versus potential (Fig. 1.1.(b)) show a complicated structure with a minimum at the pzc for dilute solutions. The capacity of the interphase on the cathodic side where cations are adsorbed tends to be largely independent of the nature and concentration of these ions, while the capacity on the anodic side is usually quite sensitive to anion type and concentration, temperature, and the applied potential.

Interphasial tension and capacitance curves have contributed much to the development of various models of the metal-solution interphase; this topic is frequently referred to as a double layer system due to the separation of charge. According to the original ideas of Helmholtz [14] the double layer may be regarded as a

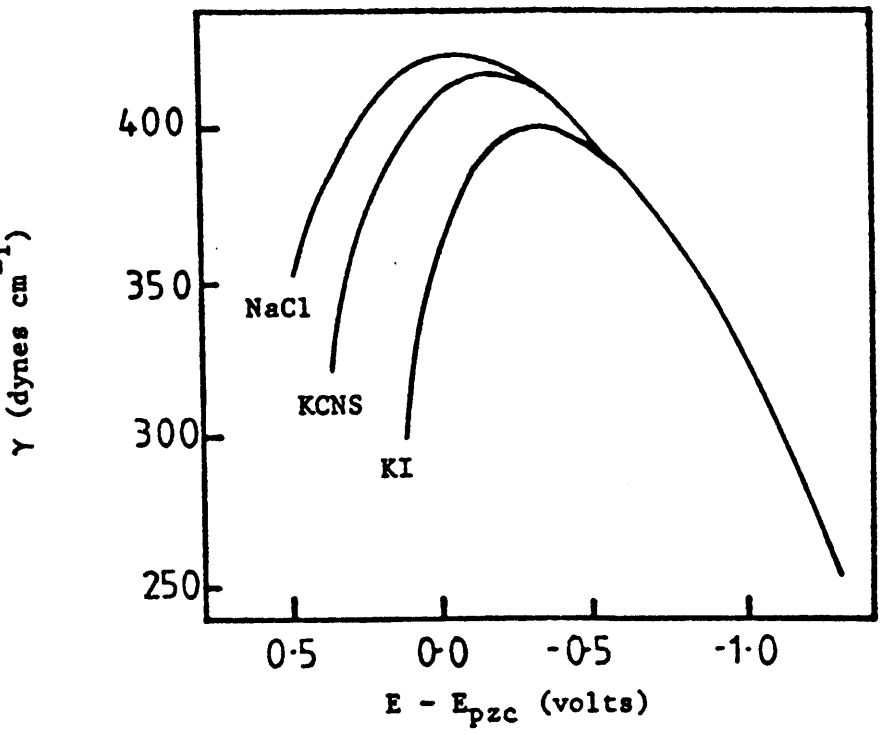

Figure 1.1(a): Electrocapillary curves for mercury and different electrolytes at 18°C. Potentials referred to E_{pzc} for an electrolyte (sodium fluoride) without specific adsorption.

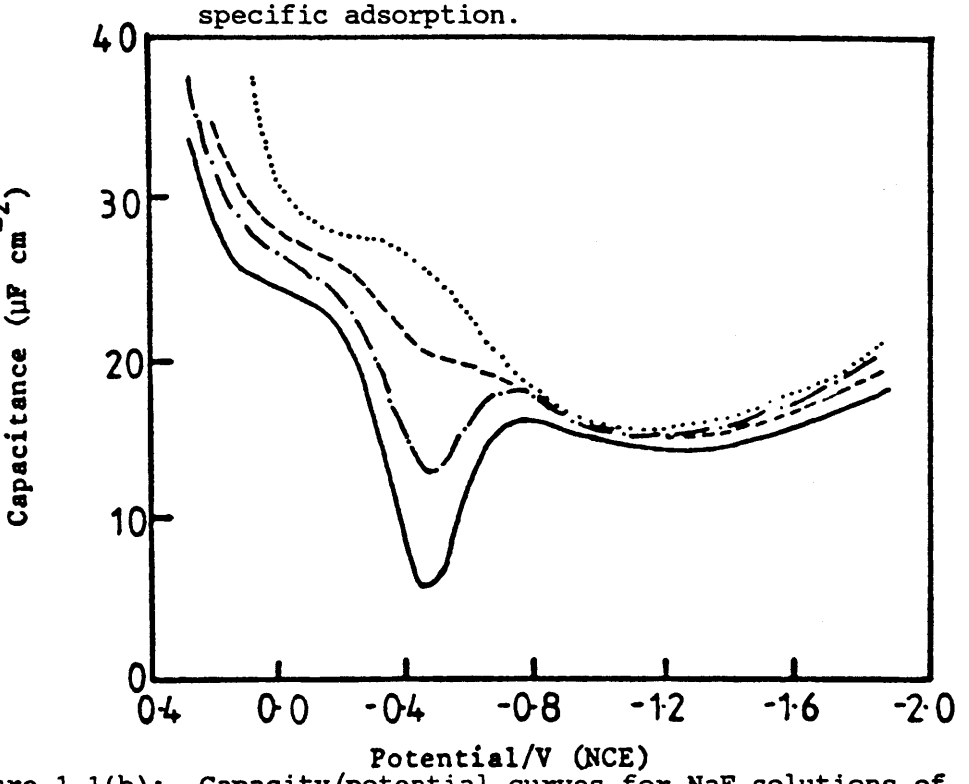

Figure 1.1(b): Capacity/potential curves for NaF solutions of different concentrations (mol dm^{-3}): ..., 0.916; ----, 0.10; -·-·-, 0.01; ——, 0.001.

simple capacitor, i.e. an array of positive and negative charges at opposite sides of the interphase, separated by a very short distance (0.3 - 0.6 nm). Gouy [15] and Chapman [16] pointed out that thermal agitation, together with high osmotic pressure within the layers, would tend to disrupt the latter. Consequently, they postulated a diffuse layer extending into the bulk solution. A combination of these two models, with some of the ions adhering to the metal surface as suggested by Helmholtz and some forming a Gouy-Chapman type diffuse layer, was suggested by Stern [17] as a more realistic way of describing the physical situation at the interphase. The major drop in potential at the interphase is assumed to occur across the compact (Helmholtz) layer with a much smaller and more gradual change in potential across the diffuse (Gouy) layer.

Grahame [7] and other workers [18,19] realised that full interpretation of the thermodynamic data for such systems required two planes of closest approach. Thus, they defined an inner layer, bounded by the Inner Helmholtz Plane (IHP), for specifically adsorbed ions or neutral molecules and solvent molecules (see Fig. 1.2). They also defined an outer layer bounded by the Outer Helmholtz Plane (OHP), for non-specifically adsorbed ions.

More recent approaches by Devanathan, Bockris and coworkers [20,21] retain the principles of Grahame's model but attempt to include more quantitatively the role played by solvent species. This is also summarised in Fig. 1.2. There is a strongly orientated layer of solvent molecules on the surface of the electrode. Specifically adsorbed ions are assumed to be capable of penetrating this inner solvent layer to interact directly with the metal. Those ions that retain their primary outer hydration shell are assumed to adsorb on a layer of solvent molecules on the metal surface.

Thus the interphase as a whole is seen to consist of three distinct regions of charge on the solution side. Since the interphasial region must be electrically neutral, the charge on the metal, q_m, has to be equal to the total charge on the solution side, i.e.

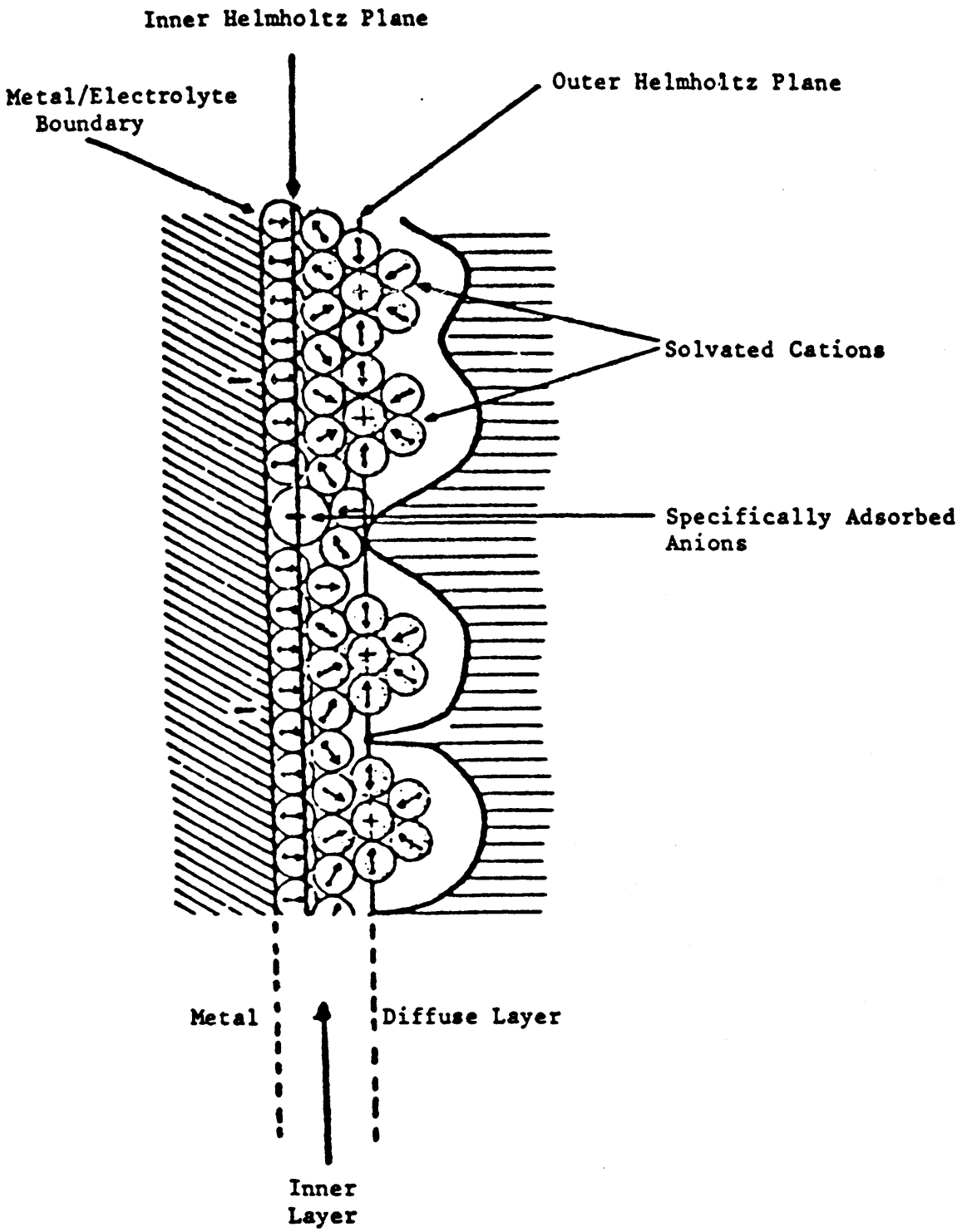

Figure 1.2: Model of the Electrical Double Layer [Ref. 20]

$$q_m = q_{IHP} + q_{OHP} + q_{diff} \qquad (1:2:4)$$

The interphase, therefore, is the electrical analogue of three capacitors in series, the total double layer capacitance, C_{dl}, being given as

$$\frac{1}{C_{dl}} = \frac{1}{C_{IHP}} + \frac{1}{C_{OHP}} + \frac{1}{C_{diff}} \qquad (1:2:5)$$

Thus the overall capacitance of the interphase is determined principally by the smallest of the three capacitances for the different regions.

Further investigation of the structure of the metal-solution interphase, for example, in order to acquire a clearer understanding of the orientation of solvent molecules at the interphase remains to be carried out [22]. Recently, reflection spectroscopy [23,24] and ellipsometry [25,26] have proved useful because of the possibility of measuring quite accurately the state of polarisation of visible light which permits changes at the interphase due to specific adsorption, and variations in the properties of solvent molecules at the interphase to be detected.

1.3. OXIDE-SOLUTION INTERPHASE

Most of the information available on the properties of the oxide/solution interface comes from studies of colloid chemistry, i.e. electrokinetic, or zeta, potentials and surface titration curves. The most important differences between oxide-electrolyte and the metal-electrolyte interphases are (i) the surface charge is higher than predicted by the Gouy-Chapman theory and is strongly dependent on electrolyte pH, and (ii) more symmetrical capacity-potential curves are observed in the case of oxides, with much higher values of capacity being observed than in the case of, for example, Hg or AgI, solution interfaces. Acid-base titrations [27] yield plots of surface charge versus pH from which the pzc is obtained, i.e. the pH at which the oxide surface has no net charge. These general characteristics have been reviewed by Ahmed [28] and Furlong, Yates and Healy [29].

The three double layers associated with the oxide-electrolyte interphase are indicated in Fig. 1.3. Firstly, a semiconductor space charge double layer which may extend up to several hundred nanometers into the solid; secondly, a Helmholtz double layer, between the solid and the OHP; and thirdly, the Gouy-Chapman double layer in the solution near the solid, in which an excess of ions of one sign exist. In the case of the space charge region in the solid the charge is in the form of uncompensated impurities or trapped holes or electrons, or possibly in the form of mobile holes or electrons, very near the surface, in the valence or conduction bands of the semiconductor. This area has been reviewed by Gerischer [30,31], Myamlin and Pleskov [32], Memming [33], and Heller and Miller [34].

Surfaces of oxides (whether conductors, semiconductors or insulators) tend to be covered by hydroxyl groups [28]. Surface hydration usually, but not always, occurs by the dissociative addition of water, viz,

$$MO + M + H_2O \rightarrow 2\ MOH \qquad (1:3:1)$$

The result is an oxide which is amphoteric, with surface groups which become protonated in acid solutions and negatively charged in basic solutions, viz.

$$MOH + H^+ \rightarrow MOH_2^+ \qquad (1:3:2)$$

$$MOH \rightarrow MO^- + H^+ \qquad (1:3:3)$$

$$MOH + OH^- \rightarrow M(OH)_2^- \qquad (1:3:4)$$

giving rise to a reversible double layer. Due to fast protonation of these surface groups, protons and hydroxyl ions are potential determining ions with nearly Nernstian dependence on electrolyte pH being exhibited by many oxides. It has been suggested that the first water layer adjacent to an oxide electrode is more structured than water dipoles at metal electrodes due to appreciable hydrogen bonding by water to the oxide surface [35].

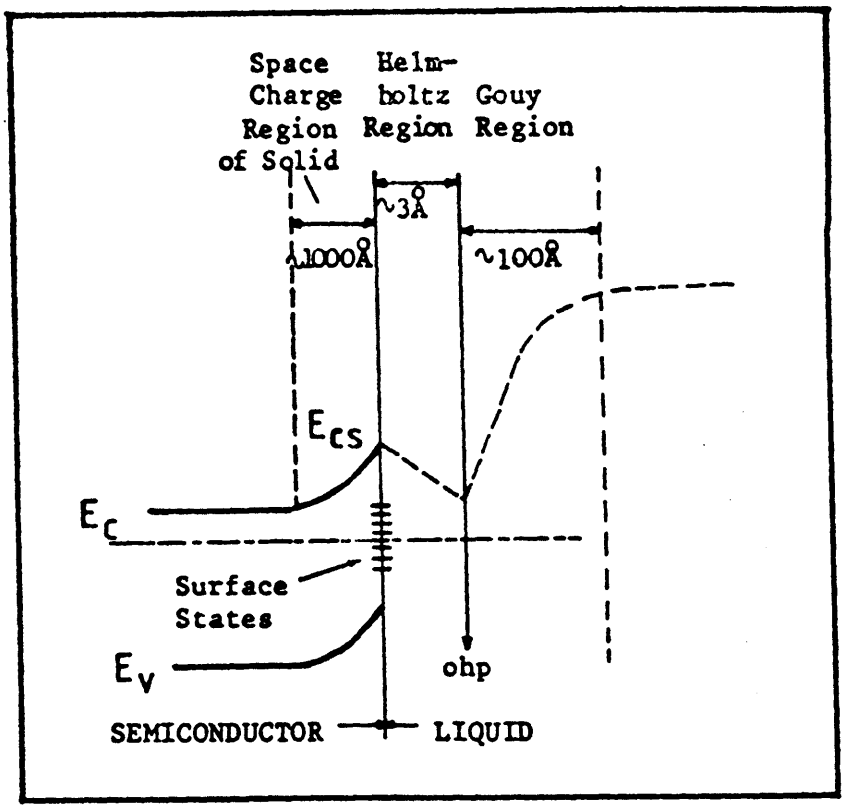

Figure 1.3: Double layers at the solid/liquid interface. The dashed line through the liquid indicates the variation in potential energy of a unit negative charge, as determined only by the double layer voltages, as it moves from the conduction band of the solid into the solution. The Gouy layer thickness indicated would represent a very dilute solution.

In solution the pzc is defined as the pH at which the surface excess of H^+ and OH^- ions on the oxide surface are equal, i.e. $\Gamma_{OH^-} = \Gamma_{H^+}$ and hence the surface charge, q, is zero. Values of the pzc for a large number of oxides have been listed by Parks [36]. The adsorption densities of H^+ and OH^- ions on the surface, and the accompanying potential drop across this layer, all vary with pH, thus confirming the reversible nature of this double layer. Hence, an oxide-electrolyte interphase subjected to an applied potential may be regarded as possessing the combined features of both polarisable and reversible double layers.

The development of surface charge [28,37,38] has been attributed to the formation of neutral or charge (±) aquo complexes of metal ions on the oxide surface, as shown schematically in the following equations;

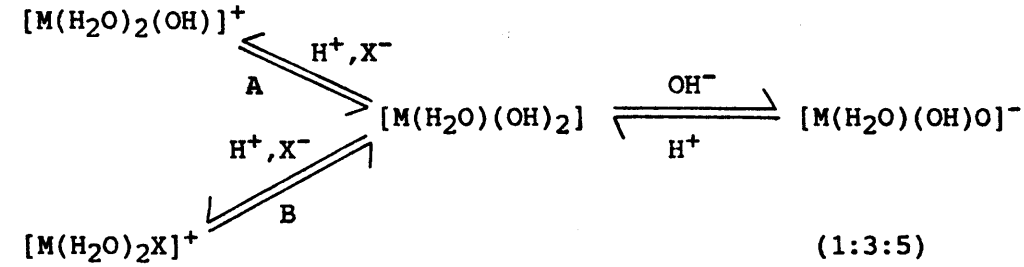

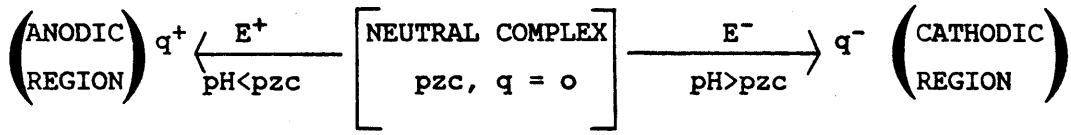

The oxide surface acquires an effective zero charge at the pzc through the formation of a neutral aquo complex. In the anodic region there is proton addition to the latter, either in the absence (mechanism A) or presence (mechanism B) of surface hydroxyl replacement by anions. Behaviour typical of mechanism A, where the oxide-electrolyte interphase is reversible to H^+ ions only, has been reported for SnO_2 [37] in NO_3^-, Al_2O_3 [39] and TiO_2 [37] in NO_3^-, ClO_4^- and Cl^- containing solutions. Behaviour typical of mechanism B, where the surface charge depends on anion concentration as well as pH, has been reported for Fe_2O_3 in Cl^-, ThO_2 and ZrO_2 in NO_3^- [38], Cl^- and ClO_4^- containing solutions [39].

The negative surface charge is assumed to originate from an acidic dissociation of the surface hydroxyl groups, and tends to increase with increasing pH as well as with increasing electrolyte concentration. Of note here is the involvement of specific adsorption of cations on the oxide surface, a phenomenon not generally observed at the metal-electrolyte interphase. This was postulated by Ahmed [38] who observed very high values for a number of oxides at pH ≈ 11 in the absence of significant dissolution. Berube and Bruyn [40] have also shown that the asymmetry of the experiment capacitance curves for TiO_2 tended to be more pronounced in the cathodic branch due to the specific adsorption of cations.

Initially, theories for the structure of the oxide-solution interphase [29], based upon the Gouy-Chapman-Stern-Grahame (GCSG) model for interphasial behaviour, were developed by Blok and Bruyn [41]. Levine and Smith [42] extended this to allow for non-Nernstian behaviour of the surface potential while Wright and Munter [43,44] used it to interpret zeta-potential behaviour of oxides. However, the major defect associated with the GCSG based models is that the surface charge values observed in certain cases exceed that developed due to ionisation of all surface hydroxyl groups.

Lyklema and Tadros [45-47] suggested a porous double layer model with both potential-determining and counter ions residing in the same region. This would account for higher charge density while zeta-potential values at the solution side of the interphase remain low, provided that the degree of counter ion penetration is extensive. Perram et al. [49-51] proposed an alternative gel layer model where a homogeneous gel-like layer of definite thickness (2-5 nm) at the interphase contains metal hydroxy groups $(MOH)_n$ into which various ions can adsorb. While Trasatti [52] showed this to be consistent with experimental facts, the presence of a gel layer has not been proven by radiotracer experiments [53]. Dignam [54,55] combined these two models and proposed a transition layer of atomic dimensions within which is established an equilibrium between oxide and aqueous species.

Yates, Levine and Healy [56], and Davis et al. [57] have formulated a so-called polyelectrolyte or site binding model. The

oxide surface is represented by a two-dimensional array of positive, negative and neutral discrete charged sites exhibiting acid/base properties. Potential determining ions and counter ions are then considered to react with, or bind to, the acid/base sites. In this model the high surface charge and low zeta-potential are rationalised in terms of ion-pair formation between surface ionized groups and counter ions.

While it appears that no totally satisfactory model for the oxide-solution interphase has emerged to date progress is obviously being made in this area. To obtain a model of general validity it is necessary to combine the factors of dispersion, hydration and hydroxylation acid/base properties.

1.4. ELECTROCHEMICAL KINETICS

Electrochemical reactions that involve the transfer of charge at the electrode-electrolyte interphase are examples of a general class of reactions referred to as heterogeneous processes; at least one stage in the overall electrode reaction must be a charge transfer [58] reaction in which a charge carrier (ion or electron) is transported from one phase into another across the electrochemical double layer.

Consider the electrode reaction $O + ne \rightleftharpoons R$ (1:4:1)

This reaction may be represented by the pathway:

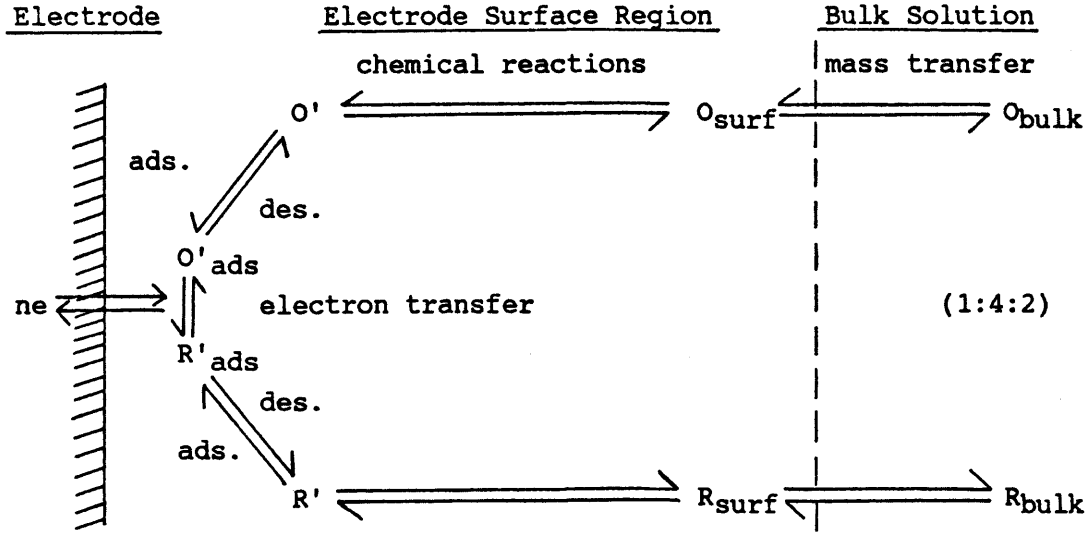

The height of the activation energy barrier, and hence the rate of the electrode reaction, can be controlled by external variation of the electrode potential, E. The potential (E_i) of an electrode through which current, i, flows differs from the equilibrium, or reversible potential, E_{rev}, established in the absence of current flow, by overpotential, η_i, which may be defined by

$$\eta_i = E_i - E_{rev} \qquad (1:4:3)$$

This overpotential may include contributions from any of the steps outlined in pathway (1:4:2), viz, (i) charge-transfer overpotential; (ii) adsorption/desorption or crystallisation overpotential; (iii) (chemical) reaction overpotential; (iv) diffusion (mass transfer) overpotential, or a combination of these processes. A further contribution, (v) resistance overpotential, arises from the presence of an ohmic solution resistance. It is usually minimised by improved cell design.

For the reaction to take place at a commensurable rate reactants and products must be transported to and from the electrode surface to sustain an electrical current across the electrode-electrolyte interphase. There are three kinds of mass transport process relevant to electrode reactions: (i) Migration - the movement of a charged body under the influence of an electric field; (ii) Diffusion - the movement of a species under the influence of a gradient of chemical potential; and (iii) Convection - the stirring and hydrodynamic transport.

The Nernst-Planck equation provides a general description of these [59] in terms of the concentration gradient, ∇C_i, the electrical gradient, $\nabla\Phi$, and the velocity of the electrolytic solution, v, viz.

$$J_i = -\frac{z_i F}{RT} D_i C_i \nabla\Phi - D_i \nabla C_i + C_i v \qquad (1:4:4)$$

where J_i is the flux of species i. The three terms in equation (1:4:4) describe respectively the migration, diffusion and convection contributions to the mass transfer at the electrode interphase.

The fundamental principles of the field of electrode kinetics were largely developed by Butler [60,61], Gurney [62,63], Frumkin [64], Volmer [65], and Horuiti and Polyani [66]. Their work dealt mainly with kinetics of hydrogen gas evolution and incorporates most of the basic principles of the subect on a macroscopic level.

(a) Macroscopic Theory

The net current density, i, which is the sum of both anodic and cathodic current densities is given by the well established Butler-Volmer equation [60,61,65], viz.

$$i = i_o \left[\exp\left(- \frac{\alpha F \eta}{RT} \right) - \exp\left(\frac{(1-\alpha) F \eta}{RT} \right) \right] \qquad (1:4:5)$$

where F is the Faraday constant, T is the absolute temperature, i is associated with an overpotential η and α is the symmetry factor; i_o, the exchange current density, denotes the reversible currents present at the equilibrium electrode ($E = E_{rev}$) and may be given by

$$i_o = F k_f a_o \exp\left(\frac{-\alpha F E^o}{RT} \right) = F k_r a_r \exp\left(\frac{(1-\alpha) F E^o}{RT} \right) \qquad (1:4:6)$$

where k_f and k_r denote the chemical rate constants present in the absence of an electric field in the electrode-solution interphase region for the forward (cathodic) and reverse (anodic) rates of charge transfer; a_o and a_r represent the activities of oxidant and reductant and E^o is the standard electrode potential.

At low overpotentials ($\eta \lesssim 10$ mV) equation (1:4:5) yields

$$i = i_o \left(\frac{F}{RT} \right) \eta \qquad (1:4:7)$$

The latter shows that at low overpotential the net current density is linearly related to overpotential. This behaviour is often observed in practice [67] and elucidation of i_o values is often

achieved by such low potential experiments.

At large overpotentials ($\eta > 100$ mV) equation (1:4:5) reduces to

$$i = i_o\left(\frac{-\alpha F\eta}{RT}\right) \qquad (1:4:8)$$

which is a form of the Tafel equation [68],

$$\eta = a - b \log i \qquad (1:4:9)$$

where

$$a = \frac{2.303\ RT}{\alpha F}\log i_o \text{ and } b = \frac{2.303\ RT}{\alpha F} \qquad (1:4:10)$$

A plot of η versus log i enables the coefficients a and b to be evaluated; i_o and α may then be determined.

At zero overpotential ($\eta = 0$) the system is at equilibrium ($E = E^o$) and equation (1:4:5) yields, on substitution of $i = 0$, that

$$E = \frac{RT}{F}\ln\frac{k_+}{k_-} + \frac{RT}{F}\ln\frac{a_o}{a_r} \qquad (1:4:11)$$

This is a form of the classical Nernst equation. This behaviour is known, for example, in the case of H_2 evolution on platinum [69,70] where the combination of H radicals is rate-determining.

(b) Microscopic Theory

On a microscopic level electron transfer reactions are treated as radiationless electronic transitions. Hence the electron must move from its initial state (in the electrode) to the receding state (e.g. an hydrated ion is the OHP) at the same energy level, i.e. it must be isoenergetic. Thus the charge transfer overpotential may be attributed to the need to raise the electron energy in the metal to the same level as that of the receding

state.

At this microscopic level it is important to classify the types of reaction that are to be encountered. There are two main reaction pathways: (i) The *outer-sphere* pathway where neither the reacting species, nor its coordinated ligands, penetrate the inner layer of solvent molecules immediately adjacent to the electrode surface in the transition state for electron transfer.

$$ML_n^{z+} + e \rightleftharpoons ML_n^{(z-1)+} \qquad (1:4:12)$$

These are related to weak overlap electron transfer reactions where the degree of interaction between the reactant and the metal surface in the transition state is sufficiently weak and non-specific that the activation free energy for the electron transfer step is largely unaffected by their proximity, being determined instead by the properties of the isolated reactant. These reactions usually occur at the OHP; (ii) The *inner-sphere* pathway involves the formation of a transition state where the inner layer is penetrated by the reacting species so that direct contact is made with the metal surface.

$$ML_n^{z+} + e \rightleftharpoons ML_{(n-1)}^{(z-1)+} + L \qquad (1:4:13)$$

These are related to strong overlap reactions which involve sufficiently strong interactions between the reactant and the metal surface in the transition state so as to significantly diminish the activation energy. These reactions usually occur at the IHP.

Fig. 1.4 shows a schematic free energy-reaction coordinate profile for a single electron electroreduction. The thermodynamic states of O and R represent the bulk-phase oxidised and reduced forms, whereas P and S represent these reactant and product species (known as "precursor" and "successor" states) formed in the interphasial region that immediately precede and follow the transition state. The curve PAS represents the elementary free energy barrier to electron transfer.

For weak overlap reactions, states O and P, and R and S will differ little in free energy. There will be little overlap between

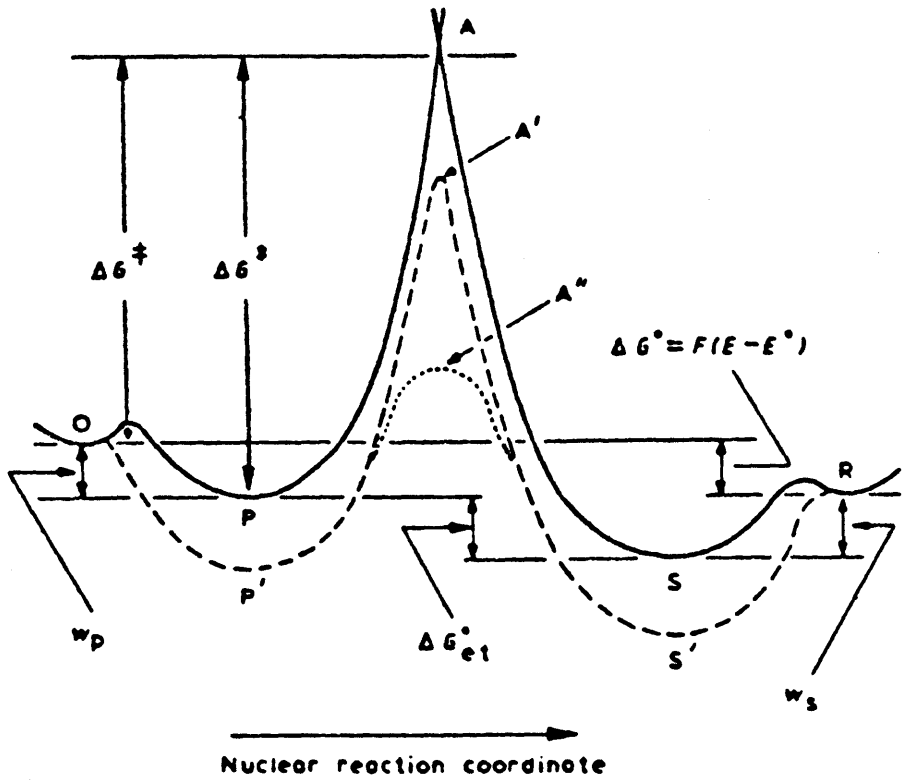

Figure 1.4: Schematic free energy-reaction coordinate profiles for a single-electron electroreduction involving solution reactant O and product R at at a given electrode potential E, occurring via three different reaction pathways PAS, P'A'S' and P'A"S'. Pathway PAS involves energetically favourable precursor and successor states (P and S) but with a weak-overlap transition state. Pathways P'A'S' and P'A"S' involve energetically similar precursor and successor states, but with the latter involving strong overlap in the transition state.

electron donor and acceptor sites due to large reactant-electrode separations. At these distances there is only a very small probability of crossing between OPA and ASR. However, due to the wave-like properties of electrons reactions can occur even in the absence of chemical bond formation between the reacting centres.

The closer the proximity of the reactant to the metal surface in electrode reactions will not only increase this "crossing probability", K_{el}, eventually to unity, but can also result in increasing energy differences between O and P, and between R and S. There are corresponding energy changes in transition state A since it is also situated in the interphasial region. The broken curve OP'A'S'R depicts the influence upon the free energy profile caused by favourable reactant-electrode interactions. The dotted curve P'A"S' represents strong overlap reactions when a chemical bond to the surface is formed. Depending on the extent of the reactant-surface interactions, the free-energy of A will be decreased to a greater extent than that of P and S, yielding a smaller free energy barrier, ΔG^*.

A standard potential, E^o, can be evaluated at which the electrochemical free energy driving force for the overall electron transfer, ΔG^o is zero. At this potential, the electrochemical rate constants for the forward (cathodic) and reverse (anodic) reactions, k_- and k_+, respectively, are equal to the so-called "standard" rate constant, k_s. The relationship between the cathodic rate constant and the electrode potential can be expressed as

$$k_- = k_s \exp(-\alpha F(E-E^o)/RT) \qquad (1:4:14)$$

where α is the cathodic transfer coefficient. Since α is often assumed to be close to 0.5, the measured rate constants are commonly very sensitive to the electrode potential, changing by tenfold for every 100-150 mV change in the latter.

The activation free energy for the overall electroreduction, $\Delta G^{\neq}$, is related to the activation free energy for the elementary step ΔG^*, at a given electrode potential E by [71]

$$\Delta G^{\neq} = \Delta G^* - w_p \qquad (1:4:15)$$

where w_p is the free energy difference between O and P. The dependence of $\Delta G^{\neq}$ upon the electrochemical driving force $F(E-E^{o})$ may be expressed as

$$\Delta G^{\neq} = \Delta G^{\neq}_{Eo} + \alpha F(E-E^{o}) \qquad (1:4:16)$$

where $\Delta G^{\neq}_{Eo}$ is the value of $\Delta G^{\neq}$ at the standard potential and α, the transfer coefficient, is also called the symmetry factor as it describes the symmetry of the reactant and product free energy wells.

A quantity of key theoretical significance is the so-called intrinsic barrier, ΔG^{*}_{int}; this equals ΔG^{*} for the particular case where the driving force for the elementary electron transfer step, ΔG^{o}_{et}, equals zero, Hence,

$$\Delta G^{*} = \Delta G^{*}_{int} - \alpha_{et}\,(F(E-E^{o}) + (w_s - w_p)) \qquad (1:4:17)$$

where α_{et} is the transfer coefficient for the elementary step and w_s is the work of forming the successor state from the bulk product. The relationship, from (1:4:15) - (1:4:17) giving,

$$\Delta G^{\neq}_{Eo} = \Delta G^{*}_{int} + (w_p + \alpha_{et}(w_s - w_p)) \qquad (1:4:18)$$

expresses the important distinction between the activation free energy for the overall electrochemical reaction in the absence of a net driving force, $\Delta G^{\neq}_{Eo}$, and the intrinsic barrier for the electron transfer step, ΔG^{*}_{int}. More generally, this may be expressed, to include any electrode potential E, as

$$\Delta G^{\neq} = \Delta G^{*}_{corr} + (w_p + \alpha_{et}(w_s - w_p)) \qquad (1:4:19)$$

where ΔG^{*}_{corr} is the work corrected free energy of activation (i.e. corresponding to $w_p = w_s = o$) at the same electrode potential as ΔG^{*} and α_{et} may be related to the observed transfer coefficient α by

$$\alpha = \alpha_{et} + \left[\alpha_{et}\left(\frac{\delta w_s}{F\delta E}\right) + (1-\alpha_{et})\left(\frac{\delta w_p}{F\delta E}\right)\right] \qquad (1:4:20)$$

Comparison of (1:4:15) and (1:4:19) shows that ΔG^* and ΔG^*_{corr} are related by

$$\Delta G^* = \Delta G^*_{corr} + \alpha(w_s - w_p) \qquad (1:4:21)$$

This relationship emphasises that only part of the double layer correction upon $\Delta G^{\neq}$ arises from the formation of the precursor state (1:4:15) since normally $w_p \neq w_s$. Equation (1:4:21), therefore, expresses the effect of the double layer upon the elementary electron transfer step, whereas equation (1:4:15) accounts for the work of forming the precursor state from the bulk reactant. These two components are combined in equation (1:4:19).

The above analysis emphasises that all reactions involving bulk solution species necessarily involve several elementary steps, each of which needs to be analysed carefully in order to relate the observed kinetics to the electron transfer barrier. Therefore, an underlying problem faced in the fundamental interpretation of electrochemical kinetics, is that it is often difficult to relate the measured rate constants to the intrinsic electron transfer barrier and other parameters referring to the electron transfer step since, often, only incomplete information is available on the thermodynamics of the individual steps comprising the overall reaction. Hence, it is desirable to treat one-electron electrochemical reactions involving an electron transfer step as occurring within a precursor state previously formed in the interphasial region. Then the overall observed rate constant, k_{ob}, may be separated into a precursor equilibrium constant, K_p, and a unimolecular rate constant, k_{et}, related by [71]

$$k_{ob} = K_p . k_{et} \qquad (1:4:22)$$

where the precursor equlibrium constant can be expressed as

$$K_p = \frac{\Gamma_p}{c_r} \qquad (1:4:23)$$

where Γ_p is the reactant surface concentration in the precursor state and c_r is the corresponding reactant concentration in the bulk solution.

Detailed study of Fig. 1.4 leads to several distinct stages as follows: (i) formation of precursor state where the reacting centres are geometrically positioned for electron transfer; (ii) activation of nuclear reaction coordinates to form the transition state; (iii) electron tunnelling; (iv) nuclear deactivation to form a successor state; and (v) dissociation of successor state to form the eventual products. The elementary electron transfer step associated with the unimolecular rate constant, k_{et} in (1:4:22), comprises of stages (ii)-(iv). This rate constant can be related to the corresponding barrier height ΔG^* by [71,72]

$$k_{et} = \nu_n K_{el} \Gamma_n \exp(-\Delta G^*/RT) \qquad (1:4:24)$$

where ν_n is the nuclear frequency factor, K_{el} is the electron transmission coefficient (i.e. the fractional electron tunnelling probability in the transition state), and Γ_n is the nuclear tunnelling factor. The theoretical model associated with this equation has been termed a semi-classical treatment in view of the inclusion of quantum mechanical correction factors [73]. The magnitudes of both ν_n and ΔG^* are determined by a combination of the various reactant vibrational and solvent reorientation modes.

The pre-exponential factor is commonly assumed to contain a collision frequency; however, to accommodate inner sphere reactions, where an intermediate precursor state is formed, it is preferable to assume that it describes the probability of forming an encounter state. This encounter pre-equilibrium model [71,72,74,75] accounts for local rates associated with a myriad of subtly distinct reaction sites, each with a different spatial position of the reactant and correspondingly different values of K_{el} and ΔG^* [74]. This idea of a reaction zone, δr, deals with the region close to the electrode surface within which the reactant has to be located in order to exchange electrons with sufficient efficiency to contribute significantly to the reaction rate. The idea of the effective electron tunnelling distance, $\delta r K^o_{el}$, where K^o_{el} is the electron transmission coefficient at the distance of closest approach, is dealt with by Hupp and Weaver [76].

Each of the pre-expotential factors contributes to the rate of electron transfer:

(i) Nuclear Frequency Factor, ν_n [71,72]:- This represents the rate at which reacting species in the vicinity of the transition state are transformed into products. It is associated with the passage of the system over the free energy barrier involving bond vibrations and solvent motion given according to a combination of the various models.

(ii) Electron Transmission Coefficient, K_{el}[72,74,77,78]:- This represents the fractional electron tunnelling probability in the transition state. It is commonly assumed to equal unity; however, it should be determined by the degree of overlap for the wave functions describing the donor and acceptor orbitals.

(iii) Nuclear Tunnelling Factor, Γ_n [72-74]:- This represents the fraction of molecules that can react without fully surmounting the free energy barrier, i.e. electron transfer can take place for nuclear configurations having energies below that from the classical transition state. It is essentially a property of energy associated with individual reactants rather than with interactions between the reacting centres and, since this effect will always act to increase k_{et}, generally $\Gamma_n > 1$. The magnitude of Γ_n depends upon both the height and shape of the barrier as well as the temperature.

In principle, using this theoretical model [79] one should be able to predict reactivities for individual electrochemical reactions, given a knowledge of the relevant thermodynamic and structural parameters. However, there are several factors which severely limit the applicability of such theory: (i) there are still relatively few situations where bond length and vibrational information is available so that inner shell barriers can be reliably calculated; (ii) many electrochemical reactions proceed via inner sphere pathways where the work terms are often unknown; and (iii) many electrochemical reactions occur via multistep pathways where one or more chemical transformations are coupled to the electron transfer stage.

1.5. TECHNIQUES FOR STUDYING ELECTROCHEMICAL REACTIONS

(a) Potential Step Techniques

In potential step experiments the potential of the working electrode is changed instantaneously, and either the current-time response or the charge-time response is recorded. These techniques are known respectively as chronoamperometry and chronocoulometry.

(i) Chronoamperometry

Consider the reaction

$$O + ne \underset{k_+}{\overset{k_-}{\rightleftharpoons}} R \qquad (1:5:1)$$

A potential-time profile, as shown in Fig. 1.5(a), is applied to the working electrode; E_1 is chosen such that no reduction of O, or indeed any other electrode reaction, occurs. Then at time $t = 0$ the potential is instantaneously changed to a new value E_2 where the reduction of O occurs at a diffusion controlled rate [82]. Fick's 2nd law can be solved with the appropriate boundary conditions [81], for a planar electrode to give the Cottrell equation [80]

$$i = \frac{nFD^{\frac{1}{2}}c^{\infty}_{O}}{\pi^{\frac{1}{2}}\, t^{\frac{1}{2}}} \qquad (1:5:2)$$

A plot of i versus $t^{-\frac{1}{2}}$ should therefore be linear, and should pass through the origin, and the diffusion coefficient of species O can be found from the gradient of the straight line. This type of behaviour is shown in curve (a), Fig. 1.5(b).

If the pulse is small, with E_2 corresponding to a low overpotential, a current-time transient of the type shown in curve (b), Fig. 1.5(b), will be observed. This corresponds to a steady state process and may be analysed with the Butler-Volmer equation as outlined earlier.

Curve (c), Fig. 1.5(b), corresponds to a mixed control reaction; $i_{t=0}$ cannot be measured directly due to finite rise-time

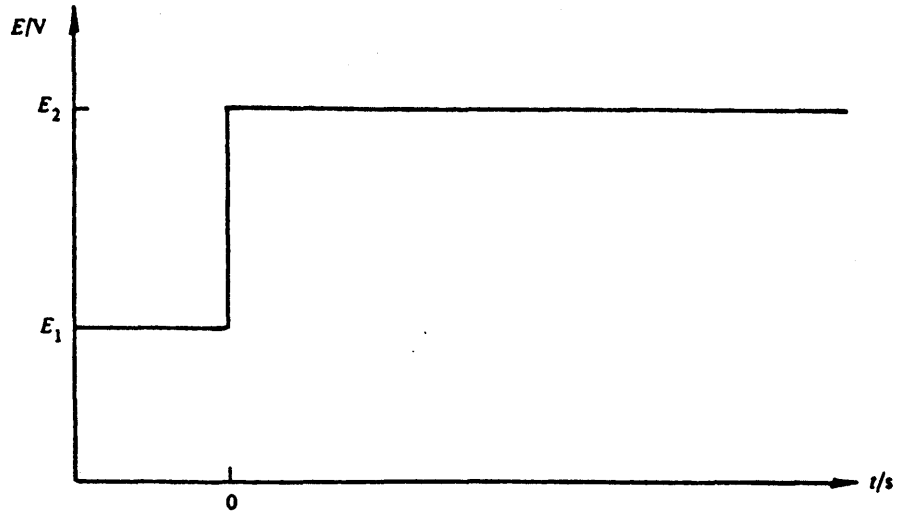

Fig. 1. 5(a): The potential-time profile for a single potential step chronoamperometric experiment.

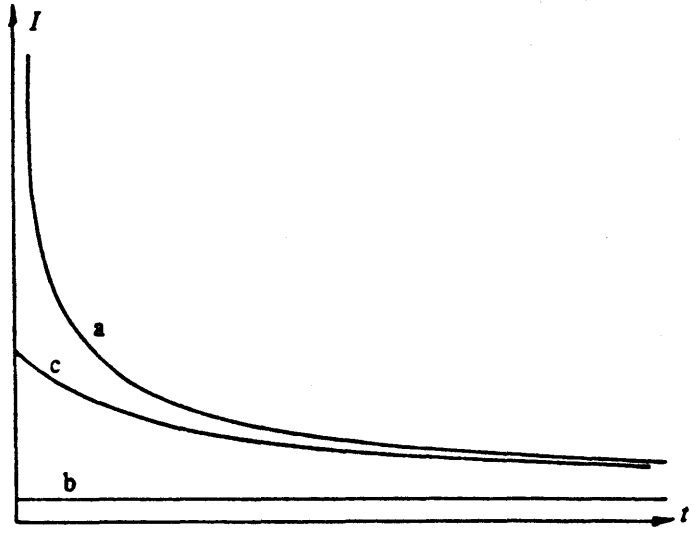

Fig. 1.5(b): I-t responses for a potential step experiment. The potential E_2 is chosen so that a: the reaction is diffusion controlled, b: the reaction is kinetically controlled, and c: there is mixed control.

and double layer charging currents which cause a sharp spike in the current at start times. To determine faradaic current at t=0, it is necessary to resort to an extrapolation procedure. Solving Fick's 2nd law with the appropriate boundary conditions [81] gives

$$i = -nFk_{-}c^{\infty}_{O} \exp \frac{(k_{-} + k_{+})^2 t}{D} \operatorname{erfc} \frac{(k_{-} + k_{+})t^{\frac{1}{2}}}{D^{\frac{1}{2}}} \qquad (1:5:3)$$

where erfc is the complement of the error function [83]. Limiting forms of this equation yield (1) at short times

$$i \simeq - nFk_{-}c^{\infty}_{O} \left(1-2 \frac{(k_{-} + k_{+})t^{\frac{1}{2}}}{\pi^{\frac{1}{2}}D^{\frac{1}{2}}}\right) \qquad (1:5:4)$$

(2) at long times

$$i \simeq - \frac{nFk_{-}c^{\infty}_{O}D^{\frac{1}{2}}}{\pi^{\frac{1}{2}}(k_{-} + k_{+})t^{\frac{1}{2}}} \qquad (1:5:5)$$

and at high cathodic overpotentials (when k_{+} is small compared to k_{-}) equation (1:5:5) reduces to the Cottrell equation.

From (1:5:4) it can be seen that at short times a plot of i versus $t^{\frac{1}{2}}$ should be a straight line of intercept $i_{t=0}$ given by

$$i_{t=0} = - nFk_{-}c^{\infty}_{O} \qquad (1:5:6)$$

from which the potential dependent rate constant k_{-} can be obtained.

By performing experiments over a range of potentials a range of potential dependent rate constants may be obtained.

Using the equations

$$\log k_{-} = \log k^{O} - \frac{\alpha_{c}nF}{2.3RT}(E-E^{O}) \qquad (1:5:7)$$

and

$$\log k_+ = \log k^o + \frac{\alpha_a nF}{2.3RT} (E-E^o) \qquad (1:5:8)$$

where k^o is the standard rate constant, and plotting log k_+ or log k_- as a function of E yields a linear graph giving values of the transfer coefficients α_a and α_c.

(ii) Chronocoulometry

As in chronoamperometry a potential-time profile, as shown in Fig. 1.5(a), is applied to the working electrode. However, in this case the total charge, Q, is recorded as a function of time. For mixed control, and where the rate of the back reaction is negligible, a plot of Q as a function of $t^{\frac{1}{2}}$ yields at long times a straight line in accordance with the equation

$$Q = \frac{4nFk_-}{\pi} C^{\infty}_o (t^{\frac{1}{2}}_L t^{\frac{1}{2}} - t_L) \qquad (1:5:9)$$

where $t^{\frac{1}{2}}_L$ is the intercept on the x-axis. The value of k_- is obtained from the slope and the value of t_L.

The advantage of chronocoulometry over chronoamperometry is that, since the charge is the integral of the current, it retains at long times information about the value of the current at short times. The charge at very short times is still distorted by the double layer charging process, but its influence on the total charge rapidly becomes negligible. This permits rate constants of an order of magnitude greater to be determined from charge, rather than current, measurements.

Whilst pulse techniques are very useful for determining the kinetics of reactions they can only be applied once the reaction mechanism has been definitely established. The reason they should not be used for mechanistic investigations is because most experiments lead to a falling transient and information is only obtained by a detailed mathematical analysis of its shape.

(b) Potential Sweep Techniques

In the area of preliminary mechanistic investigations sweep techniques [84,85], and in particular cyclic voltammetry are most useful. An 'electrochemical spectrum' indicating the potentials at which processes occur can be rapidly obtained, while from the sweep-rate dependence, the involvement of coupled homogeneous reactions is rapidly identified, and other complications such as adsorption can be recognised.

The potential-time waveforms used in sweep measurements are shown in Fig. 1.6. The simplest of these techniques is linear sweep voltammetry (LSV), and this involves sweeping the electrode potential between limits E_1 and E_2 at a known sweep-rate, ν, before halting the potential sweep. A generally more useful technique is cyclic voltammetry (CV). Initially the waveform is the same as in LSV, but on reaching the potential E_2 the sweep is reversed rather than terminated. On again reaching the initial potential E_1 there are several possibilities. The potential sweep may be halted, again reversed or alternatively continued further to a value E_3. In both LSV and CV experiments the cell current is recorded as a function of the applied potential. The applied potential varies linearly with time according to

$$E_{(t)} = E_i - \nu t \qquad (1:5:10)$$

For a reversible reaction the potential will be given by the Nernst equation as

$$E = E^o + \frac{RT}{nF} \ln \frac{c_{o(0,t)}}{c_{r(0,t)}} \qquad (1:5:11)$$

where this ratio can be shown to be a function of time given by

$$\frac{c_{o(0,t)}}{c_{r(0,t)}} = f(t) = \exp\left(\frac{nF}{RT}\right)(E_i - \nu t - E^o) \qquad (1:5:12)$$

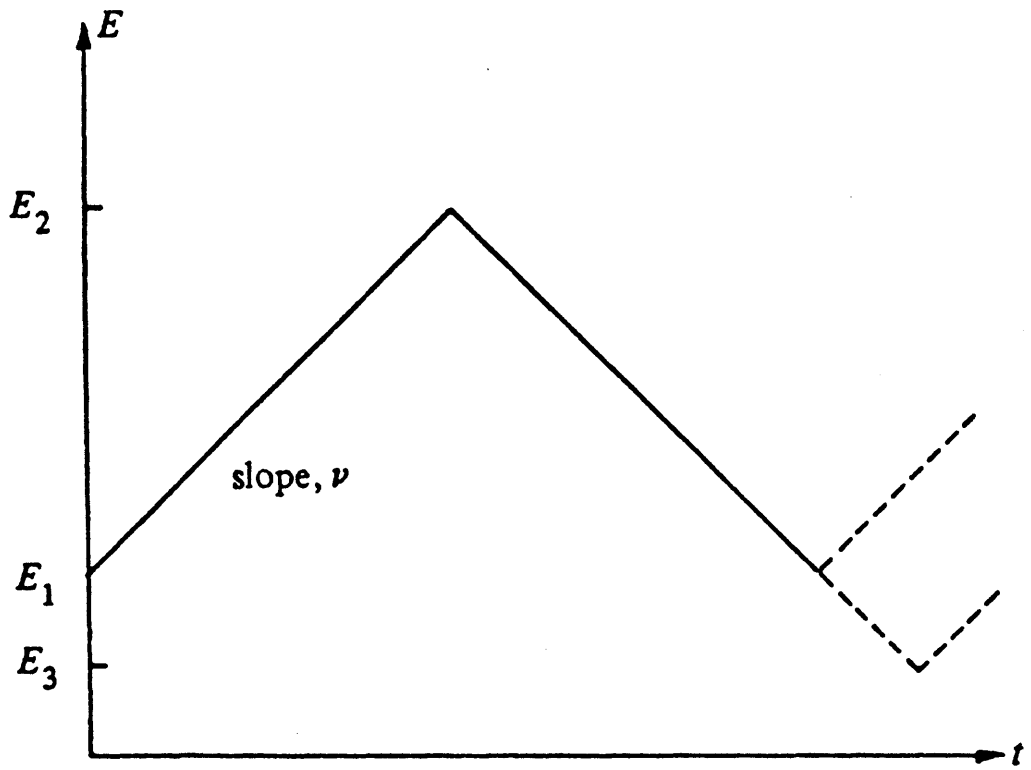

Figure 1.6: Potential-time profiles for sweep voltammetry.

A typical example is shown in Fig. 1.7(a). Randles [84], Sevcik [87] and Nicholson [88,89] have all shown that for planar diffusion

$$i_p = -0.4463\ nF \left(\frac{nF}{RT}\right)^{\frac{1}{2}} c^{\infty}_{o}\ D^{\frac{1}{2}}\ \nu^{\frac{1}{2}} \qquad (1:5:13)$$

This is called the Randles-Sevcik [86,87] equation and at 25°C reduces to the form

$$i_p = -(2.69 \times 10^5) n^{3/2}\ C^{\infty}_{o}\ D^{\frac{1}{2}}\ \nu^{\frac{1}{2}} \qquad (1:5:14)$$

where i_p is the peak current density as in Fig. 1.7(a). A linear variation of peak current with $\nu^{\frac{1}{2}}$ is predicted where D may be evaluated from the slope.

An expression for the peak potential E_p may also be found yielding

$$E_p - E_{\frac{1}{2}} = -1.109\ \frac{RT}{nF} \qquad (1:5:15)$$

Thus, for a reversible wave, E_p is independent of both scan rate (ν) and the peak current (i_p).

For an irreversible reaction, the Nernstian boundary is replaced by

$$-\frac{i}{nF} = D\left(\frac{\delta C_o}{\delta C_x}\right)_{x=0} = k_{-}(C_o)_{x=0} \qquad (1:5:16)$$

In this case, the peak current density at 25° is

$$i_p = -(2.99 \times 10^5) n(\alpha_c n_\alpha)^{\frac{1}{2}} C^{\infty}_{o}\ D^{\frac{1}{2}}\ \nu^{\frac{1}{2}} \qquad (1:5:17)$$

where n_α is the number of electrons transferred up to, and including, the rate determining step. The peak current density is proportional to $\nu^{\frac{1}{2}}$ and $\alpha_c^{\frac{1}{2}}$. For a totally irreversible system there is a total absence of a reverse peak.

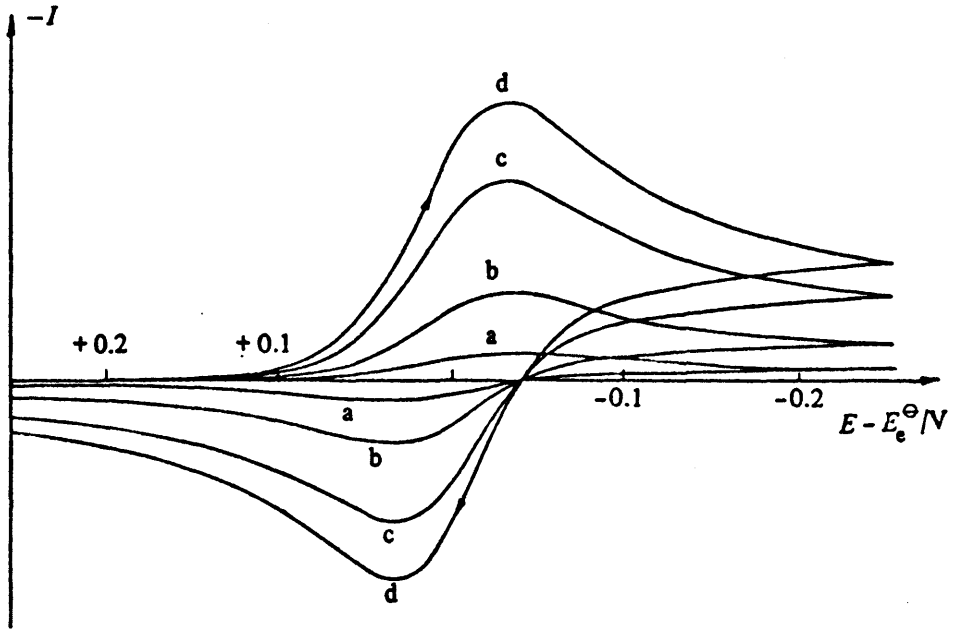

Figure 1.7(a): Cyclic voltammograms for a reversible process, O + e R when only O is initially present in solution. The potential sweep-rates are (a) ν, (b) 10 ν, (c) 50 ν and (d) 100 ν.

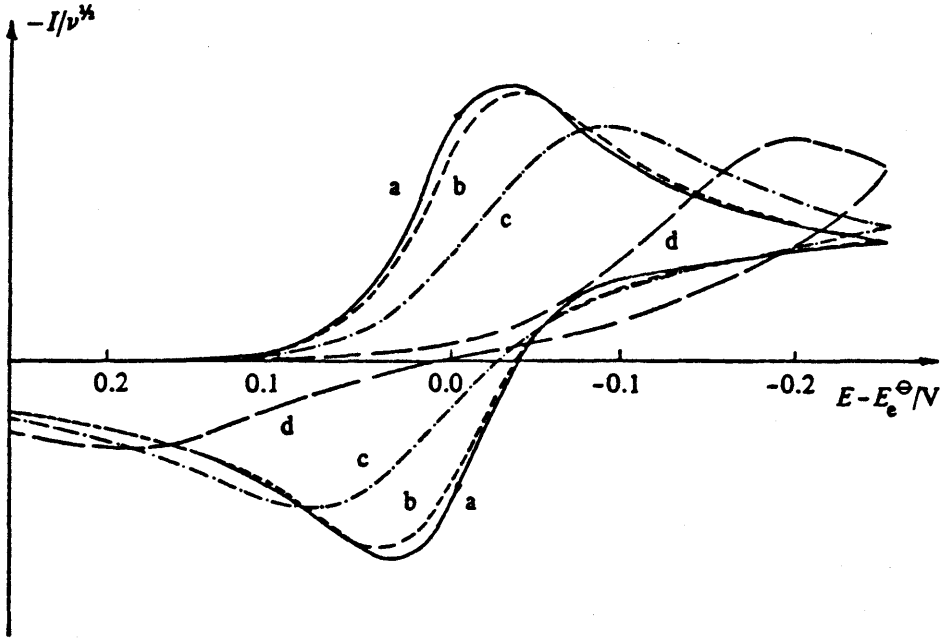

Figure 1.7(b): Normalised cyclic voltammograms. Parameters as in Fig. 1.7(a).

In this case, the peak potential is found to vary with the sweep-rate by [89]

$$E_p = E^o - \frac{RT}{\alpha_c n_\alpha F}\left(0.78\left(-\frac{2.3}{2}\log\frac{\alpha_c n_\alpha FD}{k^{o2}RT}\right)\right) \quad (1:5:18)$$

and shifts (for a reduction) in a negative direction for increasing ν by ca. $(30/\alpha_c n_\alpha)$mV for each tenfold increase in ν.

For quasi-reversible systems the boundary condition [90]

$$0.3\ \nu^{\frac{1}{2}} \geqslant k^o \geqslant 2 \times 10^{-5}\ \nu^{\frac{1}{2}}\ \text{cm s}^{-1} \quad (1:5:19)$$

yields a peak current density of

$$i_p = nFc^\infty_o D^{\frac{1}{2}}\left(\frac{nF}{RT}\right)^{\frac{1}{2}}\nu^{\frac{1}{2}}\,\psi\,(E) \quad (1:5:20)$$

where, because of the inclusion of a current function ψ (E), the peak potential currents may not be regarded as a linear function of $\nu^{\frac{1}{2}}$.

Cyclic voltammetry is probably the most powerful technique available for investigating coupled chemical reactions. The voltammograms should be recorded over as wide a range of conditions as possible before any attempt is made to interpret the data. In particular the timescale of the experiment should be varied (by using a range of sweep-rates) and the potential limits should be changed to investigate whether there are other processes coupled to the one of interest.

It is convenient to classify the different possible reaction schemes by using letters to signify the nature of the step. E represents an electron transfer at the electrode surface and C represents a homogeneous chemical reaction [92]. Thus a reaction mechanism in which the sequence involves a chemical reaction of the product after the electron transfer would be designated an EC reaction. Other common reaction types encountered include a CE reaction (preceding reaction), an EC' reaction (catalytic) and an ECE reaction. The initial investigations were carried out by

Brdicka, Wiesner et al. of the Czechoslovakian polarographic school in the 1940's. They are dealt with in detail in many review articles [81,82,89,91,93-96].

If a reactant or product is weakly adsorbed onto the surface the voltammograms generally exhibit an enhancement of peak currents in comparison with the uncomplicated charge transfer case. In the case of a reactant or product being strongly adsorbed then separate adsorption peaks may occur after or prior to the main transition peaks. The exact nature of adsorption peaks has been discussed by Wopschall and Schain [97,98], and the general problems involved in analysing electrochemical processes adsorption have been discussed by Sluyters-Rebach and Sluyters [99].

For a reversible case where the adsorption can be described by a Langmuir isotherm it can be shown that $E^A_p = E^C_p$, and that the peak current density is given by

$$i_p = \frac{qF}{4RT} \cdot \nu \qquad (1:5:21)$$

where q is the charge associated with the surface excess of O, showing that i_p is proportional to ν. Also,

$$E_p = -\frac{RT}{F\ln K} \qquad (1:5:22)$$

where $K = k_+C_O/k_-$, thus indicating that E_p is independent of ν.

Likewise, an irreversible case yields

$$i_p = \frac{q\alpha F}{RT} \cdot \nu \qquad (1:5:23)$$

with i_p being directly proportional to ν. Also,

$$E_p = \frac{RT}{\alpha F} \ln\left(\frac{\alpha qF}{kRT}\right) + \left(\frac{RT}{\alpha F}\right)\ln \nu \qquad (1:5:24)$$

The quasi-reversible case, i.e. for any degree of reversibility is considerably more complicated than the limiting cases above. It has been discussed recently by Srinivasin and Gileadi [100] and by Laviron [101,102].

(c) Other Techniques

There are many other techniques, far to numerous to discuss in detail here, which may be used for the study of electrochemical processes. These techniques include A.C. impedance measurements, polarography, and the use of rotating disc and ring-disc electrodes. These methods are outlined in detail in many comprehensive reviews and books. However, one other class of experimental techniques deserves mention.

(d) Spectroelectrochemistry

The principal disadvantage of other approaches is that such purely electrical measurements lack molecular specificity, i.e. the current only represents the aggregate rate of all processes occurring, and no direct information about the identity of reaction products or intermediates is available. Spectroelectrochemical techniques [103,104] are capable of probing the electrode/electrolyte interphasial region to provide this type of data. In particular they help (i) to identify reaction intermediates, (ii) to monitor the time dependent concentration of these, and other species, and (iii) to study surface properties such as adsorbate orientation, ordering and coverage.

(i) UV-Visible Optical Techniques

This was the first widely applied spectroelectrochemical technique and was based on the use of optically transparent electrodes (OTE). A beam of monochromatic UV-visible light is directed perpendicularly through an OTE, the diffusion layer next to the electrode and then the bulk solution; monitoring is carried out after the light has passed out of the electrochemical cell through an exit window. Information about the concentrations of

adsorbing species in the diffusion layer at the electrode may be obtained. However, this technique is limited due to the requirement of a suitable electrode material that is transparent to UV-visible light. A survey of the techniques involved in the preparation of the OTEs has been presented by Van Benken and Kuwana [105]. A similar technique of alternative design is based on the use of optically transparent thin layer electrodes (OTTLE) [106].

Reflection techniques overcome the need for transparent electrodes. The electrode surfaces need to be polished, using a combination of techniques mechanical and chemical, to a mirror finish. Ellipsometry [107] involves the determination of the change in polarisation state of an obliquely incident light beam upon specular reflection at a surface. The beam is said to be elliptically polarised if the s and p components of the electric vector are of the same frequency but different phase and amplitude. By comparing the ratios of amplitude and phase, before and after reflection, the optical constants of clean surfaces may be determined. The properties of thin surface films, e.g. oxide layers, may also be investigated [108]. Ellipsometry, however, is both expensive and relatively slow. Similar techniques of lower cost and greater speed have been developed such as specular reflectance spectroscopy. The principle is to shine a monochromatic light beam at an electrode surface at a known angle of incidence and to record the intensity of the reflected beam as a function of either wavelength, potential or time. The data obtained is then compared to calculations made using the three layer model of bulk electrode/interphasial region/bulk solution. Only very small changes in reflectivity are predicted and these must be enhanced so as to be detected. This is achieved by increasing the number of reflections or using an extremely glancing angle of incidence thereby increasing the wavelength. The electrode potential is usually modulated and reflectivity changes are detected using a lock-in amplifier.

Two techniques, which take advantage of the temperature rise in a system when it absorbs radiation are photothermal [109] and photoacoustic [110] spectroscopy. However, neither of these techniques have been widely applied to date.

(ii) Vibrational Spectroscopy

UV-visible techniques lack molecular specificity but this type of information, especially for identifying and studying adsorbate orientation, is provided by vibrational spectroscopy.

Of all the infrared (IR) spectroscopic [111] methods the most extensively applied is Electrochemically Modulated IR Spectroscopy (EMIRS) [112]. In this technique, an infrared beam is reflected off the surface of a mirror smooth electrode in solution. The potential of the electrode is modulated between two limiting potentials which affects species adsorbed on the electrode, but not species in the bulk solution. It is possible to observe differences in the IR reflectance at the two potentials by using a phase sensitive detector locked on the electrochemical modulation. Infra Red Reflection-Adsorption Spectroscopy (IRRAS) [113(a)] is similar to EMIRS but can be used at constant potential. With IRRAS the polarisation of the incident light, rather than the electrode potential, is modulated; this discriminates between variations in the plane of the electrode and those perpendicular to the electrode. A third method called Subtractively Normalised Fourier Transform Infra-Red Spectroscopy (SNIFTIRS) [113(b)] also can identify adsorbed species directly.

Absorption by solvent and window materials, which hamper infrared spectroscopy, are overcome by using Raman scattering techniques. Resonance Raman Scattering (RRS) [114] is largely used for studying species in solution. The small cross-sections of overlap of the scattering are enhanced when the frequency of the laser light overlaps with an electronic transition in the sample. Surface Enhanced Raman Scattering (SERS) [115] is used for studying surfaces and adsorbates. Enhancement, achieved by roughening the electrode, is not accounted for simply by the surface area increase [385].

(iii) Mass Spectroscopy

An electrochemical cell is interfaced directly to a mass spectrometer by connecting a porous platinum electrode to the inlet port [116]. Volatile products generated at the platinum surface

diffuse through the electrode and are detected in the mass spectrometer. In differential electrochemical mass spectrometry (DEMS) [117] the electrode is made of a porous Teflon membrane with the Pt catalyst supported on it. This approach allows discrimination between adsorbed and bulk solution species by isotopic labelling and solution replacement. By correlating the mass spectral data and the electrochemical charges it is also possible to determine clearly the number of electrons generated per molecule of product. A complementary method is the use of Electrochemical Thermal Desorption Mass Spectroscopy (ECTDMS) [118]. In this technique the electrode is emersed, transferred to an ultra high vacuum (UHV) chamber and thermal desorption spectra are obtained. A further technique called Secondary Ion Mass Spectroscopy (SIMS) [119] has also been developed to identify intermediates from secondary ions by extrapolating back to find their origin.

(iv) X-Ray Diffraction

By using a computer controlled x-ray diffraction system [120] utilising position sensitive photon counting techniques, in-situ structure at the solid/liquid interphase may be described [121]. These techniques are highly accurate when they utilise synchrotron radiation for both transmission and reflection x-ray diffraction. Cells have to be designed to minimise absorption of the x-ray beam.

(v) Other In-Situ Techniques

Electron spin resonance spectroscopy [122] (presents cell design problems), surface plasmon spectroscopy [123] (longitudual electromagnetic waves that propagate at the interphase), surface conductance [124] (a function of the concentration and mean free path of the electrons), photoemission [125] (into an electrolyte), photocurrent spectroscopy [126], scanning tunnelling microscopy (real space imaging of surfaces on an atomic scale [132], neutron diffraction and dynamic neutron scattering [127], and Mossbauer spectroscopy [128] (investigation of the resonant absorption of x-rays by certain nuclei) are other techniques which deserve mention, though not perhaps widely used.

(vi) Ex-Situ Techniques

Ex-situ techniques [129] are carried out using conventional and sensitive UHV techniques which rely on the emission or scattering of electrons by coupling the UHV chambers to the electrochemical cell using appropriate electrode transfer systems. These techniques can identify species and give information about both energetics and structure; the information provided, however, is restricted as surfaces may reconstruct [130] on transfer and are no longer under potential control in the UHV chamber; measurements on adsorbates are restricted to strongly chemisorbed species and information about species on the solution side of the interphase is inevitably lost. Some fairly sophisticated procedures have been developed to help minimise this restructuring but the use of ex-situ techniques is still problematic [131].

1.6. ELECTROCATALYSIS

1.6.1. Introduction

The role of electrochemistry may be very important in a future energy economy in which heat-engines are replaced by fuel cell devices of much higher conversion efficiency and in which energy utilisation is optimised by storage. Electrochemistry also has implications for non-traditional energy sources (e.g. solar energy). Fuel cells [133] are the only energy conversion devices which convert the chemical energy of fuels directly to electricity, without the intermediary of heat. The high theoretical efficiency of such systems is of considerable significance as the dwindling supply of fossil fuel is not capable of replacement and has valuable alternative (non-fuel) uses. The efficiency, or ratio of useful energy produced to the amount of energy supplied, of all heat engines is given by the Carnot cycle [134]. However, a much higher efficiency can be achieved in systems of energy conversion operating without the intermediate production of heat, like fuel cells.

The construction of fuel cells [135] that are competitive power sources on the market depends upon a satisfactory compromise between five basic requirements: (a) losses due to polarisation

and internal resistance of the cell should be small; (b) electrodes should be resistant to corrosion; (c) the electrolyte should be invariant; (d) the costs for electrocatalysts used in the construction of fuel cells should be low; and (e) price of fuels should be reasonable.

Fuel cells that are developed at present may be classified according to the temperature of operation: - low temperature cells operating at temperatures less than 150°C such as hydrogen-oxygen cells or cells where the hydrogen is replaced by another oxidisable material; medium temperature cells operating at temperatures between 150-300°C, e.g. phosphoric acid cells; high temperature cells operating at temperatures greater than 300°C, e.g. molten carbonate or solid electrolyte cells. Each of these types of fuel cell meet the above requirements to different degrees. However, due to corrosion at higher temperatures and the necessity to produce hydrogen by gasification reactions at low temperatures, it is clear that there are several practical advantages of low temperature cells using liquid fuels dissolved in an electrolyte. Liquid fuels are generally more easily stored than gases; no bulky and heavy cylinders are needed and the energy/mass and energy/volume ratios for the complete power units are better.

Several inorganic fuels have been examined and four of these seem to have some promise: namely, ammonia, hydrazine, hydroxylamine and sodium borohydride. However, most of the latter tend to be expensive and suffer from other drawbacks, e.g. they are explosive and/or poisonous. Organic compounds are the obvious alternative. As the longer chained carbon species suffer from solubility problems in aqueous electrolytes, simpler molecules are preferred. Earlier investigations in this area [136] indicate that the most satisfactory substances from the point of view of reactivity are methanol, formaldehyde, ethanol, ethylene glycol and formic acid.

Of the latter, methanol seems to have the most advantages: it is a liquid that dissolves readily in aqueous solution and oxidises rather directly to carbon dioxide and water; it is not expensive at the present time - being produced readily by partial oxidation of natural gas (oil, coal and even wood are alternative sources).

Since it is a liquid, methanol could readily be distributed to, and marketed by, the existing infrastructure used for gasoline [137]. Most of the other potential organic fuels listed earlier have severe disadvantages: formaldehyde has a low boiling point (-21°C) and is rather unstable; ethanol oxidises to acetic acid which is not particularly volatile; and formic acid reacts chemically with alkaline electrolytes.

No matter which fuel is selected for the cell there are still engineering and electrocatalytic obstacles to the development. Although the engineering problems, e.g. electrode sintering, are by no means trivial the key to success is the development of highly effective fuel and air electrode catalysts. Hence, the overwhelming problem to be overcome is primarily electrocatalytic [138]. Pletcher [139] pointed out that there remains a gulf between those who develop electrode materials and those who seek to understand the physical chemistry of electrocatalysis. Randin [140] also pointed out the absence of a general theory of electrocatalysis. However, as pointed out by Sakellaropoulos [141], electrocatalytic investigators have been undertaking basic research while being unable to explain even elementary processes. Bockris and Drazic [1] stated that further development depends mainly on how soon the elementary processes involved will be fully understood.

1.6.2. Basic Concepts

The term *electrocatalysis* was deliberately introduced by Grubb in 1963 [142] to identify the unique and characteristic features of catalytic electrode proceses. As in chemical catalysis (where a given reaction occurs at a different rate upon different substrates, the substrate itself suffering no change), the objective of electrocatalysis is to seek to provide alternative, lower activation energy pathways for reactions to occur. The catalysis of electrode reactions is possible both by species attached to the electrode surface and by species dissolved in the electrolyte. An example of the latter is the oxidation of propylene to propylene oxide [143] which is virtually unknown as a direct electrode reaction, but in the presence of bromide ion in

slightly alkaline solution, e.g. pH 9, the conversion is possible in high yield. The suggested route for reaction is as follows, viz.

$$2Br^- - 2e \rightarrow Br_2 \xrightarrow{OH^-} HOBr + Br^- \qquad (1:6:1)$$

$$CH_3CH{=}CH_2 + HOBr \rightarrow CH_3\underset{OH}{CH}\text{-}\underset{Br}{CH_2} \xrightarrow{OH^-} CH_3CH\text{-}CH_2 + H_2O + Br^- \qquad (1:6:2)$$

- the process occurs at the potential of the Br^-/Br_2 couple. This type of reaction is not confined to propylene [144].

The term electrocatalysis is, however, more commonly applied to systems where the oxidation or reduction requires bond formation, or at least a strong interaction of the reactant, intermediates or product, with the electrode surface. The energy consumption of an electrolytic cell is proportional to its operating voltage, V, which is usually described by an equation of the type

$$V = \Delta E_e - \eta_A + \eta_C - iR \qquad (1:6:3)$$

where ΔE_e is the difference between the equilibrium electrode potentials for the two electrode reactions; η_A and η_C are the overpotentials at the anode and cathode respectively (both will increase the numerical value of the cell voltage), and the iR term expresses the Ohm's law losses through the electrolyte and other current carrying cell components. The overpotential at each electrode will vary with current density according to the Tafel equation

$$|\eta| = \frac{2.3\ RT}{\alpha nF} \log \frac{i}{i_o} \qquad (1:6:4)$$

and it should be noted that the overpotential involved depends on both the exchange current density, i_o, and the Tafel slope, 2.3 RT/αnF. Hence, it can be seen that a good catalyst will have a high exchange current density and/or a low Tafel slope. Clearly, according to equation (1:6:3), it is most important to minimise η when these terms are significant compared to ΔE_e and the iR term.

The essential aim of electrocatalysis as a science is to establish a predictive basis for the design and the optimisation of catalysts. Predictions can be formulated only if the factors which are responsible for the electrocatalytic properties are identified. This is the fundamental goal of this area of research.

1.6.3. Selection of Electrocatalysts

The selection of electrocatalysts for a particular reaction remains largely an empirical process, and catalyst design is still very much a goal for the future. Electrocatalysts are almost always transition metal species, and, according to conventional wisdom [143], analogies with homogeneous as well as gas phase heterogeneous catalysis are to be expected. However, our knowledge of the factors which determine the activity of electrocatalysts lags behind that available in homogeneous catalysis where for example Meyer [145] has been able to discuss the choice of ligands and oxidation states involved in 1e oxidation, 2e oxidation, hydride or oxygen atom transfer carried out in the presence of Ru complexes. In electrocatalysis to date it has only been possible to consider in a very qualitative manner, the importance of the oxidation states of the metals, the spacing of catalyst centres and electronic factors due to the surrounding metal atoms, lattice type (e.g. oxide or sulphide) or ligands.

From a brief overview, it becomes apparent that selection of a suitable electrocatalyst should be based upon the following criteria:

1. optimal strength of reactant, intermediate and product adsorption;

2. maximum specificity and control of the desirable reaction path;

3. fastest reaction rate and minimal electronic energy losses;

4. inertness toward reactants, products, electrolyte and potential;

5. resistance to poisoning by molecular or ionic species and impurities;

6. optimal crystallite composition, size and surface distribution;

7. resistance to sintering and deactivation;

8. maximum effective surface area;

9. complete surface utilisation;

10. inexpensive cost.

Simultaneous satisfaction of these requirements is often impossible, and electrocatalyst selection becomes a compromise. It is possible to identify several types of electrocatalysts, for example,

(a) single metals, e.g. Pt, Ni, Pd;

(b) alloys and two component catalysts, e.g. PtSn, NiMo

(c) useful oxides, e.g. RuO_2 (metallic); also spinels, perovskites and bronzes;

(d) complexes, e.g. metal phthalocyanines and prophyrins

The predominance of transition metal species in electrocatalysis is usually attributed to their unpaired d-electrons and unfilled d-orbitals which are available for forming bonds with adsorbates. Why gold with no unfilled d-orbitals is an effective electrocatalyst in some cases, e.g. in base [385], will be discussed at a later stage. It is expected that the free energy of adsorption will depend strongly on the number of unpaired d-orbitals per metal atom and also on their energy levels, and hence, both on the choice of transition metal and its detailed

environment. Why a correlation seems to fail within the noble metal group will also be dealt with later. In the limit, the surroundings (i.e. the adjacent metal atoms in a metal or alloy, the ligands to a metal complex or the oxide ions in an oxide lattice) and the adsorbate may be considered as ligands to the central transition metal ion acting as the catalyst centre, and the surroundings will moderate all the properties of the metal-adsorbate bond.

Identification of electrode reactons, which involve surface chemistry, may be achieved by studying the i-E characteristics. These characteristics will depend very strongly on the choice of electrode material, and with some electrodes at least, the reaction will occur up to several volts away from the reversible potential. More detailed analysis of the i-E data will reveal that:

(i) the exchange current densities will vary with electrode material. For example, the i_o values for hydrogen evolution in 1 mol dm^{-3} acid range from 10^{-12} to 10^{-3} A cm^{-2};

(ii) the Tafel slope is commonly not $\beta = \alpha nF/2.3\ RT$ or $(120\ mV)^{-1}$ for a reaction where $\alpha = 0.5$, $n = 1$. Values of $\beta/2$, $\beta/3$ and $\beta/4$ are common, and the Tafel slope may also depend on electrode material, indicating a change in reaction mechanism. The Tafel slopes which are β/m may be interpreted in terms of mechanism;

(iii) the temperature dependence of the Tafel slope may not be straight forward. This was first noted by Conway et al. [146,147] for the hydrogen evolution reaction in methanol, and has also been found by Yeager [148] for oxygen reduction in phosphoric acid.

Since electrocatalytic reactions take place at the electrode surface, which is the meeting point and energy field modifier between the electrocatalyst and reactants, it is important to link catalyst activity with microscopic surface properties. The properties which determine the activity and selectivity of electrocatalysts are:

1. Surface activity - strength and mode of adsorption, adsorption isotherms, adatom formation, substrate-catalyst interactions, surface diffusion, adsorbate spillover, bulk electronic properties and surface electronic properties;

2. Surface structure and history - crystallographic parameters, crystallite size and distribution, defects and dislocations, nature of catalytic sites, and pretreatment and prior use of surface;

3. Surface stability and deactivation -sintering and redispersion, poisoning by electrolyte ions, poisoning by reactants, products or impurities and stabilisation by support;

4. Surface selectivity - structural factors, multiple surface reactions, potential effects and transport factors;

5. Physical conditions - concentration, temperature, pressure, transport phenomena and electric field.

1.6.4. The Hydrogen Evolution Reaction

The hydrogen evolution reaction (H.E.R.) is probably the most studied of electrode processes and the mechanism and kinetics of the reaction at many cathode materials have been elucidated [149,150]. This process is generally considered to involve the following steps:

$$M + H^+ + e \rightarrow M\text{-}H_{ads} \qquad (1:6:5)$$

$$2M\text{-}H_{ads} \rightarrow H_2 + 2M \qquad (1:6:6)$$

or

$$M\text{-}H_{ads} + H^+ + e \rightarrow H_2 + M \qquad (1:6:7)$$

where M represents a metal adsorption site. Equation (1:6:5) is called the Volmer reaction and represents proton discharge, equation (1:6:6) is called the Tafel reaction and represents recombination and equation (1:6:7) is called the Heyrovsky reaction and represents ion-plus-atom mechanism. The process is catalysed

by metals in the order [151]

$$Pt > Pd > W > Fe > Cr > Ag > Cu > Pb > Hg \qquad (1:6:8)$$

This is approximately the order of increasing overpotential for the H.E.R. However, all three reactions are not important on all metals. Thus, a hydrogen ion discharge rate limiting step would be enhanced by metals on which the metal-hydrogen bond is strong. On the other hand, a rate limiting step involving the ion-plus-atom mechanism would be favoured by low adsorption strength [152]. That electrocatalysis at bare metals is affected by electronic structure of the metal can easily be seen. Both mechanisms require the formation and then cleavage of a metal-hydrogen bond. Hence, while a variation of the cathode, so as to increase the free energy of adsorption, will increase the formation of the adsorbed species, it will slow down the second step in the overall process. As a result, it is to be expected that the maximum rate of hydrogen evolution will occur at intermediate values of ΔG^{o}_{ads} which leads to a significant but not monolayer coverage by adsorbed hydrogen atoms. This dependence is represented by volcano-shaped curves of exchange current density versus ΔG^{o}_{ads} for a series of metal cathodes as in Fig. 1.8.

Experimental investigations of the H.E.R. at many cathodes have shown a wide variation in the Tafel slope, exchange current density and dependence of current on pH. This is typical of reactions which involve a specifically adsorbed intermediate. More detailed study [153] of the metals in Fig. 1.8 indicates that the metals can be divided into groups depending on which mechanism is followed. Thus, metals such as Hg, Tl, Zn, Cd and Pb, which adsorb hydrogen only weakly (large positive values of ΔG^{o}_{ads}), have low values for the apparent exchange current density, Tafel slopes of $(120\ mV)^{-1}$ and the Volmer reaction is rate controlling. Metals such as Pt and the Pt family with ΔG^{o}_{ads} values close to zero have high apparent exchange current densities and kinetics which indicate that the Tafel reaction follows the Volmer reaction and is rate controlling. Metals such as Mo, Ta and W, which strongly adsorb hydrogen and have very negative values of ΔG^{o}_{ads}, again have low exchange current densities and kinetics which indicate the Heyrovsky reaction follows the Tafel reaction. It can be seen that

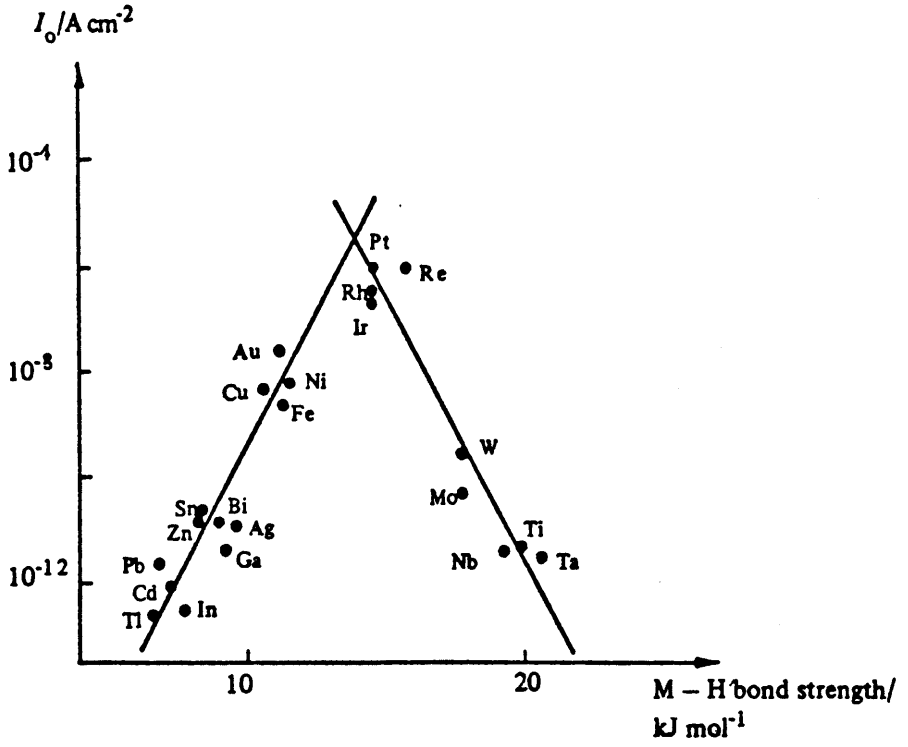

Figure 1.8: Dependence of the exchange current density for the hydrogen evolution reaction in 1 mol dm^{-3} acid on the strength of the metal-hydrogen bond formed with the metal of the electrode [Ref. 149].

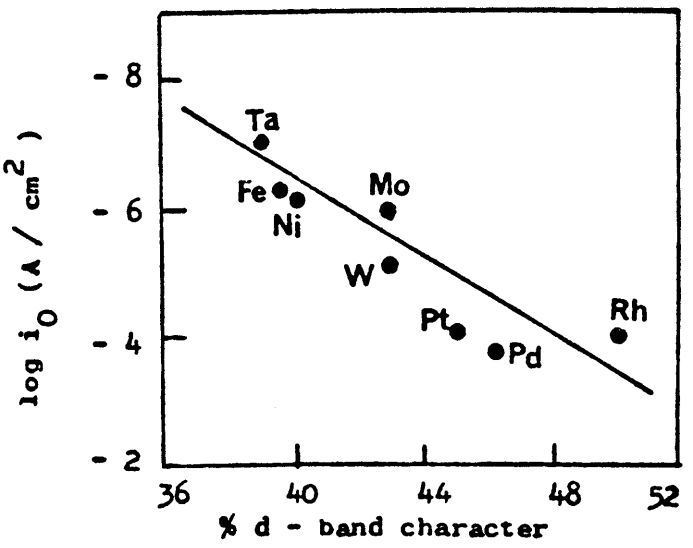

Figure 1.9: Dependence of the exchange current density for hydrogen evolution at various electrocatalysts on d-bond character [Ref. 156].

Pt has the highest exchange current density since this metal has ΔG^{o}_{ads} close to zero.

Since the strength of adsorption depends on surface electronic interactions between adsorbant and catalyst, a correlation of reaction rate and d-band character of simple metals is expected, similar to gas phase catalysis [154,155]. The correlation seems to fail within the noble metal group [156], as in Fig. 1.9 {Ta(d^3), Fe(d^6), Ni(d^8), Mo(d^5), W(d^5), Pt(d^8), Pd(d^8), Rh(d^7)}, and this may result from the existence of multiple adsorption states and the structure, history and activity of the catalysts used [141].

While the H.E.R. is influenced strongly by the strength of H_{ads} at the electrode surface it should be noted that the final product is a gaseous species. Hence the rate determining step for transfer control is effectively the need to expel hydrogen from the interphasial region where it can cause large decreases in effective electrode surface area.

The metal-adsorbate coverage at limitingly low or at limitingly high coverage is given by a Langmuir type isotherm. In intermediate cases some other isotherm, involving a coverage dependent heat or free energy of adsorption, will apply (e.g. Temkin or Frumkin). Often it is noted experimentally that the change in heat of adsorption with coverage is approximately constant, giving rise to the simplified Temkin isotherm [157] in the intermediate coverage region [158]. The linear relationship between heat of adsorption and coverage has been attributed to adsorbate-adsorbate interactions [159-161] as well as bond strength change caused by the effect of oriented dipoles at the surface, via the work function [162]. In electrolytic solutions adsorption involves displacement of adsorbed water molecules, which are bound by dispersion forces. Heats of adsorption in electrochemistry are, therefore, the difference between the heat of adsorption in vacuum and the heat of adsorption of the displaced water molecules under the appropriate potential conditions. A theory of competitive adsorption which applies particularly well to comparatively weakly adsorbing organic molecules [163] has been developed by Bockris et al. [20,164]. Their isotherm contains a number of terms involving dipole-dipole, ion-ion, and dipole-ion interactions. Such an

isotherm will be valid unless dissociation and associated strong chemisorption occurs. Under such conditions a Temkin isotherm can be expected to be a good approximation to the observed behaviour in the medium coverage range, and it can be expected that the same value of the Temkin term will apply to all species of similar chemisorbed character that are simultaneously adsorbed [158].

1.6.5. Hydrogen Chemisorption

The adsorption of hydrogen on many metals can be clearly detected using cyclic voltammetry, as outlined in Fig. 1.10; adsorption peaks are usually seen at potentials just positive to those where hydrogen gas is evolved. The desorption peaks are present on the reverse scan. These hydrogen peaks are not necessarily caused by the intermediates involved in the H.E.R. [153,165]. The adsorbed hydrogen atom is formed by the reaction

$$H_3O^+ + e \rightarrow H_{ads} \qquad (1:6:9)$$

Adsorption and desorption hydrogen peaks are characterised by their sharp symmetrical shape, their peak currents are proportional to potential scan rate, and the charges for the adsorption and desorption processes should be equal and independent of potential scan rate. The voltammogram for Pt shows that there are at least two types of hydrogen on the surface since there are two distinct adsorption peaks and probably three desorption peaks (not visible in Fig. 1.10) [153] on the reverse sweep. Indeed there have been claims of up to six different peaks being visible in weak electrolyte solutions [166]. The two main types are called 'strongly' and 'weakly' adsorbed hydrogen, the former giving rise to the more positive peak since a higher free energy of adsorption is necessary for the larger shift in potential. Various explanations have been proposed for the several peaks including different adsorption sites on a given single crystal surface, a distribution of crystallographic surfaces, induced heterogeneity associated with hydrogen adsorption itself and anion adsorption which induces heterogeneity by blocking sites to varying degrees and perturbing adjacent sites. Discussion of these different possibilities will be dealt with in section 1.7 dealing with single

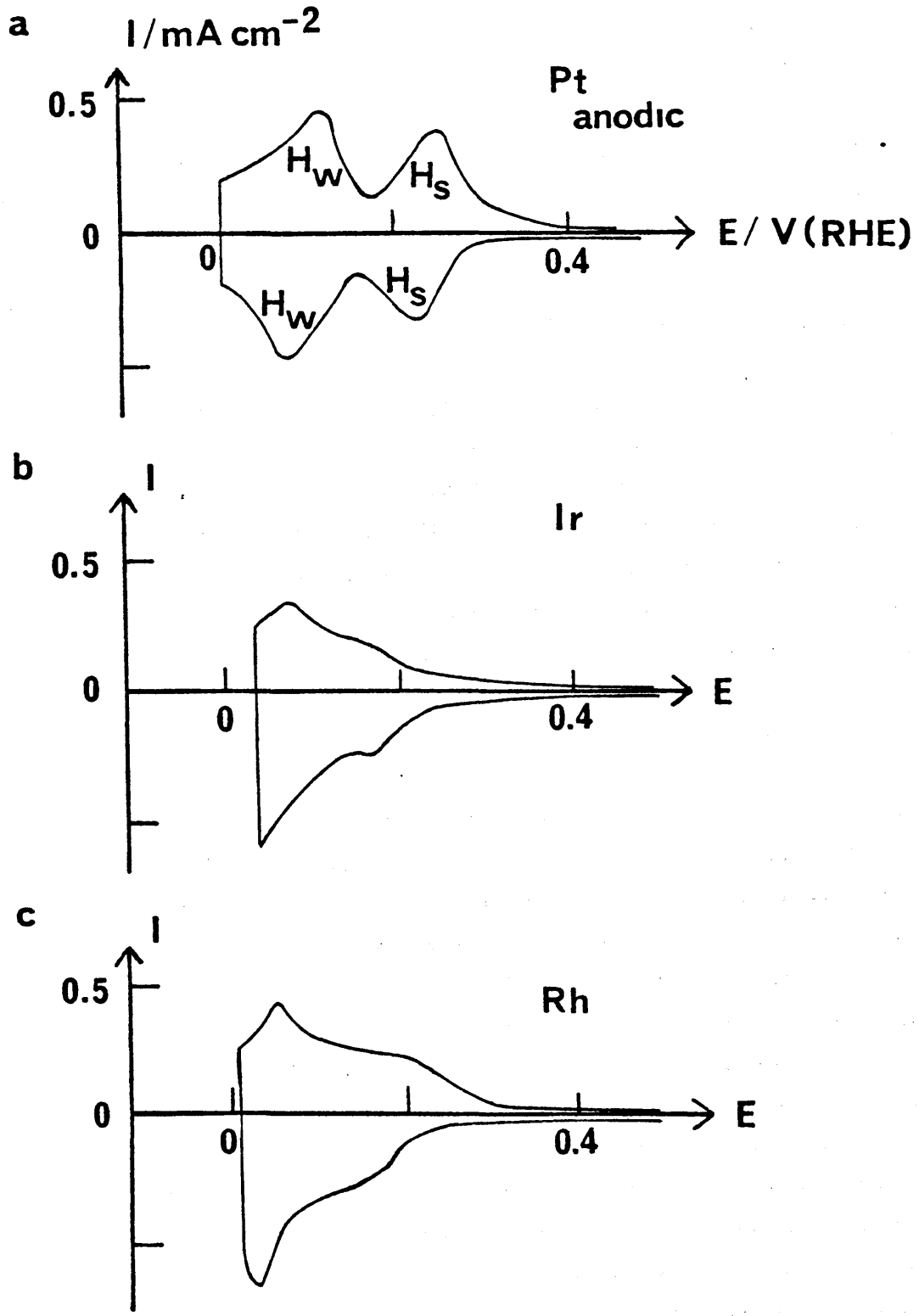

Figure 1.10: Cyclic voltammograms of (a) Pt, (b) Ir and (c) Rh run at 0.1 V s^{-1} in H_2SO_4 (1 mol dm^{-3}) to show the hydrogen adsorption and desorption regions [Ref. 143].

crystals.

The existence of different hydrogen species has also been verified by pulse modulated reflectance spectroscopy using both UV/visible [167] and IR [168] irradiation and surface conductance measurements [169,170]. Two strongly adsorbed states of hydrogen were identified on platinum between 0.4 and 0.32 V, and 0.32 and 0.2 V, respectively. The first was attributed to atomic hydrogen adsorption on grain boundaries, kinks, dislocations or the (100) plane and resulted in low coverage of the electrode surface [170]. The second was assumed to have a proton-like structure with an electron released into the metal conduction band [169]. A weak adsorption state at 0.2 - 0.05 V was considered similar to the weakly bound hydrogen which exists in gas phase studies [171] consisting of localised covalent bonds between the surface metal atoms and adsorbant. The IR spectrum for the weakly bound entity is too complex to be interpreted in terms of a simple platinum-hydrogen species (moreover, the spectrum is quite different from that for hydrogen adsorbed from the gas phase). The weakly bound structure appears to be three hydrogen atoms bridged by two water molecules, although more extensive structures are also possible. By combining these in-situ results with theoretical orbital calculations it should be possible to clarify the exact nature of the adsorbing species.

1.6.6. The Oxygen Electrode

Oxygen electrochemistry is of major importance in the areas of energy conversion and storage. Oxygen consuming cathodes are used in fuel cell systems and in metal-air batteries, whereas oxygen electrogeneration is involved in water electrolysis [172] and other industrial electrolytic processes, as well as in the recharging of metal-air batteries. The oxygen electrode has consequently been the subject of considerable investigation for many years but a clear understanding of its behaviour has not yet been attained due to the complexity of the processes involved. The complexity of the system is demonstrated in various ways, e.g. the reversible potential is rarely, if ever, observed in aqueous solution and the evolution current at constant anodic overpotential decreases almost

continuously with time. These deviations from ideal behaviour are generally attributed to the formation of an anodic oxide film which not only alters the activity of the surface but may be directly involved in the oxygen evolution reaction (O.E.R.). It follows, therefore, that any study of the latter requires a detailed understanding of the oxidation of the substrate.

A substantial portion of the energy loss in aqueous electrolyser systems is associated with the anode reaction [173], i.e. the oxygen overpotential. It has recently been determined [174-176] that among the best electrocatalysts for this reaction are those based on thermal oxides of the rarer platinum metals. Most of the fundamental work has been carried out with platinum; however, it is worth noting that several of the other noble metals, for example, iridium, rhodium and ruthenium, are more active for oxygen evolution. Their behaviour is generally more complex due to their greater affinity for oxygen and the wider range of accessible oxidation states.

The O.E.R., with accompanying standard potential values, is generally represented as

$$O_2 + 4H^+ + 4e = 2H_2O \qquad E_o = 1.229\ V \qquad (1:6:10)$$

for acid solutions, and

$$O_2 + 2H_2O + 4e = 4OH^- \qquad E_o = 0.401\ V \qquad (1:6:11)$$

for alkaline solutions. The reduction potential values here are quoted with respect to the Standard Hydrogen Electrode (SHE). Application of the Nernst equation to equations (1:6:10) and (1:6:11) leads to the following expressions for the variation of the reversible oxygen electrode potential with pressure of oxygen gas, hydrogen ion activity, and water activity, respectively, viz.

$$E = E_o + \frac{RT}{4F} \ln P_{O_2} + \frac{RT}{F} \ln a_{H^+} - \frac{RT}{2F} \ln a_{H_2O} \qquad (1:6:12)$$

and

$$E' = E'_o + \frac{RT}{4F} \ln P_{O_2} + \frac{RT}{F} \ln a_{OH^-} + \frac{RT}{2F} \ln a_{H_2O} \qquad (1:6:13)$$

where P_{O_2} represents the partial pressure in atmospheres of oxygen gas and the other symbols have their usual significance. It is therefore evident from equations (1:6:12) and (1:6:13) that the reversible potential for the oxygen electrode systems has a pH dependence of approximately 59 mV per pH unit and a 15 mV dependence per tenfold change of O_2 pressure.

The reversible oxygen electrode potential is exceedingly difficult to attain experimentally, and has only been observed by very few workers, notably Bockris and Huq [177], Hoare [178], and Watanabe and Devanathan [179]. Usually the open-circuit potentials of cells similar to the classical Grove type [180] (essentially a cell consisting of hydrogen and oxygen electrodes which use activated platinum as electrode materials) lie in the range 0.9 to 1.1 V. The difficulty in obtaining the reversible potential lies in the fact that the oxygen electrode reaction is highly irreversible even on noble metal substrates, as reflected by extremely low exchange current densities ($\approx 10^{-10}$ A cm^{-2}). Consequently, extremely low concentrations of depolarising impurities in the electrolyte are capable of interfering with the potential determining role of the oxygen reaction. Even if the electrode surface was inert, there is the problem that activation energy barriers exist along the electron reaction path. To overcome these barriers, either the potential 'hump' may be lowered by using a more active catalyst or the fraction of reactant molecules with the energy required to surmount the activation peak may be increased by raising the temperature of the system. Lewis [181] recognised early the important role the electrode surface plays as a catalyst for the electrode reaction when he pointed out that to reach the reversible oxygen potential a more powerful catalyst than platinum black was required.

Various theories have been advanced in an effort to account for the difficulty in attaining the reversible potential of Grove type cells, even in the case of stringent impurity control. According to Damjanovic et al. [182] even trace amounts of impurities (mostly organic) in the solution can affect the overall kinetics. In fact these authors realised that the path and rate of oxygen reduction are profoundly affected when the level of some impurities is in the order of 10^{-7} mole/litre.

(i) The Oxide Theory

The oxide theory was initially proposed by Lorenz and Hauser [183]. The central hypothesis of this theory is that the electrode surface is largely covered with an oxide film, and the open circuit or rest potential is accordingly determined by the oxide/oxygen couple rather than by the metal/oxygen couple. Attempts to use the oxide theory to account for the rest potential observed on any noble metal-oxygen electrode have failed. This was demonstrated by the work of Bain [184] in which he studied the rest potential on electrodes formed by plating thin films of Au, Rh, Ir and Ru on glass plates. The oxides were formed by heating the electrodes in a bunsen flame and recording the potentials in 1N H_2SO_4, 1N NaOH and 1N KCl solutions. Although the initial potentials were different, they approached a common value with time. Bain [184] reasoned that if the potential alone was determined by a metal-metal oxidereaction or by a metal oxide in equilibrium with a P_{O_2} equal to the dissociation pressure of the oxide, the rest potentials would be widely differing. However, since this was observed, the oxide theory was regarded as not being valid.

(ii) The Peroxide Theory

This theory was invoked by Brislee [185] who detected peroxide at the conclusion of open-circuit experiments and observed potential changes upon addition of H_2O_2. However, Hoare [186] has sharply criticised the intrinsic involvement of peroxide species in open-circuit potential determination; he suggested that H_2O_2 might result from the action of impurities involved in local cell phenomena.

(iii) Mixed Potential Theory

Hoar [187] was the first to propose a mixed potential mechanism for the rest potential behaviour of platinum in O_2-saturated acid solutions. He explained the deviation of the rest potential from 1.23 V by the presence of an oxide film with cracks which are at least permeable to the solution. As a result, a local cell is set up such that O_2 reduction takes place on the surface of the film, i.e. the mechanism involves an O_2/H_2O couple

and a Pt/PtO couple, where PtO refers to a layer of adsorbed oxygen atoms on the platinum surface; the activity of the surface oxygen is regarded as being potential determining in the Grove cell. Giner [188] suggested a mixed potential mechanism consisting of either the O_2/H_2O reaction (equation 1:6:10) or the O_2/H_2O_2 reaction

$$O_2 + 2H^+ + 2e = H_2O_2 \qquad E_o = 0.682\ V \qquad (1:6:14)$$

and a reaction involving bare platinum sites and those covered with adsorbed oxygen. However, he could not find any evidence for a definite oxide, and since H_2O_2 is found only in trace amounts in the reduction of oxygen, the O-O bond is evidently not broken. Therefore, the form of adsorbed oxygen important in determining the mixed potential is chemisorbed molecular oxygen, Pt-O_2, and the counter reaction is O_2/H_2O_2 (equation 1:6:14). However this is not in agreement with the evidence for dissociative adsorption of O_2 on platinum [189] and the observation that H_2O_2 is not detected under open circuit conditions at platinum electrodes in O_2-saturated solution [190].

(iv) Solvent-Dipole Inhibition Theory

At 1 atm. O_2 pressure the thermodynamic potential is ca. 1.23 V. Since the common rest potential is ca. 1.0 V there must be some hindrance. This theory proposes that at the rest potential the electric field at the interface is so high that the neutral oxygen species have difficulty in displacing water dipoles and interacting directly (or impressing its true potential) at the interface - an electrorestrictive effect may well be involved in the Helmholtz region of the double layer [186].

Hence, the complexities of the oxygen electrode reaction arise from the following reasons: (i) instability of most metals and alloys in the region of potentials where the reaction occurs in acid and in alkaline solutions; (ii) relatively slow reaction rates (with i_o of the order of 10^{-10} A cm^{-2}) compared to many other reversible electrode reactions; (iii) competing reactions such as oxide formation altering the substrate characteristics; and (iv) generation of H_2O_2 as an intermediate or in a parallel reaction in many cases.

The selection of cathodes for oxygen reduction poses a materials problem. Particularly in acid solutions, few materials are sufficiently stable to anodic dissolution at potentials close to the equilibrium potential for oxygen reduction where a good catalyst would operate. At the present time, the electrode materials which are commonly used as anodes for oxygen evolution are lead dioxide (sometimes containing another metal such as Ag) or even steel although this may lead to an overpotential of more than 0.5 V. Better materials are becoming available, for example, some semiconducting oxides (e.g. $NiCo_2O_4$) [191] work reasonably in alkaline solution which for acid RuO_2/Ir coatings on Ti [192] are probably the best available giving 100 mA cm^{-2} at about 250 mV overpotential. For oxygen reduction the most practical catalyst remains platinum; indeed, dispersed platinum on carbon electrodes with platinum loadings as low as a few mg cm^{-2}, manufactured using special techniques for creating small crystallites, allow practical current densities at an overpotential of 350-600 mV. A linear relationship between current density for oxygen reduction at a constant potential and the noble metal content seems to exist, while a crystallite size effect has also been observed in that there is a definite decrease of catalytic activity with increase of surface area [141]. Recent research studies have concentrated on various mixed oxides (e.g. spinels, bronzes and perovskites) [193,194] and transition metal macrocycles (e.g. Fe or Co phthalocyanines and porphyrins) [153,195], as well as dimeric cofacial prophyrins [196]. The macrocyclic species can be quite good catalysts but there are problems with long term stability. Moreover, it has been found that heat treatment to 950°C of the metal macrocycles adsorbed on carbon greatly enhances the catalytic activity of the surface [153,195,197] and since such strong heat treatment must destroy the metal complex, the nature of the catalyst is presently unclear. With the dimeric cofacial prophyrins it should be possible to control both the electronic environment of the two metal centres via ligand substituents and separately, the metal-metal bond distance and thus the ability of the oxygen to bond to both metal centres. However, the resulting electrodes are not yet very stable.

The geometric arrangement of catalyst centres is also important. All electrocatalytic reactions involve the formation

and cleavage of bonds, and it is likely that such processes will be substantially increased in rate if they can occur as concerted reactions, i.e. for example, in the reduction of oxygen, the bond between the surface and the oxygen atoms forms at the same time as the O=O bond is broken.

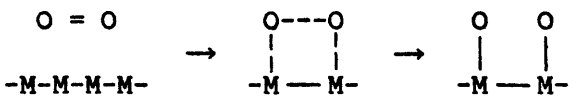

(1:6:15)

Such mechanisms require the correct spacing of the adsorption sites.

At least 14 different reaction pathways for oxygen reduction have been considered [198] and, taking into account the various possible rate-determining steps, the anodic and cathodic Tafel slopes for 53 mechanisms for the oxygen electrode system have been established. In these circumstances the mechanism can seldom be established with certainty, and reliable kinetic parameters cannot be obtained. Certainly comparison between electrode materials, where the products and mechanisms may be different, is not possible. However, a good correlation between equilibrium coverage of adsorbed oxygen at rest potential for the oxygen electrode and d-bond vacancies for the platinum group metals exist [189]. Study by Appelby [199] and others concluded that the major differences in the rate of reduction over the series of metals studied were due to changes in the pre-expotential factors rather than heat or free energy of adsorption.

1.6.7. Oxygen Chemisorption/Oxide Formation

Depending on potential, oxygen is bound on the surface of noble metal electrocatalysts as a chemisorbed species or a surface oxide [136,200]. The formation of these surface oxygen layers is independent of the presence of O_2 in the electrolyte (as the oxygen may be provided by the solvent) and irreversible [136,201-204]. Irreversibility becomes more pronounced in the order: Os < Ru < Rh < Pd ≈ Pt [136]. Reductive removal of these oxygen layers is a slow kinetic process, coming at potentials well below the characteristic potential for the layer formation on each metal. Thus, adsorption of oxygen by potential cycling techniques can

depend on the anodic potential value, the frequency of potential cycling and the number of cycles, i.e. the catalyst surface history.

In comparing the behaviour of the various metals, it may be useful to recall Pauling's treatment of the bonding in such systems [105]. Some of the outer d-orbitals are inolved as spd-hybrids in cohesive bonding, the remainder being regarded as atomic d-orbitals. The ratio and occupancy of the various orbitals is decided on the basis of such factors as atomic diameter and magnetic data. The important property, as far as surface reactions are concerned, is the number of unpaired electrons in the atomic d-orbitals. The values of the latter, given in brackets, for some metals are as follows: Au(0), Pd(0.55), Pt(0.55-0.6), Rh(1.7), Ir(1.7), Ru(2.2) and Os(2.2). Correlations have been reported between these values and both the extent of oxygen uptake from standard aqueous solution [189] and the potential required to initiate oxide growth in oxygen-free solution [206,207]. The oxygen overpotential also tends to increase with decreasing affinity of the surface for oxygen; for example, Ruetschi and Delahey [208] reported increasing oxygen overpotential with decreasing M-OH bond strength for a wide range of metals.

With regard to their involvement in electrode processes it is convenient to classify oxides into two groups:

(a) Compact, *anhydrous* oxides such as rutile, perovskite, spinel and ilmenite in which oxygen is present only as a bridging species between two metal cations and ideal crystals constitute tightly packed giant molecules.

(b) Dispersed, *hydrous* oxides where oxygen is present not just as a bridging species between metal ions, but also as O^{-}, OH and OH_2 species, i.e. in coordinated terminal group from.

(a) Anhydrous Oxides: - Compact oxides are usually prepared by thermal techniques, e.g. direct combination of the elements, decomposition of an unstable salt or dehydration of a hydrous oxide. The reversible potential of oxide systems, where both reduced and oxidised forms are insoluble, are almost invariably regarded (in terms of the RHE scale) as being pH-independent and

this assumption is undoubtably valid in many cases, a typical example being the widely used Hg/HgO reference electrode [209]. From a thermodynamic viewpoint, oxide electrodes are frequently regarded as metal/insoluble salt electrodes [209,210] in which the activity of the metal ion is modified by interaction with the OH^- or $O^=$ ligands.

Dimensionally stable anodes (D.S.A.), developed independently by Beer and Cotton during the early 1960's as a substitute for carbon in the chlor-alkali industry, are prepared by thermal decomposition of $RuCl_3$ solutions sprayed or painted onto a Ti substrate. Upon heating in air the chloride deposit is converted to a layer of RuO_2 which is an active catalyst for chlorine gas evolution. These anodes can maintain very high current densities, 0.1-1.0 A cm^{-2}, at an overpotential of only 30-70 mV. This is in contrast with the 500 mV overpotential essential with the previously used graphite anodes. In addition their stability and the consequent flexibility of cell design, including much reduced and constant inter-electrode gap, have produced very large savings both in energy and service costs. It is also interesting to note that similar performances have been claimed for other oxide materials, namely, cobalt spinels (e.g. $Zn_xCo_{3-x}O_4$ containing ZrO_2 to increase surface area) [211] and palladium oxide [212]. The chlorine evolution process has been reviewed recently [213,214].

(b) Hydrous Oxides:- In many cases the latter materials when in contact with aqueous media contain considerable quantities of loosely bound and trapped water, plus, occasionally, electrolyte species. Indeed with highly dispersed material the boundary between the solid and aqueous phases may be somewhat nebulous as the two phases virtually intermingle. These dispersed oxides are almost invariably prepared in an aqueous environment using, for instance, base precipitation or electrochemical techniques. The electrochemistry of hydrous oxides has been reviewed recently by Burke and Lyons [217].

Very often the materials obtained in oxide reactions are deposited in the kinetically most accessible, rather than the thermodynamically most stable, form; thus they are often amorphous or only polycrystalline and prone to rearrangement in a manner that

is strongly influenced by factors such as temperature, pH and ionic strength. An appreciation of the effect of such hydration is essential for the interpretation of many aspects of the behaviour of such systems [218].

The mechanism of hydrous oxide growth on repetitive cycling is now reasonably well understood, at least at a qualitative level. For most metals, but especially gold, platinum, iridium and rhodium, extension of oxide growth beyond the monolayer level under galvanostatic or potentiostatic conditions is usually quite slow, obviously due to the presence of an initial, compact, anhydrous oxide layer which acts as a barrier to further growth. Under potential cycling conditions the anodic limit plays quite a crucial role. There is probably combination of thermodynamic and kinetic factors involved but evidently the upper limit must be sufficiently anodic that compact oxide formation significantly exceeds the single monolayer level so that on subsequent reduction a disturbed, highly disordered layer of metal atoms is produced at the electrode surface. On subsequent reoxidation the disturbed layer of metal atoms is evidently converted to hydrated, or partially hydrated, oxide, complete hydration under these conditions may involve several redox cycles, with a fresh inner compact layer being regenerated at the metal surface on each anodic sweep (see Fig. 1.11). On repetitive cycling the porous outer layer increases in thickness at the expense of the underlying metal. Lack of stirring dependence in such oxide growth reactions [219,220] suggests that solution species (i.e. a dissolution/hydrolysis mechanism) are not involved.

Structural data for hydrous oxides tends to be very incomplete; the structure of oxides, hydroxides and oxyhydroxides have been discussed by Wells [221]. Hydrous oxide materials such as aluminium hydroxide and the two battery compounds, manganese oxide and nickel oxide serve as examples of the microdispersion that can occur in these systems. In the case of manganese dioxide [222] the Mn^{+4} ion is assumed to be octahedrally coordinated by six oxygen ligands, and by sharing edges and vertices the MnO_6 octahedra can combine to form almost a limitless number of phases, as illustrated in Fig. 1.12. It is clear from Fig. 1.12 that all the oxygen atoms present in the MnO_6 species in the bulk are

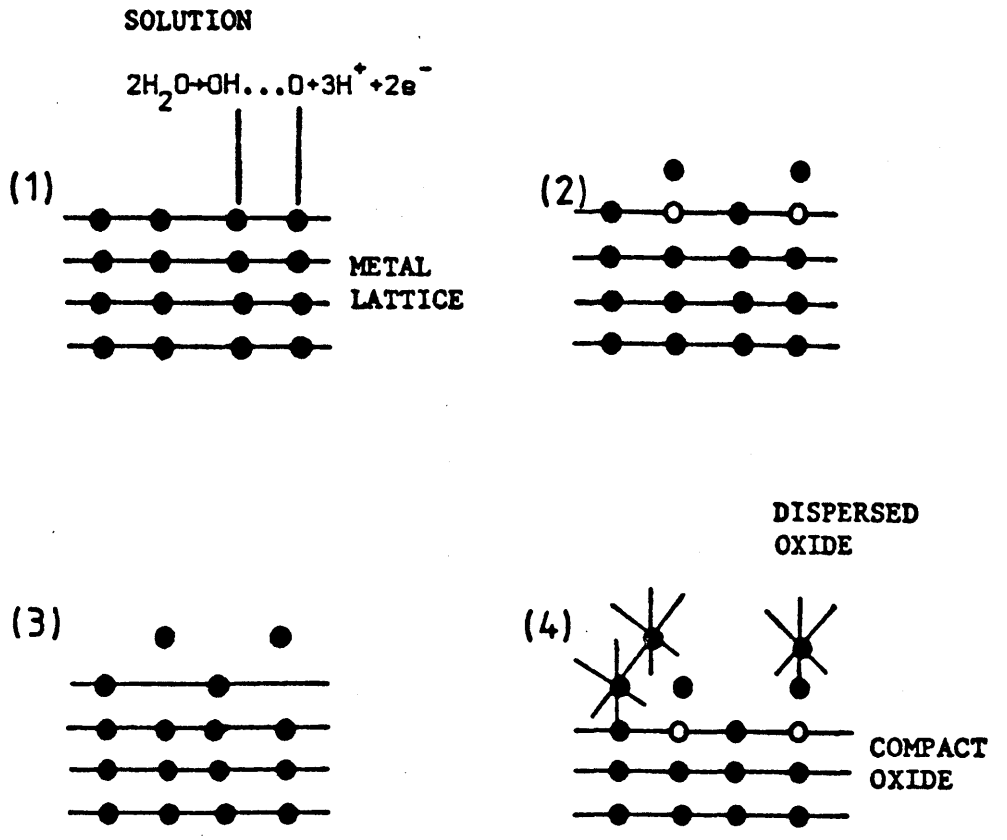

Figure 1.11: Schematic outline of the processes involved in hydrous oxide growth under potential cycling conditions,

(1) Initial Discharge
(2) Place-Exchanged Monolayer
(3) Reduction to Form Disrupted Outer Layer
(4) Initiation of Hydrous Film Growth on Second Sweep.

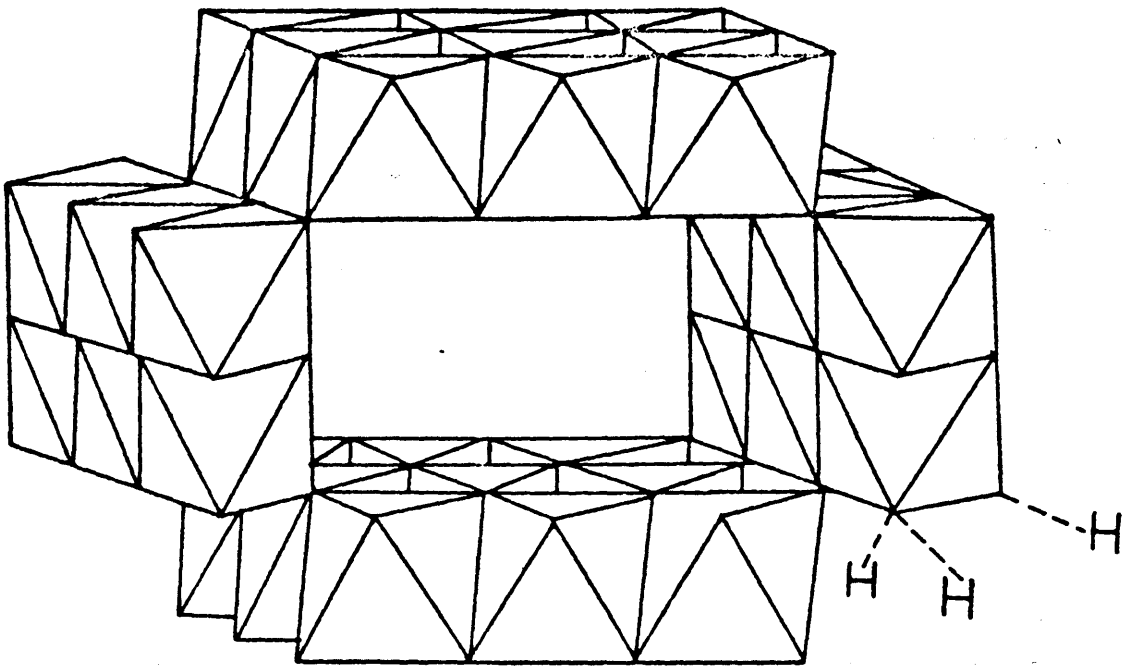

Figure 1.12: Representation of the Psilomelane structure (treble chains of MnO_6 octahedra joined to double chains of same, resulting in extended tunnel structure) of manganese dioxide. In aqueous media the terminal groups may have coordinated H_2O or OH (or their dissociated equivalents, OH^- or $O^=$) present.

bridging (Mn-O-Mn) species. However, at the surface of the lattice there are a number of terminal oxygen species - the precise number for any given octahedron varies with the bonding of the latter in the surface layer but it appears to range from 1 to 4. Such terminal groups may exist as OH_2, OH or O^-, e.g. $(-O-)_2Mn(OH)_4^{2-}$ or $(-O-)Mn(OH)_4^{2-}$ $2H^+$. Iridium dioxide can exist in two forms, anhydrous (density = 11.68 g cm^{-3}) and hydrated (density = 2.0 g cm^{-3}); the latter material, which has interesting electrochromic properties [217], can also be deposited with a variety of intermediate density values [223].

An important feature of hydrous oxides, not normally as evident with their anhydrous analogues, is their acid-base behaviour, and in particular the influence of the latter on the redox properties of the hydrous material. The relationship between typical acid and base sites at an oxide surface may be illustrated as follows:

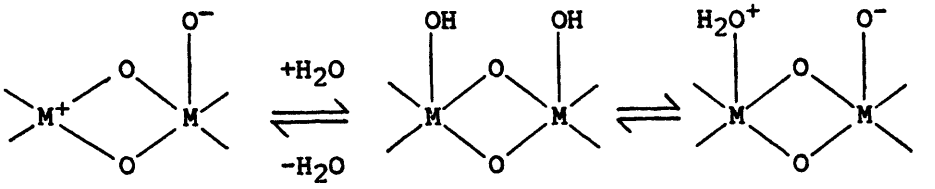

(1:6:16)

Lewis Acid	Lewis Base	Bronsted Acid	Bronsted Base

Hence, when an oxide is in contact with aqeuous media the distinction between oxide, hydrated oxide and hydroxide tends to be rather vague. There is an additional complication also that many oxides are amphoteric.

Another feature of the redox active hydrous oxide systems is the unusual variation of redox potential for metal ion valence transitions in the film with solution pH. The reversible potential of oxide systems, where both reduced and oxidised forms are insoluble, are almost invariably regarded (in terms of the RHE scale) as being pH-independent and this assumption is undoubtably valid in many cases, a typical example being the widely used Hg/HgO reference electrode [208]. However, deviations were noted in potential sweep experiments with oxide films on gold [223,224] and

iridium [219,225]. In the case of gold [223] two reduction peaks were noted with oxide films formed at high potentials (E > 2.1 V RHE) under potentiostatic conditions (t > 0.5 min). The first peak was attributed to the reduction of a layer of compact oxide (possibly with a minor degree of hydration), viz.

$$Au_2O_3 + 6H^+ + 6e = 2Au + 3H_2O \qquad (1:6:17)$$

while the second, usually much larger peak (corresponding to reduction of the outer hydrous material), showed a potential variation of ca. 1/2(2.303 RT/F) volts/pH unit (RHE), i.e. 3/2(2.303 RT/F) volts/pH unit (SHE). According to this result the ratio of hydrogen, or hydroxide ions, to electrons involved in the electrode process is 3/2. Since the most stable oxide of gold involves Au(III), the above result was attributed to the presence of an anionic, octahedrally coordinated gold species, $[Au_2(OH)_9]^{3-}$ or $[Au_2O_3(OH)_3.3H_2O]^{3-}$, present at the surface in some type of polymeric or aggregated form. Application of the Nernst equation to the reduction reaction

$$[Au_2(OH)_9]^{3-} + 6e + 9H^+ = 2Au + 9H_2O \quad \text{(acid)} \qquad (1:6:18)$$

or

$$[Au_2(OH)_9]^{3-} + 6e = 2Au + 9OH^- \quad \text{(base)} \qquad (1:6:19)$$

must obviously yield the observed potential/pH dependence.

From a thermodynamic viewpoint, oxide electrodes are frequently regarded as metal/insoluble salt electrodes [208,244] in which the activity of the metal ions is modified by interaction with the ligands, which in this case are the OH^- ions. Thus equation (1:6:19) may be regarded as a combination of the following,

$$[Au_2(OH)_9]^{3-} = 2Au^{+3} + OH^- \qquad (1:6:20)$$

and

$$2Au^{+3} + 6e = 2Au \qquad (1:6:21)$$

The dissociation constant for the complex anion, whose activity may be represented as a_c, is given by the expression

$$K_d = \frac{a^2_{Au^{+3}} \cdot a^9_{OH^-}}{a_c} \qquad (1:6:22)$$

Applying the Nernst equation to equation (1:6:21) gives

$$E = E^o - \frac{RT}{6F} \ln\left[\frac{a^2_{Au^o}}{a^{+3}_{Au^{+3}}}\right] \qquad (1:6:23)$$

Now $a_{Au^o} = 1$ and on substituting for $a^2_{Au^{+3}}$ from equation (1:6:22), it can readily be shown that

$$E = E^o - \frac{2.303\ RT}{6F} \log \frac{P^9}{K_d . a_c} - \frac{3}{2} . \frac{2.303\ RT}{F} .pH \qquad (1:6:24)$$

P being the ionic product of water. Apart from demonstrating that potential/pH values greater than zero (RHE) are of thermodynamic significance, this approach provides a simple interpretation of the unusual decrease in redox potential with increasing pH for hydrous oxide systems in general. In the case of the uncharged oxide (Au_2O_3) which may also be treated as a hydroxide, $Au_2(OH)_6$ or $Au(OH)_3$, the pH effect is less marked as the equivalent of equation (1:6:20) is as follows,

$$Au(OH)_3 = Au^{3+} + 3OH^- \qquad (1:6:25)$$

and

$$K_d = \frac{a_{Au^{+3}} \cdot a^3_{OH^-}}{a_c} \qquad (1:6:26)$$

Obviously the potential/pH dependence here will be zero (on the RHE scale) as the numbers of electrons and OH^- ions in the overall redox reaction are equal. This type of treatment can be extended to other systems notably iridium [225] and rhodium [218] where very reversible processes occur.

1.6.8. Electro-Organic Oxidation

Since hydrogen must be produced, there was a great attempt in the 'sixties to develop direct hydrocarbon-air or alcohol-air fuel cells. The published literature [226-233] in the electro-organic and fuel cell fields is voluminous, but because even the simplest hydrocarbon (CH_4) oxidation reaction occurs by an eight electron transfer reaction, while the simplest alcohol (CH_3OH) gives up six electrons to the electrode during its oxidation to CO_2, one can envisage such oxidation reactions taking place in a large number of steps involving several intermediates and yielding some by-products. Molecules studied have included methanol [137], ethanol [234], ethylene glycol [235,236], glycerol [237], propanol [238], butanol [239], and also related compounds such as formic acid [240], formaldehyde [241], carbon monoxide [242] and C_2-oxygenated compounds [243].

Methanol is the most electroactive organic fuel but its activity is considerably less than that of hydrogen. Methanol being a liquid fuel and quite soluble in aqueous electrolytes, does not cause concentration overpotential problems as with hydrogen, oxygen and the hydrocarbons. The problems connected with methanol oxidation are complex as the main reaction path in acidic media is still a subject of controversy [238]. One of the most widely accepted theories has been put forward by Breiter [136]. He proposed a "parallel paths" reaction scheme, one path going by way of formaldehyde and formic acid to carbon dioxide, and the other by adsorption and dehydrogenation of the methanol molecule on a platinum catalyst followed by further oxidation of the tenaciously held dehydrogenated organic fragment to carbon dioxide, viz.

$$CH_3OH \begin{cases} \rightarrow CHO/CO \rightarrow CO_2 \\ \rightarrow CH_2O \rightarrow HCOOH \rightarrow CO_2 \end{cases} \qquad (1:6:27)$$

Traces of formaldehyde and formic acid have indeed been identified in solution [137,138], but it is the simultaneous build up of the dehydrogenated residue (called the poisoning intermediate) that is thought to be responsible for the rapid diminution of the current with time.

Three major problems arise with anodic oxidation of methanol and other small organic molecules to carbon dioxide:

(i) the direct removal of an electron from organic fuels in solution occurs only at very positive potentials. Hence an oxidation close to the reversible potential is dependent on predissociation of the molecule to give more readily oxidised fragments. In the case of methanol the first step is [143]

$$CH_3OH \longrightarrow H_{ads} + (CH_2OH)_{ads} \qquad (1:6:28)$$

although this will be followed by other, probably faster, reactions to give CHOH, CHO and CO adsorbed on the surface. At all anode materials studied, such reactions are slow and limit severely the current density. The exception is formic acid where the cleavage of the C-H bond in the reaction

$$HCOOH \longrightarrow H_{ads} + (COOH)_{ads} \qquad (1:6:29)$$

is quite fast at several precious metals [244], and is followed by two rapid electron transfer reactions [245]

$$H_{ads} - e \longrightarrow H^+ \qquad (1:6:30)$$

$$(COOH)_{ads} - e \longrightarrow CO_2 + H^+ \qquad (1:6:31)$$

(ii) Some of the species formed in the surface reactions are very strongly adsorbed, and hence only oxidised at very high potentials. Such species act as poisons by reducing the number of catalytic sites available for the desired reaction and therefore the current density. There is little doubt now that the poisoning intermediate has been identified unambiguously as CO [152] and not COH as believed previously [245]. The disagreement seems to have arisen from differences in experimental conditions as suggested by Beden and coworkers [246]. Notable differences exist in the electrodes, time-scale, and potentials of the DEMS and IR type experiments. It has been suggested [248] that CO is the poison and CHO or COH the intermediate. Proposed mechanisms of poison formation for methanol, formaldehyde and formic acid [247] are outlined below, viz.

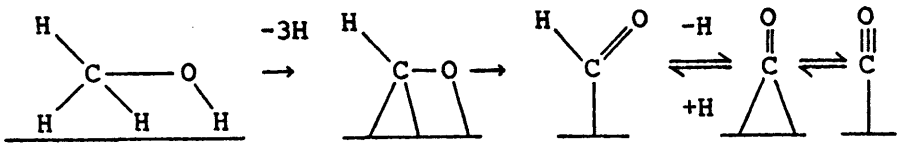

(1:6:32)

(a) methanol

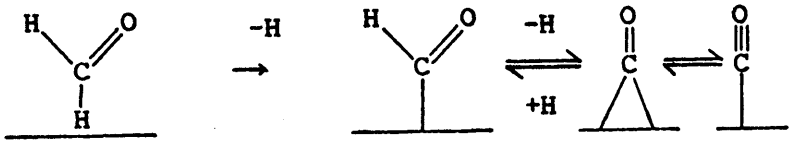

(1:6:33)

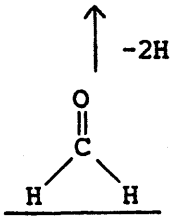

(b) formaldehyde

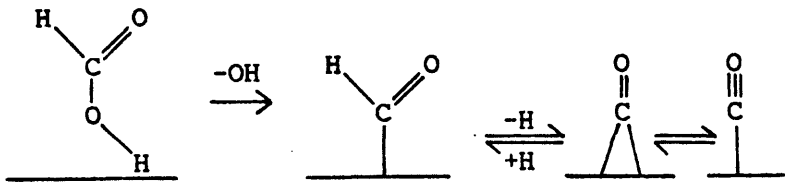

(1:6:34)

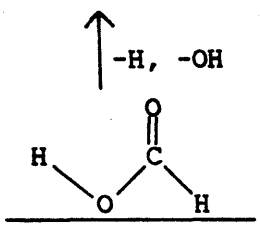

(c) formic acid

The fact that CO_{ads} does not oxidise until ca. 0.5 V means that at potentials below this(where one wishes the anode to operate) the CO effectively poisons the electrode. Thus it is necessary either to present the formation of the CO, catalyse its oxidation at lower potentials or perhaps add some species to the solution to scavenge and oxidise the surface CO.

(iii) Whether the organic oxidation occurs via the poisoning intermediate or via other organic intermediates it is clear that the next stage involves reaction with adsorbed H_2O or OH to form CO_2, as shown for methanol by

$$CH_3OH + H_2O = CO_2 + 6H^+ + 6e \qquad (1:6:35)$$

This oxygen cannot be supplied directly by a water molecule (the latter is thermodynamically stable below 1.23 V at 25°C). High potentials are required for the adsorption of oxygen-containing species and thus this reaction only proceeds at potentials substantially anodic to the methanol reversible potential. There is again some argument as to the nature of this oxygen-containing species since catalyst activity is observed at potentials lower than that at which the electrosorption of water to produce adsorbed OH species is expected, i.e. in acid media the onset of formation of these species commences on platinum [442] only above ca. 0.8 V. Wieckowski has suggested that the oxidation proceeds via an adsorbed (possibly strained and therefore reactive) water molecule [249]. However the generally accepted scheme involves reaction with OH species adsorbed on platinum as follows

$$Pt + H_2O = Pt\text{-}OH + H^+ + e \qquad (1:6:36)$$

This mechanism assumes that the catalyst must be dual functional, that is to say it must electrosorb the organic species and water in the same potential region.

The chemical nature of the electrode plays a major role in electro-organic oxidation reactions; this is illustrated by the oxidation of n-butanol on different noble metal electrodes, e.g. Pt, Rh, Pd and Au in alkaline medium [240]. Here Au gives the highest electrocatalytic activity. Palladium is much less active for alcohol oxidation whereas rhodium is usually inactive. With acid solutions, however, platinum appears to be the only effective noble metal catalyst. The electronic and geometric structures of the electrode are other important factors as reflected by studies carried out using single crystal substrates (see section 1.7).

The molecular structure of the organic compound being electrooxidised is also of significant interest. Three types of compounds are usually considered:

(a) Compounds having the same functional group, e.g. primary alcohols, but with increasing number of aliphatic carbon atoms. The electrochemical activity on a platinum electrode in acid medium decreases from methanol to butanol, but the general shape of the

voltammograms remains similar, even for a primary diol, such as ethylene glycol. However, a second oxidation wave usually occurs around 1.2 V, except for methanol.

(b) Compounds having the same number of carbon atoms but different functional groups. These compounds display very different reactivities [250]. In the series of aliphatic compounds with two carbons different functional groups (alcohol, aldehyde and carboxylic acid groups), the reactivity can be extremely high or low. The most reactive compounds in alkaline medium are ethylene glycol (15 mA cm^{-2}) and glycoxylic acid (10 mA cm^{-2}), whereas glyoxal and, above all, oxalic acid are completly unreactive at room temperature. In acid medium the reactivity pattern is quite different, with the highest current densities obtained with oxalic acid but at a more positive potential range.

(c) The same chemical compound but having different isomers. These compounds also display different reactivities. In the oxidation of the butanol isomers on Pt in alkaline medium [240] the two primary alcohols have a similar pattern with n-butanol having the highest activity. The secondary isomer, although less reactive, oxidises well with a peak at lower overpotential. However, the tertiary butanol is quite unreactive at room temperature, independent of the electrode material.

The supporting electrolyte can also modify the reaction rate, or even the reaction path, by specific adsorption of its constituent ions. The degree of coverage seems to decrease in the order $NO_3^- > SO_4^{2-} > ClO_4^-$ [234]. Currents obtained with H_2SO_4 are lower than those in $HClO_4$ and this has been attributed to adsorption by sulphate anions in competition with the fuel [251.252]. In alkaline solutions other metals, e.g. Rh, Pd, and Au, are as active as Pt [240,253-257] and there is an absence of electrode poisoning from reaction intermediates [254-257]. However, the seemingly intractable problem of carbonate build-up in cells with alkaline electrolyte [138] occurs due to the reaction

$$CO_2 + OH^- = HCO_3^- \qquad (1:6:37)$$

The main advance in the development of catalysts in recent years has been the modification of platinum by second components. Many bimetallic and trimetallic catalysts have been made but platinum group catalysts are the only systems to date to show any activity at low potentials [138]. The presence of an alloying metal either: (i) modifies the electronic nature of the surface [258]; (ii) modifies the physical structure; (iii) blocks the poison formation reactions [259,260]; or (iv) adsorbs oxygen/ hydroxyl ions which can then take part in the main oxidation reaction [259,261]. As an example [262,263], the oxidation rate of ethylene glycol in alkaline medium is greatly increased (by a factor of eight) on alloying platinum with gold (48.4 atm %) as compared with either of the individual metals. This is particularly evident at the first oxidation peak (≈ 0.76 V, corresponding to the potential range of oxidation on pure platinum). This illustrates the so-called "synergistic effect" obtained when the intrinsic catalytic activity of the alloys is much higher than that of the pure metals. Platinum/ruthenium is often reported to be the most active combination with increases of up to 40 times activity recorded [138,248].

The other technique for modification of electrodes by second components is by the deposition of foreign metal adatoms, incorporated as adsorption-stabilised submonolayers. There are five mechanisms proposed to explain their behaviour:

(a) Tsang et al. [262] claimed Bi adatoms increased the frequency factor for formic acid oxidation in acidic solutions.

(b) Many authors [263,264] believe that adsorbed hydrogen is involved in poison formation and that by blocking hydrogen adsorption adatoms enhance the activity of the electrode.

(c) Shibata and Motoo [265] suggest that the adatoms either alter the electronic properties of the substrate or act as redox intermediates.

(d) Adatoms could block the poison formation by occupying a certain number of sites of a certain type [266]. The adatoms achieve this by breaking the surface up into small local regions

[267].

(e) The electrode acts as a bifunctional catalyst [266]. The oxidation reaction of either the fuel or the poisoning intermediate is enhanced by the adsorption of oxygen or hydroxyl radicals on adatoms adjacent to the reacting species. This oxygen containing species can then be donated conveniently at the appropriate step in the reaction.

An example of underpotential deposition (u.p.d.) is fairly well illustrated by the oxidation of ethylene glycol in alkaline medium on platinum modified by the u.p.d. of seven metal adatoms: Bi, Cd, Cu, Pb, Re, Ru and Tl [264(a)]. The different adatoms used may be classified into three groups, according to their effect on the electrocatalytic activity of platinum. The first one (Pb, Bi, Tl) has a pronounced enhancement effect on the rate of oxidation, increasing the current densities by a factor of 6 to 15. The second one (Cd) does not increase the current density but shifts the oxidation curve towards more negative potentials (by ≈200 mV) which is of course a positive catalytic effect as it reduces the overvoltage. The third group leaves the catalytic activity of the electrode surface virtually unaltered. However, in acid medium the effect of the same series of adatoms is quite different, particularly for Bi and Tl, which strongly poison the electrode surface [264(b)]. The amount of u.p.d. metal is also important as shown by Pletcher et al. [268] in their study of Pb adatoms on platinum for formic acid oxidation in acid solutions.

Another type of electrocatalysis observed in the oxidation of organic molecules (mainly aliphatic alcohols and ethers) is that termed redox catalysis. In this case a layer, usually at least a monolayer, of a redox system can serve as an electron transfer mediator as well as a new surface for adsorptive interference with the reactants, viz.

$$R \rightleftharpoons O + ze \qquad (1:6:38)$$

$$S_{ads} + O \xrightarrow{k} Z + R \rightarrow P \qquad (1:6:39)$$

Obviously, the redox system itself in this scheme exhibits typical

catalyst behaviour. Ideally the surface layer plays only a mediating role and is not consumed in the overall process.

The chemical nature of the surface layer of the electrode may be monolayers of organic or inorganic compounds, covalently or adsorptively bound to the electrode surface [269]. More stable polymer layers have been formed with polyvinyl ferrocene [270,271], poly (p-nitrobenzene) [272] and ion-exchange resins loaded with redox systems [273]. Chelate complexes with iron or cobalt [274] or nickel [275] have been applied in heterogeneous redox catalysis. In-situ generated oxide layers on carbon [276], lead [277] or nickel and silver [278,279] have also been studied. Recently Beck and Schultz [280] reported an extension to oxide electrodes with a defined layer of oxide on top of an appropriate base material, which only serves as an electronically conducting support. In their paper they dealt with the Ti/Cr_2O_3 system although analogous systems are known, Pt/PbO_2, Ni/RuO_2 and Ti/VO_x. These electrodes can be regarded as similar to the activated titanium electrode of which RuO_2, as the activity oxide layer, is the most outstanding example [213].

1.6.9. Real Surfaces

Figure 1.13 depicts schematically the various surface sites that are identified by experiments as existing on a heterogeneous surface electrode. There are atoms in terraces, which are surrounded by the largest number of nearest neighbours. Atoms in steps have fewer nearest neighbours, and atoms at kink sites have even fewer. Kink, step and terrace atoms have large equilibrium concentrations on any real surface. Point defects such as adatoms (adsorbed atoms) and vacancies are also present and are important participants in atomic transport along the surface, although their equilibrium concentrations are much less than 1 percent of a monolayer even at melting point [282]. All these types of defects are present on an electrode surface when it is placed in contact with an aqueous electrolyte. These defects have a lower coordination number than bulk atoms and any unsaturated bonds must be stabilised by adsorption of solution species. These distinct sites can then give rise to different activities.

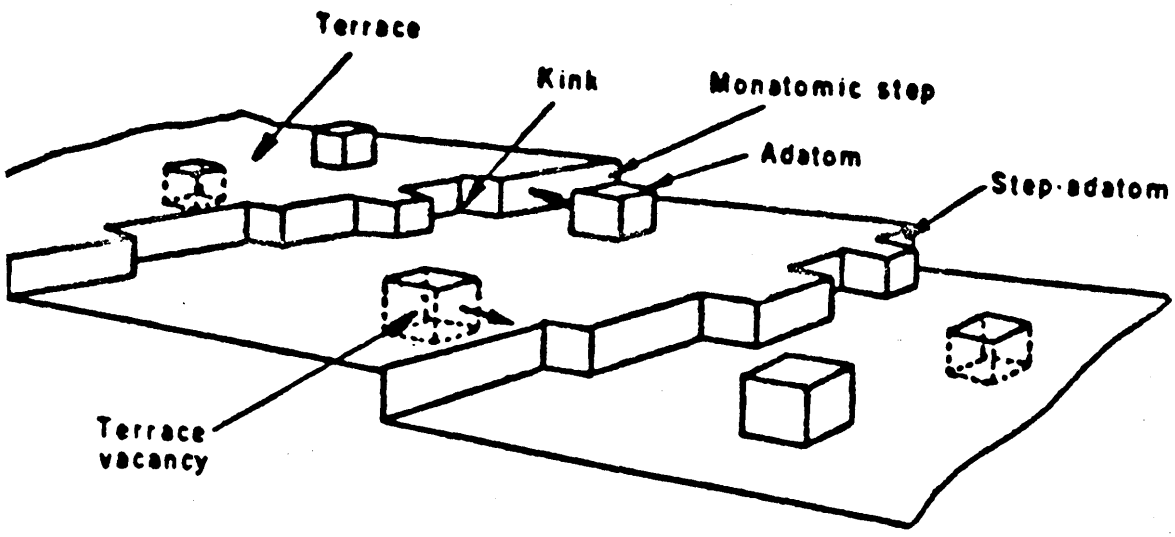

Figure 1.13: Schematic representation of the heterogeneous surface on the atomic scale. Terrace, step and kink atoms as well as point defects (adatoms and vacancies) have been identified by experiments [Ref. 282].

In electrocatalytic processes, where the rate-determining step is a surface reaction, the measured current density (in terms of the geometric area of the electrode) depends not only on the genuine catalytic activity of the surface but also on the real surface area, i.e. the roughness of the surface. This is in contrast to a mass transport controlled reaction where the current is independent of the surface roughness provided that the rugosity is small compared to the diffusion layer thickness, ca. 10^{-2} cm. Hence, clearly in catalytic electrode design the surface should be as rough as possible to give the highest apparent current density. On the other hand, in the laboratory, a knowledge of the roughness and hence, real surface area is essential to the interpretation of data at catalytic surfaces. Another recent observation is that Tafel slopes can vary with surface roughness and, for example, the success of Ni/Mo coatings on steel as catalysts for hydrogen evolution in concentrated sodium hydroxide has been attributed at least in part, to the resulting steepness of the log i-E plots [281].

1.6.10. Conclusion

From the foregoing discussion it is clear that electrocatalytic reactions are very complex. This complexity results from the great variety of reaction products and adsorbed intermediates which are formed during the course of the reactions. The best hope of elucidating these intermediates lies in the coupling of electrochemical experiments with in-situ spectroscopy. However, as pointed out earlier, the basic theory of electrocatalysis lags far behind its technological applications at the moment and it is therefore essential, for the continued progress of electrocatalysis as a science, that this be rectified. It is hoped that the present work, which combines the elements of the adsorption and surface redox models of electrocatalysis, will clarify certain areas of this complex topic, especially the reaction of organic species at noble metals anodes which is highly relevant to the operation of some types of fuel cells, electroorganic synthesis, electroanalysis, etc.

1.7. SINGLE CRYSTALS

1.7.1. Introduction

In line with similar trends in materials science, surface science and heterogeneous catalysis, electrochemists have begun to study single crystal surfaces of controlled and known structure. The main objective of such work is to elucidate the effects of site geometry on the electrocatalytic properties of the electrode surface. In particular such investigations may lead to an understanding of the origins of the multiple state adsorption of hydrogen on platinum surfaces. Surface sites, which are important for adsorption and electrocatalysis, may be charactrised in terms of the coordination number (CN) of surface atoms and the geometries of the sites in which such atoms reside. Single crystal surfaces allow a variation in both CN and site geometry and should provide information of fundamental significance.

Initial single crystal work was carried out by Will [283] who claimed voltammetric evidence for two distinct binding sites on platinum (100), (111) and (110) planes. He also proposed that when these single crystal voltammograms were combined they gave a composite voltammogram similar to that of polycrystalline platinum. However, there was considerable disagreement initially among various authors as to the true shape of the cyclic voltammograms for these surfaces [153,241]. The main cause of these discrepancies apparently revolved around the problem of surface contamination [284,285], the effect of different electrolyte anions [286] and quality of the surface, i.e. the extent of the long range order [287]. The surfaces in this early work were cleaned during the electrochemical experiment by repetitive oxidation and reduction cycles; subsequently it was proven that this procedure damaged the crystallographic structure of the surface [288]. Important progress was made in the 'seventies when apparatus allowing for a fast transfer from an ultra high vacuum (UHV) chamber to an electrochemical cell, without exposure to the ambient atmosphere, was developed in the laboratories of Hubbard [289,290], Ross [436] and Yeager [291,292]. These systems allowed the determination of structure and purity of the single crystal surfaces by low energy electron diffraction (LEED) and Auger spectroscopy just a few minutes before

or after an electrochemical experiment. In the following years, transfer systems were further developed [293]. A new technique for the production of the single crystal electrodes was developed by Clavilier [284,297] at the beginning of the 'eighties.

1.7.2. Preparation

In this new approach single crystal surfaces are prepared by melting high purity wire to form a bead. After checking the orientation the bead is mechanically cut along a plane before either polishing to a mirror finish using alumina or diamond paste, or etching in an acid bath. The surface is next annealed to ca. 1100°C to remove submicron roughness followed by slow cooling in an inert atmosphere. UHV techniques are used to characterise the surface prior to transfer in vacuum or inert gas atmosphere to the electrochemical cell [293]. To remove surface impurities sputtering (Argon plasma) or etching (aqua regia) is often used followed by annealing to obtain a clean, smooth and well oriented surface. An inexpensive technique of cleaning platinum surfaces, developed by Clavilier [284,294], consists of heating in an hydrogen-oxygen flame to 900-1100°C then quenching in ultrapure water. The electrode is subsequently transferred to the electrochemical cell with the surface protected by a drop of water attached to the crystal. Flaming destroys all organic impurities and rapid quenching protects the surface against readsorption of impurities from the ambient atmosphere. Results from this latter method are apparently extremely reproducible.

1.7.3. Single Crystal Results of Platinum

The majority of single crystal work has been carried out on platinum. Platinum crystallises in the face centred cubic system; each single crystal plane, e.g. (111), (100), and (110), has not only different symmetry and geometry, but also atom coordination number. The coordination number of the platinum atom in the bulk is 12, hence the difference between 12 and the coordination number at the surface gives the number of chemical bonds per atom cut by the dividing plane [293] which are called dangling bonds,

Fig. 1.14. At the solid surface atoms or molecules can be adsorbed at these dangling bonds. Because the number of dangling bonds per atom on each surface is different the energy of adsorption will also be different. Initially Clavilier's results [284,294] for the hydrogen adsorption-desorption process disagreed with the data obtained in the sophisticated UHV/electrochemistry systems [153]; however by improving pretreatment procedures and cleanliness of the UHV equipment similar results were obtained [285,287,295,296]. Results before 1983 seem to correspond to surfaces contaminated by adsorption of residual impurities. The results of Clavilier et al. for the (111), (110), and (100) planes are shown in Fig. 1.15 [284,297]. For a given crystallographic plane, the voltammetric profile shows several peaks which are ascribed to various hydrogen adsorption states. The total quantity of electricity measured during hydrogen desorption of the (111), (110), and (100) planes is 255, 220, and 205 $\mu C\ cm^{-2}$ respectively. This compares with the theoretical values of 243, 147, and 209 $\mu C\ cm^{-2}$ for ideal planes having a 1:1 ratio of hydrogen atoms to platinum sites on the surfaces. The high reversibility of the process should be noted for each surface. Also of note are the controversial "butterfly" peaks at ca. 0.45 V(RHE) on the (111) plane, the fine structure in the splitting of the main peaks on the (110) plane and the change from irreversibility to reversibility on the (100) plane. The most strongly bonded hydrogen state on (100) and (111) planes has been ascribed to the existence of two dimensional long range order [298] causing induced heterogeneity. The contribution of the surface arrangement in the origin of the multiple adsorption states has also been evaluated and significant relations between the proportions of the hydrogen relative to each state been found [299].

The effect of increasing the upper potential limit, Fig. 1.16, is shown to effect the character of the adsorption-desorption process of hydrogen which may be attributed to a change in the surface structure. This change is seen even after a single monolayer of oxygen is formed and shows the rapidity of the reconstruction of the surface. When oxygen atoms are adsorbed, the platinum atoms of the initial dense layer are displaced (place-exchanged) into adatom positions [290] where they are further stabilised by forming rows or small islands. The limited potentiodynamic cycling into the oxide region, which has shifted

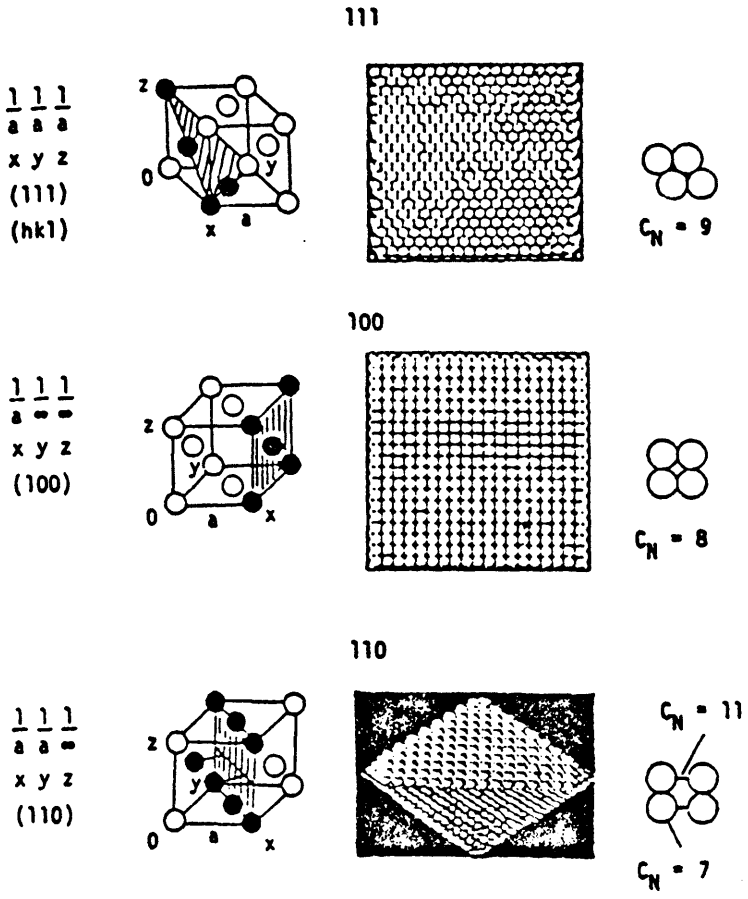

Figure 1.14: The cross-sections of the elementary cell for the face-centred cubic system with dividing plane giving the three densest atom packing. From left to right: cross-section of the elementary cell, atom packing on the surface, elementary mesh of the two dimensional lattice, C_N-coordination number of the atom at the surface [Ref. 293].

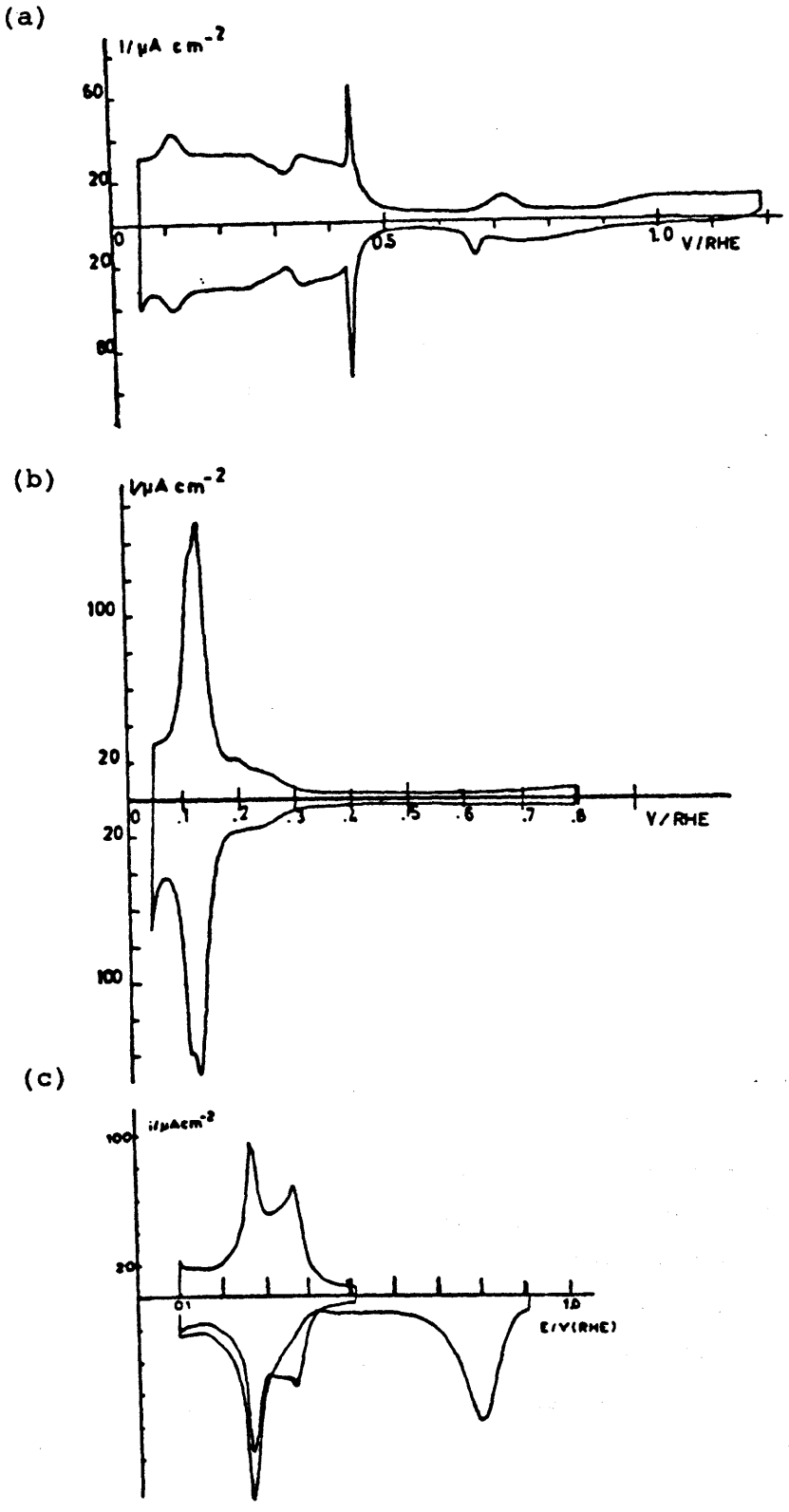

Figure 1.15: Voltammograms for the (a) (111), (b) (110), and (c) (100) directions of Pt single crystals after annealing. Sweep-rate 50 mV s^{-1}, 0.5 mol dm^{-3} H_2SO_4. (c) shows the electrochemical desorption of thermally adsorbed oxygen and change from irreversibility to reversibility of the hydrogen-desorption process [284,297].

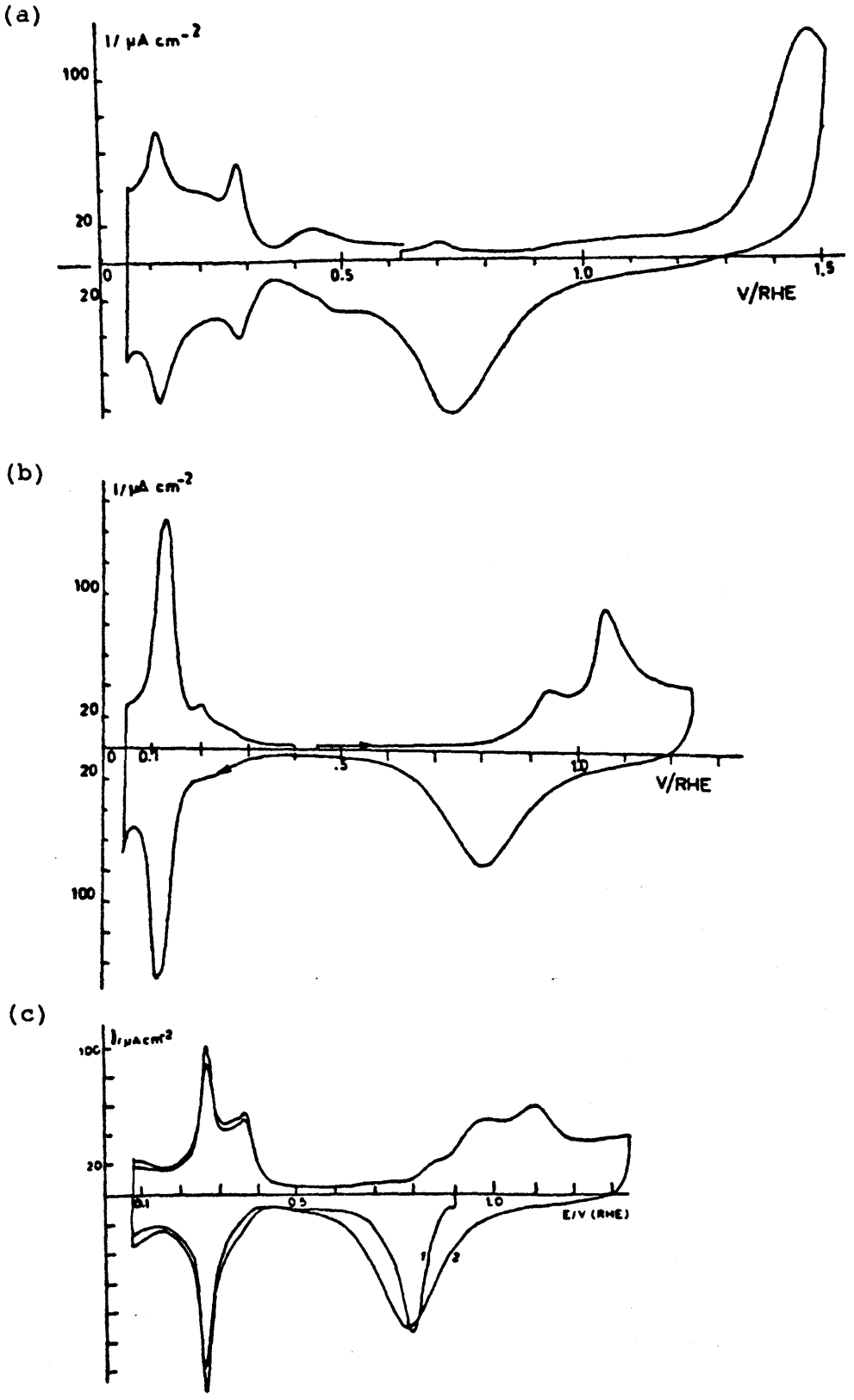

Figure 1.16: Voltammograms for the first adsorption-desorption of oxygen and the subsequent adsorption-desorption of hydrogen for the (a) (111), (b) (110), and (c) (100) directions (conditions as Fig. 1.15). (c) includes desorption of thermally adsorbed oxygen [284,297].

many atoms out of the ideal planar surface, leaves them in 3-D lattice sites, as represented by Fig. 1.17. LEED results have indicated the introduction of these random steps into (100) planes [287].

1.7.4. High Index Planes of Platinum

As studies of the low index faces of platinum did not adequately clarify the effect of site geometry on hydrogen adsorption, the approach is currently being extended to the high index faces [300-306]. By careful choice of planes it is possible to vary systematically the nature and density of the bonding sites at the surface and an estimate can be made as to how metal-adsorbate and adsorbate-adsorbate interactions contribute to the multiple state adsorption of hydrogen on platinum. An indication of how sensitive the hydrogen adsorption is to step density and step orientation is seen in Fig. 1.18 (potentials here are quoted versus SCE; 0.0 V(RHE) = ca. 0.26 V(SCE).

The platinum voltammogram [307] in Fig. 1.18 is divided into three regions: I corresponds to the hydrogen adsorption-desorption region, II corresponds to hydrogen adsorption-desorption coupled to anion adsorption-desorption and III corresponds to anion adsorption-desorption. While there seems to be no dispute over the basic observation that the crystal structure of the platinum surface plays a very important role in determining its adsorption properties, different conclusions have been proposed for the several peaks. On the basis of the results for four stepped surfaces, Ross [301] proposed that the multiple peaks were due primarily to the intrinsic heterogeneity arising from chemically different sites on the single crystal surfaces. Love et al. [293,303] concluded that, since the number, position and area under the peaks cannot be directly correlated with the number, nature and density of distinct adsorption sites on the surface, the multiple peaks may not be resolved in terms of the multiple binding sites present on the stepped surfaces. However, since the shape of the voltammetric curves clearly depends on the step density on the surface, they invoked the induced heterogeneity theory, i.e. that heterogeneity may be associated with both hydrogen adsorption

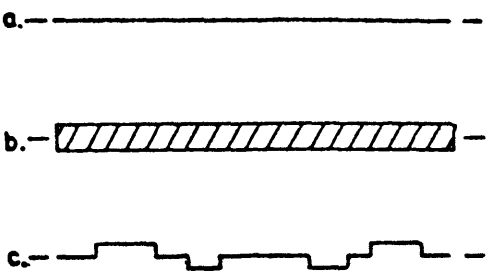

Figure 1.17: Cross-sectional scheme of Pt (100) surface: (a) before cycling, (b) oxidised at upper limit of potential sweep, (c) after electrochemical reduction of (b).

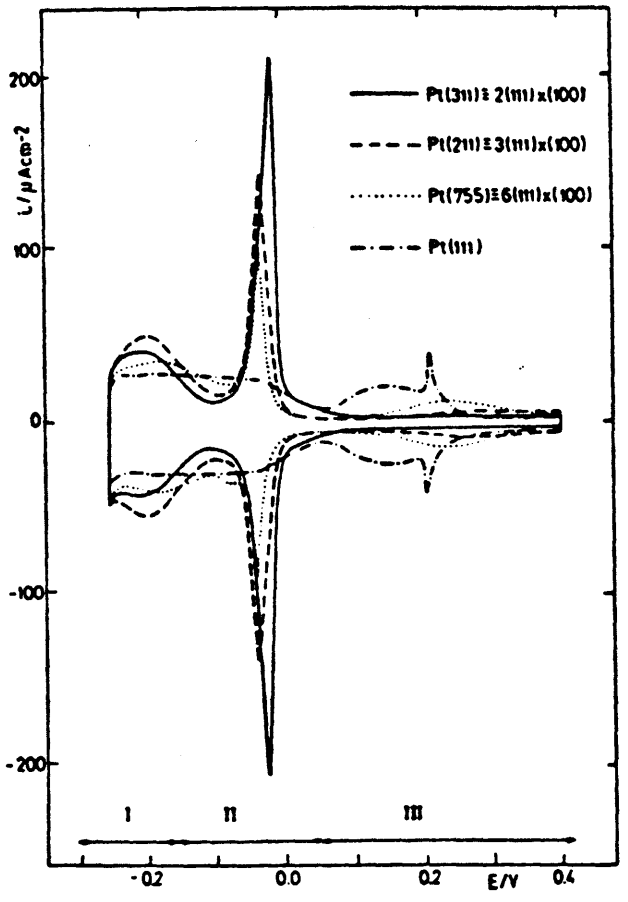

Figure 1.18: Cyclic voltammetry for Pt (111) and Pt stepped surfaces in 0.01 mol dm^{-3} H_2SO_4 versus SCE [Ref. 307].

itself and anion adsorption which influence the H adsorption process by blocking sites to varying degrees and perturbing adjacent sites. Clavilier et al. [304,308] concluded that the voltammetry is very sensitive to both terrace and step structure and hence allows a precise characterisation of the nature of the steps. They interpret the voltammograms of polyoriented surfaces by deconvolution of the low index voltammograms showing the existence of up to six separate states on the surfaces between 0.075 and 0.375 V(RHE). Adzic and coworkers [305-307] have also shown the sensitivity of hydrogen adsorption to step density and step orientation, and have pointed out the remarkable stability of some stepped surfaces with regard to oxidation. These authors also pointed out an interesting structural sensitivity of these stepped platinum surfaces to oxide formation and reduction; while the onset of oxide formation varies negligibly with the surface orientation, the shape of the curves show a pronounced dependence.

1.7.5. Organic Oxidation at Platinum Single Crystals

The oxidation of organic molecules has also been shown to be dependent on geometrical site distribution. The results shown here in Fig. 1.19 illustrate the effect of surface structure on the oxidation rate of formic acid; the latter process is obviously strongly dependent on the orientation [240]. The different peaks observed at polycrystalline platinum were assumed to correspond to the oxidation of the organic molecule at the sites having the same local symmetry as those of the low index planes and not successive electron transfers, Fig. 1.19(d). The lack of current on the anodic sweeps is associated with the blocking of the electrode surface by the poisoning intermediate common to organic oxidation reactions. The existence of current in the case of the platinum (111) electrode is due to the lack of formation of this poisoning intermediate on such surfaces. The fact that there is current on the cathodic sweeps is due to the oxidation of the poisoning intermediate at ca. 0.6 - 0.8 V(RHE). Various organic compounds have been found to form a layer of oriented adsorbed molecules on atomically smooth surfaces. Reactivity of these oriented adsorbed intermediates was sharply dependent upon orientation. These findings involved accurate packing density measurements using

(a)

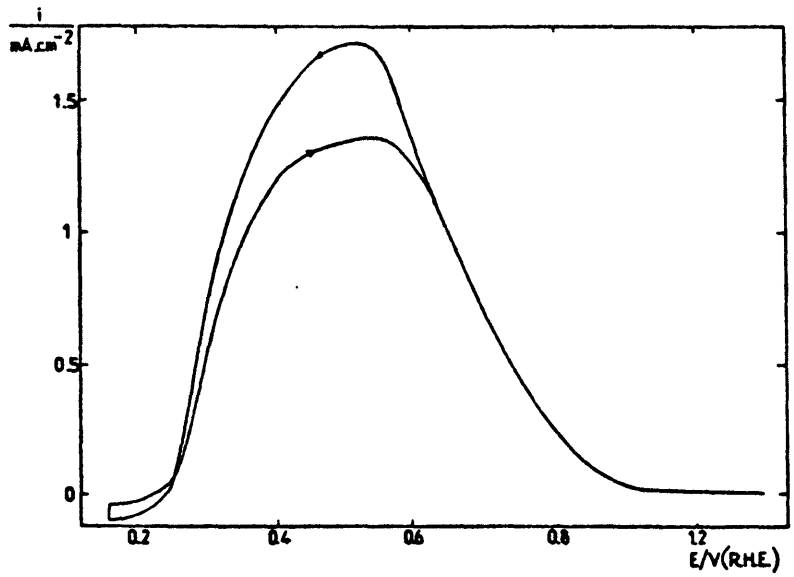

(b)

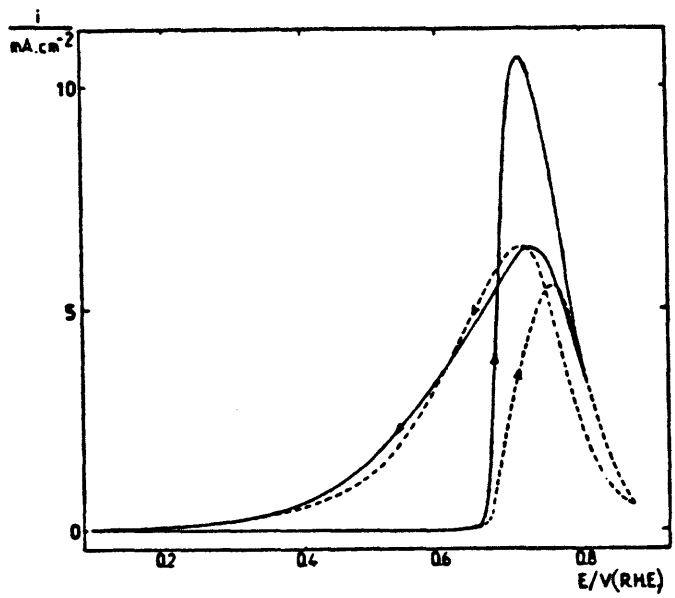

Figure 1.19: Oxidation of 0.1 mol dm^{-3} HCOOH in 0.5 mol dm^{-3} H_2SO_4 on (a) Pt (111), and (b) Pt (110) electrodes at room temperature and 50 mV s^{-1}. (——) first sweep; (-----) second sweep [Ref. 241].

(c)

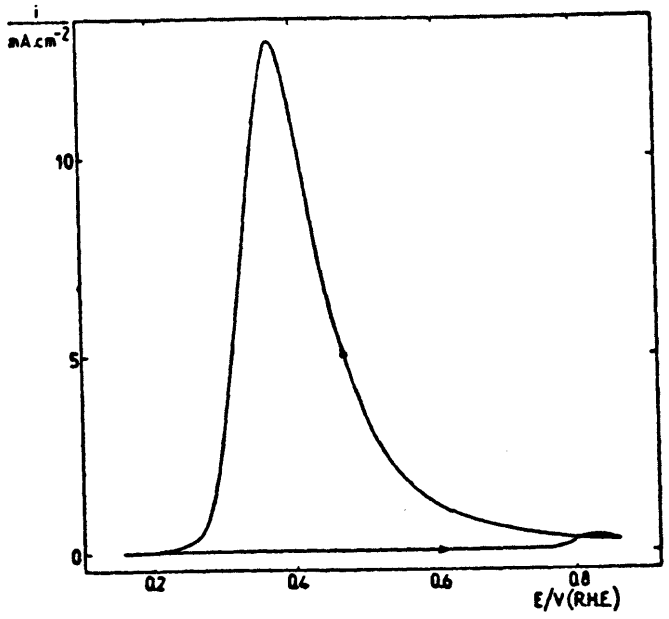

(d)

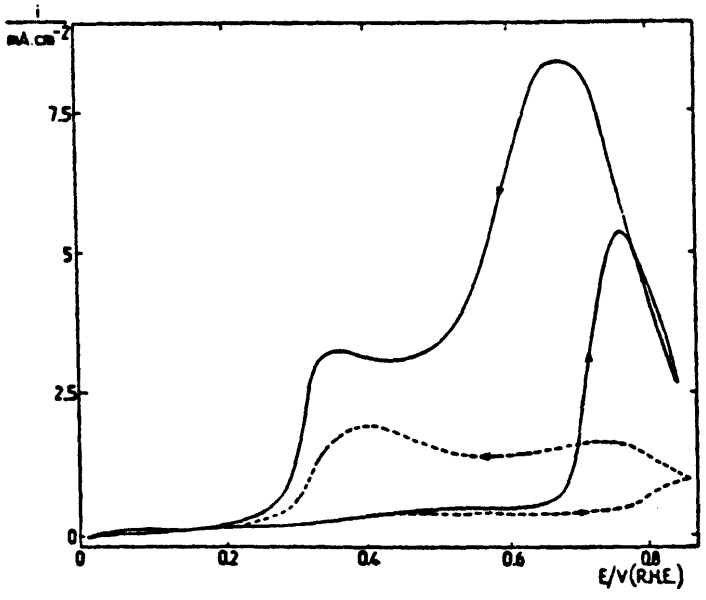

Figure 1.19: Oxidation of 0.1 mol dm^{-3} HCOOH in 0.5 mol dm^{-3} H_2SO_4 on (c) Pt (100), and (d) polycrystalline bead Pt electrodes at room temperature and 50 mV s^{-1}. (——) first sweeps; (----) second sweep [Ref. 241].

thin-layer electrodes [309]. Adsorption of CO has been shown to block between 72-99% of the surface with 87-97% recovery of unblocked surface after oxidation depending on the index surface used [310]. The number of electrons involved in this oxidation varied between 1.51-2.02 indicating that the poisoning intermediate was CO single bonded to the surface with some multibonded CO also present. Very little work on organic oxidation in alkaline electrolytes on platinum single crystals exists. However, in a study of methanol oxidation at all low index planes and at polycrystalline platinum it was shown that methanol always has the same incipient potential of oxidation and the shapes of the voltammograms are similar [311].

1.7.6. Single Crystals of Other Metals

The single crystal electrochemistry of many other elements has been studied. Iridium [312] has the same face-centred cubic lattice as platinum. However, its low index plane voltammograms show striking differences despite having the same geometrical arrangement of surface atoms. This shows that the adsorption energy of hydrogen is not solely dependent on the geometrical arrangement of the surface sites. But the fact that each plane is different supports the idea that the hydrogen adsorption energy is dependent on the geometrical site arrangement, but must also be dependent on the chemical nature of the surface site. Rhodium [313] also gives results similar to platinum.

1.7.7. Controversial Aspects of Platinum Single Crystals Results

(a) Possible "oxide" formation: Controversy still persists on the electrochemical properties of platinum single crystals due to some lack of reproducibility of results from group to group. When a single crystal electrode is cleaned by Clavilier's quenching technique [284,294] a certain amount of thermally-sorbed oxygen is produced on the surface [314,315]. This "oxide" formation has been detected on faces exposed to oxygen at high temperatures [316], and the presence of high energy hydrogen adsorption sites on the (100) and (111) platinum faces [302(b)] has been attributed to the

presence of such oxygen. It seems likely that some chemistry takes place at the platinum surface in the annealing stage, with resulting surface structures being frozen in by the quenching process [317]. This would lead to the apparently high defect concentration as shown by LEED [302(a)]. The fact that the density of the high energy hydrogen adsorption sites decreases with an increase in the density of surface steps suggest that the former are associated with lattice strain or with defects such as adatoms or vacancies [317]. The more strongly bound state on platinum (100) was attributed to the presence of self-adsorbed platinum atoms by Hubbard et al. [290], while Wagner and Ross [287] observed peaks which they proposed were due to a surface process which was complex and highly irreversible and decayed during cycling, as does the strongly bound state on platinum (100). Yeager [153] points out that the peculiar results on this (100) surface are related to some special role of oxygen in the hydrogen adsorption process due to the large changes achieved by cycling into the oxide region. Interesting splitting in the anodic peak of some high index planes is present in the first cycle after this type of treatment. This disappears on cycling but a single cycle into the oxide region reintroduces this splitting [303].

(b) The "intermediate" hydrogen peak: Another transitional state of the surface may be produced when oxygen is adsorbed or desorbed electrochemically. An irreversible well-marked desorption peak appears near 0.2 V(RHE) on the anodic sweep for the platinum (110) plane which is of the same nature as the peak observed at this potential in the same electrolyte on the conventional cyclic voltammogram of polyoriented platinum surfaces cycled over the whole potential range, Fig. 1.20, [308]. It is different from other hydrogen adsorption peaks in that it has slow adsorption-desorption kinetics and certain cathodic aging effects. The cathodic aging (below 0.15 V(RHE)) causes an increase in the size of the peak. The magnitude of this peak increases with increasing aging time or on lowering the aging potential. This could be due to surface restructuring and/or a hard-to-reduce surface oxide [153]. This is also supported by the peak becoming more pronounced by cycling in the oxygen adsorption region [308,318]. However, the aging process has also been linked with anion desorption [319]. By using time resolved staircase voltammetry [286] the slow kinetics

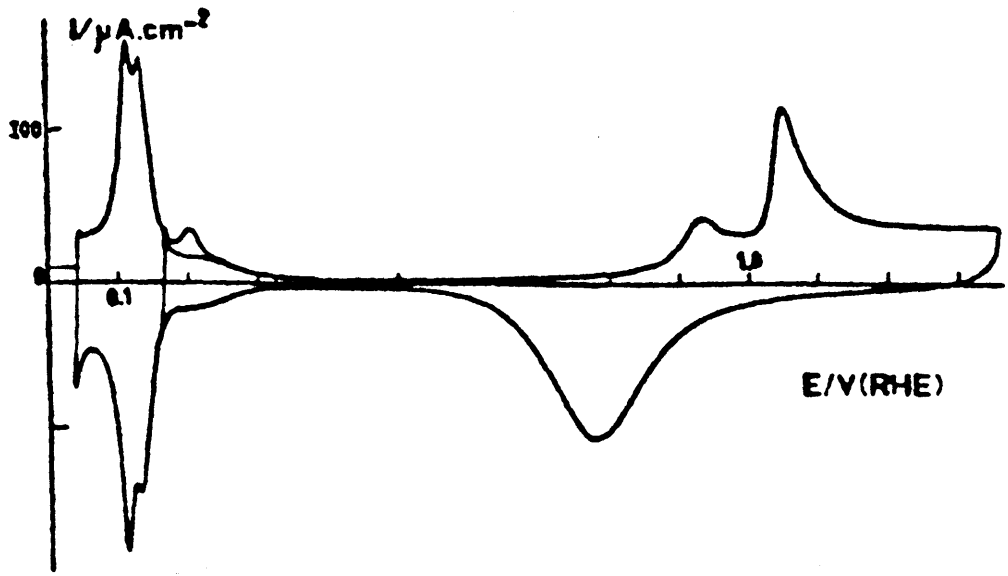

Figure 1.20: Voltammogram of Pt (110) showing the first adsorption-desorption cycle of oxygen and the two subsequent hydrogen adsorption-desorption cycles, the second one with its lower limit at nearly 0.16 V (vs. RHE). Sweep-rate 50 mV s^{-1} in 0.5 mol dm^{-3} H_2SO_4 [Ref. 308].

of this peak, Fig. 1.21, become apparent. A similar result was found for the platinum (110) face. It appears that by cycling into the oxide region certain adsorption sites are generated; those sites are lost due to surface restructuring on cycling just in the hydrogen region [308, 318]. It was suggested that the peak is made up of both a fast and slow process [286]. It should also be noted that the total charge measured in the hydrogen adsorption region increases with aging [319].

(c) Reconstruction: It has also been proposed that long range ordering of adsorbed atoms under the influence of lateral interactions cause the peaks usually assigned to individual hydrogen adsorption sites. It is well known that hydrogen adatoms may interact laterally via electronic wave function coupling to the metal valence electrons [320,321]. This indirect interaction is long range in character and its energy depends on the inter-adatom separation. As a rule, the structure of the overlayer changes with the coverage. The change from one to another arrangement of atoms usually has the characteristic of a phase transition. Phase transitions are visible as inflection points on adsorption isotherms which result in the appearance of peaks on the cyclic voltammetry curves. The multiple state adsorption of hydrogen may result from the presence of phase transitions in the ordered overlayers of hydrogen [293]. The surfaces themselves are also known to undergo reconstructions [298,323]. These reconstructions may be caused by a change in potential and modified by adsorption [322].

(d) Anion Effects: It is evident that the anions play an important role in the existence of the hydrogen adsorption states which are modified when the concentration or nature of the anion is changed [153,298]. Specific adsorption of anions influences the peak potentials for hydrogen adsorption to various degrees depending on the potential difference from the pzc of platinum [436]. In fact, contact anion adsorption is crystal-face dependent just as hydrogen chemisorption [286]. Just how sensitive the voltammogram shape is to the presence of different anions can be seen in Fig. 1.22(a). Fig. 1.22(b) shows the variation in hydrogen adsorption in 0.1 mol dm^{-3} HF with addition of H_2SO_4. This shows that very small concentrations of anions can cause appreciable changes in the

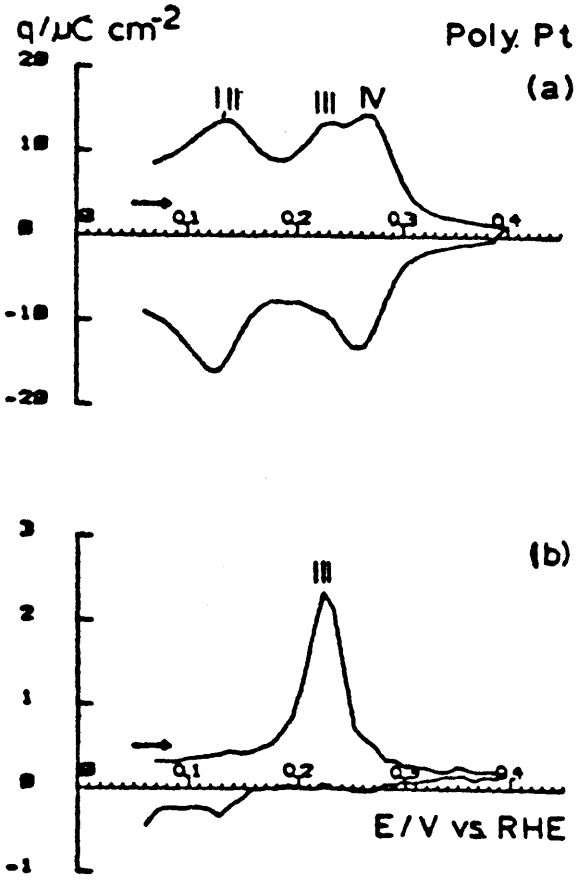

Figure 1.21: Time resolved staircase voltammograms for polycrystalline platinum in 0.5 mol dm^{-3} H_2SO_4; effective sweep-rate 1.061 V s^{-1}; potential step excitation 9.62 mV; interval between current measurements 60 μs; width of current sampling window 9 ms; integration period: (a) 0-9 ms, (b) 3-9 ms. The electrode potential was held at 0.06 V for 30 s prior to acquiring the data [Ref. 286].

(a) (b)

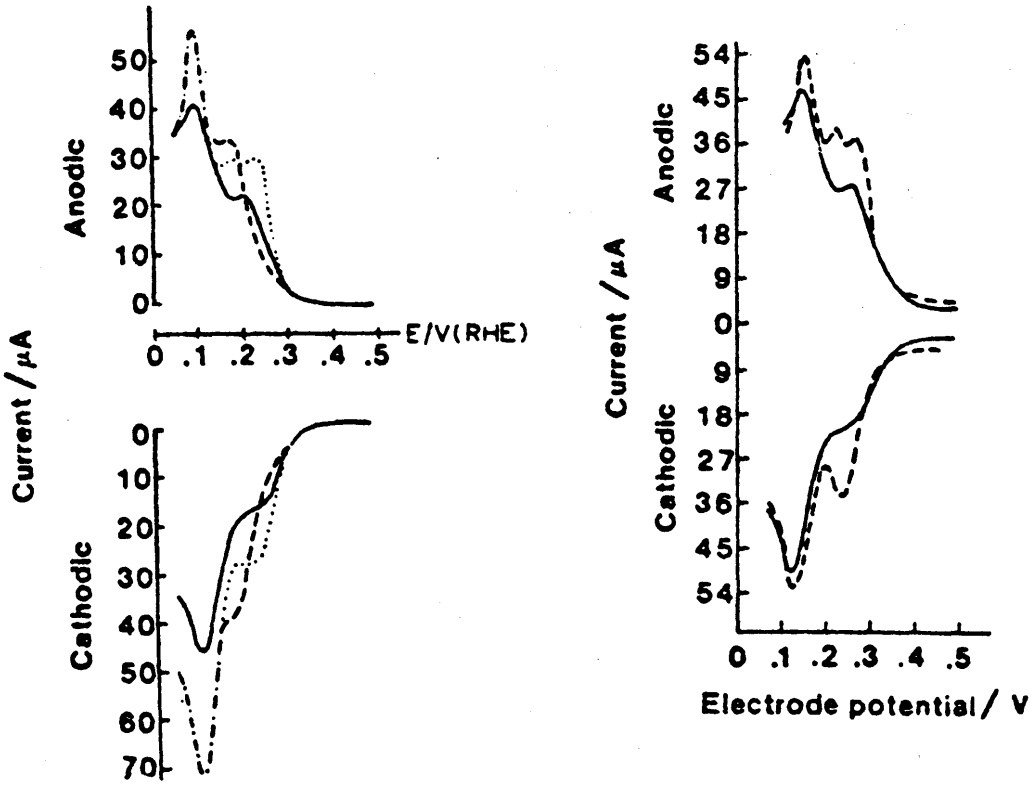

Figure 1.22: (a) Comparison of hydrogen adsorption-desorption current versus potential (corrected for Ohmic resistance) for Pt (111) after 250 cycles, 0.05-1.55 V at 1.4 V s^{-1}, in different electrolytes: (——) 1 mol dm^{-3} HF, (----) 1 mol dm^{-3} $HClO_4$, (·····) 1 mol dm^{-3} H_2SO_4.

(b) Effect of the addition of 10^{-2} M H_2SO_4 to 1 mol dm^{-3} HF on the voltammogram for Pt (111), 0.14 V s^{-1}. (——) 1 mol dm^{-3} HF, (----) 1 mol dm^{-3} HF + 10^{-2} mol dm^{-3} H_2SO_4 [Ref. 436].

hydrogen electrosorption isotherm. When studying the effects of anion adsorption note should be made of the fact that some anions are strongly chemisorbed while others are only weakly chemisorbed. In order of decreasing strength these seem to be Cl^- > NO_3^- > $SO_4^{=}$ $(HSO_4)^-$ > OH^- > ClO_4^- ≈ F^-. Fig. 1.23 shows the difference between a strongly and weakly adsorbed anion for stepped single crystal platinum surfaces. Areas under the peaks are equal but the H_2SO_4 peak is sharper and the width strongly reduced. It is mainly the peak at ca. 0.27 V(RHE) which is affected. However, the main features of the adsorption process, such as the number of voltammetric peaks and peak positions, are entirely determined by the hydrogen-platinum interactions and the morphology of the platinum surface. One explanation for this type of behaviour is that the long range ordering of the hydrogen adatoms may be assisted by hydrogen bonding to interfacial water molecules [324] and hence sensitive to the nature of the supporting electrolyte [293].

(e) Anomalous (111) Peak: The most unusual anion effect is observed on the electrochemical behaviour of a (111) platinum surface. The "butterfly" peaks at ca. 0.45 V(RHE) in Fig. 1.15(a) in H_2SO_4 electrolyte are shifted to ca. 0.8 V(RHE) in Fig. 1.24 in $HClO_4$ electrolyte. In fact, by the addition of strongly adsorbing anions to weakly adsorbing electrolytes the peak potential has been shown to shift from 0.8 V(RHE) in $HClO_4$ or HF, through 0.45 V(RHE) in H_2SO_4 and down to ca. 0.25 V(RHE) in HCl [294]. The peaks change potential (with respect to RHE) with anion concentration in H_2SO_4 and HCl electrolytes but not in $HClO_4$, HF, H_2CO_3 or OH^- electrolytes. Also, at constant anion concentration the peak potential changes with pH for H_2SO_4 electrolyte but not for more weakly bonding anion electrolytes [325]. There has been no spectroscopic identification of the species involved at the interface in these experiments.

Various explanations of the above behaviour have been suggested:-

(i) The general behaviour pattern may be dominated by impurities in the electrolyte, transfer gases or bulk platinum. However, as the "butterfly" peaks appear whether the UHV or

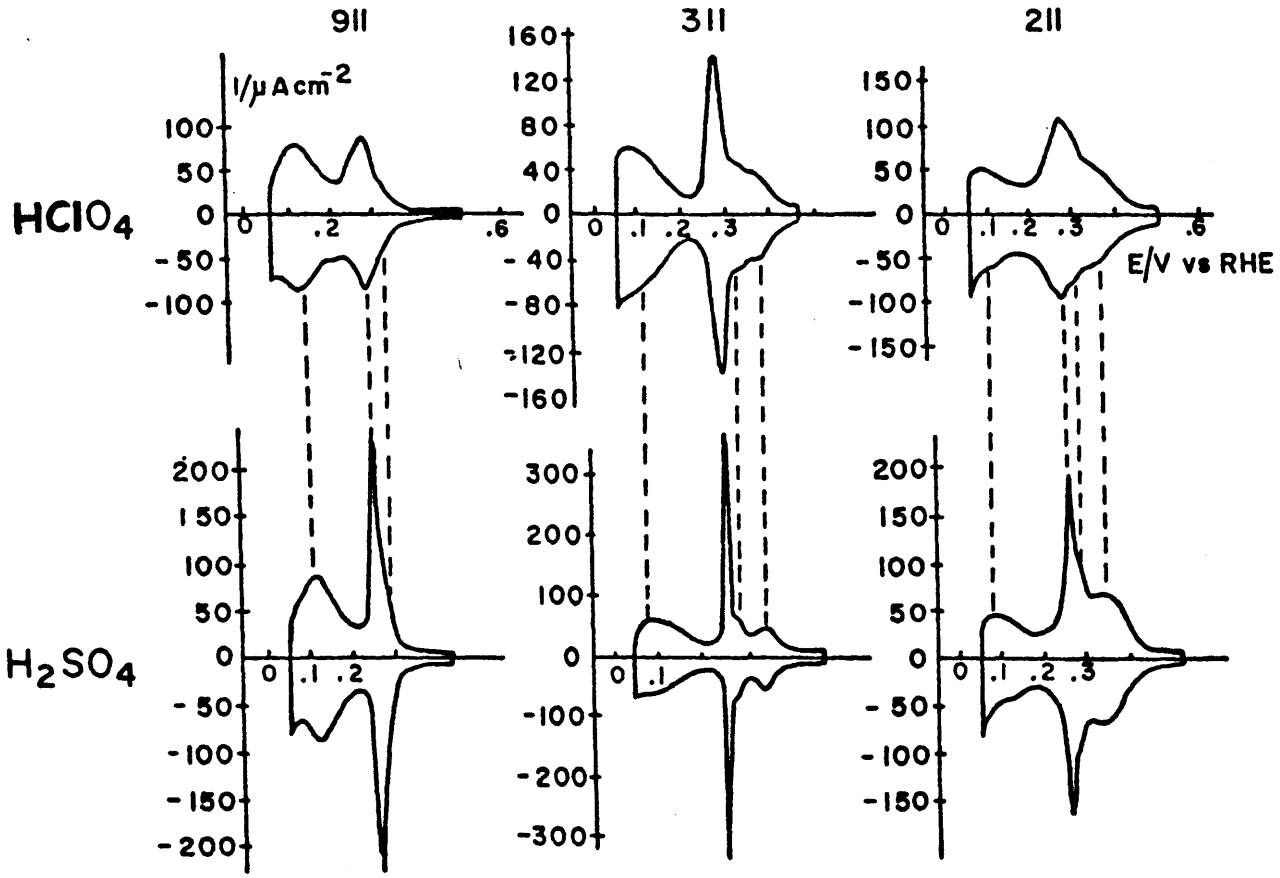

Figure 1.23: A comparison of cyclic voltammetry curves for hydrogen adsorption for 1.0 mol dm^{-3} $HClO_4$ and 0.5 mol dm^{-3} H_2SO_4 solutions on three stepped single crystal planes, sweep-rate 50 mV s^{-1} [Ref. 293].

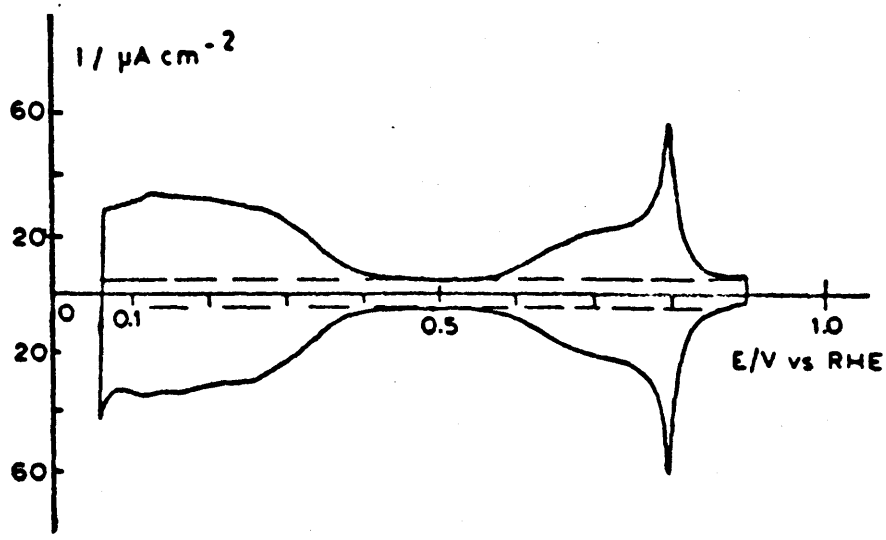

Figure 1.24: Voltammogram for the Pt (111) electrode in 0.1 mol dm^{-3} $HClO_4$ showing the splitting effect of the anion; sweep-rate 50 mV s^{-1} [Ref. 294].

quenching method of (111) surface preparation is used, this seems unlikely.

(ii) Hydrogen species are the first proposal [294,316] where the peaks correspond to the adsorption-desorption of approximately one-third of a monolayer. This view is supported by the high degree of reversibility and the fact that the charge under the voltammetry curve (ca. 240 $\mu C\ cm^{-2}$), which includes the "butterfly peaks", are independent of the nature of the anion. The difference between the mean energies of the strongly and weakly bonded hydrogen states is of the order of 63 $kJ\ mol^{-1}$ [294]. This heat of adsorption of hydrogen would be unreasonably high and not consistent with what is known about platinum-hydrogen bonding at the vacuum interface [326-328]. While the change of one-third of a monolayer may be explained by the existance of two differnt structures of hydrogen adsorbate on platinum, gold (111), [329], and silver (111), [330], which do not chemisorb significant quantities of hydrogen, also have a similar feature corresponding to one-third of a monolayer which is most likely due to a phase transition involving specifically adsorbed anions.

(iii) Oxygen like species (oxidised with respect to water) being so reversible would, according to Wagner and Ross [325], have exciting implications for electrocatalysis. It is thermodynamically possible that this peak corresponds to a water dissociation process, such as the formation of surface OH species [435]. Vacuum studies of oxygen and water on platinum (111) surfaces [331] suggest that surface OH formation is kinetically facile so it seems at least feasible that the sharp peaks could involve reversible interaction of OH species [287]. The adsorption of hydroxyl ion at a potential ca. 0.5 V more negative than that at which the actual surface oxide formation occurs has indeed been postulated in the case of gold on the basis of a voltammetry and impedance study [332]. With platinum in base reversible peaks are also visible [311] and cycling into the oxide region shows a reversible peak above the hydrogen adsorption-desorption region. The specifically adsorbed OH^- (pH>9) and the oxygen like state formed by water dissociation (pH<5) may have similar final state molecular configurations on the surface even though they derive from different initial states [325]. However, for the peaks to be

accepted as oxygen-like species it is necessary to explain why the oxidation of CO occurs at the same potential in $HClO_4$ and H_2SO_4 [325] even though the peak shifts over a range of ca. 0.35 V.

(iv) The feature in question has also been attributed to majority anion effects. While the anion effect has been pointed out already and partly discussed under (b) it should be pointed out that if the cathodic part of the peak is due to the desorption of anions there is nothing left on the surface at lower potentials to block hydrogen adsorption. Hence, the fact that the pseudo capacity value of the hydrogen region for the (111) face is one-third lower than that of the (100) and (110) faces cannot be explained.

(v) Water adsorption at the interface could cause stabilisation of hydrogen by giving long range effects [325]. Until recently it was thought that in the case of H_2SO_4 solutions the peaks were caused by the adsorption of sulphate (bisulphate) ions whereas those observed in $HClO_4$ or HF electrolytes were associated with the adsorption of hydroxyl ions [333]. However, using radio-electrochemistry Wiekowski et al. [334] show that the maximum for $SO_4^{=}$ adsorption in ClO_4^{-} solutions occurs at the "butterfly" peaks at ca. 0.8 V(RHE). However, the $SO_4^{=}$ surface coverage during this experiment only represents ca. 7% of a monolayer. As the charge associated with the anomalous peaks is $(52\pm5)\mu C\ cm^{-2}$, this yields (3.3±1.1)e/ion if the peaks are caused by anion adsorption. This value is high and scarcely consistent with the accepted models of specific adsorption of anions. It suggests strongly that the charge is generated via a process that is activated by anion adsorption but is not directly derived from the anion adsorption, i.e. the direct cause of the behaviour does not require the discharge of sulphate ions. In the concentration range of sulphuric acid studied, the desorption process begins at ca. 0.8 V(RHE). As concluded by recent electroreflectance measurements, the desorption coincides with the formation of OH radicals on platinum (111) [335].

1.7.8. Surface Characterisation

It should be noted that LEED studies show that a metallic single crystal actually consists of a mosaic of crystallites with diameters in the order of 1 μm and misorientations in the order of 0.1^{o} [287,347]. Also, scanning tunnelling microscopic (STM) images of Au (111) after flame annealing indicates the presence of distinct terraces, steps and kinks [336,347]. Similar results have also been found with UHV prepared platinum single crystals [337]. These studies have also shown that the adsorption-desorption of chloride dramatically alters the surface topography. It should be remembered that STM does not produce an image of the actual geometric structure of the surface but follows lines of constant tunnel current, which in turn are determined by the energetic and spatial distribution of electron density in front of the surface [372].

1.7.9. Electrochemically Preferred Orientations

A new electrochemical procedure to obtain platinum electrodes with preferred orientations from bulk polycrystalline platinum by the application of repetitive potential sweeps at high frequencies under carefully selected potential perturbation conditions has been developed by Arvia et al. [339-342]. The voltammograms from these electrodes produce responses very similar to those from platinum single crystal faces. The explanation of the development of these surfaces can be thought of in terms of a dynamic lattice model, where the surface atoms of platinum are oscillating principally in a direction perpendicular to the electrode surface according to the potentiodynamic induced water electrooxidation reaction. This causes a periodic separation of metal atoms in the first lattice planes which exceeds the bond length of any crystal structure yielding a jelly-like metal atom lattice which subsequently is able to accommodate preferred orientations. The development of a preferred crystallographic orientation has also been achieved independently for other metals (gold, rhodium, silver and copper) by Arvia et al. [343-346]. The importance of these type of preparations can be seen from Fig. 1.19(c) where practical electrocatalysts could be prepared having orientations which

selectively avoid formation of the poisoning intermediate formed in organic oxidation reactions.

1.7.10. Conclusion

While the study of single crystal surfaces has not solved the controversy of the origin of the multiple hydrogen adsorption states on platinum it has improved our understanding of the role of geometric surface sites in electrochemical reactions significantly. With study now expanding to higher index planes an even greater understanding of the role of particular surface sites is being obtained. While care must be taken due to results depending on surface preparation, anion concentration, etc., continued research in the single crystal area should help to increase our awareness of geometrical factors in electrocatalysis.

1.8. OBJECTIVES

As mentioned previously (section 1.6.9), when electrode surfaces are placed in contact with aqueous electrolytes, surface atoms, having lower coordination numbers than bulk atoms, must be stabilised by adsorption of solution species. Due to surface defects these surface atoms may attain a whole range of possible coordination numbers. Surface atoms, with very low coordination numbers are considered to be self-adsorbed atoms on the electrode surface and are termed adatoms. The adatoms associated with a given metal M are represented by M*. Due to the low coordination numbers associated with adatoms they are highly reactive and have a tendency to attain a more stable configuration by relaxing into a vacant lattice site on the electrode surface, viz.

$$M^* \rightleftharpoons M_{(l)} \qquad (1:8:1)$$

where $M_{(l)}$ represents a metal atom in a regular lattice site.

Alternatively, the highly reactive adatoms may attain a certain degree of stability via solvation by water molecules present in the aqueous electrolyte, viz.

$$M^* + nH_2O = M^*(H_2O)_n \qquad (1:8:2)$$

Such solvated adatoms are envisaged as being able to undergo redox transitions to form hydrous oxide species at potentials negative to regular, anhydrous, monolayer oxide formation (curve 1, Fig. 1.25), viz.

$$M^*(H_2O)_n \rightleftharpoons [M(OH)_n]^{x-} + nH^+ + (n-x)e \qquad (1:8:3)$$

The process involved may be regarded as proton loss from coordinated water molecules or excess hydroxide ion coordination by the central metal ion in the hydrous oxide material. The coverage attained is assumed to be only a small fraction (1-2%) of a monolayer as adatom concentrations at electrode surfaces is usually low due to equation (1:8:1). The reversible redox peaks due to the metal/hydrous oxide transition, represented by curve 2, Fig. 1.25, may be observed by increasing the current sensitivity of the recorder and cycling the electrode between reduced limits in cyclic voltammetry experiments. Thick films of hydroxy material can be produced by vigorous anodisation or potential cycling techniques (section 1.6.7). Reduction of this material on the cathodic sweep coincides with the potential of the metal/hydrous oxide transition (curve 3, Fig. 1.25).

It is postulated that the metal/hydrous oxide transition redox system serves as the electron transfer mediator for electrocatalytic processes with the redox system itself exhibiting typical catalyst behaviour. Reactive species, R, are oxidised by the interfacial hydrous oxide, the latter being spontaneously regenerated when the potential is above the reversible value for the metal/hydrous oxide transition, viz.

$$M^* \rightleftharpoons [M(OH)_n]^{x-} + (n-x)e \qquad (1:8:4)$$

$$R + [M(OH)_n]^{x-} \rightarrow M^* + O \qquad (1:8:5)$$

where equation (1:8:4) combines equations (1:8:2) and (1:8::3) , and O is the product of the oxidation. By a similar mechanism it is envisaged that active compounds undergoing reduction at a metal electrode surface would, if electrocatalytically demanding, be inhibited until reduction of hydrous oxide produces adatoms at the interface which are the active surface sites at which reduction

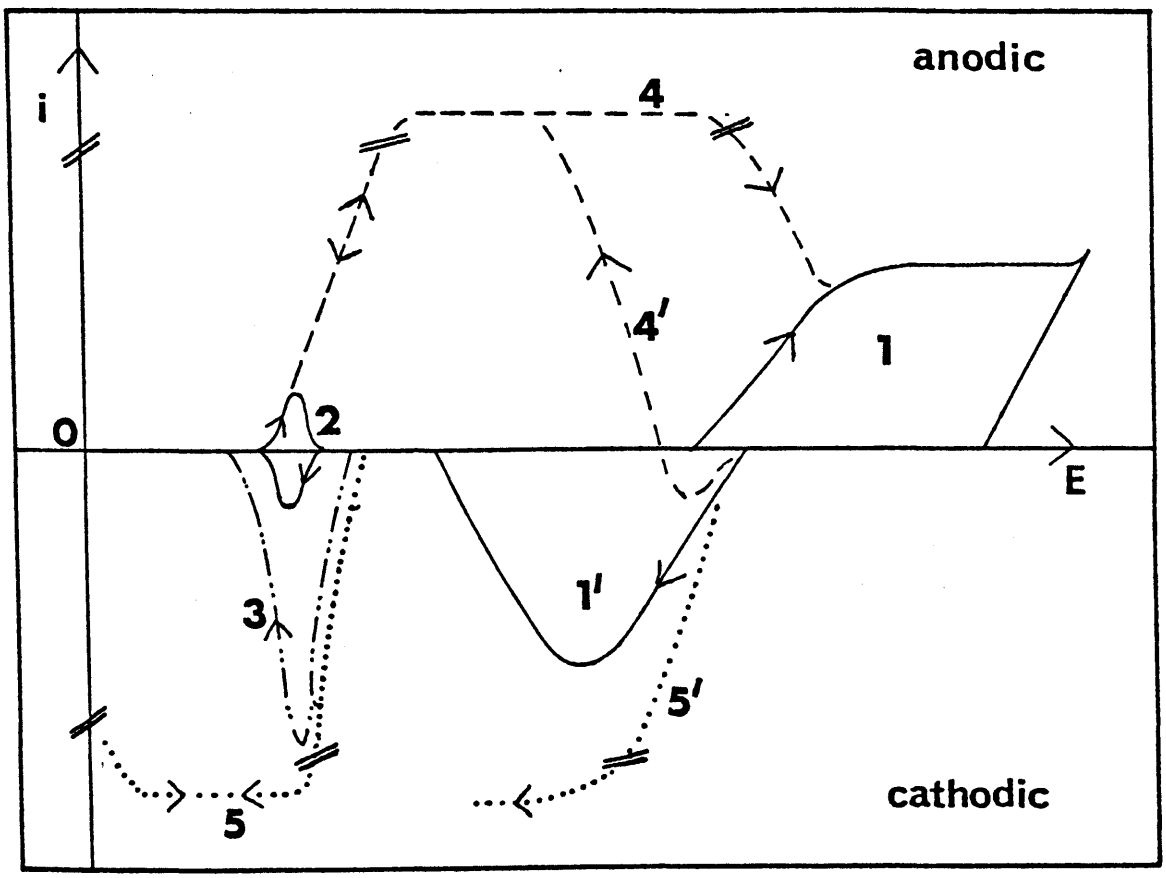

Figure 1.25: Schematic representation of the different process involved in the interfacial cyclic redox mechanism for electrocatalysis with hydrous oxide species:

(1,1') - anhydrous oxide formation and reduction
(2) - reversible, redox hydrous oxide couple
(3) - hydrous oxide reduction (thick film)
(4,4') - oxidation of oxidisable species
(5,5') - reduction of reducable species.

occurs (curve 5, Fig. 1.25). Oxidation reactions could also occur on the cathodic sweep on reduction of the anhydrous place-exchanged oxide material (curve 4', Fig. 1.25) and this process produces adatoms which are immediately converted to the incipient hydrous oxide state as long as the potential is above the adatom/hydrous oxide transition potential. Less demanding reduction reactions may occur on the cathodic sweep once the anhydrous oxide is reduced; basically, such reactions do not require adatom-type sites (curve 5', Fig. 1.25).

The kinetic characteristics of the cyclic redox catalytic mechanism are as follows:

(a) The current for the oxidation of solution species under potential sweep conditions should commence and terminate at a fixed potential determined by the nature of the redox couple at the surface (curve 4, Fig. 1.25). Similar behaviour should exist for certain reduction processes.

(b) This potential should be independent of the character of the dissolved active species undergoing oxidation or reduction (the latter will of course influence the magnitude of the current).

(c) Where the nature and the coverage of the species bound at the interface remain constant (apart from the redox change) the current should eventually attain a plateau at potentials appreciably away from the interfacial redox transition value. The expected i/E response is, threfore, rather like a polarographic wave except that the limiting current is reaction, rather than diffusion, controlled.

(d) When the cyclic redox catalytic mechanism is invoked in connection with hydrous oxide species for electrocatalytic processes it should, ideally, be possible to record the small, reversible peaks due to the metal/hydrous oxide transition at a potential usually prior to monolayer oxide formation. In cases where this is not possible the onset potential may be located by determining the potential for the reduction of thick hydrous oxide films.

The objective of the present work is to produce evidence for the nobel theory of electrocatalysis outlined above. Minor reversible peaks will be shown to exist at gold, silver and platinum electrodes in aqueous electrolytes at potentials cathodic to anhydrous oxide formation. Onset and termination of oxidation and reduction potentials will be shown to coincide with these peaks. Plateau currents will be shown to be reached. A mathematical model will also be advanced to explain this behaviour.

CHAPTER 2

Experimental

2.1. TECHNIQUES

Experiments designed to study electrode reactions can be categorised into three major types:

(I) Equilibrium Techniques: In such experiments, the measurement is made with the electrode reaction at equilibrium or perturbed only slightly from equilibrium by the application of a small amplitude a.c. signal. The more common techniques are potentiometry, amperometry, differential capacitance, measurement of surface tension and impedance. Included in such methods are measurements on reversible electrochemical cells which have been used to determine thermodynamic properties, e.g. solubility products, activity coefficients and equilibrium potentials.

(II) Steady State Techniques: In these methods the system is not necessarily at equilibrium, but the response to an applied perturbation is only measured after it has become independent of time. In practice it is commonly advantageous to use a cell with well defined convective stirring to control the mass transport. Typical techniques are voltammetry, polarography and coulometry, preferably with rotating electrodes.

(III) Transient Techniques: Here the system is perturbed from its equilibrium or steady state system and electrochemical information is obtained from the relaxation in the time domain to the new steady state condition. Double potential step, chronoamperometry, chronocoulometry and chronopotentiometry are typical examples of transient techniques.

2.2 INSTRUMENTATION

The electrochemical cell consists primarily of a vessel containing the electrodes and the electrolyte. A glass frit, separator or membrane may be incorporated to isolate the anolyte from the catholyte. Three electrodes are commonly employed, a working electrode which defines the interface under study, a reference electrode which maintains a constant reference potential and a counter (or secondary) electrode which, with the working, completes the electrolysis circuit. The cell must be designed so

that the experimental data are determined almost solely by the properties of the reaction at the working electrode.

In all experiments electronic apparatus designed to control/measure the charge passed (coulostat/integrator), current (galvanostat/current follower) and potential (potentiostat/high impedance voltmeter) are used. This apparatus may also contain instruments for signal averaging and for separating small signal responses from electronic noise. The control and measurement equipment relies on the properties of the operational amplifier which, although complex electronically, can be regarded as a three terminal box (Fig. 2.1(a)) with four useful properties.

(a) Two terminals are inputs and are referred to as the inverting (-) and non-inverting (+) inputs. They have infinite input impedance, which means they can accept an input voltage without drawing current into the device through the voltage source.

(b) The third terminal is the output, and this has zero impedance so that the output voltage remains constant irrespective of the current drawn by the load.

(c) The amplifier is essentially an inverting differential amplifier with infinite gain, A, so that:

$$E_{out} = -A\,(E_- - E_+) \qquad (2:2:1)$$

and any voltage difference at the inputs drives the output to $\pm\,\infty$.

(d) The amplifier is able to follow changes in input voltage with infinite speed.

Many of the limitations and design criteria associated with real devices arise because of the failure of the operational amplifier to meet fully these ideal properties.

The use of the operational amplifier as a control device depends upon the principle of negative feedback where part of the

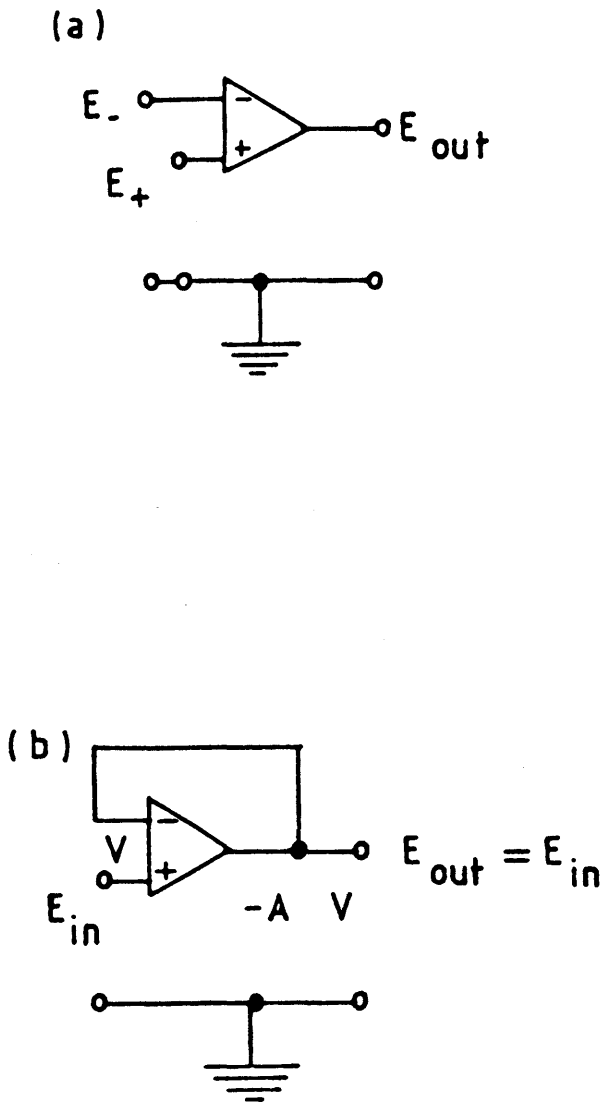

Figure 2.1: The operational amplifier: (a) the open loop configuration, (b) the principle of negative feedback.

output voltage is fed to the inverting input of the amplifier as shown in Fig. 2.1(b). In this configuration the amplifier maintains the potential difference between the inputs at zero. Any error that appears across these inputs (+ V) is amplified to give an output - A V that acts to reduce the error + V to zero. This simple configuration is an extremely useful circuit known as the voltage follower because within the limits imposed by the sensitivity of the real device, the output voltage follows exactly the input voltage. Furthermore, the input impedance of the device is infinite and the output impedance is zero. This means that the circuit can measure potential at its input without drawing current from the voltage source, and display the result on a measuring device which draws current.

The potentiostat is an instrument based on operational amplifiers, and is the basic instrument used in this study. One common configuration for potentiostatic control is shown in Fig. 2.2. The working electrode is very often connected to earth ground (or a common or virtual ground). The current flowing from the output, through the cell, is such that the two input voltages, V_1, and V_2, are equal i.e.

$$V_1 = V_2 \qquad (2:2:2(a))$$

or

$$V_1 - V_2 = 0 \qquad (2:2:2(b))$$

V_1 is equal to the potential difference between the reference electrode (R.E.) and the working electrode (W.E.), i.e.

$$\begin{aligned} V_1 &= E_R - E_W \\ &= -(E_W - E_R) \\ &= -E_W \end{aligned} \qquad (2:2:3)$$

with respect to the reference electrode.

Hence,

$$V_2 = -E_W \qquad (2:2:4)$$

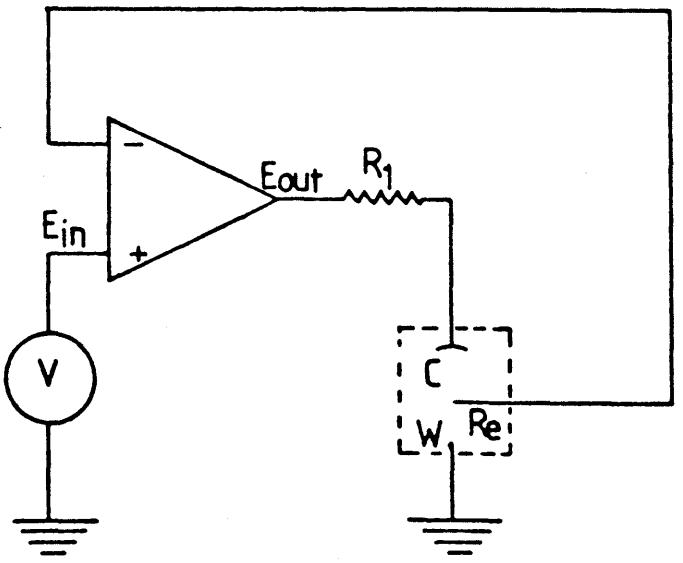

Figure 2.2: Basic Circuit for Potentiostatic Control C, R_e and W represent, respectively, the counter, reference, and working electrodes of the cell; A is an operational amplifier; V is a voltage source; R_1 is a standard resistance.

This inversion of sign can be eliminated using a more complex configuration. The current delivered by the potentiostat is commonly measured as a voltage drop across the resistor R_1. Fig. 2.3 shows the circuit used for potential sweep experiments.

A more detailed construction of a potentiostat involving several operational amplifiers (op. amps.) is outlined in Fig. 2.4. This shows some important op. amp. cof nfigurations within a typical potentiostat. Operational amps. VF and RVF are in a voltage follower or buffer configuration, i.e. the output voltage is equal to the input signal voltage, e_1. Op. amp. AP is in a voltage adder circuit.

If all the resistors on the input are equal, it adds together all the input voltages, so that one may combine different voltage signals, e.g. ramp and sinusoidal, to get a more complex input signal. It also adds the signal from RVF, which is equal to $-E_W$ (vs. R_E) and e_f (the origin of e_f is explained later). Thus

$$E_W = e_1 + e_2 + e_3 + e_f \qquad (2:2:5)$$

in Figure 2.4, B is a current booster. It is used to increase the current capabilties, if large currents are required above the capabilities of AP; CF is in a current follower configuration. The WE is maintained at virtual ground and an output voltage

$$V_i = iR_i \qquad (2:2:6)$$

where R_i is the feedback resistance, is obtained at the output. This gives a voltage proportional to the current which can be monitored using a chart recorder or other voltage measuring device. A certain fraction of V_i is fed back to overcome solution resistance, iR_u, effects.

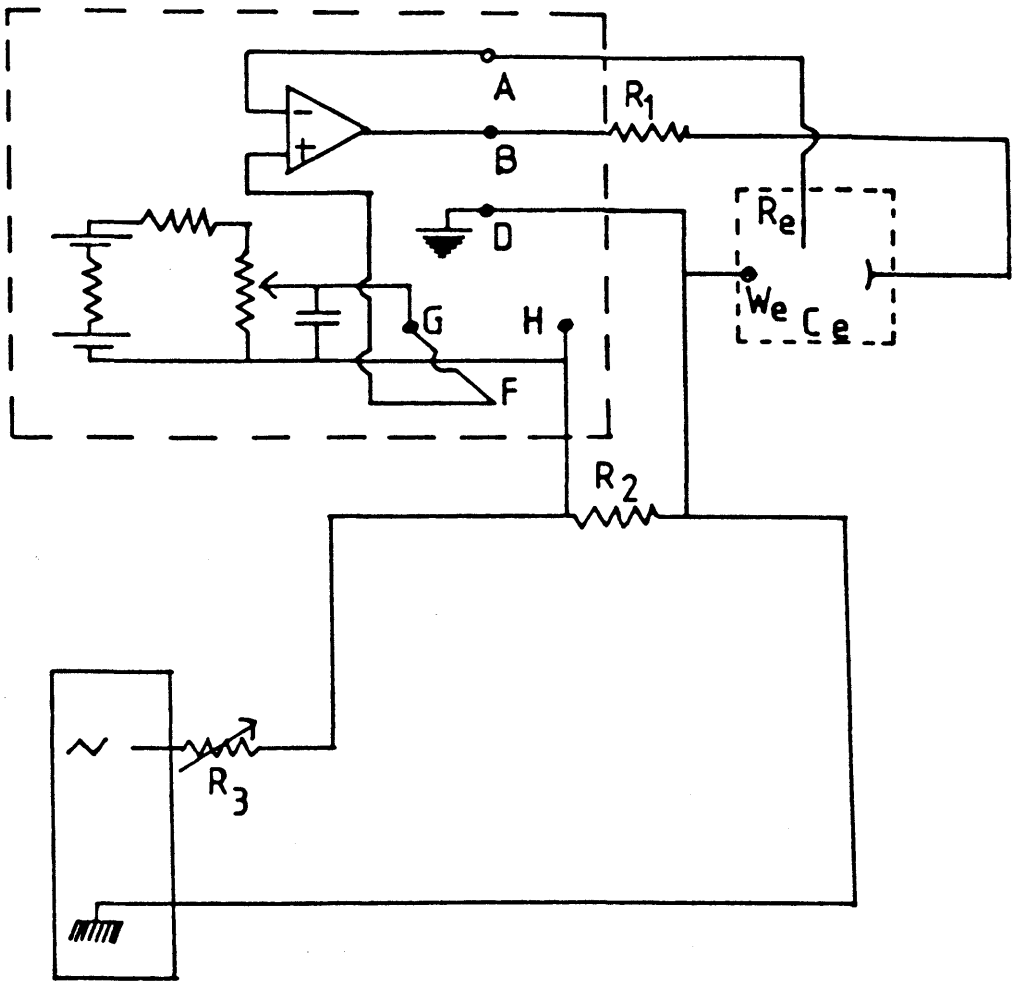

Figure 2.3: Circuit used for Potential Sweep Experiments
The potentiostat is outlined by the dashed line; A, B, D and F are the terminals for the reference electrode, counter electrode, working electrode, and control potential respectively; G and H are the output of a variable potential source available on the instrument. The function generator supplied a triangular waveform, CE, RE and WE are as in Figure 2.2; R_1 = 10Ω, R_2 = 1kΩ, R_3 variable, 100Ω - 10kΩ.

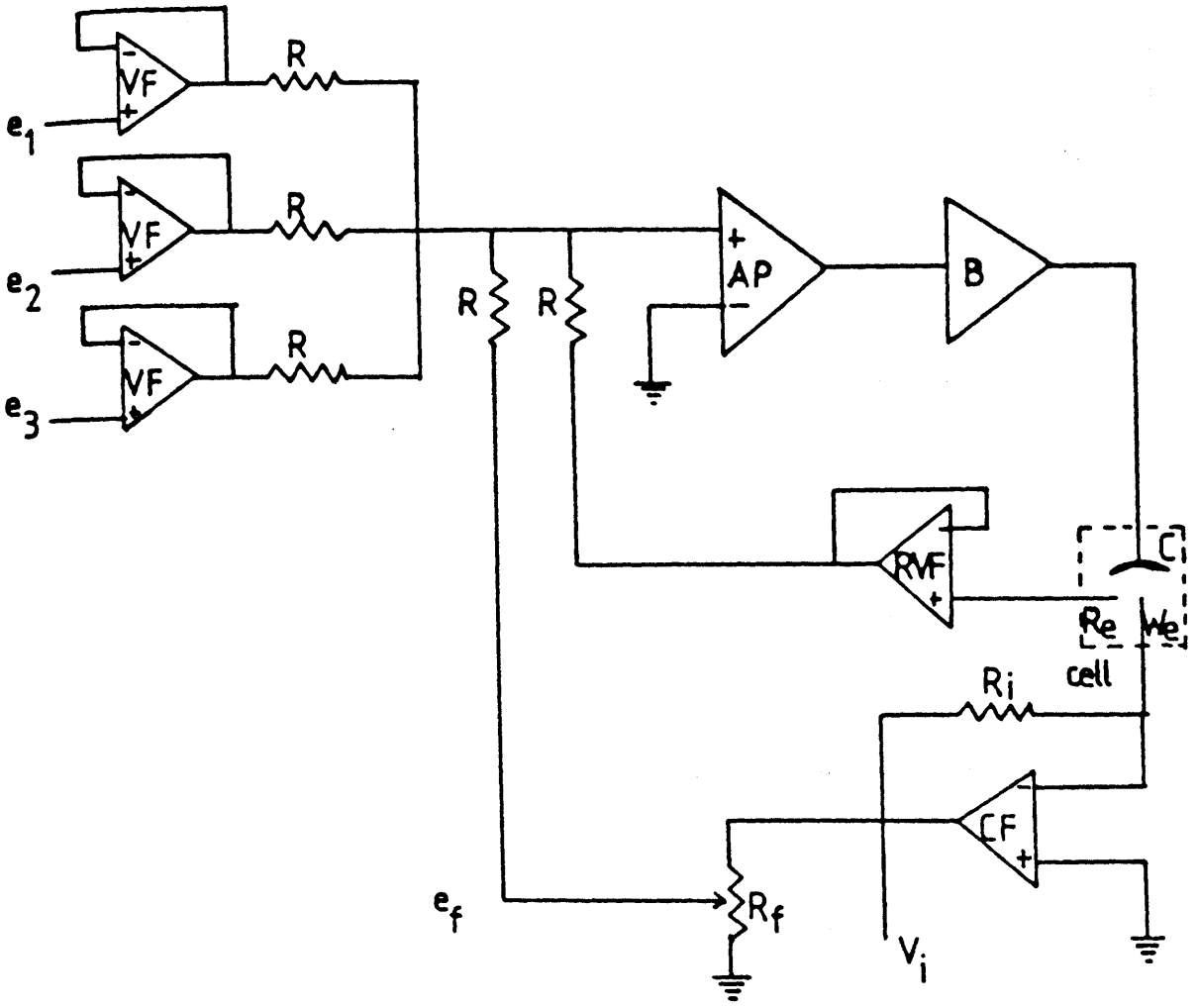

Figure 2.4: A full potentiostatic circuit based on an adder control amplifier (AP), with a current follower (CF) and iR compensation.

2.2.2. THE CORRECTION OF SOLUTION RESISTANCE, iR_u EFFECTS.

The current flowing across the solution generates a potential drop across it and a certain proportion of this potential can be observed between the reference and working electrodes. This gives rise to an error in the potential measured between them called the iR_u drop which can be appreciable in solutions of low conductivity or where high currents are used. Fig. 2.5 shows the origin of the uncompensated resistance. It can be minimised by placing the tip of the Luggin capillary from the reference electrode close to the working electrode. In principle the capillary can be moved very close to the working electrode, but as the probe is an insulator it screens the field at the electrode; this alters the current distribution and potential profile in the region where the potential is being measured. The best design for the Luggin probe [427] is one that has a narrow capillary with thin walls at its tip to prevent shielding, but has thick walls in the main body and widens rapidly away from the tip to reduce resistance.

The uncompensated resistance can be further reduced by electronic compensation, the main type being positive feedback. Here the potential E_W between RE and WE is given by

$$E_W = E^1 + iR_u \qquad (2:2:7)$$

where E^1 is the true potential in the absence of resistance errors. A voltage, e_f, proportional to the current is fed back into the input of the potentiostat, across R (see Fig. 2.4). Combining equations (2:2:5) and (2:2:7) gives

$$e_1 + e_2 + e_3 + e_f = E_W + iR_u \qquad (2:2:8)$$

We require that

$$e_1 + e_2 + e_3 = E^1 \qquad (2:2:9)$$

Therefore

$$e_f = iR_u \qquad (2:2:10)$$

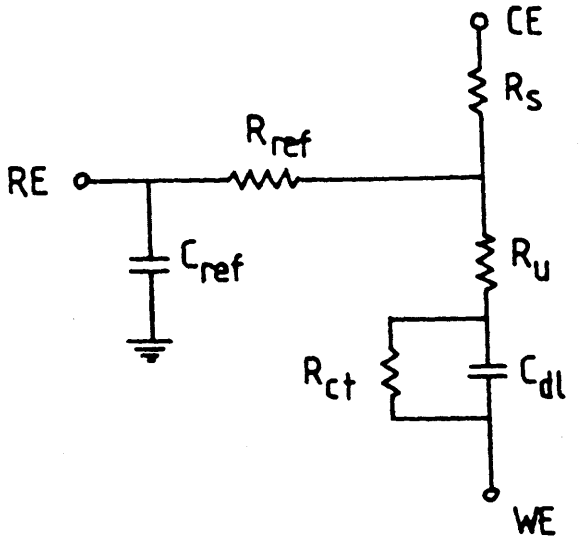

Figure 2.5: Equivalent circuit for an electrochemical cell. R_{ref} is the resistance of the reference electrode, and C_{ref} represents parasitic loss to ground in the leads. R_s and R_u are the solution and uncompensated resistances respectively, C_{dl} the double layer capacitance of the working electrode, and R_{ct} the charge transfer resistance.

This can be arranged by adjusting the voltage feedback to get the optimum iR_u compensation. In practice this is an unstable electronic configuration and only ca. 80% to 90% compensation is achievable.

A second real time method of measuring iR_u is the current interruption technique [428,429]. When the current through the electrochemical cell is interrupted suddenly, the potential of the working electrode does not immediately return to its steady state value but decays in a complex manner determined by the discharge of the double layer capacitance through the faradaic process. However, any potential drop that is purely ohmic in character will be reduced to zero at the moment of current interruption and this allows the uncompensated resistance to be measured from the potential time transient.

In an alternative (a.c.) approach the solution resistance can be measured from the high fequency intercept of the impedance semicircle on the real axis.

2.3. ELECTROCHEMICAL CELLS, APPARATUS AND ELECTRODES

Experiments were carried out either in a thermostatted cell (Metrohm, Type EA 880 T-20) (Fig. 2.6) or a conventional three compartment (Fig. 2.7) containing a central working electrode and counter electrodes, of the same material as the working electrode, in their own compartment with a fine glass frit separating the solutions. Potentials were measured with respect to either a saturated calomel electrode or a hydrogen reference electrode in the same solution. All potentials are quoted with respect to a reversible hydrogen electrode in the same solution (RHE). A Luggin capillary whose tip was positioned ca. 1 mm from the surface of the working electrode was used to minimise iR_u drop in solution. The cell temperature was controlled to within 0.1°C of the desired temperature and the solution was deoxygenated or stirred as required by a flow of purified nitrogen gas.

The formaldehyde solution (B.D.H. Chemicals Ltd.) was stabilised by about 12% methanol (preliminary experiments showed

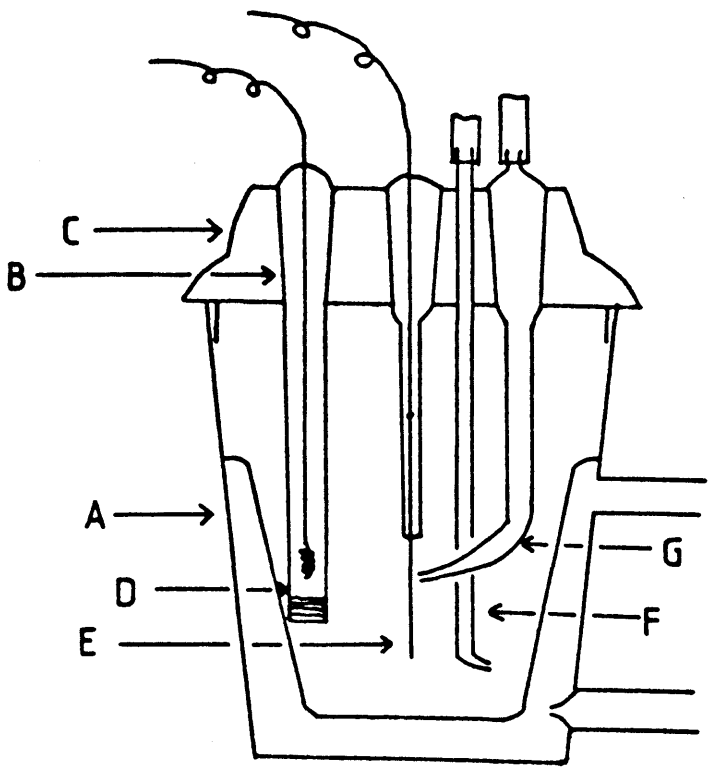

Figure 2.6: Cell No. 1.

A = water jacket; B = B14 joint; C = cell lid;
D = counter electrode; E = working electrode;
F = nitrogen inlet; G = Luggin capillary.

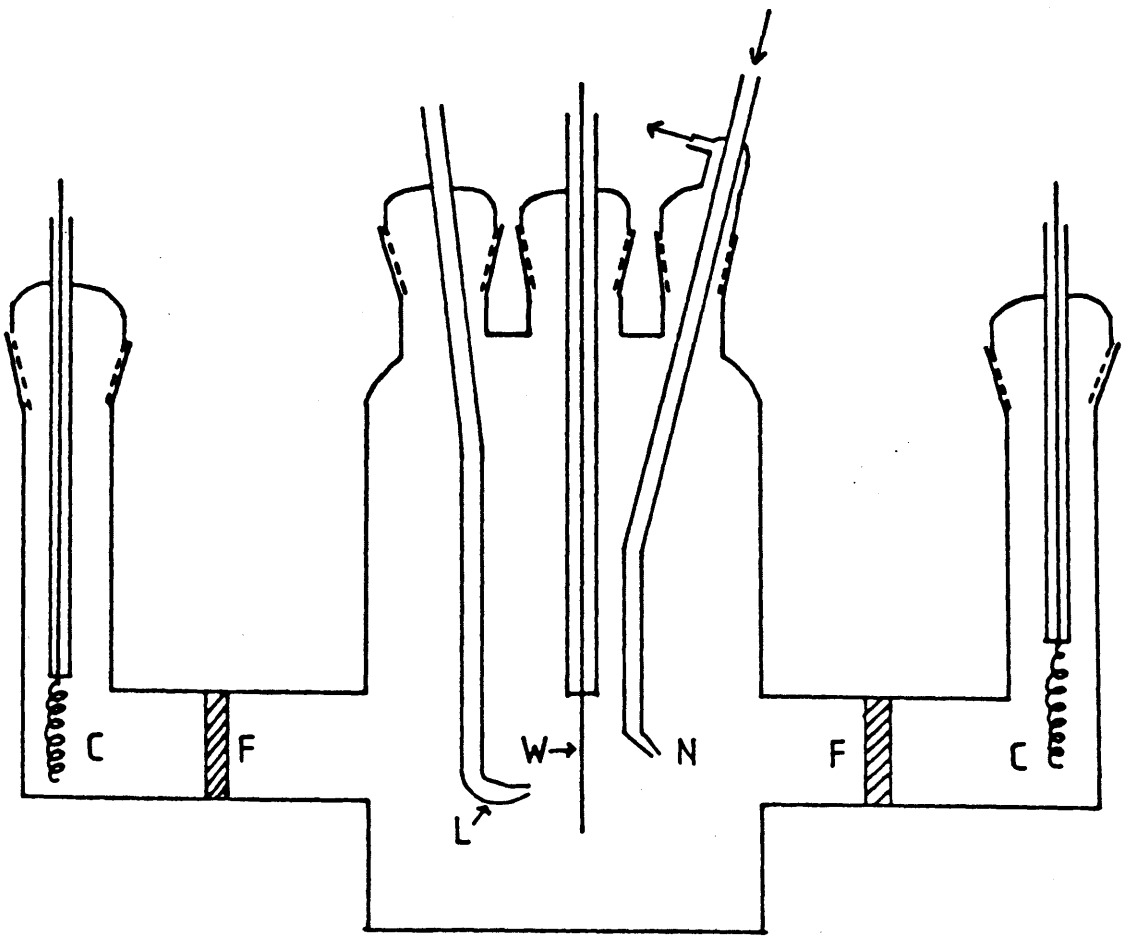

Figure 2.7: Cell No. 2.

C = counter electrodes

F = glass frits

L = Luggin capillary

N = nitrogen stirring inlet

W = working electrode

that both methanol and formic acid, in aqueous media, were virtually inert with regard to oxidation on gold and silver in base). All other solutions used were made up using Analar grade chemicals (where possible) and water which was triply distilled; the first distillation involved the use of potassium permanganate to destroy organics and the latter ones were carried out using quartz glassware).

The potential control of the working electrode was affected with the aid of a potentiostat (Wenking, Model LT-78). The signal for triangular potential sweep and potential stepping experiments was produced by a Metrohm VA Scanner (Model E612), which had wide sweep speed capabilities with a sweep hold facility and potential stepping capabilities. Both i/E current characteristics and i-t current decay profiles were recorded using a potentiometric chart recorder (Rikadenki, Model RW-21, X-Y recorder, with built-in Y-t capibilities).

The working electrode consisted of a length of smooth wire (gold (Goodfellow Metals, 99.95% purity), silver and platinum (Johnson Mattey Metals, 99.995% purity)), 0.5 - 1 mm diamter, ca. 0.25 - 1 cm^2 exposed area, sealed directly into glass. The working electrode was periodically cleaned by brief (10s) immersion in boiling HNO_3 or aqua regia followed by washing with triply distilled water; in some instances this was followed by mild abrasion to roughen the surface and again the electrode was washed before use. In experiments involving the platinum electrode the surface was often activated by platinisation - a platinum black layer was deposited by cathodising at 20 mA cm^{-2} for 5 min. in H_2PtCl_6 solution (1 g in 100 mls of 0.01 mol dm^{-3} HCl): typically this resulted in an increase in surface area (as measured in terms of adsorbed hydrogen capacity) by a factor of 150 as compared with smooth platinum.

CHAPTER 3

Gold

3.1. INTRODUCTION

Gold, considered to be the most noble of metals, is soft and yellow (melting point 1063°C) with the highest ductility and malleability of any element. This nobility has resulted in the usage of the metal not only as a corrosion-free (and therefore low resistant) contact material in modern electronic instrumentation but also as a substrate for electrochemical oxidations which, until recently, have been believed to be achieved on an unoxidised gold metal electrode. The situation however is more complex than may be immediately apparent and a precise understanding of the factors influencing the formation of oxide films on gold is clearly of considerable fundamental interest.

It is generally accepted that the main oxide formation region on a gold electrode commences at ca. 1.35 V in acidic solutions [85,203,214,348] and that the reduction of films formed at potentials less than 2.0 V gives rise to a single cathodic peak at ca. 1.2 V [214,215,349]. The anodic behaviour of gold in basic solutions has not received as much attention; however, a shift in the onset of oxidation of the metal to less anodic potentials (ca. 1.2 V at pH ≈ 14) with increasing solution pH has been noted [350,351]. The cathodic counterpart of this oxide peak occurs at ca. 1.1 V. The oxidation reaction of this metal is interpreted for both acidic and basic solutions, in terms of a Au/Au (III) transition [352] represented by

$$2Au + 3H_2O = Au_2O_3 + 6H^+ + 6e \qquad (3:1:1)$$

- the quoted E^o value for this reaction, assuming the involvement of an anhydrous oxide, is 1.511 V (pH = 0).

Increasing the oxide formation potential above 2.0 V, i.e. well into the oxygen gas evolution region, in either acidic or base results in a substantial increase in the charge associated with subsequent oxide reduction [214,224,353-355]. This effect is generally attributed to formation of a multilayer oxide - as demonstrated by the appearance of more than one reduction peak. Burke and McRann [224] attributed this second type of oxide to a hydrous hyperextended oxide which is now assumed to be [361] an

aggregate of $[Au_2(OH)_9^{3-}]_n$ or $[Au_2O_3(OH)_3(3H_2O)^{3-}]_n$ species. This is assumed to have the following type of polymeric or aggregate structure, viz.

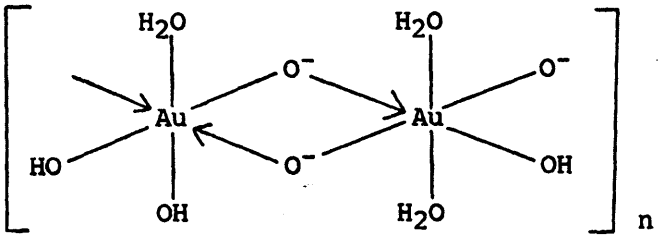

(3:1:2)

The evidence for the latter species at the present time is not very satisfactory (structural analysis for instance is totally lacking); however, the monomeric units outlined above are in agreement with the electrochemical data, notably the potential/pH shifts [224,361]. Reduction of the hydrous oxide species occurs at ca. 1.0 V in acidic media but is shifted to ca. 0.65 V in basic media, i.e. there is increased stability of the hydroxy complex, and hence a lower level of Au (III) activity, in the porous film, with increasing levels of hydroxide ion concentration in solution.

The former anhydrous oxide shows a potential/pH shift of (2.303 RT/F) V/pH unit, i.e. a 59 mV/pH shift, SHE scale or zero shift per pH unit on the RHE scale. However, the latter hydrous oxide shows a shift of 3/2(2.303 RT/F) V/pH unit, i.e. a 88.5 mV/pH shift on the SHE scale or a 29.5 mV/pH unit shift on the RHE scale. There is a need to modify the Pourbaix diagram for gold to take the acid-base effects in the hydrous oxide system in account [362].

XPS data from Peuckert and coworkers [363,364], who have surveyed the work of earlier authors, was interpreted on the basis that the thick film of oxide grown above 2.0 V was AuO.OH. This may well be valid as far as the material in the ultra high vacuum of the XPS apparatus is concerned; however, the question remains as to what extent this film is hydrated when it is in contact with an aqueous environment. It seems impossible to reconcile the simple AuO.OH formation (or its oxide, Au_2O_3, or hydroxide $Au(OH)_3$, equivalents) with the large cathodic shift, ca. 3/2(2.303 RT/F) V/pH unit (SHE scale), observed with gold oxide [224,361]. However, these two conflicting assignments for the thick film oxide

may be reconciled by assuming that hydrous gold oxide can undergo the following type of chemical transition, viz.

$$Au_2(OH)_9^{3-}.3H_f^+ = Au_2(OH)_6.3H_2O = 2AuO.OH + 5H_2O \quad (3:1:3)$$

in high vacuum (H_f^+ here represents a counter ion present in the hydrated regions of the film). It is assumed here that the layer is almost totally dehydrated in the ultra high vacuum chamber of the XPS equipment. An alternative possibility is that the less hydrated material alters to the anionic form as it undergoes reduction.

The growth of thick film hydrous oxide, above 2.0 V at gold in both acidic and basic solution, is accompanied by vigorous oxygen evolution [356]. According to Krasil'schikov [357] this reaction includes (among others) the following two steps with the involvement of a higher oxidation state, viz.

$$Au_2O_3 + O^- = Au_2O_4 + e \quad (3:1:4)$$

and

$$Au_2O_4 \rightarrow Au_2O_3 + \tfrac{1}{2}O_2 \quad (3:1:5)$$

In equation (3:1:4), the first step, the primary coordination state of the Au(III) cations in the initially anhydrous film is altered, and in the subsequent decomposition of the unstable Au(IV) oxide loss of oxygen may involve its replacement by H_2O or OH^- species to give hydrated or hydroxylated oxycations. The latter may reoxidise and evolve further oxygen via the above equations, or rearrange to form the nucleus of an outer hydrated film [224]. Such repetitive changes in both the oxidation and oxygen coordination states of gold cations in the surface layer are assumed to be the primary cause of hydrous oxide layer formation.

Many early workers [358,359] reported minor oxidation of gold surfaces at potentials considerably more cathodic than the main anodic oxidation peak. For example, Hoare [358] suggested the presence of an oxide at potentials as low as 0.87 V in acidic sulphate solutions. This proposal was supported by the ellipsometric studies of Sirohi and Genshaw [359] who suggested the formation of chemisorbed species in the potential regions 0.5 to

1.4 V in acidic solution and 0.3 to 1.12 V in alkaline solution prior to regular surface oxide formation at more anodic potentials. These reports were dismissed by Woods [215] as arising from impurities in either the metal surface or the electrolyte solution. However, publications have continued to appear in the literature [360-370] indicating the occurrance of a reversible reaction, apparently involving adsorbed OH species, at potentials substantially lower than generally associated with monolayer oxide formation. Thus Conway and coworkers [365] have observed two small, highly reversible transitions in the region 0.5 to 0.6 V (RHE) in cyclic voltammograms recorded for gold in highly purified base (0.2 mol dm^{-3} $Ba(OH)_2$). This assumption of incipient surface oxidation of gold prior to the regular monolayer oxide region is confirmed by the spectroscopic data of Nguyen Van Huong and coworkers [366]. A more dramatic illustration of these reversible peaks at ca. 0.7 V(RHE) can be found in the work of Gonzales-Velasco and Heitbaum [367] who used a mixed (NaOH + $NaClO_4$) electrolyte. The ClO_4^- anion evidently does not participate directly in the redox process as similar peaks of lower magnitude were observed in this work at the same potential in pure 1.0 mol dm^{-3} NaOH.

Angerstein-Kozlowska and coworkers [368,369] studied the single-crystal planes of Au electrodes and found substantial differences in the patterns of the early stages (0.0 to 1.3 V(RHE)) of oxidation in 0.01 mol dm^{-3} $HClO_4$ solutions. These differences were attributed to the different strengths of adsorption of anions on the different planes. The anions, which were assumed to be specifically adsorbed with some charge transfer, were considered to form overlay lattices on the surfaces. Kirk and coworkers [360], outlined the behaviour of gold in 1.0 mol dm^{-3} KOH. Three peaks, at ca. -0.9, -0.45 and +0.1 V(SCE), i.e. ca. +0.2, +0.65 and +1.2 V(RHE), were identified as being due to the formation of Au(I) hydroxide on the (110), (110), and (111) single crystal planes, respectively. However, the possibility that hydrous oxide species could be involved at these low potentials was not taken into account.

Support for the notion that hydrous oxide species are involved in the incipient oxidation process is given by the work of Scheron

and Kolb [370]. They observed, using gold single crystal material in 1.0 mol dm^{-3} H_2SO_4, a highly reversible redox transition at ca. 0.72 V(SCE) - for the pH in question the latter corresponds to ca. 1.0 V(RHE), this is the region where hydrous oxide material reduces at low pH [224,361]. It is assumed, therefore, that the current over the range 1.0 V to 1.36 V(RHE) corresponds to $[Au_2(OH)_9]^{3-}$ formation at various types of coordinatively unsaturated metal atom sites (considered to be adatoms, Au*). Such atoms have an unusual degree of access to solution entities, e.g. H_2O and OH^-. Usually currents in excess of double layer charging values are observed in base [224,365] over the region 0.5 V to the start of the compact monolayer formation process, i.e. ca. 1.15 V in base. This may also be due either to the formation of identical hydrous oxide species, represented by $[Au_2(OH)_9]^{3-}$, at different types of adatom sites or, alternatively, to the formation of a range of oxyspecies of slightly different degrees of hydration.

The amount of hydrous oxide material formed at the polycrystalline gold surface prior to the conventional compact monolayer is not large - an estimate based on the area of the two reversible peaks reported by Conway and coworkers [365] for base is ca. 2% of monolayer capacity - taking the anodic charge over the region 1.2 to 1.5 V to represent a monolayer. However, these authors have also pointed out that in base there is a region (0.5 to 1.2 V) prior to monolayer oxide growth where a reversible i/V profile is observed, with currents well above double layer charging values; the net charge value here corresponds [365] to ca. 35% of an OH monolayer. Nguyen Van Huang and coworkers [366] in their work assumed that ca. 10-20% of the surface of gold in acid was involved in incipient oxidation.

In the present work the involvement of incipient oxidation products in electrocatalytic behaviour will be outlined with particular attention to formaldehyde oxidation on gold in base; some data for nitrate reduction will also be presented to show that hydrous oxides, in other instances, can play an inhibiting role. This section may be viewed as a continuation of earlier work on the electrocatalytic properties of gold carried out in this laboratory [351]. In this earlier work by Burke and Cunnane [351] oxidation of organic species, e.g. ethylene glycol and pyrrolidine, in base

was shown to coincide with the Au*/Au(III) hydrous oxide transition. These reactions were assumed to occur via an interfacial cyclic redox with the $[Au_2(OH)_9]^{3-}$ species acting as the mediator, viz.

$$2Au^* + 9OH^- = [Au_2(OH)_9]^{3-} + 6e \quad (3:1:6)$$

$$[Au_2(OH)_9]^{3-} + \text{organic material} = 2Au^* + \text{oxidation products} \quad (3:1:7)$$

3.2. RESULTS

3.2.1. Anodic Behaviour of Gold in Base

A typical voltammogram for gold in base solution is shown in Fig. 3.1. As previously reported by other authors [350,351]] surface oxidation apparently commenced just above 1.36 V(RHE) on the anodic sweep which may be attributed to conventional monolayer oxide, Au_2O_3, or hydroxide, $Au(OH)_3$, formation [215]. This anhydrous deposit was reduced on the subsequent cathodic sweep at ca. 1.1 V(RHE) with full reduction apparently achieved by ca. 0.96 V. However, many minor transitions, labelled here A to E, are also indicated in this diagram. These lower transitions gave rise to very low and variable responses at A, ca. 0.1 V; B, ca. 0.35 V; C, ca. 0.65 V; D and E, ca. 1.1 V.

Fig. 3.2 also shows a cyclic voltammogram for gold in base solution - in this case using reduced limits (-0.1 to 0.4 V). However, the gold electrode was preanodized at ca. 1.6 V for 5 minutes prior to recording the cyclic voltammogram at a quite fast sweep-rate (500 mV/s). A significant decrease in peak height was observed on repetitive cycling; only the first, second and tenth cycle are shown here. The peak involved here is assumed to correspond to A in Fig. 3.1. The cathodic response here is quite broad, i.e. the peak extended over a considerable range of potential.

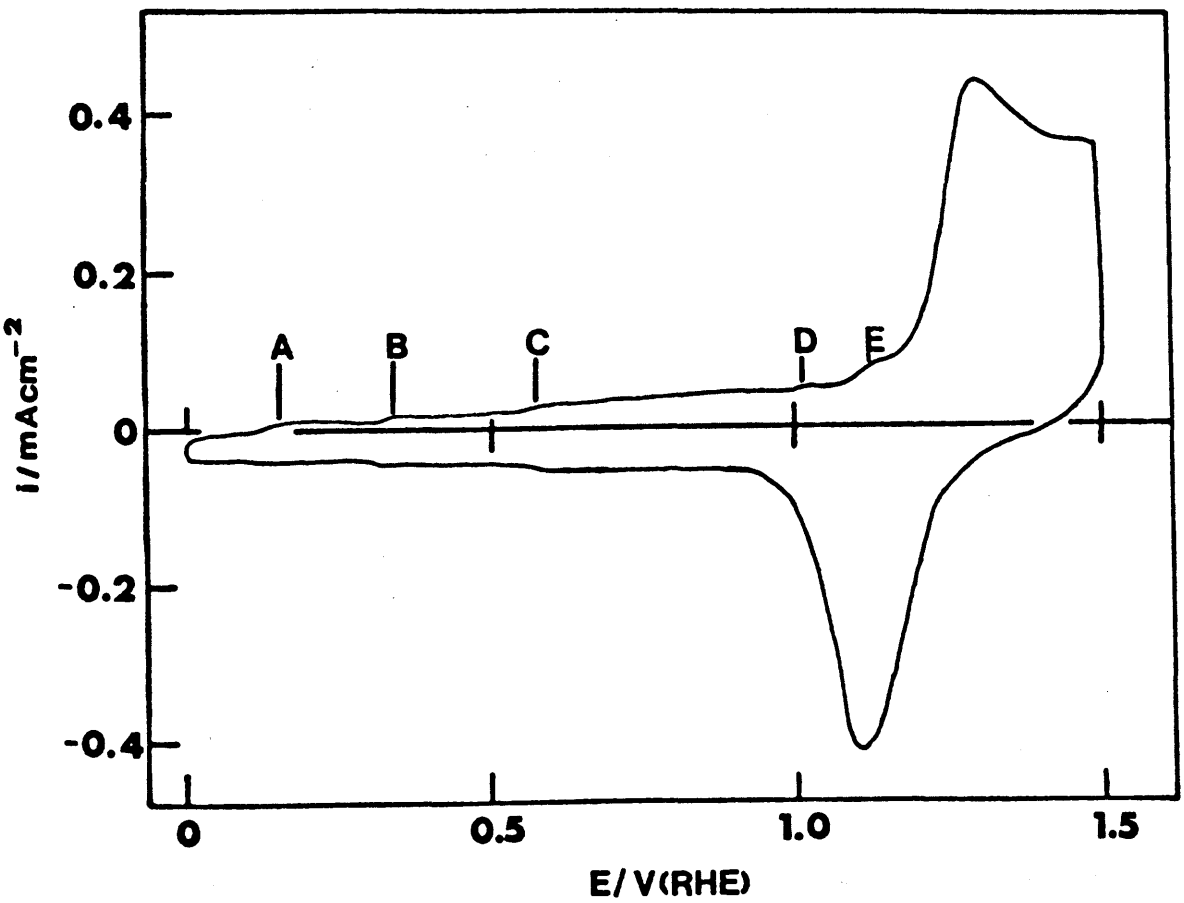

Figure 3.1: Cyclic voltammogram (0.0 to 1.5 V, 50 mV s^{-1}) for gold in N_2-stirred 1.0 mol dm^{-3} NaOH, T = 20°C.

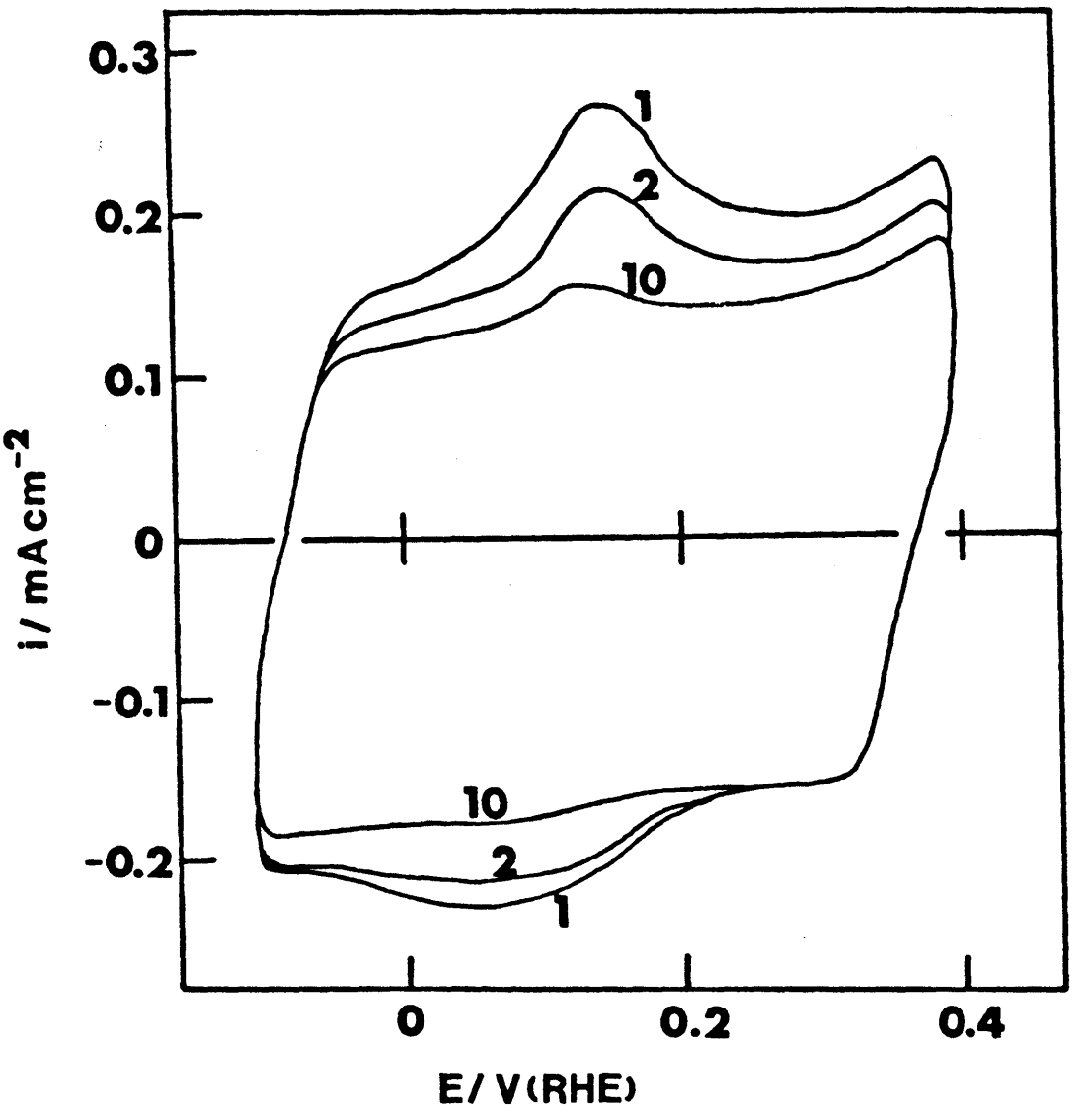

Figure 3.2: Cyclic voltammograms for gold in base: same conditions as in Fig. 3.1 except at reduced limits (-0.1 to +0.4 V) and a faster sweep-rate (500 mV s^{-1}). The electrode was preanodized at 1.60 V for 5 min: the first, second and tenth cycle are shown.

3.2.2. Participation of Incipient Hydrous Oxide Au(I) Species in Electrooxidation and Electroreduction Processes.

Some typical examples of formaldehyde oxidation on gold in base are shown in Fig. 3.3. At all concentrations reaction commenced (anodic sweep) and terminated (cathodic sweep) at ca. 0.1 V. In most cases the current, on the anodic sweep, rose to a plateau. However, in the region of ca. 0.4 V a further increase in current was usually observed. At low formaldehyde concentration this again was followed by a further plateau which extended up to the start of the regular monolayer-type oxide formation region at ca. 1.15 V. For very low formaldehyde concentration, Fig. 3.3(a), the oxide formation peak was still evident - the recorder sensitivity was usually quite high in this case as the net oxidation was low. However, as the formaldehyde concentration was increased the main feature at high potentials on the anodic sweep was the drop in current occurring at the potential where the monolayer oxide commenced of the gold surface - see, e.g. Fig. 3.3(e).

On the subsequent cathodic sweep the surface reactivated for formaldehyde oxidation when the oxide layer was removed. It can be seen that as the oxide layer was removed in Fig. 3.3(a) vigorous formaldehyde oxidation recommenced but at this low bulk concentration the current dropped and a portion of the oxide removal peak reappeared at ca. 1.0 V. At higher formaldehyde concentration values no indication of this main oxide removal step was evident. At intermediate formaldehyde concentrations, Figs. 3.3, (b)-(d), a high oxidation current was observed in the oxide layer removal region.

In many cathodic sweeps, Figs. 3.3, (c)-(e), an increase in surface activity for formaldehyde oxidation was observed over the range 1.0 to 0.5 V. This was followed by a plateau before current dropped to terminate at ca. 0.1 V. In (a) and (b) in Fig. 3.3 the oxidation currents below 0.5 V are significantly lower on the cathodic sweep.

As outlined in Fig. 3.4 the plateau currents for the anodic sweep were virtually a linear function of formaldehyde

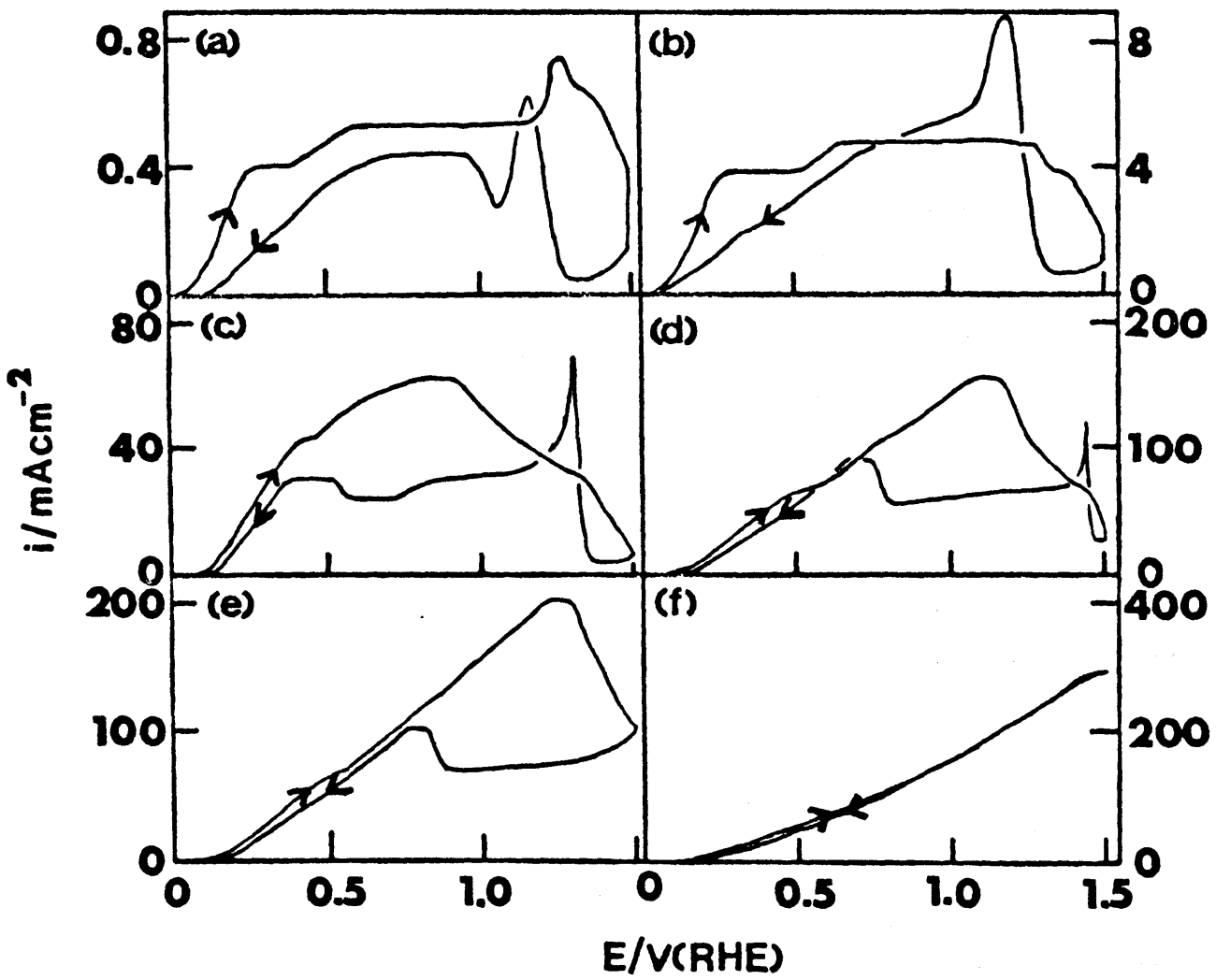

Figure 3.3: Cyclic voltammograms (0.0 to 1.5 V, 50 mV s^{-1}) recorded for gold in unstirred 1.0 mol dm^{-3} NaOH + increasing concentration of formaldehyde, T = 20°C: HCHO concentration (mol dm^{-3}): (a) 0.01, (b) 0.06, (c) 0.30, (d) 0.50, (e) 0.60, (f) 0.70. The data shown here refer, in each case, to the third cycle.

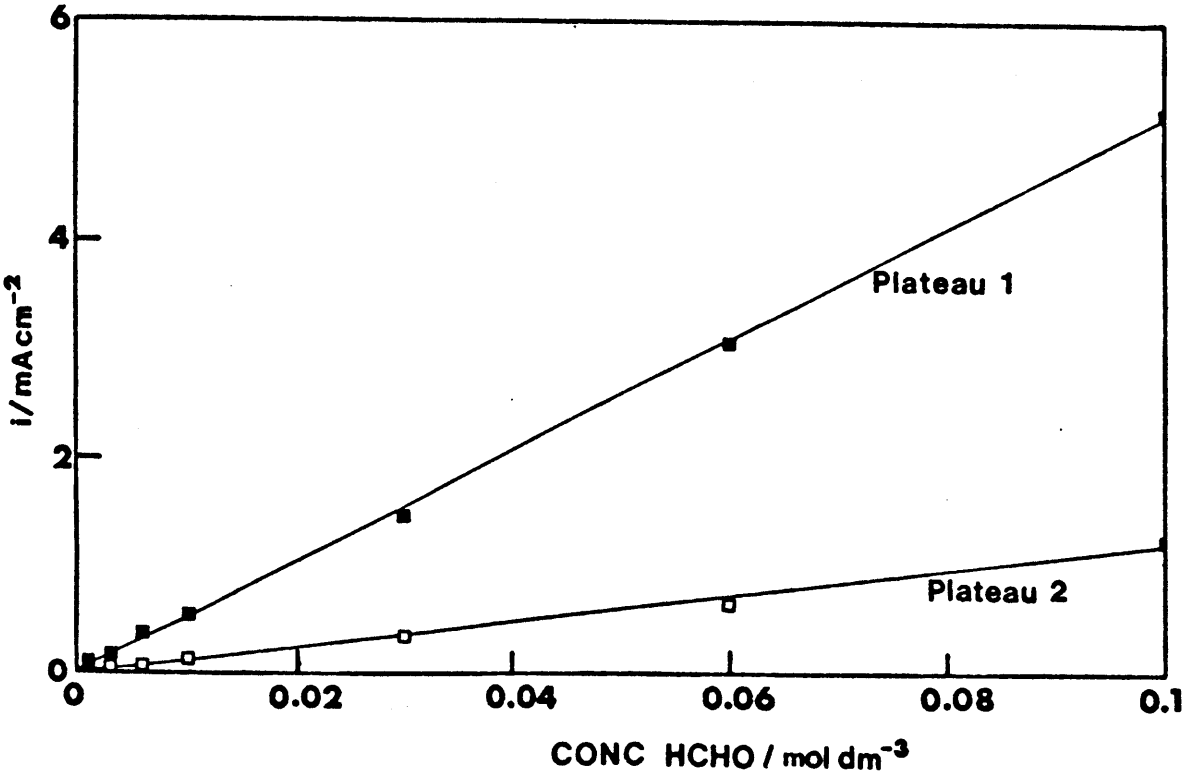

Figure 3.4: Variation of the plateau currents (at ca. 0.3(1) and 0.8 V(2) - see Fig. 3.3(a)) with formaldehyde concentration for gold in 1.0 mol dm^{-3} NaOH at 20°C. The values were taken from voltammograms (0.0 to 1.5 V) recorded at 50 mV s^{-1}. Plateau 1 values were measured from the current baseline while plateau 2 values were measured as the difference from plateau 1.

concentration, at least up to the value of the latter of ca. 0.5 mol dm^{-3} HCHO. The current values for plateau 1 in Fig. 3.4 were measured with respect to the base line (i = 0) while the values for plateau 2 in Fig. 3.4 were taken as the difference in current values between the two plateaus. The behaviour at higher concentrations is uncertain as well defined plateaus are not observed under such conditions.

A typical cyclic voltammogram for nitrate reduction on gold in base is shown in Fig. 3.5. Significant nitrate reduction currents were observed only below ca. 0.15 V. The response for NO_3^- (or HNO_3) reduction on gold at low pH is shown in Fig. 3.6; reduction in this case became significant only below -0.1 V.

3.3. DISCUSSION

In the cyclic voltammogram for gold in base there are quite a number of minor transitions, A-E in Fig. 3.1, prior to the onset (at ca. 1.2 V) and removal (at ca. 1.1 V) of the regular monolayer oxide. Although the level of response for any of these minor transitions is quite low (and rather variable), there is independent evidence for their presence, viz.

A: This transition can be more clearly observed on incresing the sweep-rate (Fig. 3.2); a reversible peak (showing some hysteresis) appears at ca. 0.1 V. Independent evidence for this transition is provided by the work of Kirk and coworkers (peak A in Fig. 2, [360], is at ca. -1.0 V(SCE) which corresponds to ca. +0.05 V(RHE) for the pH in question). Other indications of a reversible transition at ca. 0.05 V are evident in work by Kita and coworkers (see Fig. 6(b) in [371]) and Burke and coworkers (see Fig. 5 in [372]). The minor peak is visible even on the cathodic sweep; thus some reaction, possibly an Au/Au(I) transition, occurs at low potentials. In some cases it is possible that the Au(I) species is stabilised by complex formation with CO [371] or pyridine [372].

B: A small increase in current may be observed at ca. -0.35 V on the anodic sweep in Fig. 3.1. A distinct cathodic peak in the same region was observed by Burke and Hopkins (Figs. 8 and 9 in [371])

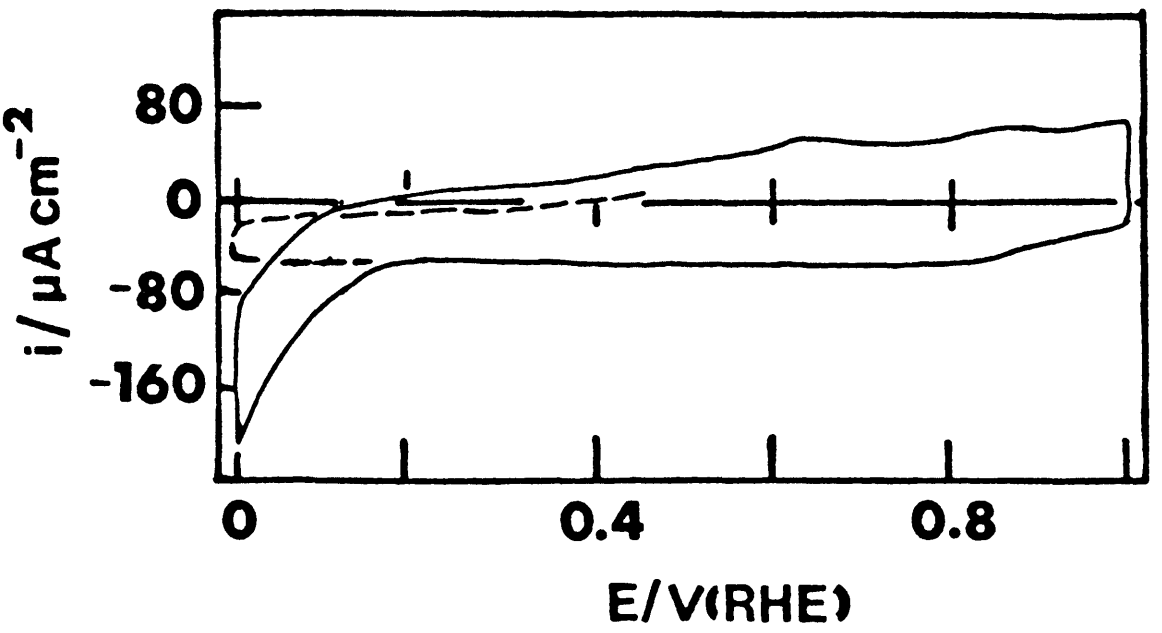

Figure 3.5: Cyclic voltammogram (0.0 to 1.0 V, 100 mV s^{-1}) in N_2-stirred 1.0 mol dm^{-3} NaOH containing 1.1 mol dm^{-3} $NaNO_3$ at 20°C: the dashed line indicates the behaviour of gold in the absence of nitrate (the cathodic current at low potential in the latter is assumed here [255] to be due to the presence of some subsurface oxygen).

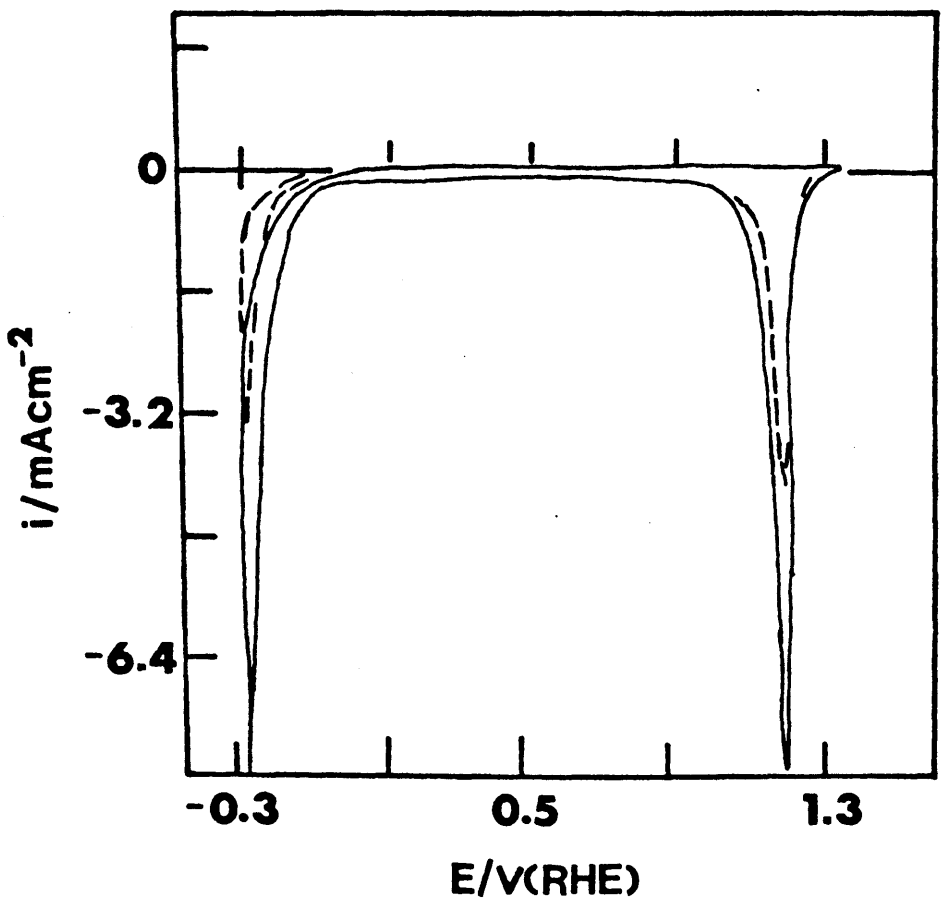

Figure 3.6: Cyclic voltammogram (0.0 to 1.6 V, 100 mV s^{-1}) for gold in N_2-stirred 1.0 mol dm^{-3} H_2SO_4 (----) and 1.0 mol dm^{-3} H_2SO_4 + 0.1 mol dm^{-3} HNO_3 (———) at 20°C.

during the reduction of thick hydrous gold oxide films in base. A similar peak at ca. 0.33 V was reported more recently [351] when thick gold oxide films were reduced at a slow sweep-rate in pyridine-containing base.

C: As discussed in the introduction to this chapter, there is ample evidence by Conway andcoworkers [365], Gonzales-Velasco and Heitbaum [367], Burke and Cunnane [351] and many other workers [358-360] for a transition at ca. 0.65 V for gold in base. As already mentioned, this may be due to formation of an hydrous oxide species at adatom sites on the metal surface, viz.

$$2Au^* + 9H_2O = [Au_2(OH)_9]^{3-} + 9H^+ + 6e \qquad (3:3:1)$$

D and E: A peak (or two peaks in some instances in the present work) was observed just prior to regular monolayer oxide formation at ca. 1.1 V - see the dashed line for gold in ClO_4^--free base in Fig. 1 [367], (in fact the minor peaks at ca. 0.1, 0.65 and 1.2 V for gold in NaOH are quite clear in the latter diagram). Two peaks in the upper region in question have also been reported by Adzic and coworkers (Fig. 4 in [255]) for Au(100) single crystals in organic-free NaOH solution.

The other, more indirect, evidence for these transitions at low potentials is the onset of electrocatalytic processes at the various potentials quoted above. This aspect will be dealt with in the next section. The basic question at this stage is why the magnitude of these lower peaks are so small and variable and what reactions or processes are involved.

It is assumed here that special, adatom sites are involved and that at least in the case of A, and possibly B, an Au/Au(I) transition occurs. At ca. 0.1 V those metal adatoms protruding from the surface, and virtually surrounded by solvent species, are assumed to ionise according to the following reaction

$$Au.xH_2O = Au^{+1}.OH^-(x-1)H_2O + H^+ + e \qquad (3:3:2)$$

The response is low because the adatom state (Au*) is of high energy and most of the metal atoms at the interface revert readily

to a high bulk lattice metal coordination state (Au_l). This latter reaction, viz.

$$Au^* \rightleftharpoons Au_l \qquad (3:3:3)$$

explains why on repeated cycling in the low potential region the response (Fig. 3.2) decreased with time or number of cycles. The process at B in Fig. 3.1 also gives a low response: the same reaction, equation (3:3:2), may be involved but a slight difference in site geometry and energy is assumed to shift the potential from ca. 0.1 to 0.35 V - the possibility of formation of an Au(III) species at the latter value cannot, at present, be definitely disproved. Other features to be borne in mind are the effect of cycling to the high anodic limit (Fig. 3.1) which may not only roughen the surface, i.e. increase the Au adatom concentration on subsequent reduction, but introduce subsurface oxygen into the metal - the possibility of subsurface oxygen is considered in more detail in the present thesis in connection with the work on silver. Some minor dissolution of the product formed on oxidation is also possible (most of these lower anodic peaks for Au in pure base have cathodic counterparts [367] but - as the shapes differ - it is difficult to decide if the magnitudes for formation and removal are exactly equal). Finally, it is clear that the process represented by equation (3:3:2) could also be considered as a form of adsorption process - accompanied by charge transfer.

Before considering electrocatalytic processes at gold in base at low potentials, it is worth considering briefly the interaction of non-reacting organic molecules, e.g. pyridine, in this region, as mentioned under A above. Such molecules also give rise [351,374] to a reversible peak (or peaks) at low potentials (0 to 0.2 V). The SERS technique has been applied here [374] and this pronounced optical effect is first observed on the anodic sweep only at the potential corresponding to the first (minor) anodic peak. Unlike other systems, e.g. silver, the SERS effect for pyridine on gold in base is not totally quenched at very negative potentials, i.e. the active sites on gold are retained to a significant degree. It has been suggested [372] that the reason why the SERS effect is so pronounced with the Gp. 1(b) metals (Cu, Ag and Au) is that these readily form the +1 state which, because

of the low charge on the cation, do not strongly bind the OH^- counterion and thus permit the organic ligand to interact directly with the surface cation in the presence of a strong electric field. It is also noteworthy that Ca^{+2} ions ($c = 2 \times 10^{-5}$ mol dm^{-3}) in base (0.1 to 1.0 mol dm^{-3} NaOH) commence to adsorb [375] on gold in the region of the lower peak (A in Fig. 3.1). As the authors point out, this cannot be direct cation adsorption (the adsorption increases with increasing positive potential - the opposite of what one would expect for cationic species). It is suggested that the gold adatoms are oxidised to the Au^+ state at one plane; outside this (and possibly solvent separated from it) are the OH^- counterions - it is into the latter region that the highly charged Ca^{+2} ions are assumed to be attracted by electrostatic forces. Also relevant here is the fact that the Ca^{+2} uptake is time dependent: the charge, or Au^{+1} concentration, at the interface apparently increases with time presumably as some surface metal atoms transform to the adatom - and then the Au(I)-state. Thus, in electrocatalysis involving such species the concentration of active sites may be both potential and time dependent.

The current/voltage behaviour for formaldehyde oxidation on gold in base (Fig. 3.3) shows the coincidence between the onset (anodic sweep) and termination (cathodic sweep), at all concentrations, at ca. 0.1 V, i.e. in the region of the lower anodic peak represented by A in Fig. 3.1. This is a prime requirement of the interfacial surface redox cyclic mechanism outlined earlier (section 1.8). Electrooxidation evidently cannot occur at a potential below which the oxidized (Au^{+1}) state cannot exist. The fact that the current rises to a plateau, in most cases, on the anodic sweep is also expected in terms of either a kinetic or diffusion controlled step. The further increase at ca. 0.4 V is apparently due to the intervention of a new surface redox process corresponding to the minor increase in current shown as B in Fig. 3.1. Deactivation of the gold surface towards formaldehyde oxidation occurs above ca. 1.15 V - the onset potential for the formation of regular, anhydrous oxide. This is not seen in Fig. 3.3, (e) and (f), presumably because the aldehyde concentrations in these cases are so high that little monolayer oxide can exist even at 1.5 V - especially in (f).

As soon as the monolayer oxide begins to be removed on the subsequent cathodic sweep at ca. 1.3 V, Au adatoms become available at the gold surface. The adatoms can undergo redox transitions and hence reactivate the gold surface towards formaldehyde oxidation. At high formaldehyde concentrations the oxide may well be removed by direct reaciton with the organic species - although this type of reaction probably also involves an electrochemical route [376]. At intermediate formaldehyde concentrations, Fig. 3.3, (b) to (d), a high oxidation current observed in the oxide layer removal region indicates that as the monolayer oxide material is reduced a high, but transient adatom concentration or activity is generated.

The increase in current, evident in several of the cathodic sweeps between 1.0 and 0.5 V, indicates an increase in surface activity. This is probably due to reduction of some Au(III) hydrous oxide sites, which occurs, C in Fig. 3.1, at ca. 0.65 V. The Au/Au(I) cycle is assumed to be more active than the Au/Au(III), or Au(I)/Au(III), for aldehyde oxidation because the OH^- ion is not easily displaced from the more highly charged Au(III) centres. This effect is not observed in Fig. 3.3(f) because the monolayer oxide, high adatom concentration, and Au(III) hydrous oxide - in this sequence - are not formed to a significant extent under these conditions.

The above outline of formaldehyde oxidation on gold in base confirms the work of other authors. Beltowska-Brzezinska and coworkers [254,377], Enyo [378], and Adzic and coworkers [255] have all pointed out that formaldehyde oxidation on gold in base commenced at ca. 0.05 V(RHE) and anodic sweeps showing two plateaus are shown in several instances [254,377]. The work of Sibille and coworkers [379], and Van Effen and Evans [380] is also significant as it shows the potential of onset of aldehyde oxidation on Au in base is virtually independent of the nature of the aldehyde - again as is required by the interfacial redox model. Kita and coworkers (see Fig. 5(b) in [371]) have shown that carbon monoxide also commences to oxidise in base at ca. 0.05 V(RHE). In addition, on allowing the gold electrode to age in base at -0.1 V for 12 min. the onset of the CO oxdiation was observed to shift anodically to ca. 0.55 V(RHE). These reactive organic compounds seem to form complexes with the Au(I) species by acting as Lewis bases and are

evidently activated with respect to oxidation by the process. Hence, the aging at -0.1 V [371] for the CO case outlined above leads to a lowering of the activity for the CO oxidation as it allows the adatoms more time to be incorporated into regular surface lattice positions so that little of the Au(I)/CO complex (a vital ingredient in the interfacial redox cycle at 0.05 V(RHE)) is generated at the interface during the subsequent anodic cycle. Under such circumstances the onset of CO oxidation shifts anodically to the Au/Au(III), incipient hydrous oxide formation, region.

Other organic compounds which cannot act as Lewis bases, and hence cannot form activated complexes with the Au(I) state (which is a Lewis acid), commence oxidation in the region of the incipient hydrous oxide transition, i.e. Au/Au(III). Hence, compounds such as methanol [381], mesoxalate [382], 1,2-propanediol [383], pyrrolidine and piperidine [351] all commence and terminate oxidation at ca. 0.65 V(RHE) on gold in base, i.e. process C in Fig. 3.1. The mechanism of such oxidations, where the $[Au_2(OH)_9]^{3-}$ species is used as the mediator in a cyclic redox fashion, is dealt with in detail by Burke and Cunnane [351].

An example of the different reactivities for gold in 0.1 mol dm^{-3} NaOH was provided recently by Larew and Johnson [426] for the oxidation of glucose and its derivatives. Aldehyde group containing compounds, e.g. glucose, glucuronic acid and 2-deoxy-D-glucose, commenced oxidation at ca. -0.7 (SHE), i.e. ca. +0.05 V(RHE). However, compounds void of aldehyde groups, e.g. gluconic acid and glucaric acid, commenced oxidation at ca. -0.2 V(SHE), i.e. ca. +0.55 V(RHE). This behaviour highlights the fact that compounds which are capable of acting as Lewis bases, and hence forming activated complexes with the Au(I) state, commence oxidation in the region of peak A in Fig. 3.1, while other organic compounds commence oxidation at a potential which coincides with the hydrous oxide transition, peak C in Fig. 3.1. The behaviour of the current with increasing glucose concentration, i.e. an initial increase followed by a plateau region, is also as expected by an interfacial cyclic redox mechanism.

The work related to the oxidation of formaldehyde in base by Beltowska-Brzezinska and coworkers [254,377], not only for gold but also platinum and platinum/gold alloys, is important. These two metals have significantly different electronic properties and one would expect a much lower rate of oxidation on gold - especially in terms of the activated chemisorption model for electrocatalysis - as gold in only a weakly chemisorbing metal. However, in 1.0 mol dm^{-3} NaOH the oxidation rate at -0.4 V(SCE), or ca. +0.6 V(RHE), is ca. 0.6 mA cm^{-2} on Pt and ca. 4 mA cm^{-2} on Au: the conditions quoted for these data (Figs. 1 and 3 in [377]) are not quite identical but they illustrate the unusual activity of gold which cannot be explained in terms of the conventional activated chemisorption model of electrocatalysis.

The initial oxidation product formed according to equation (3:3:2) on the gold in alkaline electrolyte is a strong base; the OH^- ion is not strongly held at the Au^+ site and strong interaction occurs between the latter, which is a Lewis acid, and the gem-diolate anion (a Lewis base) produced by interaction of HCHO with a hydroxide ion in bulk solution, viz.

$$HCHO_{aq} + OH^-_{aq} = H_2CO^-.OH_{aq} \qquad (3:3:4)$$

$$H_2CO^-.OH_{aq} = H_2CO^-.OH_{ads} \qquad (3:3:5)$$

There are two routes for further reaction, one predominating at the start of the first current increase, viz.

$$H_2CO^-.OH_{ads} + OH^- = HCOO^-_{aq} + H_2O + \tfrac{1}{2}H_2 + e \qquad (3:3:6)$$

and the other at higher potentials, viz.

$$H_2CO^-.OH_{ads} + 2OH^- = HCOO^-_{aq} + 2H_2O + 2e \qquad (3:3:7)$$

The release of hydrogen gas (equation (3:3:6)) under anodic conditions is an interesting phenomenon (it supports the view that gold metal is not a good catalyst in the chemisorption mode): however, release of this gas is not observed beyond the end of the first wave [254,377]. Kinetic isotope studies [380] indicate that aldehyde oxidation on gold involves cleavage of a carbon-hydrogen

bond in the rate-limiting step - hence the linear variation (Fig. 3.4) of the plateau currents with aldehyde concentration (although diffusion control may also be important [254] at this point). This does not conflict with the idea that incipient surface oxidation is important as such cleavage is assumed to occur only at Au(I) sites, i.e. it is the generation of the latter that triggers the organic oxidation reactions.

The oxidation of formaldehyde at the gold/solution interface is quite fast - possibly in some cases diffusion controlled [254]. However, it is assumed here that only a small fraction of surface sites, i.e. adatom or Au(I) centres, are effective. If on reaching ca. 0.35 V on the anodic sweep (B in Fig. 3.1) a new type of Au(I) centre is generated then the second increase in current in this region observed here in many cases, even at relatively slow sweep-rate (Fig. 3.3), is understandable. In terms of the interfacial redox model the surprising feature in the present work was the lack of an increase in current on the anodic sweep above ca. 0.7 V, i.e. above point C in Fig. 3.1 where the Au/Au(III) hydrous oxide transition is known to occur, and where other organics, e.g. pyrrolidine and piperidine [351] are known to oxidise strongly. Initially the second increase in current in Fig 3.3 was assumed to be due to this transition, but the onset potential is clearly too low. In fact the strong binding of OH^- ions at Au(III) centres appears to have an inhibiting effect in the case of formaldehyde whose oxidation seems to occur by an inner sphere mechanism. Another factor involved in the inhibition may be the anionic character of the gem-diolate which will give rise to repulsion at the anionic hydrous gold oxide, $[Au_2(OH)_9]^{3-}$ [217], species at the interface (pyrrolidine and piperidine, on the other hand, are neutral bases and such repulsion is far less).

The gradual disappearance of the plateau after the first peak with increasing formaldehyde concentration (Fig. 3.3) is evidently due to the effect of the increasing current on the overpotential associated with the reaction giving rise to the first peak. At high values for the oxidation current (or HCHO concentration) just above the first surface transition the potential becomes so anodic (due to the incresed overpotential) that as it reaches the limiting value or plateau it coincides with or exceeds the value for the

start of the second plateau, i.e. both processes merge at high concentration, Fig. 3.3(f), to give a smooth continuous current increase.

The behaviour of formaldehyde on gold in acid, as compared with base, is worth considering. At low pH this compound does not oxidise [384] below ca. 0.8 V, i.e. its oxidation commences at a potential corresponding to the onset of Au(III) hydrous oxide formation. The trivalent state is more active at low pH due to the low OH^- ion activity while formaldehyde in acid is assumed to be present in the neutral - rather than in the gem-diolate, anionic-form. There is no oxidation due to Au(I) species in acid because, as shown by Burke and coworkers [372], the Au/Au(I) transition occurs well below 0 V at low pH, i.e. the HCHO is thermodynamically unable to reduce Au(I) species (if the latter do exist) at adatom sites under such conditions.

Although nitric acid and nitrate anions are strong oxidising agents, unstable with regard to reduction at pH = 0 below ca. 1.26 V [352], their reduction, even with active cathode materials, e.g. Pt, is highly inhibited (an overpotential of 1.5 V has been mentioned [385]); prior to the present work of the origin of the inhibition was not clear. At pH values significantly above zero the reduction may be represented [352] as

$$2NO_3^- + 12H^+ + 10e = N_2 + 6H_2O \qquad (3:3:8)$$

- although a range of products, including nitrous acid, ammonia and hydroxylamine [386], can be produced. It is clear from Fig. 3.5 that with gold in base significant nitrate reduction currents are observed only below ca. 0.15 V, i.e. below peak A in Fig. 3.1. It appears that nitric acid reduction occurs only at highly reactive adatom (Au*) sites which are easily deactivated by incipient oxidation according to equation (3:3:2). NO_3^- (or HNO_3) reduction on gold at low pH is even more inhibited; as shown in Fig. 3.6 hydrogen evolution currents on gold become significant at ca. -0.25 V but reduction in the prsence of NO_3^-/HNO_3 becomes significantat ca. -0.1 V. This increased inhibition of nitrate species reduction on lowering the solution pH is again in agreement with the incipient surface oxidation model because, as demonstrated

earlier [372], the potential of the Au/Au(I) transition decreases significantly on lowering the pH. In fact the inhibition at low pH is expected to be appreciably larger than observed here but a number of factors must be considered: (1) the current in acid, even in the presence of NO_3^-, may be predominantly hydrogen gas evolution (promoted by the presence of NO_3^-); (2) the presence of a trace of hydrogen on the surface may effect the Au/Au(I) potential; (3) the overpotential in acid is so great (due to the absence of unoxidised Au* sites) that a new route (involving, for instance, less active surface species) for NO_3^- reduction may operate.

Collaboratory evidence that reduction at gold in base occurs via the incipient cyclic redox mechanism was obtained by Nishihara and Shindo [387] in their work on nitrobenzene. After polishing the gold electrode - a process which causes the formation of adatoms at the interface - two reduction waves were obtained on a current-potential curve for nitrobenzene in 0.1 mol dm^{-3} KOH. The half-wave potentials, one at ca. -0.7 V and the other at -1.0 V(SCE), i.e. +0.35 and +0.05 V(RHE), respectively, correspond aproximately, to the potentials of processes A and B in Fig. 3.1. However, upon either holding the potential of the electrode at -2.0 V(SCE), i.e. ca. -0.95 V(RHE), or cycling the electrode in the sample solution, between -0.4 and +0.5 V(SCE), i.e. +0.65 and +1.55 V(RHE), for an extended period - both techniques which lead to a greater degree of hydration of adatoms and hence the formation of the $[Au_2(OH)_9]^{3-}$ species as in equation (3:3:1) - a single wave was obtained commencing at ca. -0.5 V(SCE), i.e. +0.55 V(RHE), just below the Au/Au(III) transition potential at C in Fig. 3.1. This behaviour is analogous to the case of Kita and coworkers [371] outlined earlier for CO oxidation in relation to aging the electrode at low potentials. Plateau regions were observed [387] at potentials cathodic to potentials where processes A, B and C in Fig. 3.1 occur for the nitrobenzene reduction as would be expected in the present mechanism.

3.4. CONCLUSIONS

Detailed investigation of the voltammetric behaviour of hydrous oxides of the noble metals is a relatively novel area and the involvement of such species in the electrocatalytic behaviour of gold was outlined earlier [351] in terms of the Au/Au(III) hydrous oxide couple. These species are produced in such small amounts under normal anodic sweep conditions that both their formation and participation in interfacial processes is easily overlooked. In the present work evidence for two additional, possible Au(I), species in base is provided and these are used to rationalise the unexpectedly high activity of gold at high pH for the oxidation of certain compounds, e.g. aldehydes and CO [351]. The low coverage of such species at the interface is rationalised in terms of the requriement of a high degree of metal atom hydration at the interface before the hydrous oxide species, Au(I) or Au(III), can be generated. The connection between the present work and SERS has been briefly mentioned here and, for work with the Gp. 1(b) metal electrodes (Cu, Ag and Au), this technique has interesting possibilities. Indeed it has already provided evidence [388] for the formation of hydroxy species on gold in base at potentials well below the onset of (and differing substantially in character from) the regular monolayer oxide product.

The nitric acid work outlined here demonstrates another important aspect of incipient hydrous oxide formation, namely inhibition of cathodic procesess at adatom sites. If the latter are oxidised then, despite the large dirving force, species such as HNO_3 or NO_3^- are unable to react as they apparently cannot displace OH or OH_2 groups at the active sites. Once such sites are reduced reaction can commence. Overall, this work shows how the cyclic redox mechanism utilising incipient hydrous oxides provides plausible explanations for all aspects of electrocatalysis at gold - which the activated chemisorption model fails to accommodate.

CHAPTER 4

Silver

4.1. INTRODUCTION

As early as 1908 Luther and Pokorney [389] described a study of the electrochemical behaviour of silver and its oxides. Since then further interest in the system has been generated by the development of silver-zinc and silver-cadminum battery systems (in which silver oxide is used as an anode) and a number of reviews of the area have been written [186,390,391]. Lewis [392] concluded that the only stable components of the system are O_2, Ag and Ag_2O.

The accepted values for the standard potentials exhibited by the various couples involved in electrochemical transitions are [393] given as

$$Ag^+ + e = Ag \qquad E^o = 0.799\ V \qquad (4:1:1)$$

and

$$Ag^{2+} + e = Ag^+ \qquad E^o = 1.98\ V \qquad (4:1:2)$$

A number of workers have also determined the potential of the Ag/Ag_2O couple [389,394]

$$Ag_2O + H_2O + 2e = 2Ag + 2OH^- \qquad E^o = 1.173\ V \qquad (4:1:3)$$

and the potential of the Ag_2O/AgO couple is given as

$$2AgO + H_2O + 2e = Ag_2O + 2OH^- \qquad E^o = 1.398\ V \qquad (4:1:4)$$

Most investigations of the system have been performed by means of constant current charging curve techniques. A typical curve is illustrated below for silver in 1.0 mol dm^{-3} NaOH. From simultaneous x-ray diffraction studies, Wales and Burbank [395] concluded that Ag_2O was formed during the first region (a) and AgO during the first plateau (c). Other x-ray [396], electron diffraction [397], and chemical [398] analyses appear to be in agreement with these assignments. The first plateau, (c), is preceded by a small, but distinguishable, peak (b) for which various explanations have been offered. Hickling and Taylor [399] ascribed it to the formation of an oxide higher than AgO which decomposes to give the latter; Jones et al. [400] suggested that it might be due to a difficulty associated with AgO nucleation in

the Ag_2O layer, and third suggestion, by Dirske, [401] attributed it to a maximum ohmic potential drop associated with a complete film of Ag_2O.

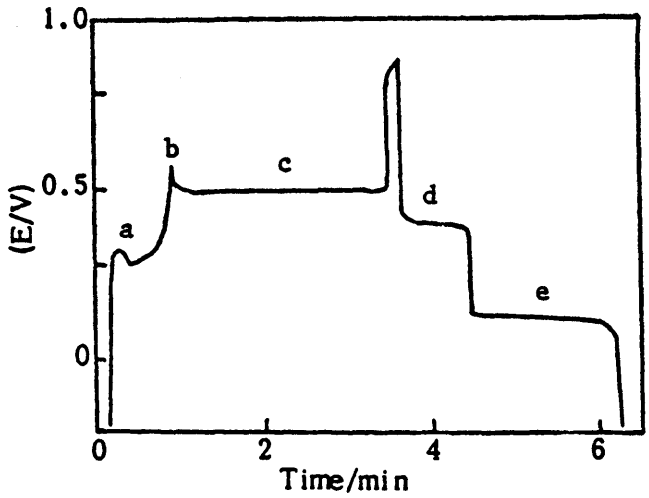

Typical charging curve of reformed silver in 1.0 mol dm^{-3} NaOH. Oxidation at 0.95 mA, reduction at -1.05 mA, electrode area 0.2 cm^2 [410].

On discharge, the potential immediately drops to a short plateau (d) where AgO is reduced to Ag_2O [395]. Transition from this plateau to the subsequent larger one (e) involving an Ag_2O/Ag reduction appears to occur [395,398] before complete AgO/Ag_2O conversion has taken place, hence both reactions occur simultaneously at the lower potential value, a layer of Ag_2O always covering that of AgO [186,395].

In the charging situation, it may be noted that most of the oxide is deposited at the Ag_2O/AgO potential, whereas on discharge most of the reduction takes place at the Ag/Ag_2O potential. It has been suggested [402] that the Ag/Ag_2O reaction continues to occur alongside that of the Ag_2O/AgO transition on charging.

The first potential sweep studies of the silver electrode were undertaken by Dirske and DeVries [403] and by Croft [404]. Cyclic voltammograms for the system generally show four oxidation peaks in the anodic sweep and two reduction peaks in the cathodic sweep [405]; a secondary anodic peak is often observed in the early stages of the cathodic sweep. General agreement in the literature

attributes the major anodic peaks to Ag_2O and AgO formation with the cathodic peaks resulting from the corresponding reductions. Minor anodic peaks have been variously attributed to AgOH formation [403], preferential oxidation of an activated lattice [406], or silver dissolution as $Ag(OH)_2^-$ [407]. The activated lattice is favoured by Droog [408] on observation of the differing voltammetric profiles exhibited by the (111) and (110) silver crystal faces, the (110) being much more reactive.

For the formation of AgO from Ag_2O [407] as well as for Ag_2O reduction to Ag [409] an autocatalytic effect has been reported, i.e. upon potential sweep reversal before the current has reached its peak value, a characteristic current increase is observed. This would imply the process to be nucleation-controlled. Recent results [408], however, performed on the Ag (110) face have failed to confirm this phenomenon, thus indicating the process to be perhaps a random rather than nucleation-controlled deposition.

As in the case of gold, many early workers [411-417] reported minor oxidation of silver surfaces at potentials considerably cathodic to the main anodic oxidation region. Shumilova et al. [411] observed waves at ca. 0.35 and 0.75 V during both the anodic and cathodic sweep for voltammograms recorded for silver between 0.1 to 1.1 V, in 1.0 mol dm^{-3} KOH saturated with argon. These waves were attributed to the formation or reduction of two "adsorption compounds" of oxygen. In later work, these authors [412] reported up to five waves during the anodic sweep and three on the cathodic sweep, on variation of the electrode pretreatment. Loobmaa et al. [413], however, assigned the peaks to the removal or formation of a layer of H_{ads}. Both Hamelin et al. [414] and Valette [415] reported peaks within this same region but attribute these peaks to specific ion adsorption about the point of zero charge for silver in base. Bindra and Roldan [416], and Kita et al. [417] also reported the presence of these minor peaks but do not comment on the origins of such features.

4.2. RESULTS

4.2.1. Anodic Behaviour of Silver

A typical voltammogram for silver in base solution is shown in Fig. 4.1(a). As previously reported by other authors [410,418,419], surface oxidation apparently commenced just above 1.0 V (RHE). Three peaks were noted on the positive sweep; according to Stonehart and Portante [407] the first two peaks at $E_{max} \approx 1.24$ and 1.38 V (RHE) are due to Ag(I) formation, possibly AgOH (with perhaps some $Ag(OH)_2^-$ ion formation [409]) and Ag_2O. The third anodic peak with $E_{max} \approx 1.67$ V (RHE) is attributed to formation of AgO; the latter, however, is generally considered [420] to be an equiatomic [Ag(I)Ag(III)] compound. On the subsequent negative sweep in base two reduction peaks were observed. The peak at $E_{max} \approx 1.36$ V (RHE) is attributed to reduction of AgO to Ag_2O, while the peak at $E_{max} \approx 1.09$ V (RHE) is attributed to reduction of Ag_2O to Ag. However, when the same electrode was cycled subsequently between reduced limits (Fig. 4.1(b)), and the current sensitivity of the recorder increased, minor peaks, corresponding to a reversible transition at ca. 0.3 V and a cathodic process at ca. 0 V were observed. Evidently a small fraction of the silver surface is capable of undergoing a reversible redox transition at a quite low potential.

When the voltammetric behaviour of silver in base was examined in greater detail the pattern observed was found to be affected by sweep-rate. Data recorded at slow sweep-rates, showing the effect of electrode pretreatment, are outlined in Fig. 4.2. After nitric acid pretreatment (curve A) cathodic currents were recorded over the entire range - even during the anodic sweep; the transient cyclic voltammetry response was apparently superimposed on a cathodic background current due to reduction of oxygen diffusing to the interface from within the metal where it was inserted earlier during the course of the HNO_3-pretreatment. The ability of oxygen, under oxidising conditions, to penetrate into the bulk silver lattice (or at least the outer regions of the latter) has been demonstrated by the work of Zhutaeva and coworkers [421]. The surface, and subsurface, oxygen or silver oxide species are assumed to play an important role both in the bonding of charged silver

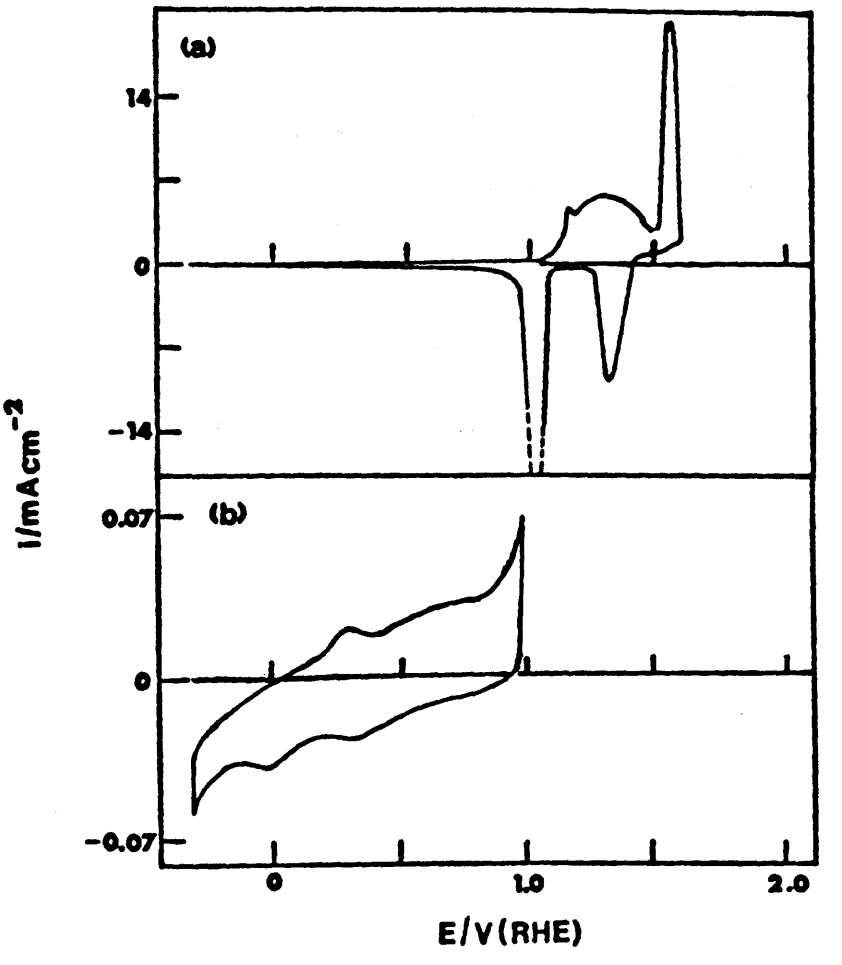

Figure 4.1: Cyclic voltammograms (40 mV s^{-1}) for Ag in 1.0 mol dm^{-3} NaOH (T = 20°C):
(a) -0.3 to 1.6 V;
(b) -0.3 to 1.0 V.

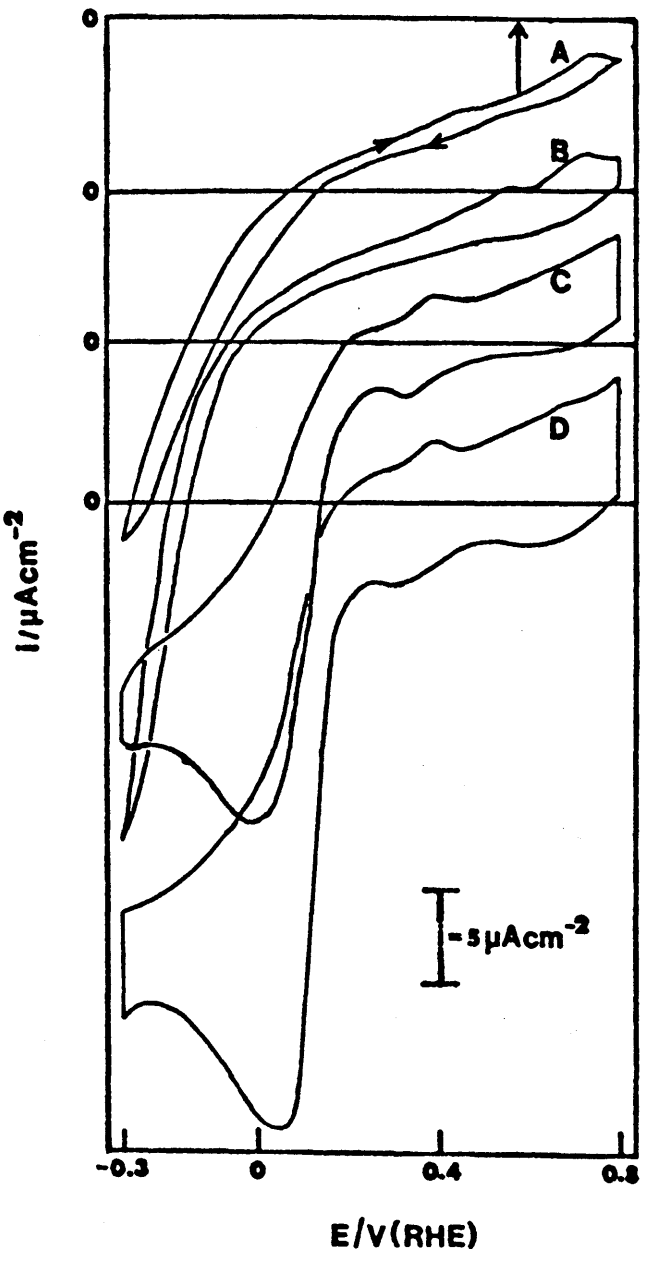

Figure 4.2: Effect of electrode pretreatment on cyclic voltammograms recorded at a slow sweep-rate (10 mV s^{-1}) for Ag in 1.0 mol dm^{-3} NaOH at 20°C: (A) HNO_3-dip, (B) abraded, (C) potential cycled, -0.3 to 1.6 V, 100 mV s^{-1} for 5 min., (D) anodized at 1.6 V for 5 min.

adion species at the surface and modifying the redox properties of the interfacial species, i.e. shifting the potential of the lower peak. Indications of minor peaks at 0.75 and 0.45 V were also just about visible on the anodic sweep (curve A); transitions in the same region for this system have been reported by Bindra and Roldan [416]. After HNO_3 pretreatment and abrasion (curve B) the two peaks on the anodic sweep were slightly enhanced; one was still at ca. 0.75 V but the other was at ca. 0.55 V. After potential cycling pretreatment, using a relatively high anodic limit of 1.6 V, the cyclic voltammetry behaviour (curves C and D) was considerably different. A reversible pair of peaks now appeared at ca. 0.35 V (as in Fig. 4.1(b)) and a cathodic peak (with no anodic counterpart) was observed in the region of OV. There is obviously reduction of some species, most likely subsurface oxygen diffusing to the interface, at the latter potential; this reaction may be catalysed by the deposition of traces of hydrogen on the silver at ca. O V - hence the cathodic peak in this region. The passage of cathodic currents at the early stages of the anodic sweep may also be attributed to the reduction of subsurface oxygen which continues to diffuse to the interface in this region.

The corresponding behaviour at faster sweep-rates is shown here in Fig. 4.3; for clarity only the anodic sweeps are shown here. As the transient currents were larger at faster sweep-rates the voltammograms were more symmetrical about the voltage axis. With a fresh silver electrode (no pretreatment, curve A) two peaks were recorded, one at ca. 0.55 V and the other ca. 0.78 V. This behaviour pattern was significantly modified (in particular the peak at ca. 0.78 V which virtually disappeared) by subsequent treatment of the electrode (e.g. abrasion or acid dip) and, despite considerable endeavour, was never fully restored with a used electrode. As outlined earlier this alteration in the behaviour of silver is probably due to significant oxygen penetration into the outer layers of the metal lattice. Most of the other pretreatments listed in connection with Fig. 4.3 resulted in a drop in the peak potential for the first anodic peak, i.e. one at ca. 0.55 V in curve A. In most cases a distinct increase in anodic current commenced just above 0.2 V.

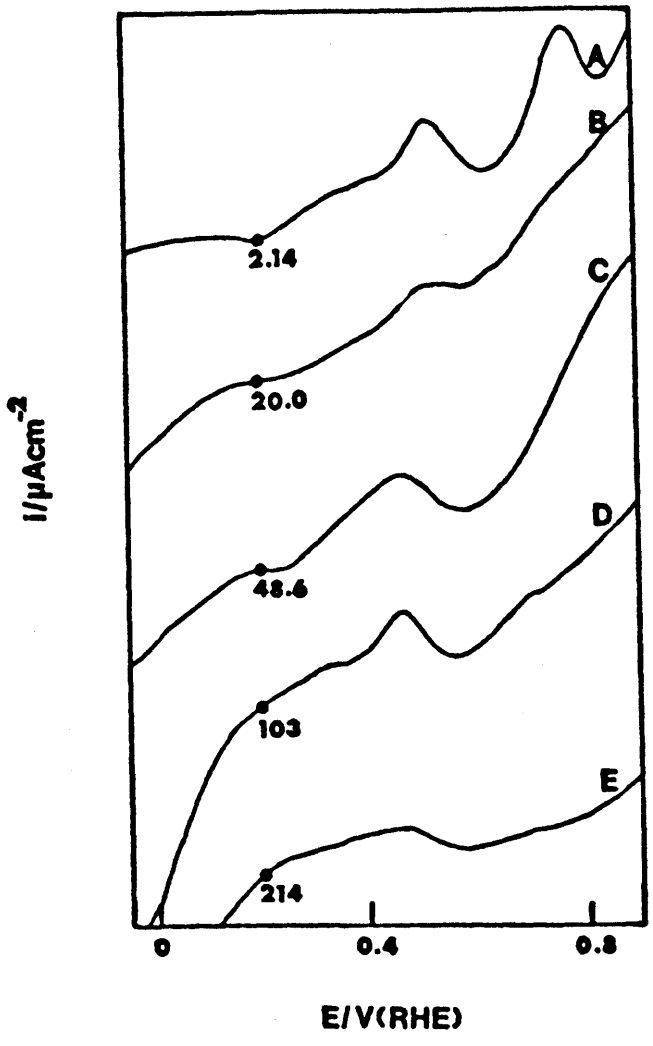

Figure 4.3: Effect of electrode pretreatment on the anodic sweep recorded at a fast sweep-rate (250 mV s^{-1}) for Ag in 1.0 mol dm^{-3} NaOH at 20°C: (A) untreated surface (5), (B) abraded (10), (C) HNO_3-dip (25), (D) potential cycled, -0.3 to 1.6 V, 100 mV s^{-1} for 5 min. (25), (E) anodized at 1.6 V for min. (50) - the figures in brackets here are the current sensitivies (μA cm^{-1}) while the figures in the diagram are the current densities (μA cm^{-2}) at 0.2 V.

It must be borne in mind here that the peaks in question are only minor features on the double layer charging current. They vary in magnitude, and to a lesser extent in peak potential, for electrodes pretreated under similar conditions; in addition, it is difficult to control the magnitude of the peak (the above pretreatments were adopted with this objective in view; peak area, which is a measure of interfacial adatom or adion concentration, would be an interesting variable to study). In some instances, as in the case of gold [351], the lower peak appeared as a poorly resolved doublet on both the anodic and cathodic sweep - this type of behaviour was observed more frequently in the anodic behaviour.

The effect of sweep-rate on the peak potentials of the doublet observed in the lower region is illustrated in Fig. 4.4. The values were virtually independent of the rate of change of potential, indicating that the interfacial redox transition is a rapid, reversible process. This is confirmed by the data shown in Fig. 4.5 where a linear increase in peak current with sweep-rate was recorded. Accurate data for this plot was difficult to obtain as - apart from the high background due to double layer charging currents - peak resolution was not good (especially in the cathodic case); however, the general trend was not in doubt.

As pointed out earlier (section 1.6.7) study of reversible peak potential variation with solution pH, i.e. $\delta E_p/\delta pH$ values, is a very useful technique for the investigation of hydrous oxide behaviour at interfaces. However, it requires the use of buffer solutions which entails the introduction of foreign anion, e.g. sulphate and borate species, and with Group 1(b) metals in general where the binding of the OH^- ligand by M^+ species is not strong [372] these foreign anions can coordinate to cationic species at the interface. Such salt formation reactions were probably the origin of the broad peaks at, or above, 0.4 V in the anodic sweeps recorded for silver in these buffer solutions (Fig. 4.6). The sharp peaks (or doublets) at more cathodic values were attributed here to an Ag/Ag^+ transition without foreign ion interference. It was clear that the E_p values for these lower peaks shifted anodically with increasing solution pH (the same trend was evident when the potential taken was that corresponding to the first major rise in current on the anodic sweep). Some data from these

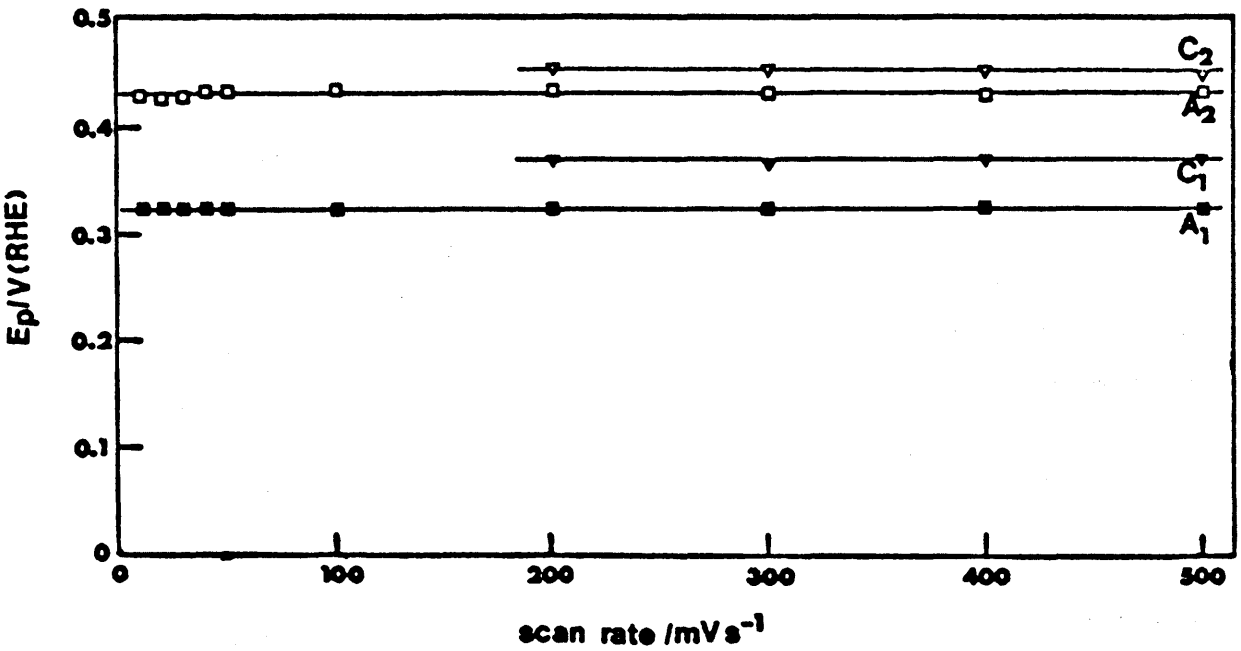

Figure 4.4: Effect of sweep-rate on the peak potentials for Ag in 1.0 mol dm^{-3} NaOH at 20°C; pretreatment, - 0.3 to 1.6 V, 100 mV s^{-1} for 10 min.; analytical scan range, -0.3 to 0.8 V.

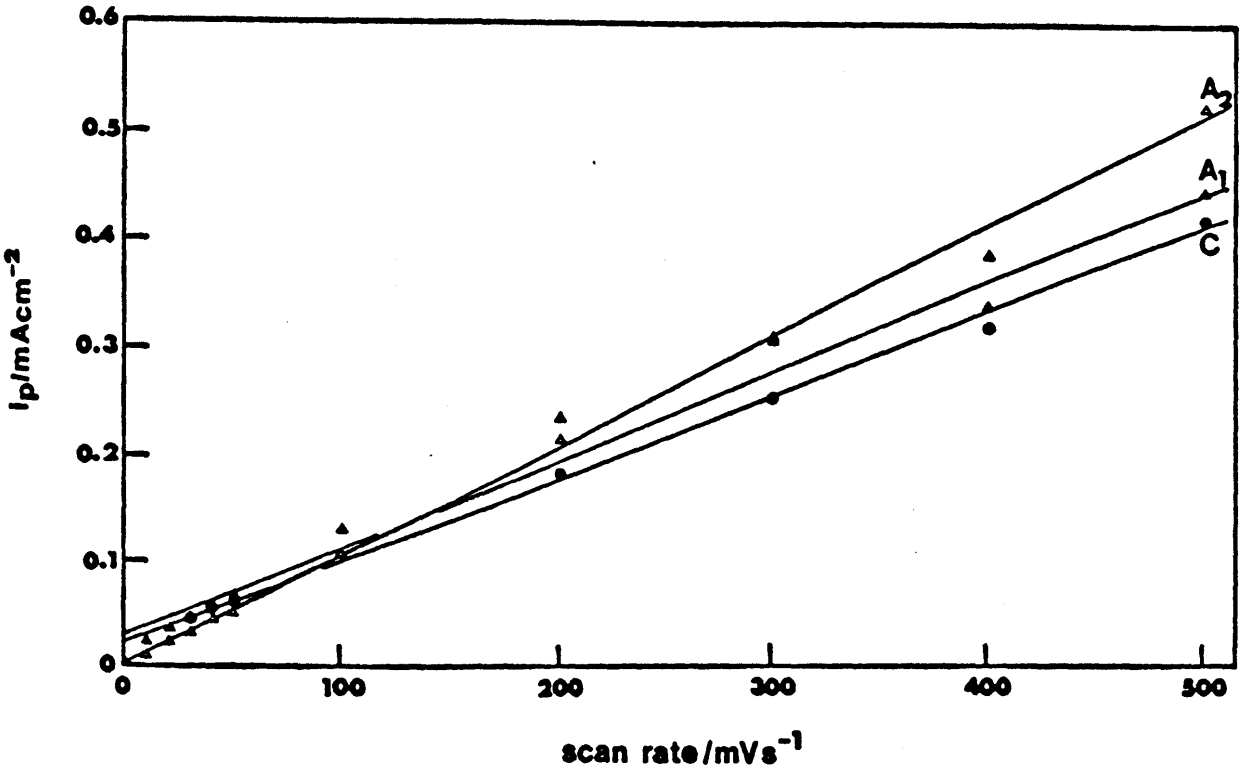

Figure 4.5: Effect of sweep-rate on peak current density - same conditions as in Fig. 4.4. The peaks in question are those at ca. 0.35 V, in Fig. 4.1(b) which frequently appeared as ill-resolved doublets - especially on the anodic scan - at fast sweep-rates.

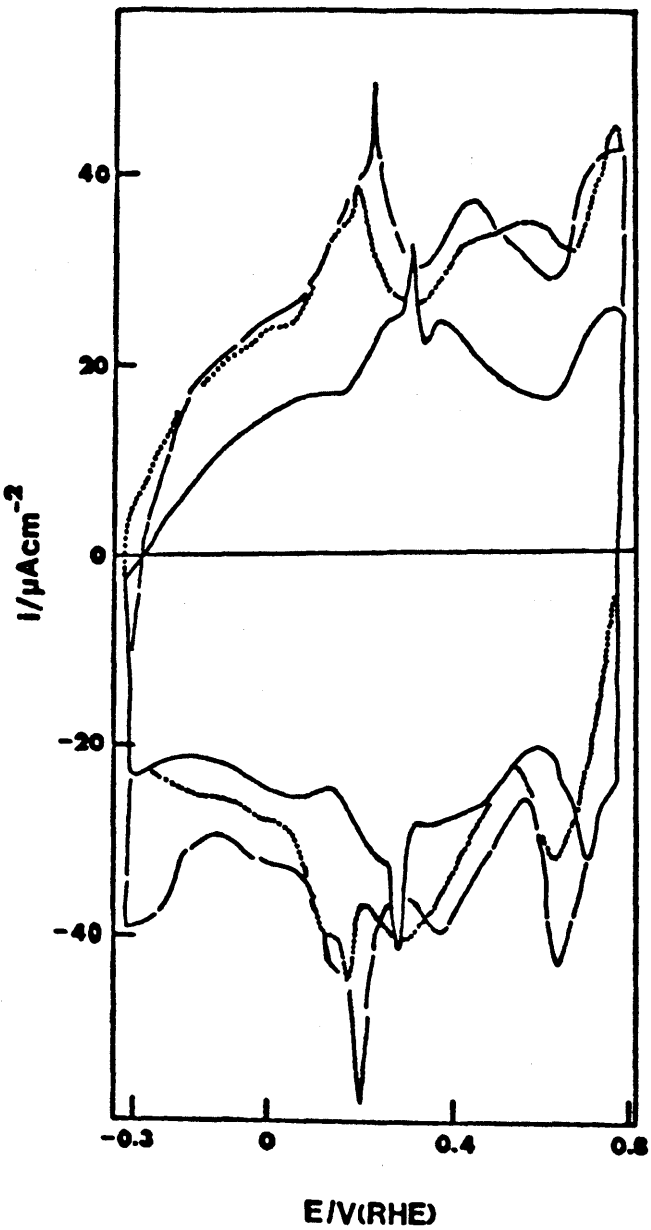

Figure 4.6: Examples of sweeps (50 mV s^{-1}) recorded for Ag in borate buffer solutions of constant ionic strength (Na_2SO_4 added - the composition of the solutions is given in ref. 430), T = 20°C: (——), pH = 12.3; (---), 11.3; (·····), 10.8.

diagrams was plotted in Fig. 4.7 and it is clear that, with some exceptions (notably peak A_2), the slopes were in the region of 59 mV, i.e. 2.303 RT/F V, per pH unit. In terms of the SHE scale this corresponds to a zero shift with pH; the latter result implies that there is no hydroxide ion involvement in the oxidation of the silver adatoms.

The somewhat anomalous behaviour of peak A_2 in Fig. 4.7 is difficult to explain; as outlined later there appears to be a complication in the anodic sweep associated with a step preceding adatom oxidation (on a polycrystalline surface there are a wide variety of adatom sites, some being more reactive than others). Such a complication is expected to be of a lesser significance on the cathodic sweep - an assumption borne out by the fact that in this case the E_p/pH behaviour is more regular.

4.2.2. Participation of Incipient Hydrous Oxide Species in Electrooxidation and Electroreduction Processes

Fig. 4.8 shows a cyclic voltammogram for silver in 1.0 mol dm^{-3} NaOH to which formaldehyde - to a level of 0.1 mol dm^{-3} - had been added (superimposed on Fig. 4.1(b)). A large increase in current was noted at ca. 0.2 V where oxidation commenced (anodic sweep) and terminated (cathodic sweep) - this latter value coincided with the lower (cathodic) end of the minor reversible peaks at ca. 0.3 V for silver in the organic-free base. At slow sweep-rates (Fig. 4.9) the initial increase in current in the region of the lower peak was followed by a plateau where the rate of oxidation was virtually independent of potential. Data recorded at faster sweep-rates (Fig. 4.8) showed little sign of a plateau.

The effect of formaldehyde concentration on the plateau current observed (Fig. 4.9) for the oxidation of this compound at slow sweep-rates at silver in base is shown in Fig. 4.10. The rate of oxidation was linearly dependent on the reactant concentration in solution at low values of the latter and virtually independent of reactant concentration at high values (above ca. 0.01 mol dm^{-3}) of the latter.

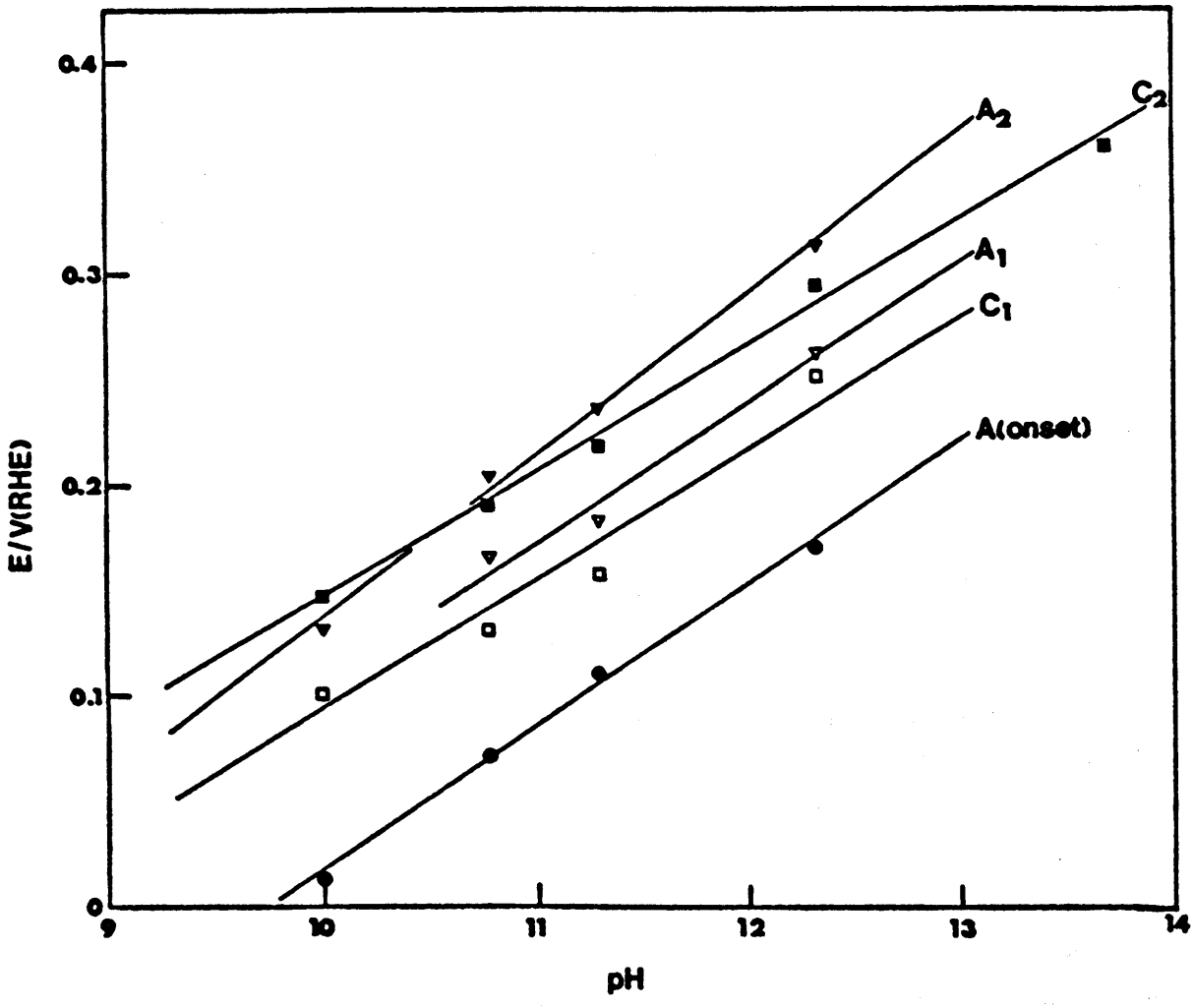

Figure 4.7: Peak potential shifts recorded for Ag in borate buffer solutions (same conditions as in Fig. 4.6). Slope values (mV/pH unit): A_1 64±11; A_2 81±4; C_1 66±9; C_2 59±3. The lower line (slope = 68±4) shows the variation with pH of the potential for the first significant rise in oxidation current on the anodic sweep.

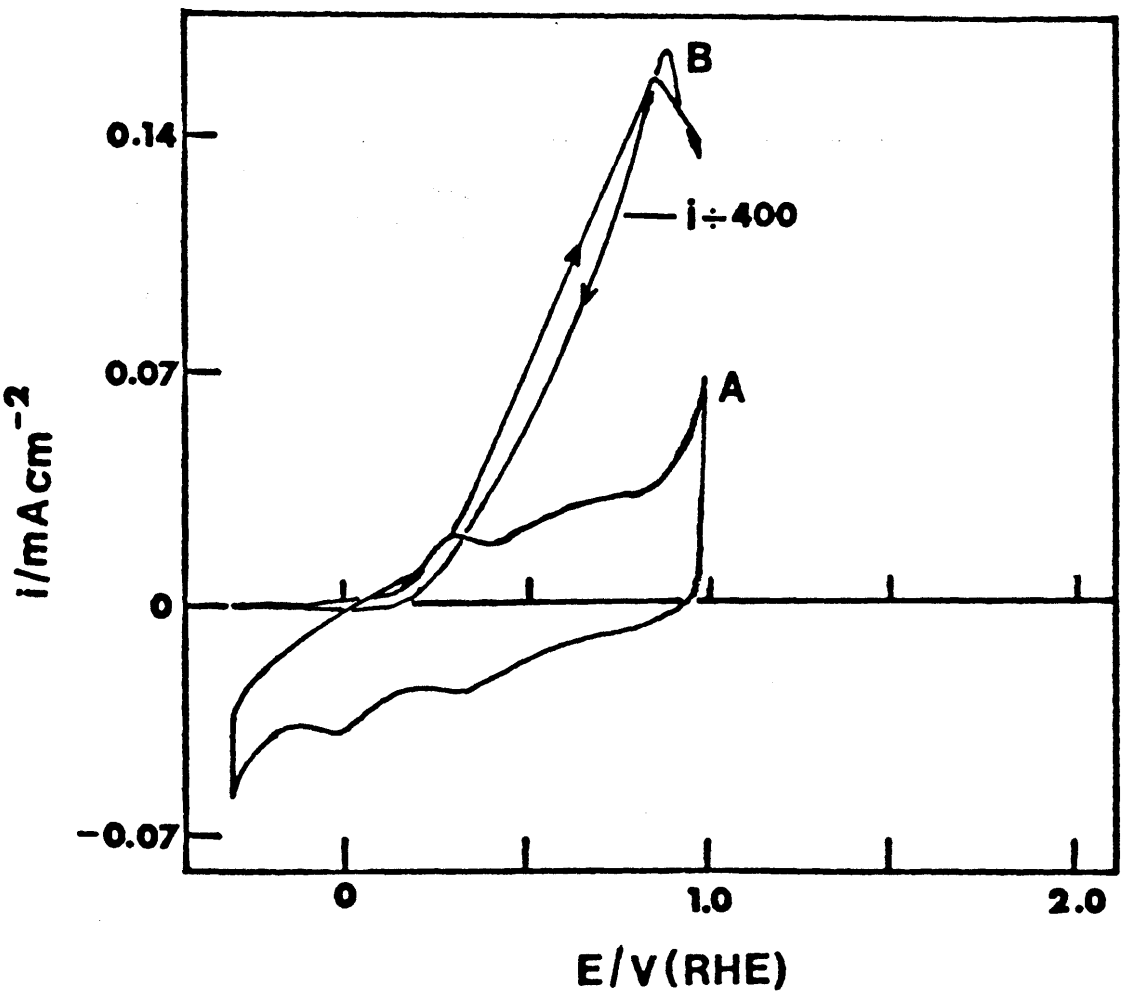

Figure 4.8: Cyclic voltammogram for Ag (40 mV s^{-1}, 20°C) in 1.0 mol dm^{-3} NaOH (-0.3 to 1.0 V) - curve A; the effect of adding HCHO (to a level of 0.1 mol dm^{-3}) to the base - curve B.

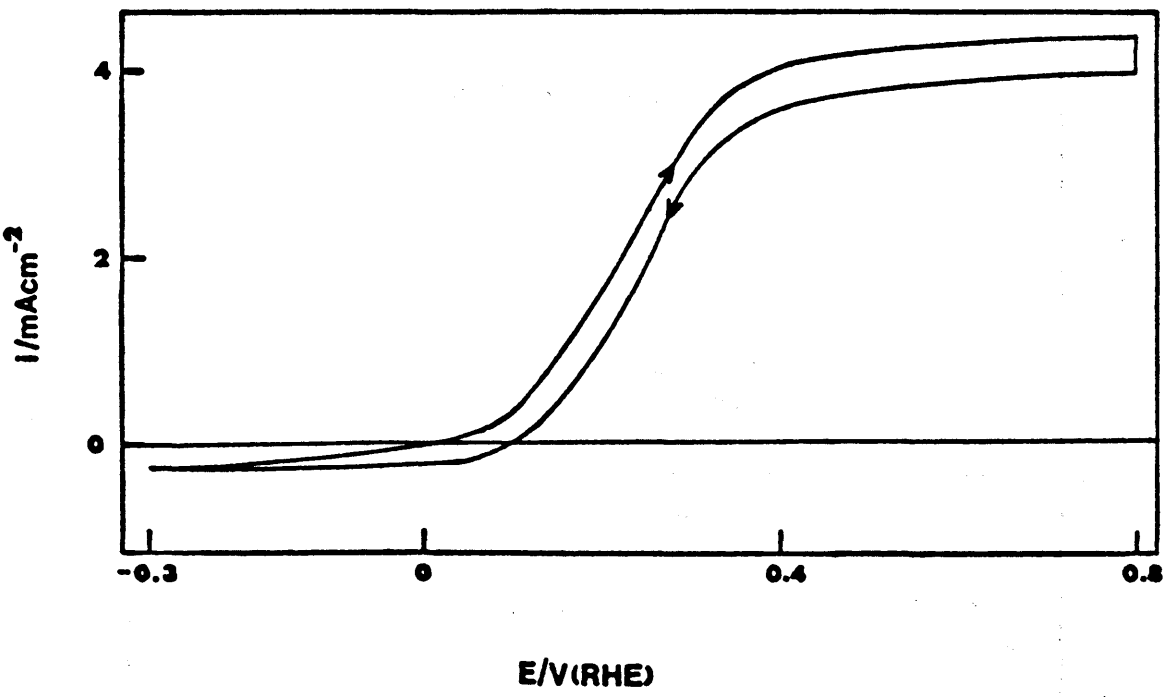

Figure 4.9: Example of a cyclic voltammogram recorded at a slow (10 mV s^{-1}) sweep-rate for Ag in 1.0 mol dm^{-3} NaOH + 0.1 mol dm^{-3} HCHO solution at 20°C.

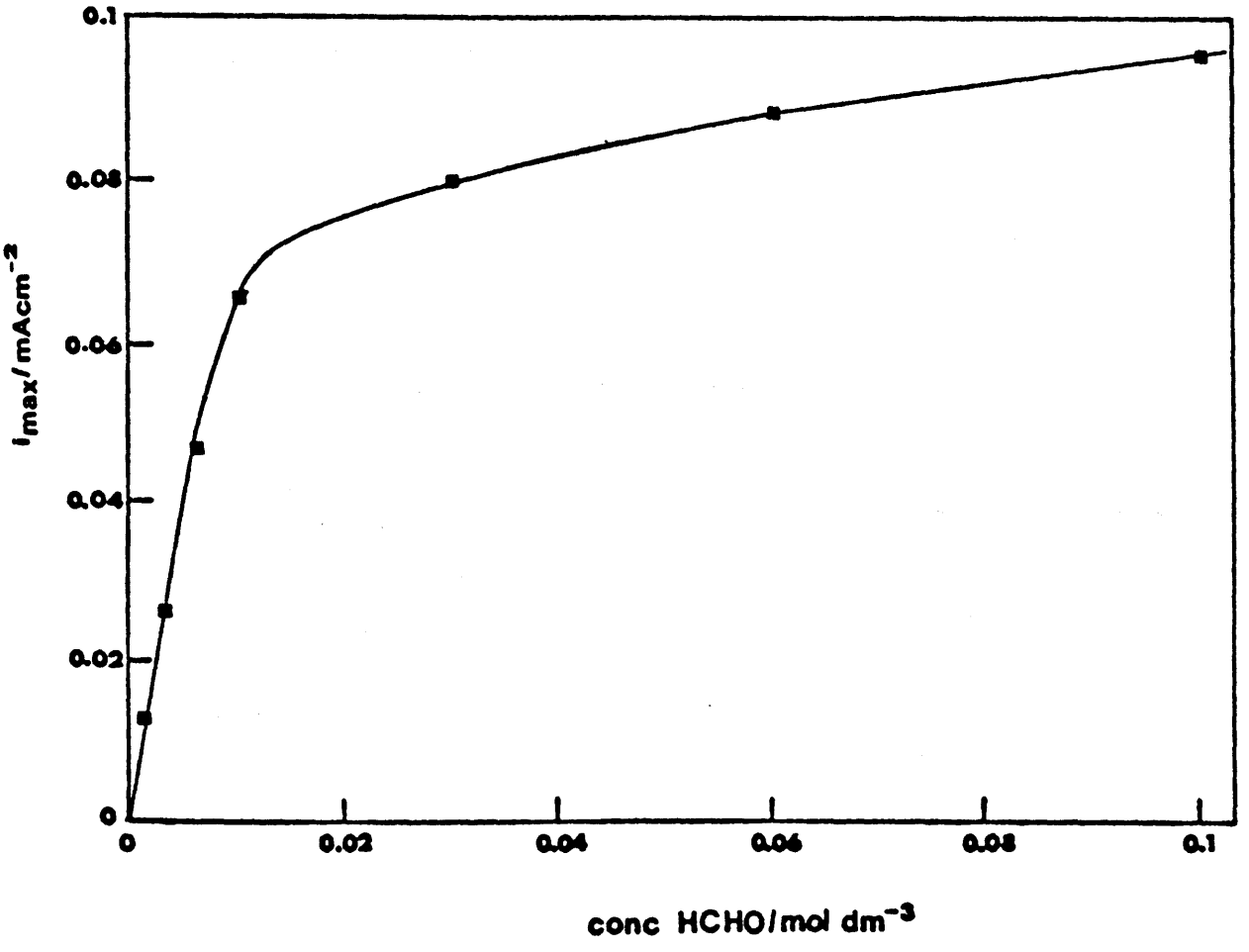

Figure 4.10: Effect of HCHO concentration on the limiting current recorded for Ag in 1.0 mol dm^{-3} NaOH (+HCHO) solutions (C.V. conditions as in Fig. 4.9).

Fig. 4.11 shows a cyclic voltammogram for silver in 1.0 mol dm^{-3} NaOH to which $NaNO_3$ - to a level of 0.02 mol dm^{-3} - had been added (superimposed on Fig. 4.1(b) also). Reduction of $NaNO_3$ commenced at ca. 0.25 V on the cathodic sweep and terminated at approximately the same potential on the anodic sweep. The current again appeared to reach a limiting value below ca. -0.1 V.

4.3. DISCUSSION

In agreement with the cyclic redox mechanism postulated earlier (section 1.8), a pair of small reversible peaks can be identified on silver in aqueous alkaline electrolyte at ca. 0.3 V in Fig. 4.1(b). This potential value compares with ca. 1.24 V for the onset of anhydrous oxide formation for silver in base (Fig. 4.1(a)). The inability of the Ag^+ cation in its adion state to retain the OH^- anion [372] is due to the low charge on the cation (relative for instance to Pt^{+4} which coordinates an excess of OH^- species). Thus the initial oxidation of silver at low potentials in base is attributed to the reaction

$$Ag^* + nH_2O = Ag^{*+1}(H_2O)_n + e \qquad (4:3:1)$$

The fact that on a polycrystalline silver surface there are a wide variety of adatom sites, some more reactive than others, is borne out by the variety of peaks observed in Figs. 4.2 and 4.3. Variation of pretreatment was adopted in an attempt to vary the quantity of adatom sites on the silver surface. Villullas et al. [422], used a silver electrode which, by pretreating by mechanical polishing and holding the potential at fixed potentials, was considered to undergo a surface restructuring process that rendered an increased concentration of active sites (Ag^*). Mayer and Muller [423] postulated that the formation of silver oxide layers proceed via a dissolution/precipitation process. Such a mechanism, possibly prevalent in some pretreatments used in the present work, would obviously product adatoms on a silver surface. Hence the history of a silver electrode is considered relevant to the voltammetric response yielded by silver surfaces in base. This may explain the variety of minor features observed for silver voltammograms in base at potentials negative to the onset of

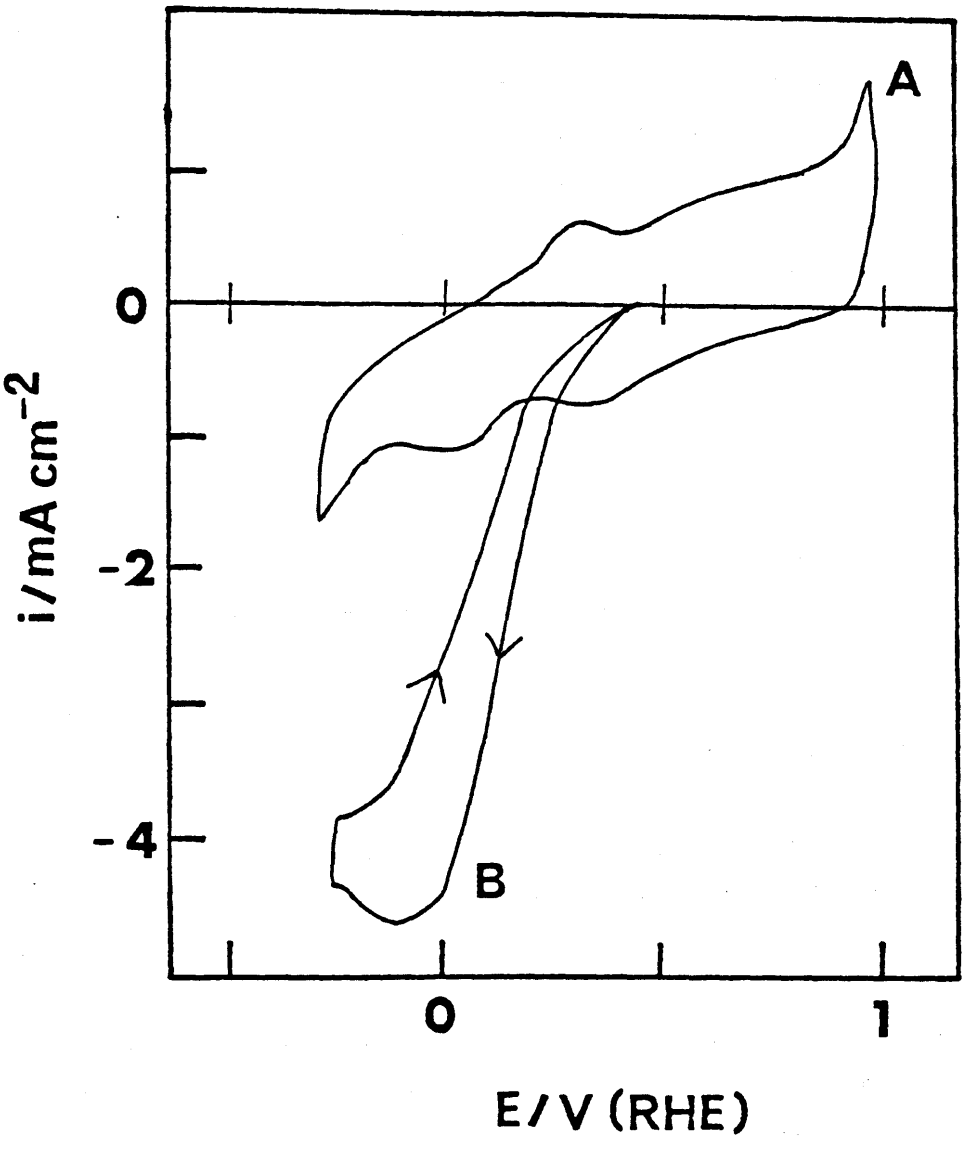

Figure 4.11: Cyclic voltammogram for Ag (40 mV s^{-1}, 20°C) in 1.0 mol dm^{-3} NaOH (-0.3 to 1.0 V) - curve A; the effect of adding $NaNO_3$ (to a level of 0.02 mol dm^{-3}) to the base (1 mV s^{-1}) - curve B.

anhydrous oxide formation.

The value of ca. 59 mV/pH unit for the slopes in Fig. 4.7 appears to be at variance with the expected super-Nernstian shifts usually reported for hydrous oxide systems [217]. This unusual behaviour of silver is evidently due to the small charge of the central metal ion. At a simple level AgOH (or $Ag_2O.nH_2O$) may be considered as an Arrhenius acid, similar to NaOH except not at all as soluble; it is a strong base, i.e. the OH^- tends to separate from the monovalent cation - the latter (which is present only at quite low coverage) is assumed to remain attached, in hydrated form, at special sites at the interface. The conversion of the AgOH to solvent-separated ionic species may involve Grotthus-type proton transfer reactions, viz.

$$AgOH.nH_2O + H_2O \;=\; Ag^+.(n-1)H_2O + OH^-_{(aq)} \qquad (4:3:2)$$

It follows, therefore, that the redox process for the silver ion, viz.

$$Ag^+.(n-1)H_2O + e \;=\; Ag^* + (n-1)H_2O \qquad (4:3:3)$$

has no direct OH^- ion involvement; hence, as observed $\delta E/\delta pH = 0$ V/pH unit on the SHE scale, i.e. 59 mV/pH unit on the RHE scale.

The current/voltage behaviour for formaldehyde oxidation at silver in base, (Figs. 4.8 and 4.9), shows the coincidence between the onset and termination of the oxidation potential with the potential of the metal/hydrous oxide transition; this is in agreement with the cyclic mechanism postulated earlier for such reactions. Evidently the anodic product of the redox transition promotes rapid oxidation of reactive molecules. The earlier results of Beltowska-Brzezinska [424] have also shown that the onset and termination of formaldehyde oxidation on silver in base occur at ca. -0.8 V (SCE) which corresponds to ca. 0.25 V (RHE). Furthermore, by using a cyclic treatment on the silver electrode before the experiments and using a rotating silver disc electrode [424] a second wave was shown to appear at ca. -0.35 V (SCE), i.e. ca. 0.7 V (RHE) which corresponds to a potential where another

minor peak is found on the silver electrode in base.

At slow sweep-rates (Fig. 4.9) the increase in current for formaldehyde oxidation is followed by a plateau where the rate of oxidation is virtually independent of potential. This behaviour is in agreement with the kinetic theory proposed by Beck and Suhultz [280] for interfacial cyclic redox processes involving surface-bonded mediators at oxide surfaces. Their expression for the limiting current is of the form

$$i_{max} = zFkK(C_S) \qquad (4:3:4)$$

However, at faster sweep-rates (Fig. 4.8) there is little sign of a plateau. The plateau behaviour can only be expected under conditions where the number of redox sites at the interface is constant. While in the case of many metals either surface deactivation or adatom/lattice atom conversion (i.e. adatom decay) may give rise to variation in active site coverage, there may be another factor involved in the present case. As mentioned earlier there is probably a range of surface site energies involved in polycrystalline silver; therefore, at faster sweep-rates the adatom/adion conversion is incomplete in the surface redox peak region, and hence the oxidation current increases significantly at higher potentials due to the increasing number of redox sites participating in the interfacial reaction. This view is supported by the results of Beltowska-Brzezinska [424] which show no plateau region for formaldehyde oxidation on silver in base until the potential is greater than ca. -0.2 V (SCE), i.e. ca. 0.85 V (RHE) at sweep-rates of 35 mV/s; in the latter case adatom, and hence hydrous oxide coverage, is assumed to reach a limiting value at ca. 0.85 V (RHE) - hence the limiting or constant rate of formaldehyde oxidation at more anodic potentials.

Van Effen and Evens [380] studied the oxidation of a whole range of different aldehydes at silver anodes in base; these commenced oxidation at potentials negative to onset of anhydrous oxide formation. They noted that the currents achieved for aldehyde oxidation at silver in base were always much less than the level expected for diffusion controlled reactions; this is again as expected by the cyclic redox theory. It was also observed

[377,424] that the formation of the anhydrous oxide film inhibited aldehyde oxidation. Hydrous oxide species at the interface are generally assumed [351] to be converted to regular anhydrous oxide when the potential rises to the regular monolayer oxide region; such a transition causes loss of the interfacial mediators, i.e. the surface becomes largely deactivated with respect to electrocatalytic oxidation.

The effect of formaldehyde concentration on the plateau current observed for the oxidation of this compound at slow sweep-rates in base (Fig. 4.10) shows a behaviour which is rather similar to that observed in enzyme-catalysed reactions, [425], i.e. the rate is linearly dependent on the reactant concentration in solution at low values of the latter and virtually independent of reactant concentration at high values of the latter. In the case of enzyme-catalysed reactions the rate of reaction (v) is related to the reactant concentration (C_S) and enzyme concentration (C_E) by the Michaelis-Menten equation

$$v = \frac{k_c C_E C_S}{k_m + C_S} \qquad (4:3:5)$$

where k_c is known as the catalytic constant and k_m the Michaelis constant. The similarity in rate behaviour between the enzyme-catalysed and electrochemical processes (at $i = i_{max}$) is obviously due to the fact that in both cases reaction is occurring at a fixed number of active sites - the latter in the present electrochemical case being the number of adspecies at the electrode surface which have undergone the $Ag^*/Ag^*(I)$ transition.

The Michaelis-Menten equation has exactly the same form as the Langmuir adsorption isotherm and the latter may be incorporated into the approach used by Beck and Schultz [280] to interpret the kinetic behaviour of the present system, viz.

In the general reaction scheme R and O are the reduced and oxidised form, respectively, of the surface couple; S represents the solution species that is oxidised in its adsorbed state by chemical reaction with O.

$$R = O + ze \qquad \text{(fast)} \qquad (4:3:6)$$

$$S_{ads} + O = Z + R \qquad \text{(slow)} \qquad (4:3:7)$$

[A] = net conc. of active surface sites = [R] + [O]

$$E = E^{O} - \frac{RT}{zF} \ln \frac{[R]}{[O]}$$

$$= E^{O} + \frac{RT}{zF} \ln \frac{[O]}{[R]} = E^{O} + \frac{RT}{zF} \ln \frac{[O]}{[A]-[O]} \qquad (4:3:8)$$

E^{O} is the standard potential of the surface redox couple. If the transport and adsorption of S is fast

$$[S_{ads}] = \theta[A] = \frac{KC_S[A]}{1 + KC_S} \qquad (4:3:9)$$

$$i = zF\, k[S_{ads}]\, [O] \qquad (4:3:10)$$

But $$\ln \frac{[O]}{[A]-[O]} = \frac{zF}{RT} (E-E^{O})$$

$$\frac{[A]-[O]}{[O]} = \frac{[A]}{[O]} - 1 = \exp\left[-\frac{-zF}{RT} (E-E^{O}) \right]$$

$$[O] = \frac{[A]}{1 + \exp[-\frac{zF}{RT} (E-E^{O})]} \qquad (4:3:11)$$

$$i = \frac{zFkKC_S[A]^2}{(1 + KC_S)\{1 + \exp[-\frac{zF}{RT} (E-E^{O})]\}} \qquad (4:3:12)$$

Special cases

(1) At low reactant concentration θ is low, therefore

$$\frac{\theta}{1-\theta} \simeq \theta = KC_s$$

$$S_{ads} = \theta[A] = KC_s[A]$$

(the same result is obtained from (4:3:9) by letting $1 + KC_s \simeq 1$).

Hence,

$$i = \frac{zFkKC_s[A]^2}{1 + \exp\left[-\frac{zF}{RT}(E-E^o)\right]}$$

At potentials well above the reversible peak potential $E >> E^o$ and

$$1 + \exp\left[-\frac{zF}{RT}(E-E^o)\right] \simeq 1$$

Therefore

$$i_{max} \simeq zFkK[A]^2.C_s \qquad (4:3:13)$$

i.e. for low reactant concentration the limiting current is proportional to C_s as already demonstrated by Beck and Suhultz [280]; see also Fig. 4.10 for [HCHO] < ca. 0.01 mol dm^{-3}.

(2) At high reactant concentration

$$K[C_s] >> 1$$

$$i \simeq \frac{zFk[A]^2}{1 + \exp\left[-\frac{zF}{RT}(E-E^o)\right]}$$

For $E >> E^o$ this expression reduces to the form

$$i_{max} = zFk[A]^2 \qquad (4:3:14)$$

i.e. for higher reactant concentration the limiting current, as also demonstrated in Fig. 4.10, is independent of C_s. It is also clear from these equations that a constant value for i_{max} is observed only when the active site concentration at the interface, [A], is a constant.

The oxidation of formaldehyde on silver in base is assumed to be preceded by a chemical step involving the reversible nucleophilic addition of a hydroxide ion to the carbonyl group resulting in the formation of the electroactive gem-diolate species [380,416] which is oxidised in a two-electron irreversible process to the corresponding carboxylate. This oxidation of formaldehyde is accompanied by evolution of hydrogen gas [377,424] - an unusual product for an organic oxidation process. The scheme proposed by Bindra and Roldan [416] to explain this reaction is as follows:-

$$HCHO_{aq} + OH^- = H_2CO^-.OH_{aq} \qquad (4:3:15)$$

$$H_2CO^-.OH_{aq} = H_2CO^-.OH_{ads} \qquad (4:3:16)$$

$$H_2CO^-.OH_{ads} + OH^- = HCOO^- + H_2O + H_{ads} + e \qquad (4:3:17)$$

$$H_{ads} = \tfrac{1}{2}H_{2(g)} \qquad (4:3:18)$$

The overall reaction is therefore

$$HCHO + 2OH^- = HCOO^- + H_2O + \tfrac{1}{2}H_2 + e \qquad (4:3:19)$$

As pointed out here, equation (4:3:1), adatom oxidation leads to formation of hydrated, cationic adspecies which tend to coordinate Lewis bases such as $H_2CO^-.OH$. However, this adsorption, equation (4:3:16), at active sites is a competitive process during which H_2O or OH^- species have to be displaced. Extensive coordination or saturated coverage is apparently achieved only at significant reactant concentration.

Reduction of $NaNO_3$ (Fig. 4.11) is assumed to occur by a similar type of mechanism as outlined for the oxidation of formaldehyde, except that instead of the active mediator being the anodic product of the redox transition it is now the reduced form

of the interfacial couple, i.e. the Ag^* adatom. This latter assumption is supported by the coincidence of $NaNO_3$ reduction onset and termination at ca. 0.25 V (RHE) with the potential of the redox transition for silver base. This behaviour, outlined here in Fig. 4.11 for 0.02 mol dm^{-3} $NaNO_3$ in base, shows a limiting current occurring at potentials below ca. -0.1 V (RHE). This limiting current behaviour is not as well defined - especially on the cathodic sweep - as that for formaldehyde oxidation (Fig. 4.9); presumably loss of silver adatoms occur due to relaxation of the latter into regular silver lattice sites at the surface.

The results shown here for nitrate reduction are in reasonable agreement with those of Nishihara and Shindo [387] who found that reduction of nitrobenzene is aqueous alkaline solution occurred with two reduction waves at ca. -0.5 and -0.8 V (SCE), i.e. ca. 0.5 and 0.2 V (RHE) at 50 mV/s. These potential values correspond to values where cathodic peaks appear for silver in base. The reduction of both nitrate and nitro groups are assumed to be electrocatalytically demanding reactions, i.e. they only occur at active sites which in the present case may be assumed to be silver adatoms which can only exist at potentials cathodic with respect to the adatom/hydrous oxide transition.

4.4. CONCLUSIONS

The current results for silver in base support the general view that the electrocatalytic behaviour of polycrystalline metal electrodes in aqueous media is strongly influenced - probably dominated - by the behaviour of adatom species. Reactive organic molecules, such as formaldehyde, oxidise at potentials above the adatom/hydrous oxide transition - the process involved being mediated, in a cyclic redox manner, by the oxidised state of the adatom, the latter being the effective, electrochemically generated, oxidant. It may be pointed out here that cyclic redox schemes for electrocatalysis are not particularly novel; they are widely invoked, for instance, in the case of oxygen gas evolution at metal anodes [219] - but in such instances the metal is usually coated with a thick oxide layer and the interfacial transition is usually an oxide/oxide interconversion. The major novelty of the

present approach is the emphasis placed on the low coverage hydrous oxide species which are widely ignored in deriving electrochemical data on the basis of thermodynamic information - the classical approach in this area is the work of Pourbaix [352] who largely ignored the difference between hydrous and anhydrous oxides (both were assumed to be equivalent) and was apparently unaware of the importance of the influence of the acid-base properties of the hydrous oxides on the redox behaviour of the latter. According to Pourbaix silver is unoxidable at potentials below ca. 1.173 V (RHE); as will be outlined in more detail for platinum this may be valid for regular silver lattice atoms but not for silver atoms in the adatom state.

The kinetic treatment developed here for this type of electrocatalysis can account for most features of the reaction; e.g. the constant value of the limiting current in the upper region of the potential sweep, and the influence of reactant concentration on this limiting current. Factors that require further attention include (a) the precise nature of the bonding of the adspecies at this interface (it is assumed that subsurface oxygen plays a role here but the precise nature of the bonding is at present indefinite), (b) it would be most interesting to have control of the coverage of such species at the interface - especially with a view to increasing the density of such active sites, and hence the electrocatalytic activity of the surface. However, the very low coverage and response of the active site species means that progress in the latter area is difficult.

CHAPTER 5

Platinum

5.1. INTRODUCTION

Platinum is frequently the substrate of choice for fundamental work in electrocatalysis due to its marked resistance to corrosion, high electrocatalytic activity, and apparently clear separation between the potential regions for hydrogen and oxygen adsorption.

The electrochemical behaviour of platinum in aqueous media is usually summarised by the cyclic voltammogram shown in Fig. 5.1. In such diagrams four main potential regions are usually distinguished on the anodic sweep: 0-0.4 V, ionisation of adsorbed hydrogen; 0.4-0.8 V, double layer charging (this process occurs over the entire potential range but it is the sole process over the intermediate region quoted here); 0.8-1.5 V, deposition of hydroxy and oxy species at the metal surface; above 1.5 V, oxygen gas evolution plus continued growth of the surface oxide layer (formation of a thick, yellow, hydrous oxide film occurs under constant polarisation conditions [432-434] at 2.1 V < E < 2.5 V). On the subsequent cathodic sweep the corresponding regions are as follows: the peak at 0.8 V, reduction of the monolayer oxide film; 0.5-0.4 V, double layer discharging (again this process occurs over the entire cathodic sweep); 0.4-0 V, adsorbed hydrogen formation (plus reduction of any hydrous platinum oxide formed under highly anodic conditions); below 0 V, hydrogen gas evolution. The potential ranges quoted here are approximate and refer mainly to acidic media. The hydrogen region was discussed in some detail in section 1.7.

The formation of monolayer oxide films on platinum (anodic conditions) has been extensively investigated by Conway and coworkers [434]. It was demonstrated [435] that with a highly purified aqueous 0.5 mol dm^{-3} H_2SO_4 electrolyte three poorly resolved peaks (O_{A1}-O_{A3}) could be identified in the anodic sweep below monolayer (i.e. one electron per Pt atom) coverage. These authors also designated the broad flat region from Q_{OH} = 1 (E≈1.1 V) to the oxygen gas evolution stage as O_{A4} (where Q_{OH} is the charge for OH coverage). Hysteresis was always observed between the regions O_{A2}, O_{A3}, and O_{A4}, and the single peak on the subsequent cathodic sweep; the only region showing signs of reversibility was that associated with the start of the O_{A1} peak

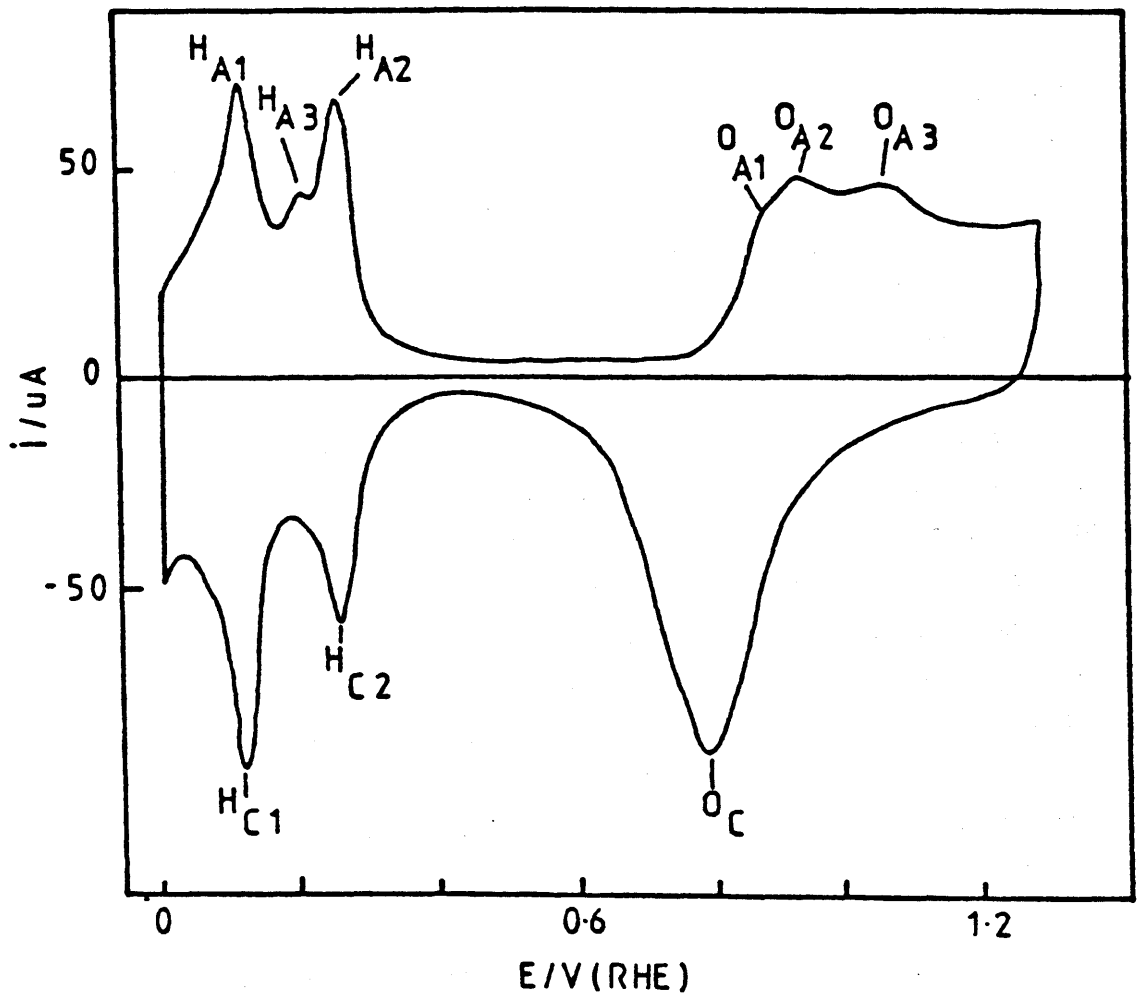

Figure 5.1: Potentiodynamic i/E profile for a platinum surface in high purity 0.5 mol dm^{-3} H_2SO_4 at 25°C, V = 0.1 V s^{-1}.

(up to ca. 0.88 V at a sweep-rate of 100 mV/s). Based on the recorded charge values, the three peaks were assigned to the following processes:

$$4Pt + H_2O = Pt_4OH + H^+ + e \qquad E_p(O_{A1}) \approx 0.89 \text{ V} \quad (5:1:1)$$

$$Pt_4OH + H_2O = 2Pt_2OH + H^+ + e \qquad E_p(O_{A2}) \approx 0.95 \text{ V} \quad (5:1:2)$$

$$Pt_2OH + H_2O = 2PtOH + H^+ + e \qquad E_p(O_{A3}) \approx 1.05 \text{ V} \quad (5:1:3)$$

The formulae in these equations represent only surface lattice occupancy ratios, not chemically distinct species.

The hysteresis in the oxide formation/removal process at anodic limits above ca. 0.9 V was attributed to a slow post-electrochemical step in the surface oxidation reaction. It was assumed that interaction between neighbouring OH, or PtOH, species induced place-exchange reactions in the surface layer (adsorbed OH groups switching positions with metal atoms in the surface layer of the metal lattice) resulting in significant formation of "OHPt" species. The fact that the three peaks on the anodic sweep are quasi-reversible in character (the peak potentials being virtually independent of sweep rate, a feature that seems in conflict with the marked hysteresis between the oxide formation/removal reactions) was attributed to the continued existence, at any part of the sweep, of species such as OH_{ads} and its place-exchanged equivalent, OHPt; at higher anodic limits, up to 1.1 V, an increased thickness of OHPt is assumed to be present; only at higher anodic limits was it postulated that PtO species were present in the surface layer.

The above approach by Conway and coworkers has been questioned by a number of authors. Ross [436], for instance, has shown that the fine structure at the initial stages of surface oxidation depends strongly upon the solution composition and is absent in the presence of a hydrogen fluoride electrolyte; according to this author the fine structure in the voltammogram is due to anion adsorption in solutions of low pH. Bagotzky and Tarasevich [437] observed only two very broad peaks on the anodic sweep in base, the first of which they attributed to OH and the second to O

adsorption. They also postulated that in acid media the main product of oxidation at any point of the anodic sweep is O_{ads}. Attempts have been made to simulate the experimentally observed current/voltage response obtained under cyclic voltammetry conditions for the platinum oxide formation/removal reactions by Appleby [438], and Bagotzky and Tarasevich [437]; the fact that both approaches yield reasonable agreement between experimental and recorded voltammograms, using significantly different reaction schemes and assumptions as to the origin of the irreversibility, illustrates the absence of a diagnostic role in this approach as used to date.

One feature that seems to have been largely ignored in earlier work is the fact that the species formed in the initial stages of the platinum oxidation reaction may be charged, rather than neutral in character. Evidence for this is found in the work of Vetter and Berndt [439] whose charging curve data is reproduced here in Fig. 5.2. It is clear from this diagram that the potential (E_i) for the onset of oxidation (dotted line in Fig. 5.2) decreases with increasing pH by ca. 3/2(2.303 RT/F) V/pH unit; since the authors were apparently unaware at that time of the significance of oxide acidity, they automatically assumed a conventional 2.303 RT/V variation, which is obviously in poor agreement with the experimental data in this initial oxidation region. The unusual decrease in E_i with increasing pH is now widely accepted; Conway and coworkers [440] attributed it to the effect of anion adsorption while Bagotzky and Tarasevich [438] attributed it to a change in oxidation mechanism with variation in pH. According to Burke and Roche [441] the effect is due to the formation of an initial acidic or anionic product according to the following reaction schemes:

$$2Pt + 2H_2O = [Pt_2O.OH]^- + 3H^+ + 2e \qquad \text{(acid)} \qquad (5:1:4)$$

$$2Pt + 3OH^- = [Pt_2O.OH]^- + H_2O + 2e \qquad \text{(base)} \qquad (5:1:5)$$

The product of this reaction, O^-_{ads} ..... $H\text{-}O_{ads}$, is assumed to be stabilised to a significant extent by hydrogen bonding between species coordinated at adjacent Pt sites. Apart from inducing hysteresis, place-exchange reactions are also assumed to destroy the anionic character of the surface oxide species, the return to

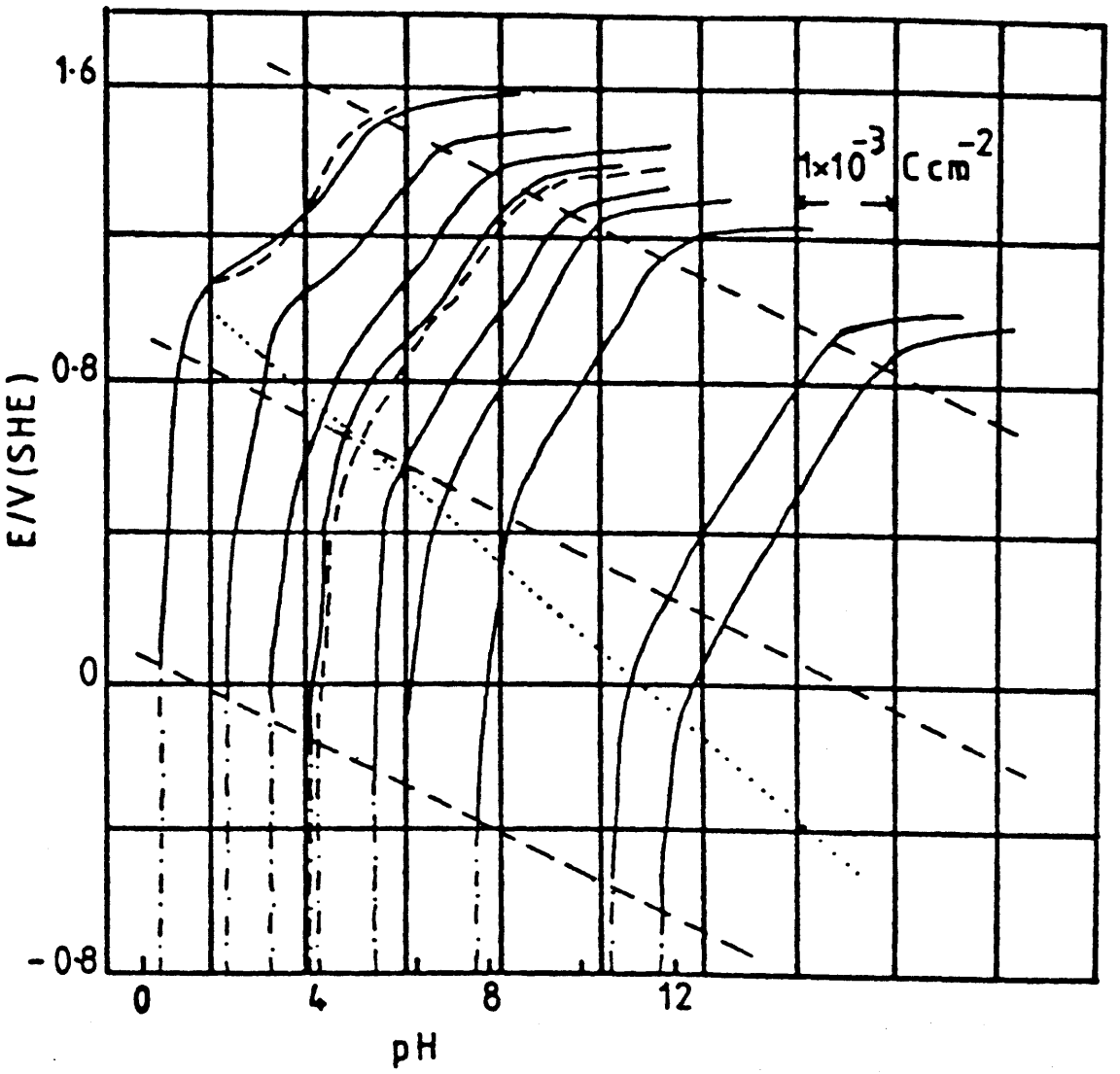

Figure 5.2: Anodic charging curves (i = 5.0 μA cm^{-2}) for platinum in aqueous buffer solutions at different pH values, T = 25°C. The dotted line of slope 3/2(2.303 RT/F) V/pH unit has been added [Ref. 439].

conventional 2.303 RT/F behaviour at the onset of oxygen gas evolution is clear from Fig. 5.2. The high OH^- ion activity in base stabilises the $[Pt_2O.OH]^-$ species; it effectively lowers the Pt^{+1} activity by driving the dissociation equilibrium of the surface hydroxy species, viz:

$$[Pt_2O.OH]^- + H_2O = 2PtOH + OH^- \qquad (5:1:6)$$

to the left hand side. Thus from a simple Nernstian viewpoint (which should be applicable to the initial stage of oxidation as this apparently occurs under reversible conditions [435], the equilibrium potential for the process

$$Pt^{+1} + e = Pt \qquad (5:1:7)$$

must be considerably lower in base than in acid (it is clear from equations (5:1:4) and (5:1:5) that $\delta E/\delta pH = 3/2(2.303\ RT/F)$). Because the oxidation starts at a higher potential in acid, and the voltage is changing at the same rate in cyclic voltammetry experiments carried out under similar conditions, the currents in the reversible region must be greater at low pH (the point of completion of the largely anhydrous O_{ads} monolayer at 1.4-1.5 V is virtually pH-independent) - clearly the arrest in the charging curves for acid just after the onset of oxidation has the same origin. Thus charges in the acidic or anionic character of the species involved in the early stages of surface layer formation extert a strong influence on the current/voltage behaviour in this region.

The mechanism of monolayer oxide formation on platinum above 1.0 V is still a topic of considerable controversy. Visscher and Devanathan [442] suggested that the rate of reaction was controlled by the entry of metal ions into the film and derived rate equations on the assumption that this was predominantly a field-assisted process. Vetter and Schultze [443,444], Schultze [445], and Ord and Ho [446] proposed a model involving migration of platinum and oxygen ions across the oxide layer under the influence of a high electric field; this approach has been extensively employed in recent times by Damjanovic and coworkers [447-449]. Such a mechanism, however, is not universally accepted; as Belanger and

Vijh [214] have pointed out it is in conflict with the finding of a limiting coverage (oxygen/platinum ratio) of just above 2.0 at ca. 2.2 V by Biegler and coworkers [450,451]. This point may not be quite valid because (as outlined later) hydrous oxide growth commences in this region, i.e. there may be a change in the nature of the film at this potential, perhaps making it more susceptible to dissolution (Visscher and Blijlevens [452] have shown also that the limiting coverage is dependent on the acid concentration). A possibly more serious objection is the fact that quite large currents may be passed through a platinum electrode in the thin oxide layer region providing a suitable simple redox species is present in solution [453]. Even the occurrence of the oxygen gas evolution reaction, which is quite vigorous above 1.6 V, suggests that the surface layer is not highly resistive, as would be required if a large electric field (which has been suggested [453] to be as high as 10^7 V cm^{-1}) were to be developed across the surface layer.

A more detailed criticism of the high-field theories of oxide growth as applied to platinum can be found in the work of Gilroy [454,455]. The author has proposed an alternative, low-field theory based on the assumption that surface oxidation occurs, from the onset, by a nucleation mechanism, the process being controlled by the rate at which growth sites are initiated. The basis of this approach has been reviewed by Fleischmann and Thirsk [456].

Hydrous oxide growth on platinum, whether produced by d.c. polarisation or a.c. cycling (Fig. 5.3), yields a thick surface oxide layer [457,460-463]; the process involved needs active centres, or defect sites, for initiation [458]. Reduction of the hydrous oxide is observed at 0.2-0.4 V in acidic media; however, due to the unusual potential/pH shift discussed earlier, the hydrous oxide deposit on platinum is quite difficult to reduce in alkaline electrolytes. The charge for this reduction peak in acid varies with the duration of growth and greatly exceeds that for monolayer reduction. It may also split after growth into a doublet [458], suggesting the presence of two types of hydrous oxide material. Altmann and Busch [459] have proposed that the hydrous oxide may be described as $PtO_2.nH_2O$. The existence of a Pt(IV) species was confirmed by Allen et al. [460] by the use of x-ray

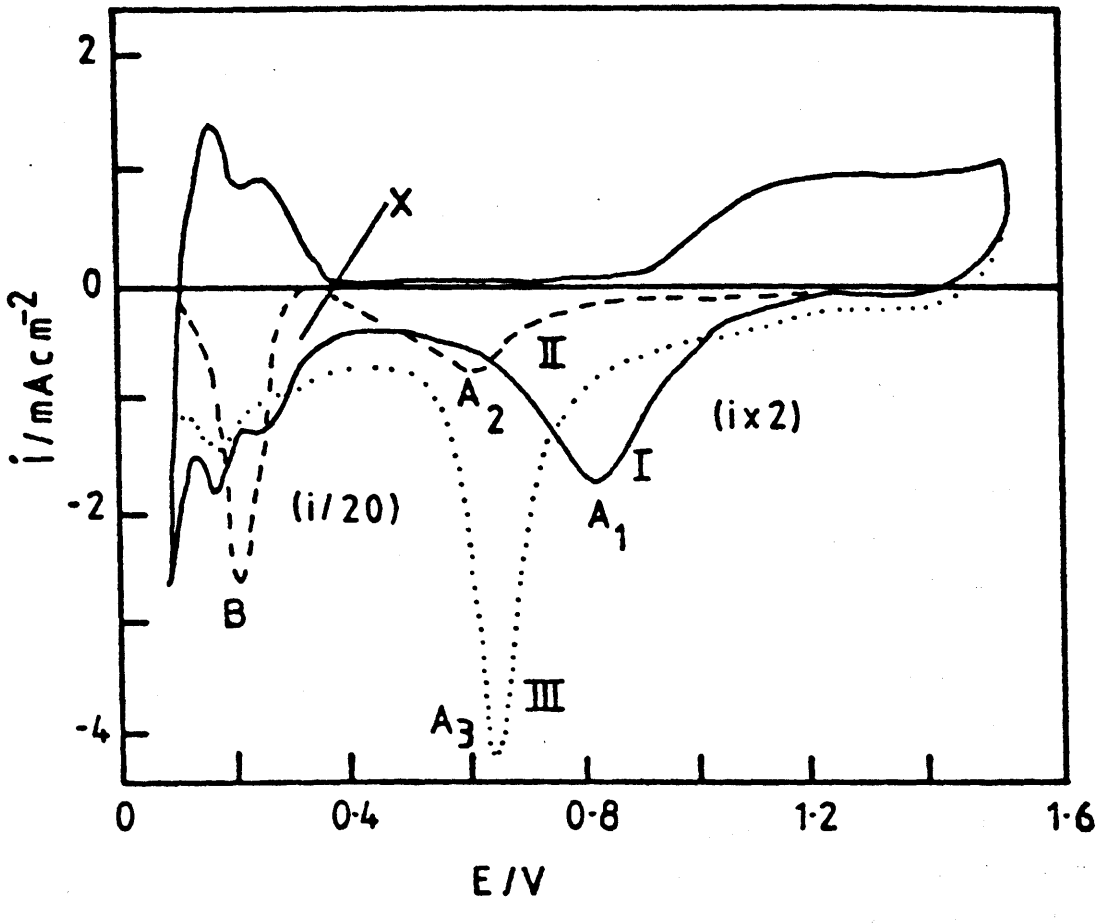

Figure 5.3: Curve I (——) is a typical cyclic voltammogram for polycrystalline platinum in 1.0 mol dm^{-3} H_2SO_4 at 25°C, V = 0.3 V s^{-1}. Curve II (---) is a reduction sweep for the same electrode coated with a thick hydrous oxide layer (at point X on this sweep the recorder sensitivity was considerably reduced). Curve III (···) is a similar reduction sweep (2.0 to 0 V, 40 mV s^{-1}) recorded without growing the hydrous oxide layer [Ref. 462].

photoelectron spectroscopy.

The hydrated oxide of platinum may also be considered as an acidic species, viz.

$$Pt^* + 6H_2O = [Pt(OH)_6]^{2-} + 6H^+ + 4e \quad (5:1:8)$$

$$+ 2H^+ \;\downarrow\uparrow\; - 2H^+$$

$$PtO_2.4H_2O$$

Here the hydrated oxide is assumed to be in equilibrium with the anionic (or acidic) hydroxy species - the above formulation is in accordance with the observed super-Nernstian E/pH shifts recorded for many metal/hydrous oxide (and even oxide/oxide) transitions - a reversible 90 mV/pH unit shift requires a ratio of $3H^+$ (or $3OH^-$) to 2e [217].

The platinum hydrous oxide system may be treated as a metal/insoluble salt electrode involving the metal/metal ion reaction

$$Pt^{+4} + 4e = Pt^* \quad (5:1:9)$$

From a thermodynamic viewpoint, the generation of hydrous oxide films on platinum at low potentials on the anodic sweep is feasible, especially in base. The inhibition here is evidently related to the need for six hydroxide ions to have access to coordination sites at the same platinum atom, an improbable condition for a metal atom in a regular surface site. Hence the need for active centres (Pt*), or defect sites, for initiation as mentioned above. Formation of hydrous oxide layers of thickness (measured in terms of the charge required for reduction) in excess of 2.5 C cm^{-2} (geometric area) is readily achieved by cycling [464]; this corresponds to over 1,000 monolayers of oxygen. The rate of hydrous oxide growth decreases with increasing cycling time or thickness, probably due to gradual accumulation of poorly hydrated material at the compact oxide/hydrous oxide interface. Little hydrous growth was observed under cycling conditions [464] within the pH range 4.0 to 9.0; it was suggested that hydrous oxide growth requires some type of rearrangement of the initial amorphous surface oxide layer, a reaction requiring H^+ adsorption at low pH and interaction with OH^- at high pH values. With both acid and

base grown films reduction results in the generation of a finely divided, platinum black type surface.

5.2. THE ANOMALOUS "HYDROGEN" PEAK, H_i

5.2.1. Introduction

The greatest problem in applying the theory that electrocatalysis at platinum involves mediation by a hydrous oxide in a cyclic redox mechanism is the difficulty in establishing, unambiguously, that a reversible transition occurs at a potential cathodic to regular anhydrous oxide formation. The problem here is the high affinity of platinum for hydrogen; as already pointed out in sections 1.6.5 and 1.7 this metal has an extensive hydrogen adsorption/desorption region, and the currents due to the latter tend to mask the much lower response associated with formation or reduction of low level (or incipient) hydrous oxide species. As previously mentioned, in section 1.7, there is a peak at low potentials (assigned H_{A3} in Fig. 5.1) that behaves in an anomalous fashion compared with the other peaks in the hydrogen region. This peak is referred to here as the intermediate hydrogen peak, H_i, and was investigated using cyclic voltammetry procedures.

5.2.2. Results

Generally, peak H_i was clearly observed under repetitive sweep conditions only when the upper limit was well into the monolayer oxide region - ca. 1.0 V(RHE), Fig. 5.4. Once established using a high anodic limit, e.g. 1.6 V(RHE), the peak in question disappeared again on repetitive cycling between reduced limits, e.g. 0 to 0.6 V(RHE), Fig. 5.5(a); restoration of H_i was achieved in the latter case by either raising the upper limit above 1.0 V or holding the potential constant, for a significant period of time, at potential values close to 0 V, Fig. 5.5(b). It can be seen that in the latter case the holding process diminished the height of H_w while slightly accentuating the height of H_i and H_s. The same trend was observed when the cycle limits used were 0 to 1.6 V; H_i was observed on continuous cycling in this case but the peak was again more pronounced after interrupting the scan and holding the potential constant for short periods at 0 V(RHE).

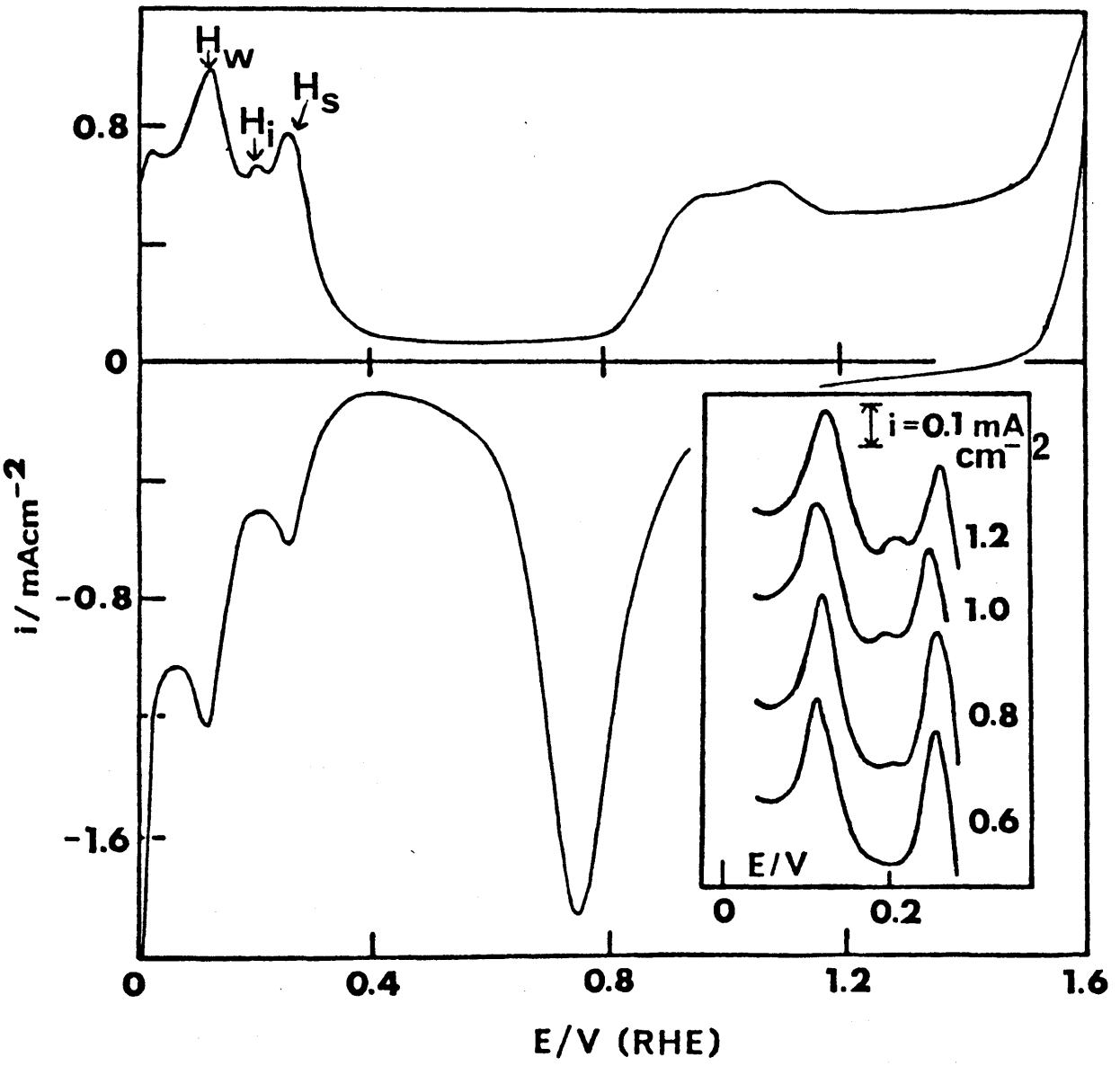

Figure 5.4: Effect of the upper limit on the appearance of the H_i peak. The cyclic voltammogram shown here (0-1.6 V, 50 mV s^{-1}) was for smooth Pt in N_2-degased 1.0 mol dm^{-3} H_2SO_4 at 25°C. The inset shows the changes observed in the hydrogen desorption region on changing the value of the upper limit (the values are given in the diagram). Before recording each voltammogram the electrode was multicycled - 0 to the chosen upper limit, 0.5 V s^{-1}, for 5 min.

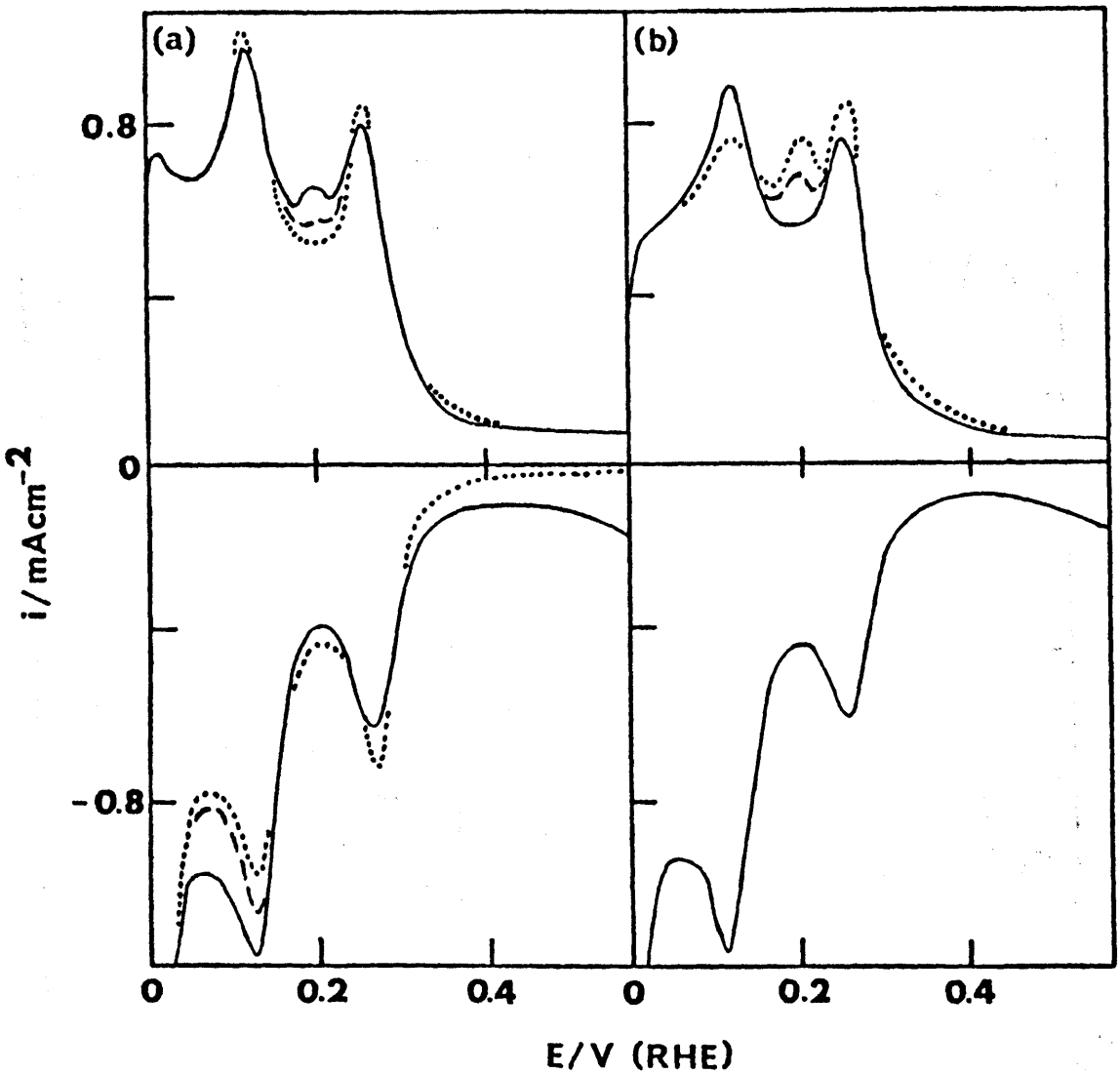

Figure 5.5: (a) Effect of cycling on the disappearance of the H_i peak: (——), cyclic voltammogram 50 mV s^{-1}, 0-1.6 V (only the H-region is shown here), for smooth Pt in N_2-degased 1.0 mol dm^{-3} H_2SO_4 at 25°C; (····), the 100th cycle after altering the scan limits to 0-0.6 V; (----), the 20th cycle (where it differed significantly from the 100th).

(b) Restoration of the H_i on holding the potential at 0 V: (——), steady state scan recorded on repetitively cycling the electrode, 0-0.6 V, 50 mV s^{-1}; (----) and (····), the electrode was held at 0 V for 10 sec and 5 min, respectively, prior to recommencing the scan in the anodic direction. The electrolyte was N_2-stirred during the holding period to minimise accumulation of H_2 about the interface; most conditions for (b) were similar to those quoted here for (a).

When an electrode was subjected to extensive cycling under reducing conditions (0 to 0.6 V, 500 mV/s, for 20 min) it gave a response similar to the dotted line in Fig. 5.5(a). Then after holding the electrode at 0 V for 15 minutes, the next cycle showed a clear response for H_i; however, this peak virtually disappeared on the next cycle, Fig. 5.6, while H_w (and to a lesser H_s) was slightly enhanced.

Essentially the same type of behaviour for H_i was obtained using $HClO_4$ as an electrolyte. For instance, the H_i peak was not observed with the latter electrolyte, under repetitive sweep conditions, until the upper limit of the sweep was extended to ca. 1.0 V(RHE). In general the resolution of the peaks in the hydrogen region was significantly less in this case. An example is given in Fig. 5.6(b); this again illustrates the effect of holding at 0 V. H_i can be seen on the first anodic scan recorded after such pretreatment but, with the low anodic limit used in this case (0.6 V), it is virtually absent in subsequent scans.

While the height of H_s was approximately the same on the anodic and cathodic sweep, for voltammograms recorded in H_2SO_4, with a variation of the upper limit, the height of H_w tended to be greater when the sweep was in the cathodic direction. This is represented in Fig. 5.7 by a graph of the ratio of the height of the cathodic to anodic wave, h_c/h_a, against the increase in the upper limit. The platinum electrode was cycled, for ca. 5 min. (500 mV/s) between 0 V and the upper limit in question, prior to the ratio h_c/h_a being calculated.

5.2.3. Discussion

The results outlined above indicate some of the ways the H_i peak differs from other peaks in the hydrogen region of platinum. It is postulated here that the H_i peak is not in fact a hydrogen peak and hence does not behave as expected for one of the latter. The above data, and other data discussed later, is more consistent with the idea that the small intermediate peak, H_i, on the anodic sweep is due to an adatom (Pt*)/hydrous oxide transition of the form indicated in equation (5:1:8).

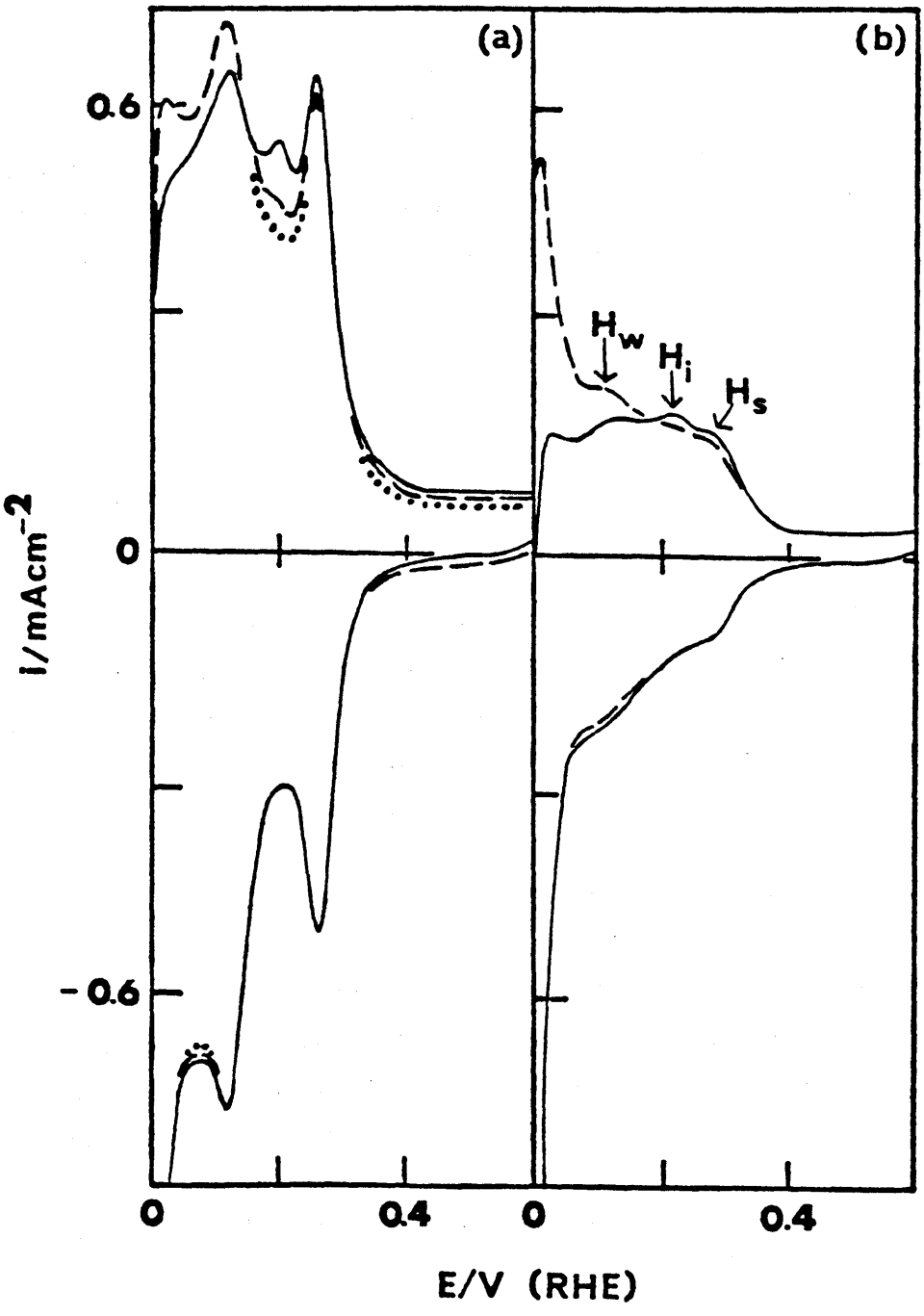

Figure 5.6: (a) Loss of H_i after holding at 0 V: (——), (----) and (····) show the 1st, 2nd and 5th voltammogram (0-0.6 V, 50 mV s^{-1}) recorded after holding the potential at 0 V for 15 min; same general conditions as in Fig. 5.5.

(b) Similar experiment using 1.0 mol dm^{-3} $HClO_4$ as electrolyte. The 1st (——) and 2nd (----) cycles (0-0.6 V, 50 mV s^{-1}) shown here were recorded after holding the Pt electrode at 0 V for 5 min.

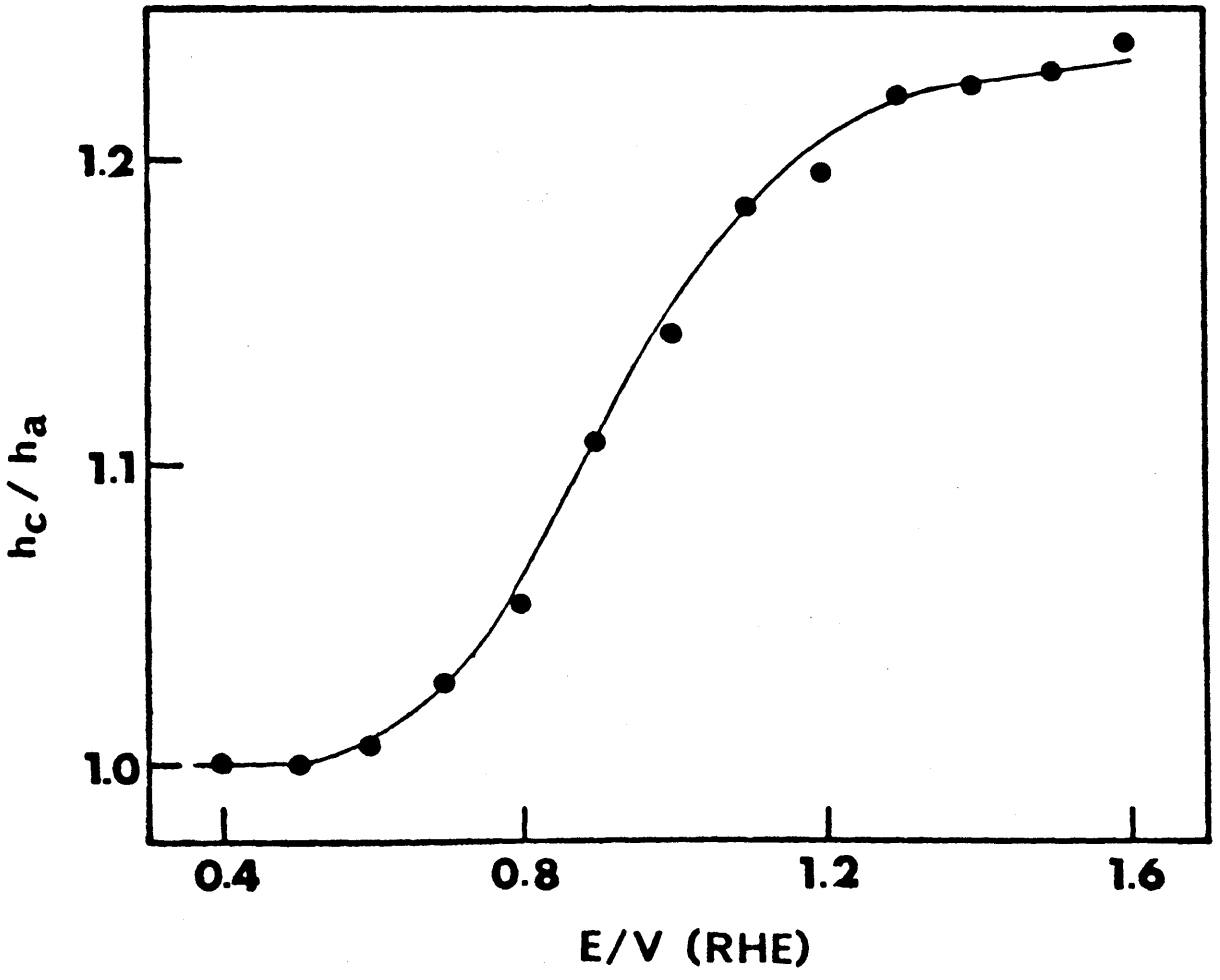

Figure 5.7: Variation of peak height ratio (h_c/h_a) for the cathodic (h_c) and anodic (h_a) response in the H_w region (Fig. 5.4) as a function of the value of the upper limit (E) of the scan (0-E, 50 mV s^{-1}); smooth Pt in N_2-degased 1.0 mol dm^{-3} H_2SO_4 at 25°C. The platinum electrode was cycled, for 5 min (500 mV/s) between 0 V and the upper limit in question, prior to the ratio h_c/h_a being calculated.

The anomalous behaviour of the H_i peak was clearly established by Conway and co-workers [465] who found the entropy change associated with the reaction involved here (ca. 0 JK^{-1} mol^{-1}) to be totally different to that associated with the other hydrogen adsorption/desorption peaks examined in their work. However, if the peak is considered to be due to formation of an hydrous oxide species then the entropy change associated with the conversion outlined in equation (5:1:8) (where an adatom, already surrounded with six water molecules, is converted to an hydrous oxide species) would be expected to be low as no great difference occurs in the atomic environment. Confirmation of the anomalous behaviour of the H_i peak was obtained using staircase voltammetry [287]; it was shown for instance that there was a slow component in the reaction involved - though only on the anodic sweep. This may be explained in terms of the hydrous oxide viewpoint by assuming that in the latter case the electrochemical step, equation (5:1:8), is preceded at longer times by a slow adatom formation step, i.e. a decrease in lattice coordination number (LCN) value for Pt surface atoms of intermediate values of the latter. The absence of such a slow response on the subsequent reduction step is understandable as in this case the electrochemical step now precedes any change in LCN value likely to occur after adatom formation.

The data for reflectance changes, and in particular the time dependence of the latter in response to square wave potential perturbation in the hydrogen region of platinum, as reported by Bewick and Tuxford [466], are quite interesting. Using a fixed anodic value of +320 mV (NHE) in 1.0 mol dm^{-3} $HClO_4$ and a series of cathodic values ranging from +20 to +170 mV (NHE) the following results were obtained. Stepping from +20 to +320 mV, Fig. 10(a) in ref. 466, gave a dual response - a rapid increase in reflectivity followed by a slow decrease. On reversing the perturbation, i.e. switching from +320 to +20 mV, an initial spike, i.e. an increase in reflectivity, was observed, followed by a decrease but with little if any time dependence of the reflectivity at the lower potential. As the lower limit was raised from +20 to +170 mV (in a series of steps) the square wave component diminished and the feature remaining, according to the authors, was the slow decrease following the anodic step. The data in this work was averaged over many runs and essentially the same results were obtained by fixing

the cathodic limit at +70 mV and varying the upper value from +120 to +570 mV. The slowly-forming component (and the two reflectance spikes) appeared with the anodic limit above +220 mV but the time scale for the fall decreased with increasing value for this limit.

While the interpretation suggested here for the fast component in the square wave response is the same as that proposed by Bewick and Tuxford [466], i.e. high hydrogen coverage (at potentials well into the region of weakly bound hydrogen) caused a decrease in reflectivity, the interpretation of the slow response, and spikes, is different. Switching from +70 to +320 mV cleared the surface of hydrogen giving a rapid jump in reflectivity. This, however, is followed by adatom oxidation - a slow process because such oxidation is generally preceded by a lowering of LCN value. Thus at the anodic limit a slow decrease in reflectance is (as expected) observed. Switching once more to the cathodic limit leads to immediate reduction of all hydrous oxide species - a rapid rise in reflectance is observed here as there is no pre-electrochemical step in this case (hence the second spike). This is followed immediately, at the lower potential, by the fast decrease in reflectance to a constant value as the surface becomes appreciably covered with hydrogen. The observed decrease in time scale for the slow reflectance change on stepping from a lower limit (+70 mV) to increasing values of the upper limit, Figs. 11(d)-11(h) in ref. 466, is evidently due to the effect of increasing over-potential on both the hydrous oxide formtion and, in particular, the preceding, slow adatom formation step. It may be noted that this interpretation of the reflectance changes is very similar to that suggested here earlier to explain the staircase voltammetry data [287].

It may be noted that in order to explain the slow response Bewick and Tuxford [466] had to assume slow ionisation of strongly bound hydrogen on platinum - however, there is no direct evidence that this type of hydrogen reacts significantly slower than weakly bound hydrogen. It is interesting to note also that the maximum reflectivity for the Pt/0.5 mol dm^{-3} H_2SO_4 system, according to Conway and Angerstein-Kozlowska [467], is at ca. 0.2 V(RHE), i.e. in the region of the H_i peak where the surface is free of both hydrous oxide and weakly bound hydrogen.

Bewick and coworkers [267] assumed that whereas the weakly bound hydrogen exists at the interface as a layer of hydrated atoms, viz.

$$Pt + H_3O^+ + e = Pt—H—O\begin{matrix}H\\H\end{matrix} \qquad (5:2:1)$$

the strongly bound hydrogen exists in an interstitial protonic form at hollow sites ($Pt_{h.s.}$) at the interface, viz.

$$Pt_{h.s.} + H_3O^+ + e = Pt_{h.s.}—H^+ + H_2O + e \qquad (5:2:2)$$

The electron involved in the discharge of the hydrogen is assumed to be denoted back to the conduction band of the metal. However, it is not easy to see why an electron should leave the proton and return to the electron-rich conduction band. Furthermore, one would expect the entropy changes associated with equations (5:2:1) and (5:2:2) to differ significantly - which, according to experimental data [465], is not the case.

The same type of controversy as outlined here in connection with reflectance data also arises with regard to the interpretation of thin film conductance results for platinum in acid solution. According to Fujihira and Kuwana [468] the increase in film conductivity as the potential enters the hydrogen region may be due to the strongly bound hydrogen existing in a protonic form; however, the authors stress that even at that stage (1975) such a view was controversial. The possibility of oxide being involved in the hydrogen region of platinum was obviously not given serious consideration at that time. However, it is now clear that just as removal of the monolayer oxide film at higher potentials resulted in an increase in Pt film conductivity [468], the removal of the low coverage hydrous oxide film at the start of the hydrogen adsorption region should give (as observed) a similar conductivity charge - though of much smaller magnitude.

The results quoted here largely confirm data produced by other authors. For instance Woodard and coworkers [286] showed that holding polycrystalline or (110) platinum surfaces at potentials

below 0.15 V(RHE) caused the peak associated with H_i to increase - these authors refer to still earlier data of the same type and one of their suggestions to explain this effect involves participation of a "hard-to-reduce surface oxide". In a later paper Scortichini and Reilley [302(c)] reconfirmed the enhancement of H_i on holding the electrode at low potentials (see also Breiter [135], pp. 59-60) and also stated that to continue to observe this peak the upper limit of the scan should include the monolayer oxide formation region. The presence of H_i was demonstrated by Hoare [469] for bright platinum in both H_2SO_4 and HF solution - and is therefore unlikely to be associated with anion adsorption phenomena (the F^- anion is assumed not to adsorb specifically at metal surfaces), in both solutions H_i vanished on cycling between reduced limits, ca. 0.0 to 0.46 V(RHE). An interesting account of the behaviour of the H_i peak has also been produced by Loo and Furtak [318]; these authors report an anodic and cathodic peak in this region for an aqueous $NaHCO_3$ electrolyte but the resolution of some of the cathodic peaks in the diagram in question, Fig. 1(A) in ref. [318], is quite poor. The unusual character of the H_i peak was also pointed out by Woods [200] who reported that this peak was not observed at fast sweep-rates or at low temperature. The appearance of the H_i peak on platinum single crystal surfaces has been dealt with in section 1.7.7(b) with both Clavilier and Armand [308] and Woodard et al. [286] reporting the existence of such a feature.

With regard to the results quoted here for the appearance of the H_i peak one of the most important points is the low magnitude, under any condition outlined here, of the charge associated with H_i. Very special sites of extremely low coverage are apparently involved; therefore direct observation of such sites, or the species generated at them, will obviously be extremely difficult. This in turn means that the interpretation of the behaviour of the H_i peak must be largely speculative.

An interesting account of hydrogen absorption by platinum, and a discussion of the possibility that this form of hydrogen is responsible for the H_i peak, has been given by Woods [200]; however, the author was unable to establish the identity of the species or reaction involved in this region. Cycling the platinum into the monolayer oxide formation region causes place-exchange,

i.e. a disturbance in the outer layer of metal atoms, so that on reduction an increased density of adatoms is obtained at the interface and hence H_i - if the latter is attributed to the process shown is equation (5:1:8) - becomes more clearly visible. Adatoms are high energy species that readily decay by increasing their bulk metal lattice coordination number, viz.

$$Pt^* \rightarrow pt_{(\ell)} \qquad (5:2:3)$$

Consequently, peak H_i emerges clearly on successive cycles only when the upper limit of the sweep is such that significant surface oxidation is involved so that the highly disturbed state of the surface is regenerated during the cathodic sweeps, Fig. 5.4.

However, the data shown in Fig. 5.6(a) suggests that monolayer oxide formation and reduction is not essential in order to observe H_i, i.e. to generate adatoms. Holding the electrode at 0 V for a significant period of time may result not only in the formation of H_{ads} but also some intrusion of hydrogen into the outer layers of the metal lattice - evidence to support the latter view has been summarised by Woods [200]. On recommencing the anodic sweep the reduction of this surface hydride evidently yields a significant coverage of platinum adatoms - hence the appearance of peak H_i. As pointed out earlier these adatom species decay rapidly and thus H_i is virtually absent on subsequent anodic sweeps, Fig. 5.6(a).

The claim that oxide formation occurs within the hydrogen region for platinum in aqueous media is likely to be controversial and alternative interpretations of the H_i peak, in terms of both hydrogen absorption and adsorption (a H_3^+ species was mentioned in the latter case), have been outlined by Woods [200]. However, the latter author has pointed out that there are observations apparently inconsistent with the conclusion that peak H_i can be simply ascribed to hydrogen absorption in the bulk metal.

It is assumed here that the adatom/incipient hydrous oxide peak appears clearly only when the metal surface is pretreated so that its adatom coverage is high and, furthermore, such high adatom coverages are rather unstable - the adatoms decay readily by increasing their lattice coordination number. This may well be the

reason why H_i is not easily seen with platinised platinum surfaces; the latter are so highly defective that adatoms can decay rapidly by interacting with neighbours in defect sites (on this basis the ideal situation with regard to high adatom activity is to have such atoms in contact with a perfect single crystal surface).

Another feature noted during the course of this work was that while the height of peak H_s was approximately the same on the anodic and cathodic sweep, the height of H_w tended to be greater when the sweep was in the cathodic direction (this can also be seen in data quoted by Woods - see curve 1, Fig. 14, in ref. 200). The main surface oxidation process is clearly involved in this effect as the peak height ratio (h_c/h_a) was found, Fig. 5.7, to depend upon the anodic limit of the scan. This effect cannot be due simply to general roughening as the latter should affect the height of the H_w on both the anodic and cathodic sweep to the same extent. It is assumed here that reducing the oxide monolayer yields a significant level of Pt* adatoms - some of which oxidise to the hydrous oxide state. The reduction of these just below 0.2 V (there may be some hysteresis associated with the reaction shown in Fig. 5.1 as peak H_i is usually not observed on the cathodic sweep) should increase the charge in the H_w region of the cathodic sweep. There may also be some loss of subsurface oxygen from the outer layers of the metal lattice in this region. Support for this view of incomplete oxide removal in the monolayer oxide reduction region can be found in earlier reports [469] that for smooth platinum electrodes the charge for formation of the monolayer oxide film is significantly larger than that for its reduction. If the material produced on reduction below 0.2 V is in an active state, e.g. of somewhat higher than normal surface area, that rearranges rather readily, then both the greater value of h_c compared to h_a as well as the dependence of the ratio h_c/h_a on the anodic limit of the scan, Fig. 5.7, are understandable.

5.3. OXIDATION OF ORGANIC COMPOUNDS AT PLATINUM

According to the present model, electrocatalysis of anodic processes are mediated, or triggered, by low levels of incipient hydrous oxide species formed at adatom sites on the metal surface. If this view is valid then oxidisable species should commence (anodic sweep) and terminate (cathodic sweep) their oxidation on platinum in the hydrous oxide reduction region which is at ca. 0.2 V(RHE) in acid [463]. However, such reactions of carbonaceous species are difficult to investigate as they are generally complicated by the formation of CO_{ads}-type poisoning species [470]. One way of minimising the effect of the latter (at least for short periods of time) is explored in this section; it was also demonstrated that the oxidation of other compounds, in particular hydrazine, is free of complications arising from surface deactivation.

5.3.1. Results

A typical voltammogram for hydrazine oxidation on platinum in acid is shown in Fig. 5.8. The reaction commenced (anodic sweep) and terminated (cathodic sweep) at ca, 0.2 V. The oxidation current increased over the potential range ca. 0.2 to 0.6 V before levelling out to give a plateau response. The absence of significant poisoning in this case was evident from the fact that the i/E profiles for the anodic and cathodic currents virtually coincided. The dashed line in Fig. 5.8 shows the anodic response in the hydrogen region for the same electrode and conditions - except in the absence of hydrazine.

The behaviour of platinum in base, with and without hydrazine present, is illustrated in Fig. 5.9. The behaviour of platinum in pure base (the dashed line) followed the same overall pattern as for platinum in acid giving hydrogen, double layer and oxide regions. The main differences noted were the cathodic shift in the onset of oxide formation and, of particular interest to the present theory, the disappearance of the intermediate hydrogen peak, H_i, from the hydrogen desorption region. The onset and termination of hydrazine oxidation on platinum in base shifted cathodically to ca.

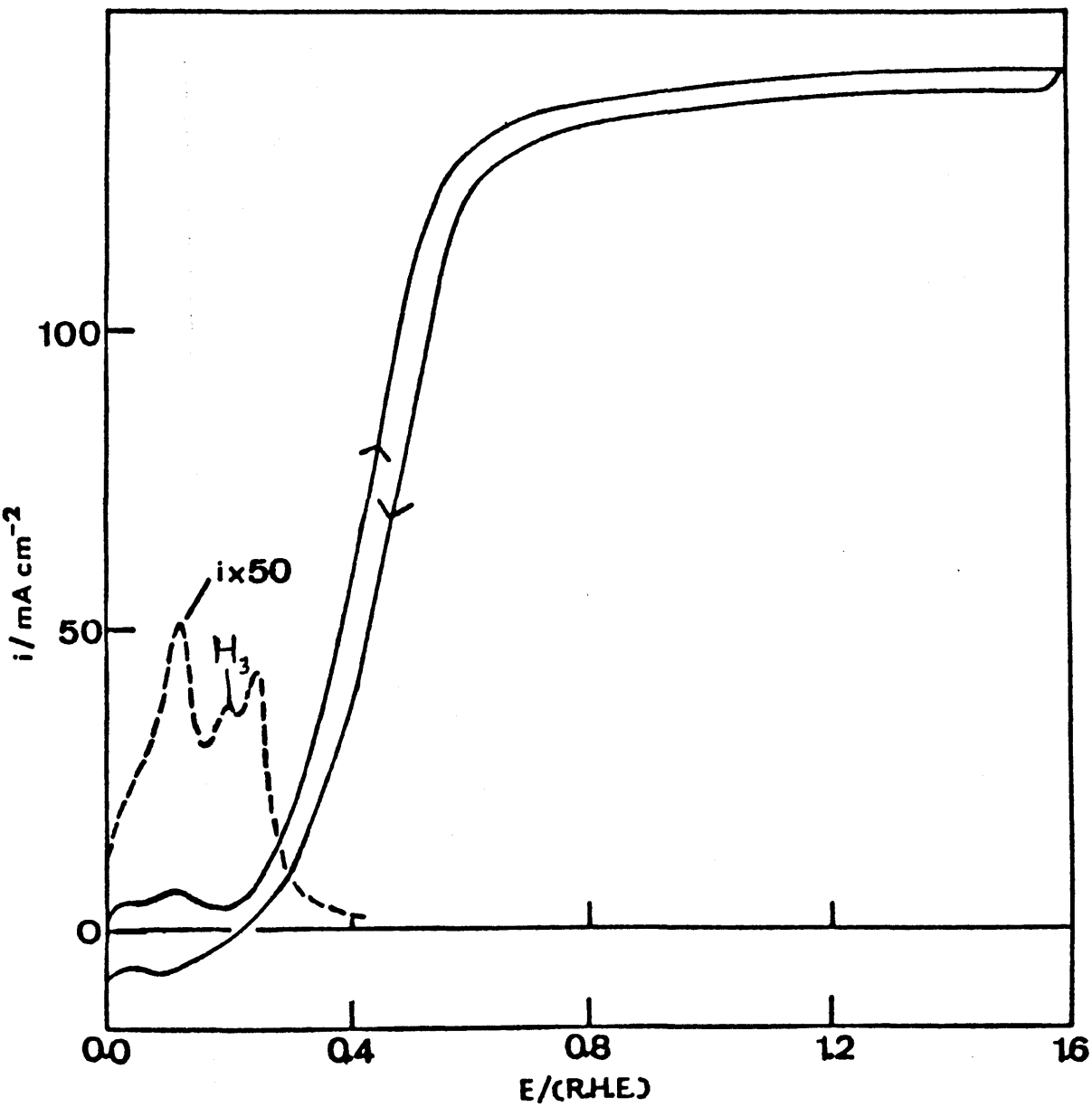

Figure 5.8: Cyclic voltammogram (0-1.6 V, 50 mV s^{-1}) for a platinised platinum electrode in 1.0 mol dm^{-3} H_2SO_4 solution containing 0.1 mol dm^{-3} N_2H_4 (full line); the dashed line shows the anodic response in the hydrogen region for the same electrode and conditions - except in the absence of N_2H_4. The solution was nitrogen stirred, T = 25°C.

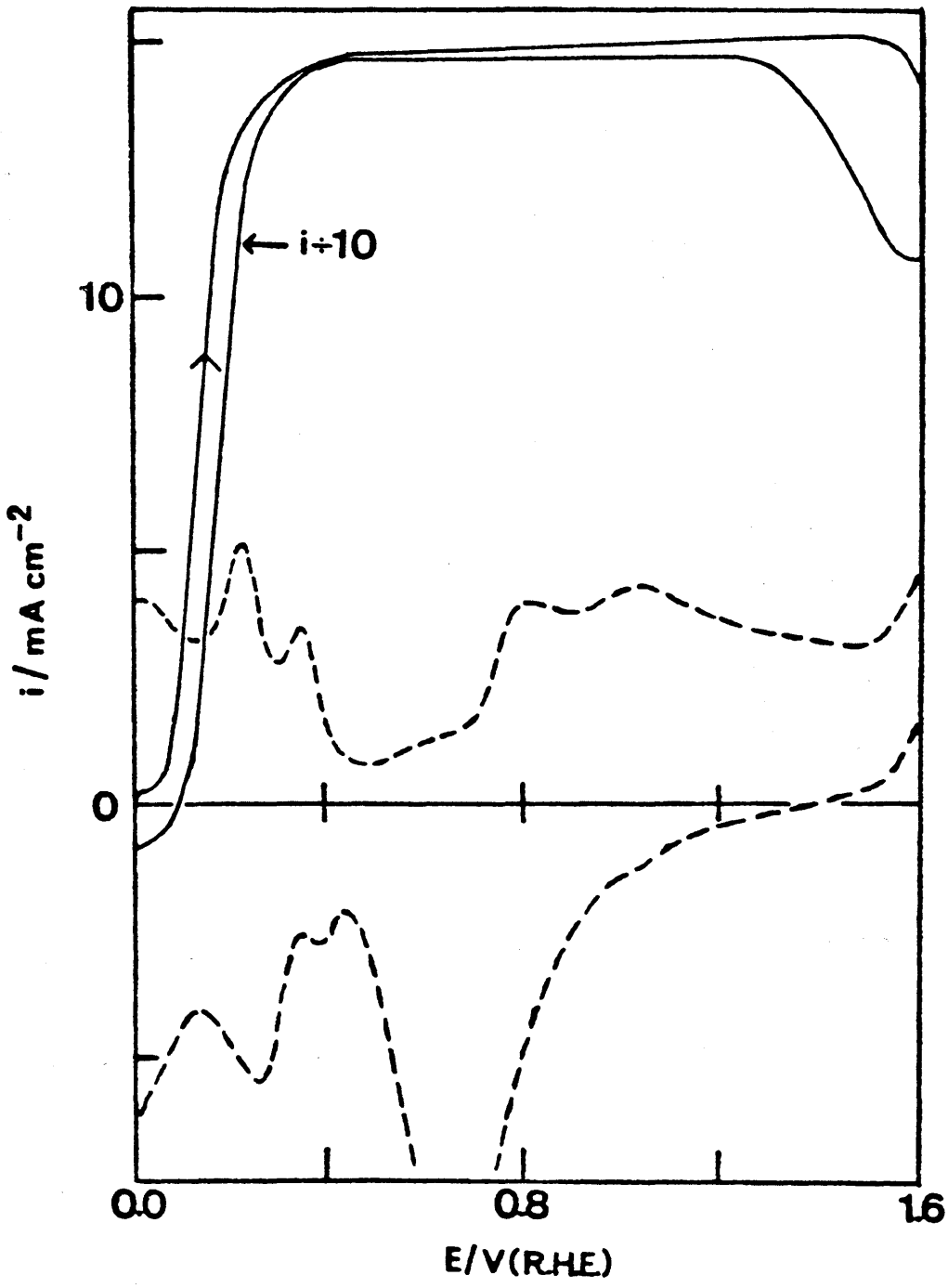

Figure 5.9: This is the equivalent to Fig. 5.8 in base; the solution was 1.0 mol dm^{-3} NaOH, and cyclic voltammograms were recorded both in the absence (----) and presence (——) of N_2H_4 (0.1 mol dm^{-3}).

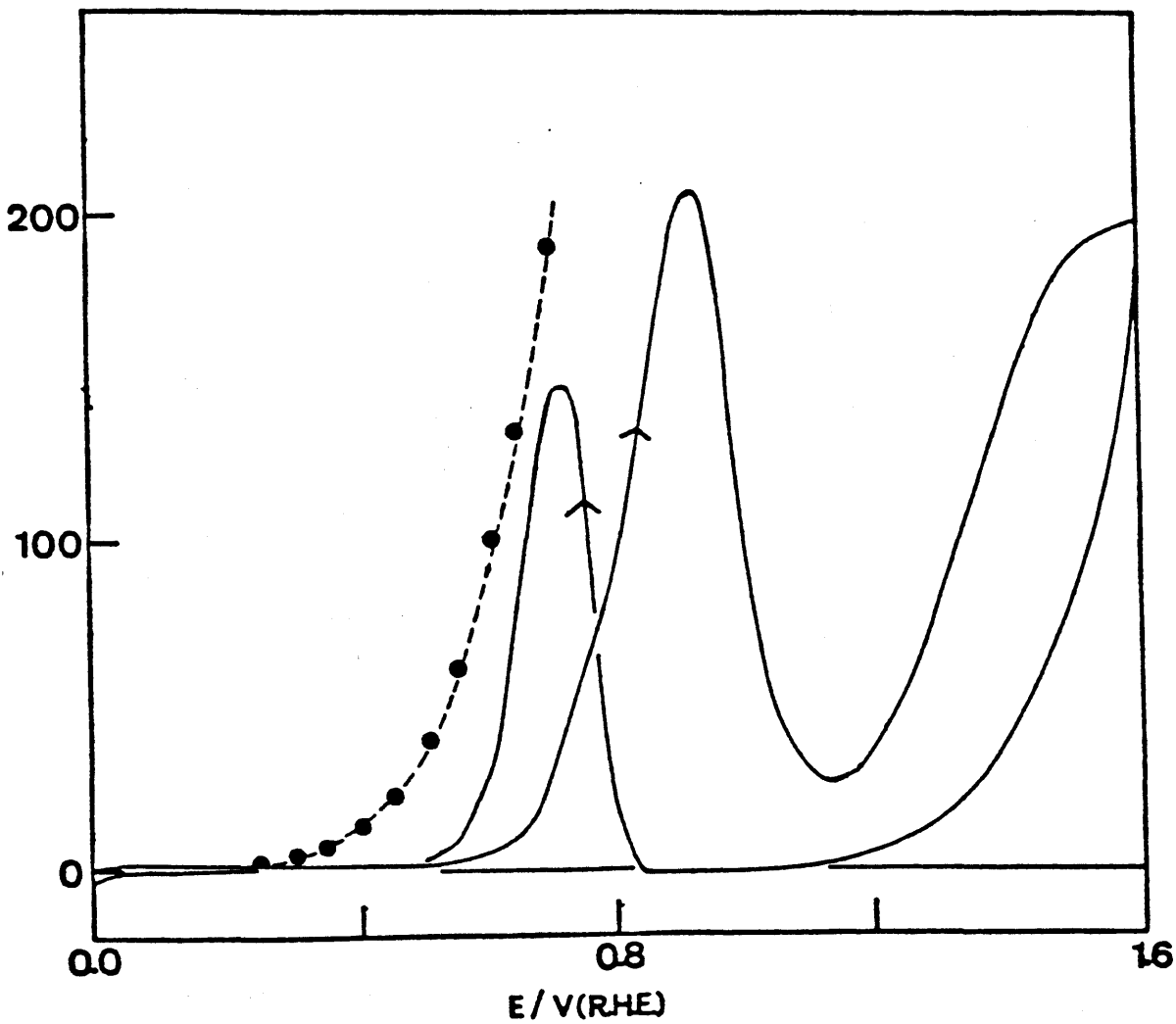

Figure 5.10: The response for methanol oxidation at a platinised Pt electrode in N_2-stirred 1.0 mol dm^{-3} H_2SO_4 + 0.5 mol dm^{-3} CH_3OH solution (T = 25°C; 50 mV s^{-1}) is given by the full line. The dashed line is for methanol oxidation under poison-free conditions; the electrode was preanodized at 1.1 V for 30 s before stepping to the lower potentials (●). The current density values here correspond to t = 0 following the step.

0.05 V. Also, the rate of current increase with potential in the presence of hydrazine was much sharper in base than in acid and the plateau current was attained in base just above 0.3 V. There was a slight drop in oxidation current at ca. 1.5 V which was still evident after potential reversal at 1.6 V but the plateau current was reattained at ca. 1.3 V on the cathodic sweep: the anodic and cathodic curves virtually coincided at lower potential values.

The cyclic voltammetric response for the oxidation of methanol at platinum in acid, Fig. 5.10, appears at first glance, to contradict the present model of electrocatalysis as oxidation on the anodic sweep apparently commenced at ca. 0.5 V rather then 0.2 V. This oxidation increased to a maximum at ca. 0.9 V with a small shoulder at ca. 0.7 V on the anodic sweep. A second oxidation response occurred between 1.2 to 1.6 V; however, reaction in this region was significantly less marked during the cathodic sweep. Oxidation on the cathodic sweep recommenced at ca. 0.8 V and terminated at ca. 0.5 V.

However, as mentioned previously, there is a well-known [470,471] complication at the platinum surface due to CO_{ads} deactivation, possibly at reactive Pt* sites. Such species can be removed by anodizing in the oxide monolayer region. Results were obtained for the variation of platinum electrode current with time, after anodizing at 1.1 V for 30s in acid solution in the absence of any oxidisable material, and stepping from the latter potential value to a series of lower values. All currents recorded were cathodic with an initial spike which was probably associated with oxide film reduction plus deposition of hydrogen. An experiment similar to that outlined above was carried out in the presence of methanol and the results obtained are shown in Fig. 5.11. In this case a predominantly anodic current response was observed providing that the lower potential value was above ca. 0.2 V. This anodic response decreased with time presumably due to deactivation of the electrode surface by the CO_{ads}. Current values for methanol oxidation in acid at a clean platinum electrode, i.e. at t=0 (where t is the time after the step), were obtained by extrapolating the anodic current decay profiles (Fig. 5.11) back to zero time at the step. These current values are shown by the dashed line (or points) as a function of the lower value of the step in Fig. 5.10.

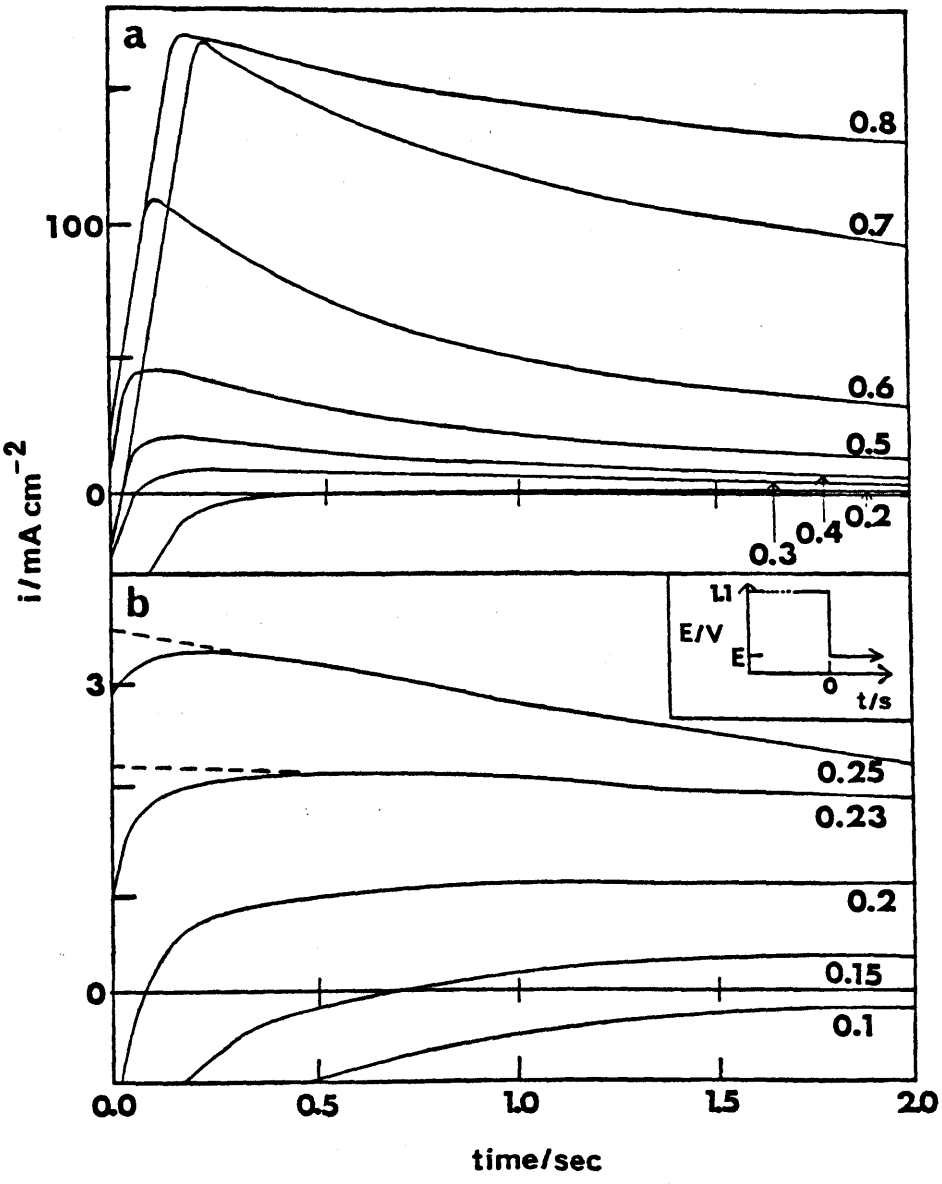

Figure 5.11: Decay curves for current against time upon stepping the potential from 1.1 V (hold for 30 s) to a series of lower values (on graphs) for a platinised Pt electrode in 1.0 mol dm^{-3} H_2SO_4 + 0.5 mol dm^{-3} methanol, T = 25°C. (b) inset shows potential profile used in stepping. The time axis for (b) is divided by 10.

This plot, which confirms earlier results by Russian authors [472] and Clavilier [473], shows that on a clean platinum electrode in acid methanol oxidation also commences at ca. 0.2 V.

Cyclic voltammetric responses for formic acid and formaldehyde at platinum in acid are given in Figs. 5.12 and 5.13 respectively. In both cases, three anodic peaks were observed on the anodic sweeps, at ca. 0.6, 0.9, and 1.45, respectively. On the subsequent cathodic sweeps oxidation of the organic species commenced at ca. 0.8 V, yielded a peak at ca. 0.6 V and terminated at ca. 0.2 V. In stepping experiments, similar to those outlined above for methanol, oxidation of both formic acid and formaldehyde was shown to commence at ca. 0.2 V (dashed lines, Figs. 5.12 and 5.13).

An example of a cyclic voltammogram recorded for the oxidation of isopropanol to acetone on platinum in acid is shown in Fig. 5.14. The isopropanol oxidation current commenced on the anodic sweep towards the end of the hydrogen removal region, i.e. above 0.3 V, followed by two peaks, one at ca. 0.6 V (A_1) and the other at ca. 1.3 V (A_2). Anodic peaks at approximately the same potentials values, labelled here as A_1' and A_2', were observed on the subsequent cathodic sweep. There was also an enhancement of charge in the cathodic sweep on the hydrogen region (C_1). Isopropanol oxidation currents, obtained by the stepping procedure outlined above, over the range 0.3 to 0.5 V, were the same as in the cyclic voltammetry experiments (dashed line, Fig. 5.14).

A series of cyclic voltammograms for isopropanol oxidation at platinum in acid recorded at different sweep-rates is shown in Fig. 5.15. At high sweep-rates, 500-50 mV s^{-1}, Fig. 5.15 (a)-(c), the main anodic peak (A_1) exceeds its cathodic equivalent (A_1') or the upper anodic peak (A_2). However, at low sweep-rate values, 10-1 mV s^{-1}, Fig. 5.15 (d)-(f), the peak height ratios are reversed - note also the emergence of a new intermediate peak, at ca. 0.9 V, on the anodic sweep at sweep-rates of 10-1 mV s^{-1}.

The response for the reduction of acetone on platinum in acid is shown in Fig. 5.16. A reduction peak was observed on both the anodic and cathodic sweep at 0.05 V with a decrease in acetone reduction current at potentials below the latter value. It was

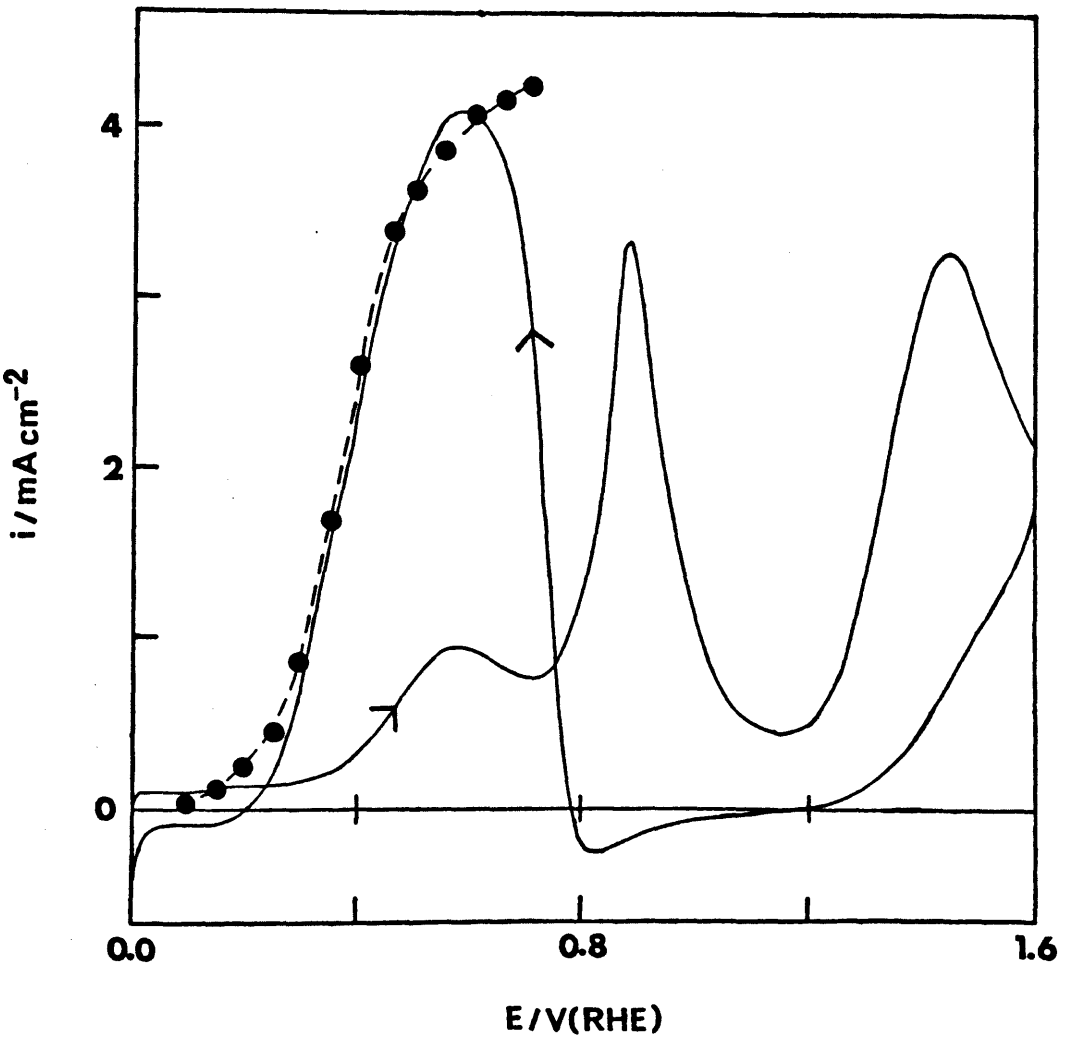

Figure 5.12: The response for formic acid oxidation at a platinised Pt electrode in N_2-stirred 1.0 mol dm^{-3} H_2SO_4 + 0.1 mol dm^{-3} formic acid solution (T= 25°C, 50 mV s^{-1}) is given by the full line. The dashed line is for HCOOH oxidation under poison-free conditions (as given in Fig. 5.8).

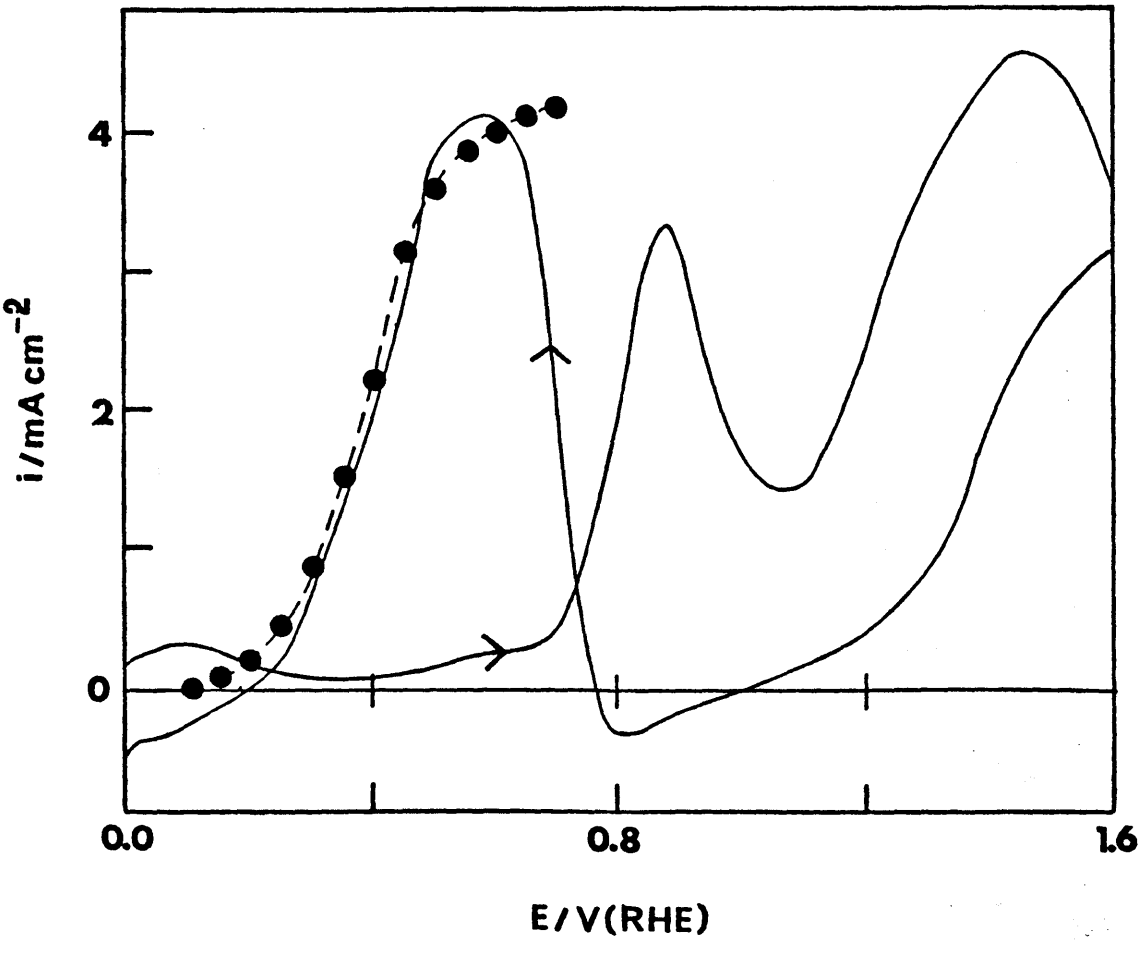

Figure 5.13: The response for formaldehyde oxidation at a platinised Pt electrode in N_2-stirred 1.0 mol dm^{-3} H_2SO_4 + 0.1 mol dm^{-3} HCHO solution (T = 25°C, 50 mV s^{-1}) is given by the full line. The dashed line is for HCHO oxidation under poison-free conditions (as given in Fig. 5.8).

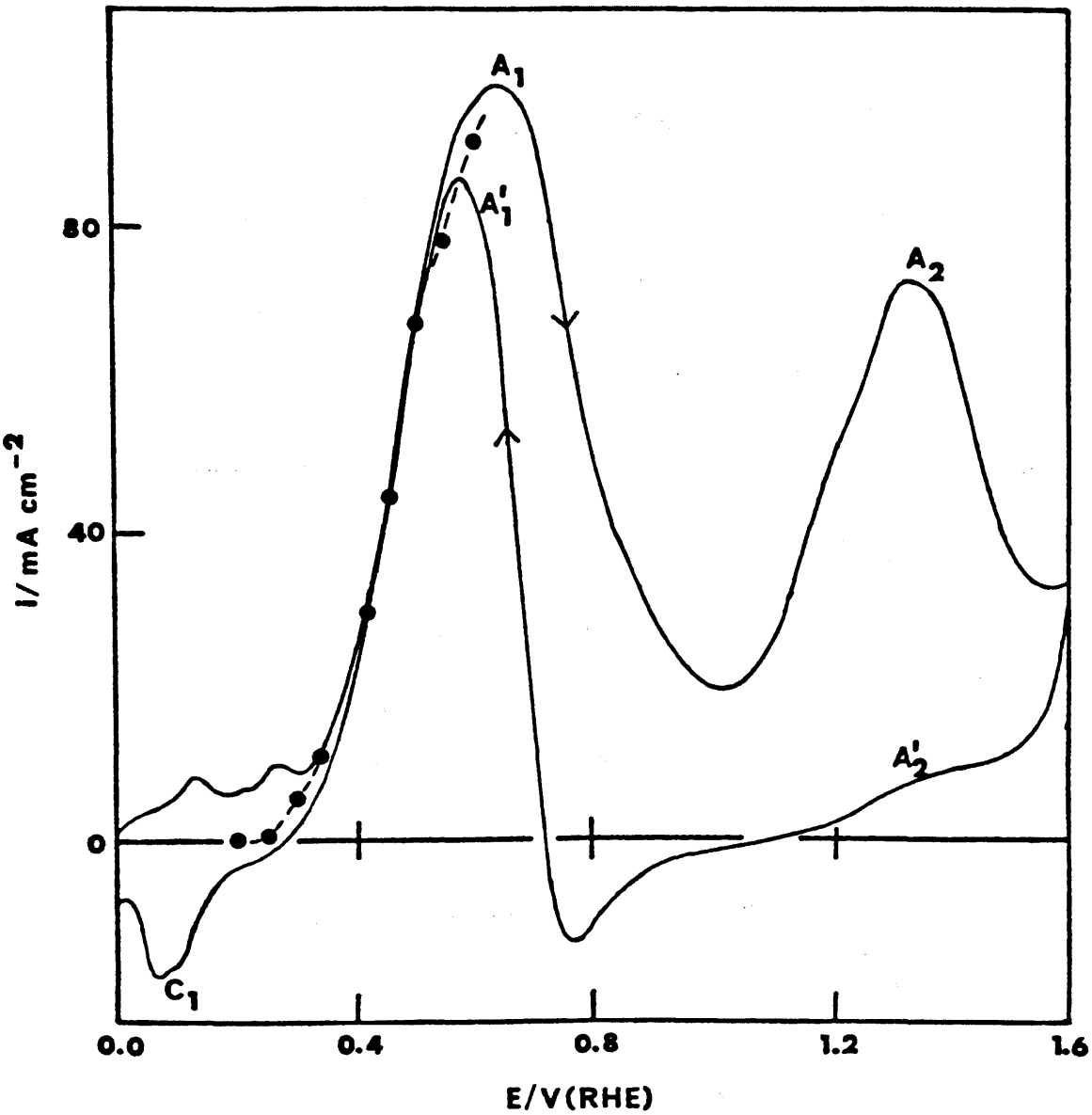

Figure 5.14: Cyclic voltammogram (full line) for isopropanol (0.5 mol dm^{-3}) oxidation at a platinised platinum surface (50 mV s^{-1}, 25°C) in N_2-stirred 1.0 mol dm^{-3} H_2SO_4. The broken line (or points) is the response for t = 0 (got by extrapolation) observed on stepping the potential of a preanodized electrode (30s at 1.3 V) to a variety (●) of lower values.

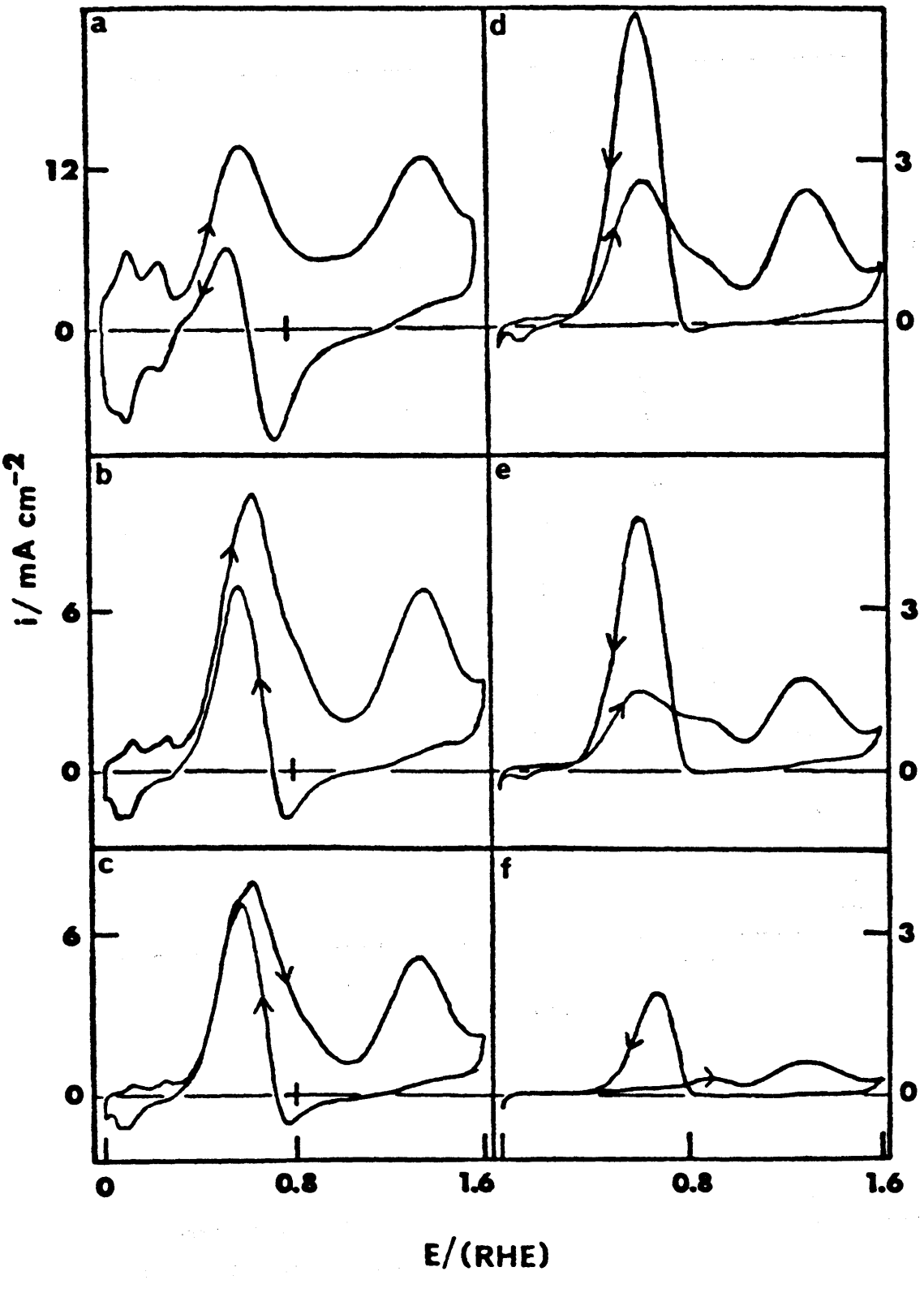

Figure 5.15: Effect of sweep-rate on the i/E response for a platinised Pt electrode in N_2-stirred 0.5 mol dm^{-3} isopropanol + 1.0 mol dm^{-3} H_2SO_4 at 25°C: sweep-rate (mV s^{-1}): (a) 500; (b) 100; (c) 50; (d) 10, (e) 5; (f) 1.

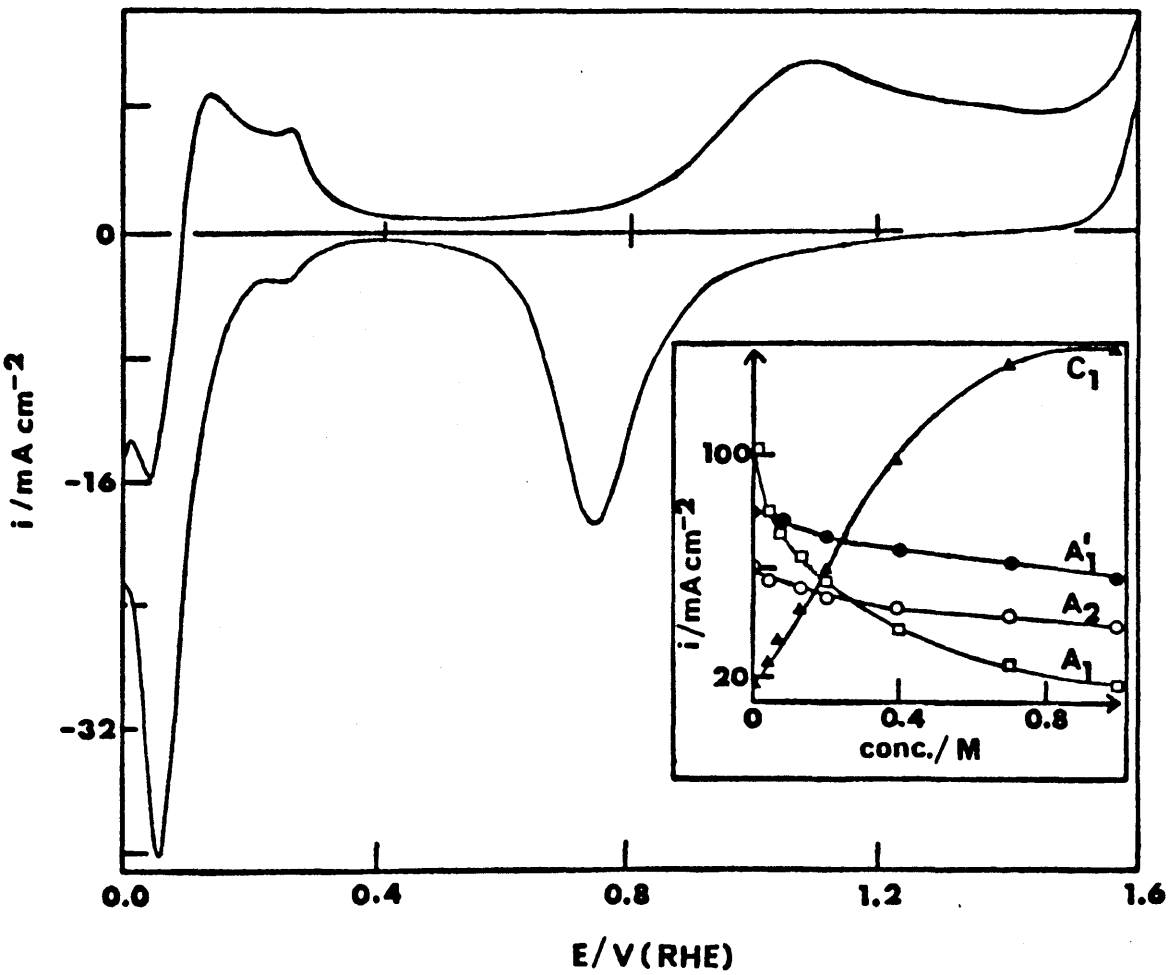

Figure 5.16: Cyclic voltammogram (50 mV s^{-1}) for acetone (0.1 mol dm^{-3}) reduction at a platinised platinum surface in N_2-stirred 1.0 mol dm^{-3} H_2SO_4 at 25°C. Inset shows the effect of the concentration of added acetone on the peaks for isopropanol (0.5 mol dm^{-3}) oxidation. The cyclic voltammetry conditions were as given here for the main diagram; peak labelling as in Fig. 5.14.

also noted that in the double layer region, e.g. at 0.45 V, the current in the anodic sweep in the acetone case (compared with the behaviour at this potential in Fig. 5.1) exceeded that in the cathodic sweep. The presence of the acetone also slightly modified the i/E response at the start of the oxide formation region, giving rise to a slightly larger rate of oxidation at ca. 0.8 V. Note also that the poorly resolved triplet at the start of the surface oxidation region (Fig. 5.1) is replaced by a single peak (Fig. 5.16) in the presence of acetone. The effect of acetone concentration on the oxidation of isopropanol in acid is summarised in the inset in Fig. 5.16. The most notable features here are the significant decrease in peak A_1 and increase in peak C_1; A_2 and A_1' also decrease (to a much lesser extent) with increasing acetone concentration.

The effect of temperature on the rate of isopropanol oxidation at peaks A_1 and A_1' is summarised, for two alcohol concentration values, in Fig. 5.17. A notable feature was the decrease in the rate of oxidation with increasing temperature on the anodic sweep in the case of the more concentrated alcohol solution. The alcohol oxidation in the region of peak A_1' on the cathodic sweep increased quite significantly with increase in temperature.

The oxidation behaviour of a range of other organic compounds was examined in the same manner as outlined here for methanol, formic acid, etc. The relevant data for all these compounds is summarised in Table 5.1; some of these species, e.g. glycine, methylamine, dimethylamine, dimethyl sulphoxide, appeared to be rather inert with respect to oxidation; others, e.g. oxalic acid, were capable of oxidation only at relatively high potentials. The important result here is that the vast majority of reactive organic compounds commenced oxidation on poison-free (stepped) platinum surfaces in acid at approximately the same potential, ca. 0.2 V(RHE).

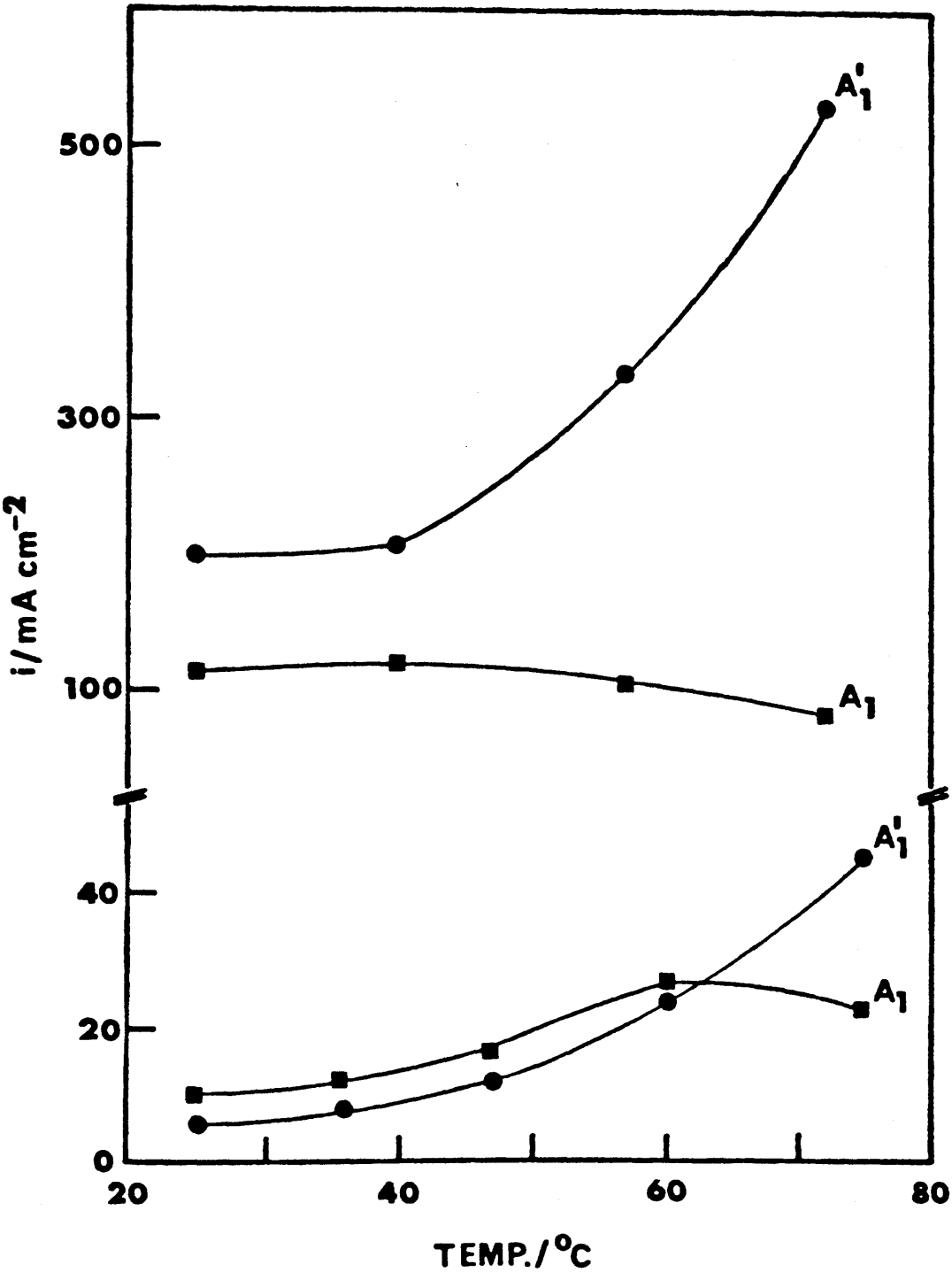

Figure 5.17: Variation of current density with temperature for isopropanol oxidation in 1.0 mol dm^{-3} H_2SO_4 (50 mV s^{-1}). Lower values are for 0.1 mol dm^{-3} isopropanol; upper values are for 3.0 mol dm^{-3} isopropanol.

TABLE 5.1: OXIDATION BEHAVIOUR FOR ORGANIC COMPOUNDS UPON STEPPING

List of organic compounds giving their onset oxidation for cyclic voltammetric experiments (50 mV s^{-1}, T = 25°C, conc. 0.1 mol dm^{-3}) and after stepping experiments (as detailed earlier for methanol, Fig. 5.10) for platinum in acidic electrolyte. Values are quoted versus RHE.

Compound	Cyclic Voltammetry	Stepped
Methanol	0.45	0.18
Formic Acid	0.35	0.18
Formaldehyde	0.5	0.15
Isopropanol	0.25	0.21
2-Ethoxyethanol	0.3	0.17
Diglyme	0.4	0.15
Hydrazine	0.2	0.21
Ethylene Glycol	0.4	0.18
Diformyl Hydrazine	0.4	0.15
Acetaldehyde	0.7	0.16
Ascorbic Acid	0.6	0.26
Glycine	-	-
Methyl Amine	-	-
Diethylamine	-	-
Dimethylsulphoxide	-	-
Hydroxylamine	0.9	-
Dimethyl Hydrazine	0.7	0.4
Oxalic Acid	0.9	-

5.3.2. Discussion

According to the interfacial redox model of electrocatalysis the 0.2 V region is a critical potential for platinum in acid: above this $Pt(OH)_6^{2-}$ species should exist at a low coverage and accelerate hindered anodic reactions. Hydrazine, free of the complications of CO-type poisoning species [470], should commence oxidation above the thrermodynamically reversible potential, -0.35 V(SHE) [474], for this compound (the SHE and RHE scales virtually coincide at low pH). However, since oxidation does not occur until 0.2 V(RHE) the following cyclic redox mechanism for the reaction is assumed to operate, viz.

$$Pt^* + 6H_2O = Pt(OH)_6^{2-} + 6H^+ + 4e \qquad (5:3:1)$$

$$Pt(OH)_6^{2-} + N_2H_4 + 2H^+ = Pt^* + N_2 + 6H_2O \qquad (5:3:2)$$

The onset of hydrazine oxidation coincides with the appearance of the small intermediate peak, H_i, in hydrazine-free solution. the i/E profile for hydrazine oxidation, Fig. 5.8, certainly resembles a polarographic wave, yielding a plateau region; this is in excellent agreement with the general mechanism for electrocatalysis postulated in this thesis. The current variation over the potential range 0.2 to 0.6 V may reflect a change in the concentration, and stability, of hydrous oxyspecies over this region; this feature of the reaction is discussed later.

As pointed out in section 5.1, thick hydrous oxide layers grown on platinum in base cannot be readily reduced in this medium [463]; this is understandable as according to equation (5:3:1) the potential for hydrous oxide reduction should shift in the cathodic direction by 0.5(2.303 RT/F) V per unit increase in pH. Since the hydrous oxide on platinum reduces at ca. 0.2 V(RHE) in acid (pH≈0) it should reduce at ca. -0.18 V(RHE) in base (pH≈13.6). Such a potential is difficult to attain with platinum due to the low overpotential of this metal for hydrogen gas evolution. The absence of the intermediate (H_i) peak in base may be explained in terms of this cathodic shift in the hydrous oxide formation potential.

According to the postulated model traces of hydrous oxide should commence formation on platinum in base at ca. -0.18 V and thus oxidation of hydrazine should commence in this region. Since the standard potential of the cell based on the reaction

$$N_2H_4(\ell) + O_2(g) = N_2(g) + H_2O(\ell) \qquad (5:3:3)$$

is 1.56 V [198] the reversible potential for hydrazine oxidation in base is ca. -0.33 V(RHE). In fact, as shown in Fig. 5.9, hydrazine commences oxidation on platinum in base at a significantly lower value (0.05 V) than in acid (0.2 V); however, this value for base is not quite as low as expected. The reason why the onset potential for hydrazine oxidation in base is not lower is not quite certain but it may be that the hydrous oxide species cannot form readily on a fully hydrided surface. Even if the hydrous oxide does form initially (it being thermodynamically more favoured) it may be removed by reaction with weakly bound hydrogen, viz.

$$Pt(OH)_6^{2-} + 4H_{ads} + 2H^+ = Pt^* + 6H_2O \qquad (5:3:4)$$

and have difficulty in reforming in the presence of so much hydrogen. Another possibility is that low levels of hydrous oxide may exist below 0 V in base but are unable to react with hdyrazine because the latter cannot adsorb on a surface totally covered with hydrogen. In any event it appears that only when some of the surface is clear of hydrogen at ca. 0.05 V(RHE) that N_2H_4 oxidation is observed in base.

The process of hydrazine oxidation in base shows many of the characteristics of the interfacial cyclic redox, or hydrous oxide catalysed, route for reaction, e.g. the existence of a plateau region. Another significant feature of the reaction in base is the sharp increase in current at the start of the hydrazine oxidation process at ca. 0.05 V. The adatom/hydrous oxide transition for Pt in base was estimated earlier to be ca. -.0.18 V; however, significant hydrazine oxidation occurs only when the surface is partially clear of adsorbed hydrogen at ca. 0.05 V. Evidently, the rate of increase of oxidation, once this value is exceeded, is dramatic because the system is already well above the $Pt^*/Pt(OH)_6^{2-}$ value, i.e. the oxidant concentration at the interface is large and

virtually constant in the region 0.05 V.

The oxidation of most organic compounds, as outlined in section 5.3.1, is complicated due to CO_{ads} deactivation [470,471]. This deactivation process leads to a cyclic voltammetric response of the type given for methanol, formic acid or formaldehyde oxidation in Figs. 5.10, 5.12, and 5.13, respectively. Initial oxidation occurs at ca. 0.6 V probably due to partial removal (via oxidation) of CO-type deactivating species. The most active potential for oxidation of these compounds is ca. 0.9 V(RHE), i.e. just after the onset of regular monolayer oxide formation - a region where significant formation of hydrous oxide is known to occur [441] (hence the rapid rate of reaction). The current decay above 0.9 V is obviously due to the rapid decrease in the hydrous oxide component in the monolayer-type film [435]. Oxidation of the organic compound at ca. 1.3 V is assumed to involve a different mechanism as at this stage the oxide coverage of the platinum surface is quite high.

The slow rate of oxidation at the early stages of the cathodic sweep clearly establish the inhibiting character of the monolayer oxide material. Platinum atoms, which had been displaced from the surface lattice via the place-exchange reaction during oxide formation, evidently give rise to hydrous oxide species once the monolayer material starts to reduce below ca. 0.8 V - and hence oxidation of organic species recommences. This oxidation may fall off quickly if a poison is again formed as an intermediate (as in the case of methanol); however, if poisoning does not occur, oxidation will invariably terminate at ca. 0.2 V, e.g. formic acid in Fig. 5.12 and formaldehyde in Fig. 5.13.

The stepping experiments described earlier provide a means of examining the behaviour of organic oxidation reactions occurring at an unpoisoned platinum surface. On stepping to lower potential values an initial cathodic response is observed due to reduction of the monolayer oxide. In organic-free electrolyte the current decreases quickly to zero current, the rate of decrease probably being determined mainly by the oxide reduction process - a reaction (especially removal of residual, i.e. subsurface oxygen) that is much slower than adsorbed hydrogen formation. However, with

reactive organic in solution this cathodic response is replaced by organic oxidation which results in a net anodic current; it is possible in these circumstances that the electrons required for oxide reduction are supplied mainly by the reactive organic material rather than the external circuit. The decay of anodic current after the step is probably due to a gradual accumulation of poisoning species and relaxation of Pt adatoms at the platinum surface.

Strong evidence for the participation of surface hydrous oxide species in oxidation reactions in general may be found in the fact that diverse compounds, e.g. methanol, isopropanol, and hydrazine, all commence oxidation on the anodic sweep in the H_i peak region (observed by stepping). The different types of bonds (O-H, C-H, N-H) in these molecules may weaken on chemisorption but the participation of OH ligands from the metal hydroxy complex is evidently required to initiate oxidation.

As pointed out in Table 5.1, a large variety of other organic compounds behave in a manner similar to that described above, i.e. these organic compounds commence oxidation at ca. 0.2 V on stepping the potential from the monolayer oxide region to a range of lower values (the organic concentration in each case was 0.1 mol dm^{-3}). Certain compounds either did not oxidise to any significant extent, e.g. glycine, or commenced reaction at a potential well above 0.2 V, e.g. oxalic acid (0.9 V). It is evident, however, that most reactive organic compounds, although thermodynamically able to undergo oxidation at lower potentials, e.g. methanol (0.02 V), formic acid (-0.25 V), formaldehyde (-0.13 V), and hydrazine (-0.35 V) - all potential values quoted versus SHE at 25°C [474], commence oxidation on a platinum surface, free from deactivating species, in acid in the region of the intermediate (H_i) peak, i.e. at ca. 0.2 V(RHE).

Independent evidence for the significance of the 0.2 V potential in the case of platinum in acid may be seen in the work of Lamy and coworkers [250], and Sun and coworkers [471]. For formic acid oxidation the current on the cathodic sweep almost invariably drops to zero (irrespective of the orientation of the surface, see Fig. 1.19 in the present thesis) at this potential.

Since it does not involve a CO intermediate, formic acid oxidation on platinum is less susceptible to poisoning than the same type of reaction with methanol: some poisoning in the formic acid case is evident on the anodic sweep; evidently some CO_{ads} species are formed on reduction of CO_2 formed by catalytic decomposition of HCOOH at low potentials.

The oxidation of isopropanol at platinum in acid, as shown in Fig. 5.14, is assumed to involve the following reaction, viz.

$$(CH_3)_2CHOH = (CH_3)_2CO + 2H^+ + 2e \qquad (5:3:5)$$

Although there is some inhibition of this reaction [475] above 0.6 V, possibly due to strong adsorption of the product (acetone), the effect is not as marked as in the case of methanol; evidently CO-type species are not formed extensively in the case of isopropanol. The lower current densities in this case clearly demonstrate that isopropanol is not as reactive as hydrazine. An interesting feature is the prolonged, reversible change in current with potential over the approximate range 0.2 to 0.6 V. It is assumed here (and further evidence will be given later in connection with a reduction process) that the concentration of interfacial species (Pt* and $Pt(OH)_6^{2-}$) alters in a reversible manner in this region.

The variation of the rate of oxidation (or reduction) with potential, over the region in question, may be explained in terms of the following scheme, viz.

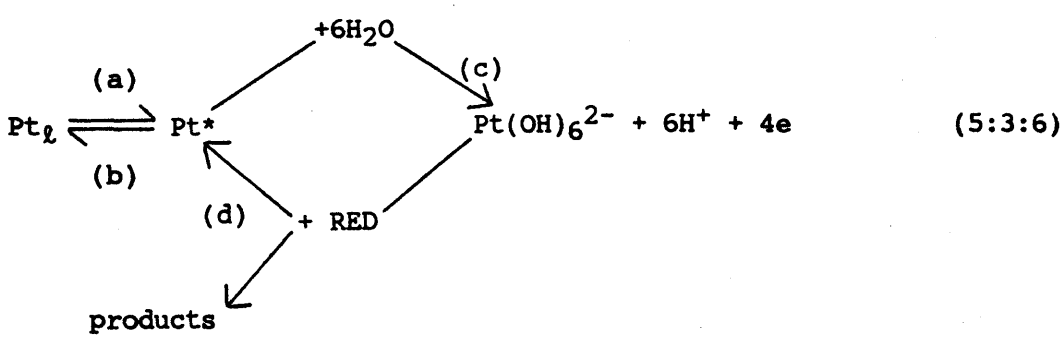

On the right-hand side is represented the interfacial cyclic redox process for oxidation of the reductant (RED), e.g. methanol, isopropanol, or hydrazine. On the left-hand side is shown the

complication in this system arising from the gain and loss of adatom species. Since the adatom is a high energy state, the equilibrium shown here by (a) and (b) will generally be far to the left: also at the polycrystalline metal surface there are probably a range of surface lattice atom (Pt_ℓ) states, i.e. the bulk-metal-lattice coordination number of Pt_ℓ (surface species) is assumed to be variable.

At the lower end of the potential range, ca. 0.2 V, the activity of the reduced state in the electrochemical step, (5:3:6(c)), will be high: this will promote loss of adatoms via (5:3:6(b)) thereby creating a low level of Pt(IV) and hence a low rate of oxidation. As the potential is increased the activity of the reduced state (Pt*) will be low because now the electrochemical equilibrium, (5:3:6(c)), will be driven to the right; under such conditions the Pt_ℓ/Pt* equilibrium will also tend to move to the right, yielding a higher coverage of Pt(IV) and, as observed, a higher rate of oxidation. The reversible character of the i/E response outlined in Figs. 5.8 and 5.14 is understandable in terms of the scheme outlined here in equation (5:3:6). It may be noted that the potential range in question here, 0.2 to 0.6 V, is similar to that recorded for the peak potential (E_p) variation during the course of thick hydrous oxide reduction on platinum (Fig. 3 in ref. 463) as the cathodic sweep-rate involved was varied from 50 to 5 mV s^{-1}.

The decay of current above 0.65 V in the case of isopropanol, Fig. 5.14, is probably due to an inhibition effect due to strong adsorption of the oxidation product (acetone) or an intermediate formed by chemisorption of the oxidation product. A plateau, rather than a decrease, was observed in this region in the case of the oxidation of less reactive compounds, e.g. 2-ethoxyethanol. The potential at which the decrease occurs with isopropanol is below the value expected for the onset of compact monolayer oxide formation. There is evidently some species, other than CO_{ads}, deactivating the electrode surface in the isopropanol case.

The effect of the surface deactivation can be seen more dramatically in cyclic voltammograms recorded for isopropanol at different sweep-rates, Fig. 5.15. Initial isopropanol oxidation

(A_1) occurs at low potential due to mediation of hydrous oxide species in a cyclic redox mechanism. The peak at ca. 0.9 V, Fig. 5.15 (d)-(f), may correspond to isopropanol oxidation either by an alternative mechanism to that involved in the A_1 peak or by the same mechanism at a surface at which the activity of hydrous oxide undergoes a transient increase. The latter explanation seems more likely as earlier work by Burke and Roche [441] indicated that the initial product at the onset of monolayer oxide formation is a hydrated species, as explained in section 5.1. Such a reactive product is assumed to be capable of oxidising the isopropanol over the region in question, 0.8 to 1.0 V; at high potentials this mechanism is inoperative because the degree of hydration of the interfacial oxide decreases with increasing coverage, i.e. $Pt(OH)_6^{2-}$ is replaced by $Pt(OH)_2$. Further oxidation, at A_2 in Fig. 5.14, occurs by a different mechanism as at this potential there are few reactive platinum metal sites remaining at the interface.

The cathodic peak, C_1 in Fig. 5.14, apparently involves acetone reduction. This can be seen from the aeffect of adding acetone to the isopropanol-free acid solution in Fig. 5.16. The decrease in acetone reduction current at potentials below 0.05 V is attributed to displacement of organic material from the interface at high hydrogen coverage. While the presence of acetone did not dramatically influence the voltammetry of platinum, the acetone (or a derivative formed by partial oxidation) evidently coordinates to, and inhibits the oxidation of, the more reactive surface platinum sites. The dramatic lowering of the A_1 peak for isopropanol oxidation on addition of acetone, as outlined in the inset of Fig. 5.16, is not unlike that recorded on lowering the sweep-rate over the range 10 to 1 mV s^{-1} with initially acetone-free solutions, Fig. 5.15. Obviously, at low sweep-rates, acetone (or an oxidation product of same) formed by isopropanol oxidation has a greater opportunity of accumulating at, and deactivating, the electrode surface.

The accumulation of acetone at the platinum surface also occurred at higher temperature in the case of concentrated isopropanol solutions, Fig. 5.17. The rate of oxidation in the latter case was high and the accumulation of acetone around the interface is assumed to enhance the deactivation process -

especially if the latter involves slow adsorption or further oxidation of acetone, either of which may be accelerated by increasing the temperature. The alcohol oxidation at peak A_1' on the cathodic sweep is less inhibited, Fig. 5.17, as this occurs just after the monolayer removal process which yields, initially, an unpoisoned surface. Cyclic voltammetry is of course a transient technique; under constant potential conditions, e.g. at 0.6 V, the current for isopropanol is known [476] to decay with time.

In the case of isopropanol the surface activity for oxidation could be renewed either by holding the electrode at a high anodic potential (30 sec. at 1.3 V) or at a low potential (30 sec. at 0 V). The initial level of oxidation attained in both cases on stepping to an intermediate potential, e.g. 0.6 V, was ca. 25 mA cm^{-2} for 0.1 mol dm^{-3} isopropanol solution. Extended work in this area showed that while the initial increase in alcohol oxidation current commenced at ca. 0.2 V, the major increase occurred at ca. 0.4 V. These two values are close to the two oxide reduction peaks reported for thick hydrous oxide films grown by potential cycling techniques [477].

Earlier proposals with regard to the mechanism of isopropanol oxidation [475] now need modification to incroporate the role of hydrous oxide species in this reaction at low potentials. The question of acetone oxidisability is controversial; one group [476] reported a direct i/E response for this reaction, but radioactive tracer studies [431] suggest the opposite. This latter work also showed that acetone adsorption on platinum, although irreversible, is quite slow - this explains the apparent absence of poisoning of the electrode for isopropanol oxidation at low potentials (0.3 to 0.5 V, Fig. 5.14). The Tafel slope for isopropanol oxidation in the region of 0.4 V was high, ca. 200 mV $decade^{-1}$; this evidently reflects the influence of inhibition of the interfacial reaction owing to strong adsorption of product species.

5.4. REDUCTION AT PLATINUM

5.4.1. Results

The voltammetric response for dichromate on platinum in acid is given in Fig. 5.18. The main reduction current commenced here below ca. 0.6 V followed by a dramatic increase in activity over the approximate range 0.6 to 0.2 V. Maximum reduction occurred at ca. 0.2 V, followed by a slight decrease. On reversing the potential at 0 V the i/E response was similar to that of the cathodic sweep over the range 0 to 0.6 V. However, attention is directed mainly to the anodic sweep; the cathodic sweep here is complicated by the presence of an additional feature, namely the compact oxide removal peak at ca. 0.65 V. At higher potentials the response was similar to that for pure acidic electrolyte.

Some data for HNO_3 reduction on platinum at low pH is shown by the dashed line in Fig. 5.19. On the cathodic sweep the reduction current for this reaction commenced just below 0.4 V (this was just above the value for hydrogen adsorption which commenced at ca. 0.36 V, represented by the solid line in Fig. 5.19). A short plateau was seen at ca. 0.2 V but then, following the peak for the adsorption of weakly bound hydrogen, the surface appeared to be significantly deactivated for HNO_3 reduction. This deactivation continued into the start of the anodic sweep but the current dropped again at ca. 0.1 V as nitrate reduction recommenced at the beginning of the first hydrogen reduction peak. The reduction current predominated above ca. 0.25 V, however, the HNO_3 reduction decayed gradually above ca. 0.35 V.

The behaviour for $NaNO_3$ reduction for platinum in base is outlined by the dashed line in Fig. 5.20. There appeared to be some reduction of the nitrate in the region of 0.25 V but the rate was much slower in base than in acid. Note the much higher concentration of the oxidant in Fig. 5.20, with 0.1 mol dm^{-3} NO_3^- in base no cathodic current was observed on the anodic sweep. The full line in Fig. 5.20 shows the voltammetric response for platinum in pure base electrolyte for comparison.

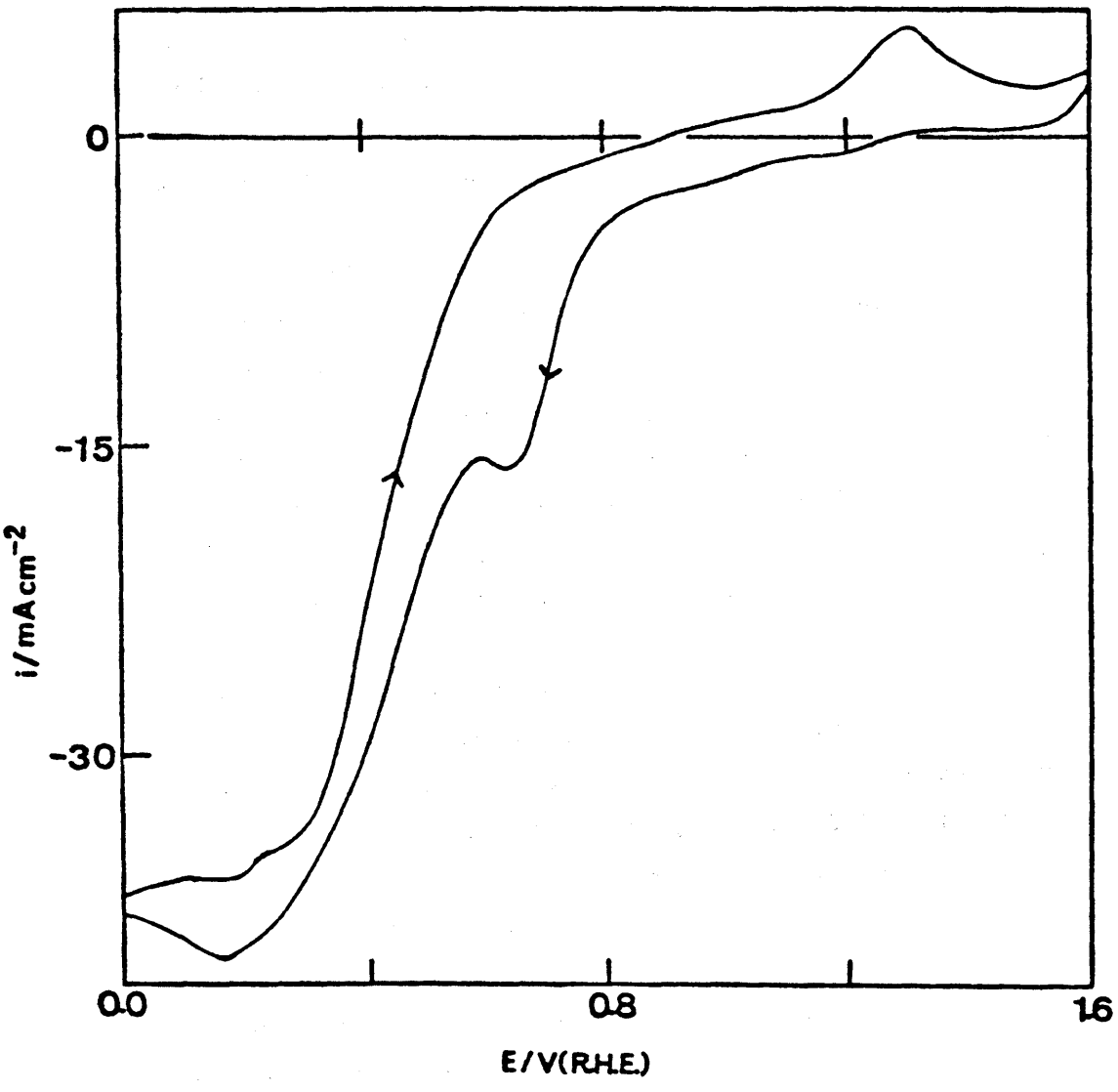

Figure 5.18: Cyclic voltammogram (0 to 1.6 V, 50 mV s^{-1}) for $Na_2Cr_2O_7$ (0.1 mol dm^{-3}) reduction at a platinised platinum electrode in 1.0 mol dm^{-3} H_2SO_4 solution at 25°C.

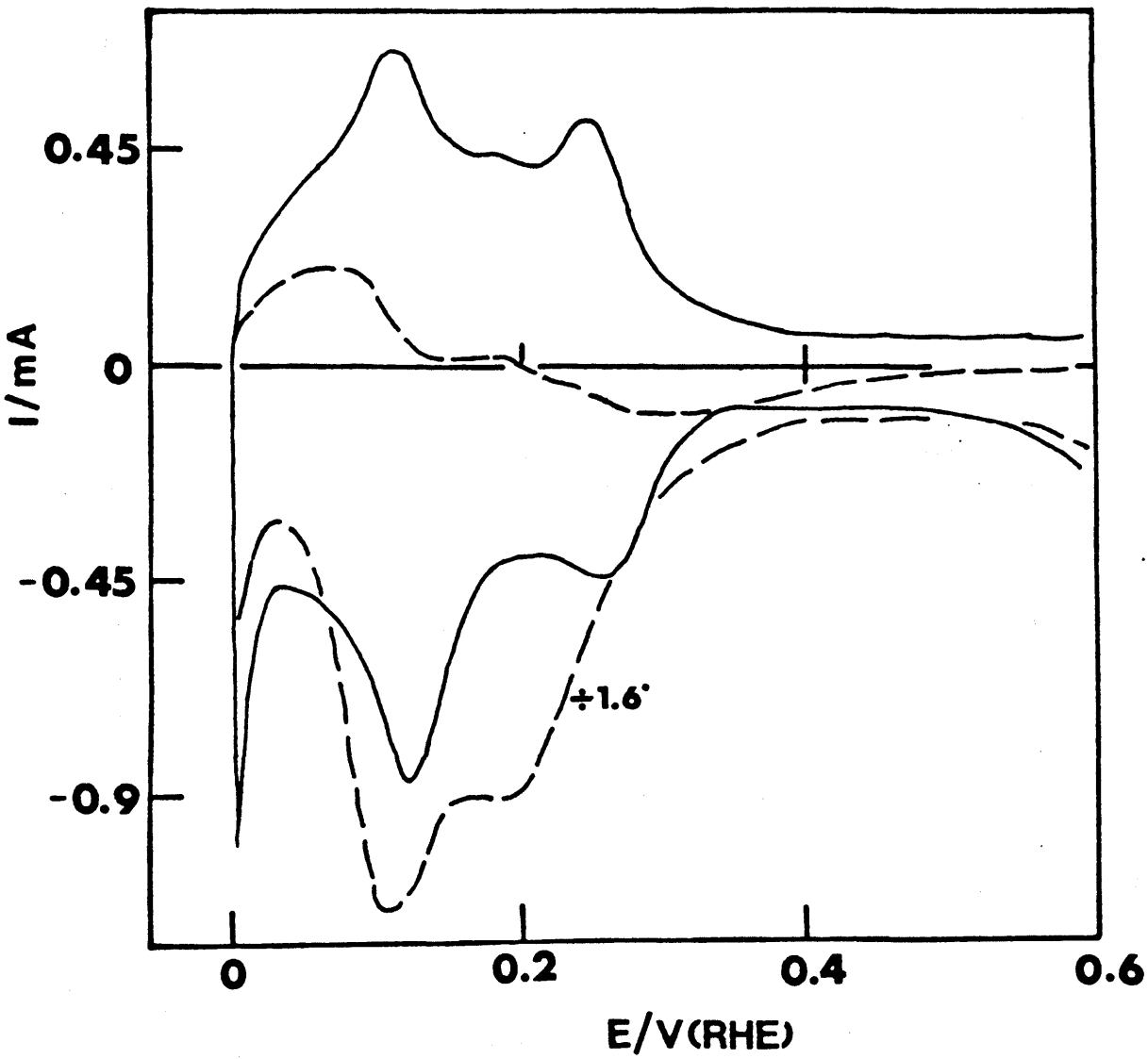

Figure 5.19: Cyclic voltammograms (0 to 1.6 V, 10 mV s^{-1}) for a platinised platinum electrode in (a) N_2-stirred 1.0 mol dm^{-3} H_2SO_4 (——) and (b) N_2-stirred 1.0 mol dm^{-3} H_2SO_4 + 0.1 mol dm^{-3} HNO_3 (----); T = 20°C. Only 0 to 0.6 V shown; note that the the true current density in the latter case is larger (by a factor of 1.6) than shown in this diagram.

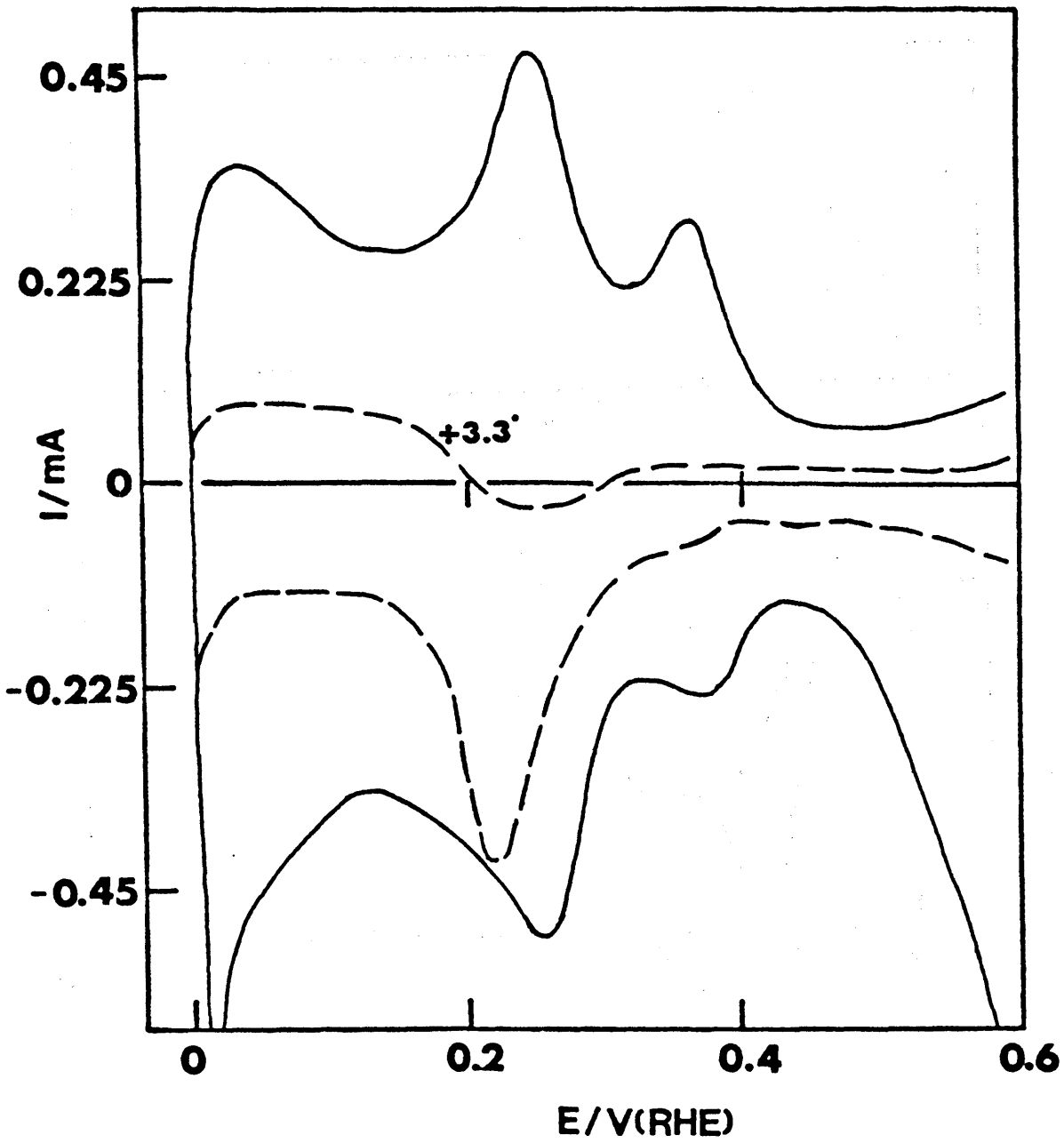

Figure 5.20: Cyclic voltammograms (0 to 1.6 V, 10 mV s^{-1}) for a platinised platinum electrode in (a) N_2-stirred 1.0 mol dm^{-3} NaOH (——) and (b) N_2-stirred 1.0 mol dm^{-3} NaOH + 1.1 mol dm^{-3} $NaNO_3$ (----). Only 0 to 0.6 V shown; note the true current density in the latter case is larger (by a factor of 3.3) than shown in this diagram.

5.4.2. Discussion

The ideas outlined above in section 5.3.2. are relevant not only to oxidation but also reduction processes. As pointed out previously for oxidation proceses at Pt electrodes the dramatic increase in activity is over the approximate range of 0.2 to 0.6 V. For the reduction of dichromate in the same system the range is the same but the trend is reversed, the higher potential end now being the region of low activity, Fig. 5.18. As pointed out by previous workers in this area [478], dichromate reduction occurs only at an unusually high overpotential, i.e. it is an electrocatalytically demanding reaction which evidently only occurs at high energy, adatom (Pt*) sites. Above 0.55 V these sites are totally converted to hydrous oxide, i.e. the equilibrium represented by equation (5:3:6) is totally on the right-hand side. As the potential is decreased below 0.55 V the adatom activity increases, unoxidised Pt* sites are accessible and the dichromate reduction current increases dramatically. It is worth noting here that the acceleration of dichromate reduction commences well before the onset of proton discharge on platinum, i.e. H_{ads} is not the reducing agent. Maximum dichromate reduction occurs at the same potential as where maximum Pt* adatom activity occurs, i.e. at 0.2 V where nearly all hydrous oxide species are reduced. Slight current decay below this potential of 0.2 V may be attributed either to Pt* adatom decay or blocking of the Pt* adatom sites by H_{ads}.

The reduction of nitrate ions at platinum and at related metal electrodes is a reaction of considerable interest in connection with radioactive waste handling [479]. As in the dichromate case, the reduction of nitrate at low pH occurs above the potential value for hydrogen adsorption. The deactivation which occurred below the maximum current at 0.2 V could be due either to anion (NO_3^-) repulsion by the surface at potentials below the pzc or (perhaps more likely) to the inability of the NO_3^- or $Pt(OH)_6^{2-}$ anions to compete with hydrogen (at high coverages of the latter) for adsorption sites at the interface. On the anodic sweep the current is initially the net sum of HNO_3 reduction and H_{ads} oxidation. However, above 0.25 V the reduction current predominates as at this stage most of the adsorbed hydrogen has been removed. Above 0.35 V

the various types of Pt* adatom sites are converted to the hydrous oxide state and hence the reduction current decays. The HNO_3 reduction currents are larger during the cathodic sweep as the Pt* adatom concentration at the interface is greater in this case following reduction of the oxide monolayer material.

Essentially the same behaviour for nitric acid reduction on platinum in acid as observed here has been reported by Horanyi and Rizmayer [375] who carried out a much more extensive investigation of this reaction using polarisation and radiotracer techniques. Their conclusion with regard to the importance of competitive adsorption of NO_3^- and $SO_4^=$ anions is accepted here - with the proviso that the sites being competed for are adatom centres which are gradually deactivated above 0.2 V due to hydrous oxide formation. Similar type results have been reported for many other compounds including nitrous oxide reduction [486], azide reduction [480] and compounds containing carbon-halide bonds [481] - these results may be interpreted as the HNO_3 case outlined above.

The behaviour of $NaNO_3$ in base, Fig. 5.20, is explanable in terms of the super-Nernstian ion shift that hydrogen oxide reduction undergoes when the electrolyte is changed from low to high pH (as explained in section 5.1), i.e. the hydrous oxide is reduced, or the Pt* adatoms for NO_3^- ion reduction are produced, only at much lower potentials (here inhibition due to H_{ads} is much more marked) in base. Hence, at concentrations of 0.1 mol dm^{-3} $NaNO_3$ no reduction is observed at platinum electrodes in base. Evidently only at high NO_3^- concentration can the latter species compete with OH^- ions - over a short potential range - for Pt* adatom sites in base.

5.5. CONCLUSIONS

In summary it can be seen that an appreciation of the quasi-stabilisation of adatom intermediates due to hydration at interfaces leads to an understanding of the unexpected stability (or metastability) of hydrous oxide films at noble metal electrode surfaces, in general, in aqueous media. Diverse aspects of platinum behaviour, e.g. hydrous oxide formation and reduction,

unusual entropy values in the hydrogen region, staircase voltammetry data, electrocatalytic behaviour and spectroscopic data, can all be rationalised on the basis of this one model. While there is no difficulty in growing thick films of hydrous oxide materials under special conditions [217], the coverage at which such species are involved in single sweep reactions (to judge from the magnitude of the charge of the H_i peak relative to that involved in the hydrogen monolayer) is extremely small. Thus direct evidence for participation of such species is extremely difficult to obtain for platinum - however, note should be taken of some direct evidence for the existence of a Pt(IV) oxidised species on platinised carbon and Pt-Ru alloy electrodes as shown by XPS investigation [246,482]. The role of Ru in such systems is considered to be that of a co-catalyst, i.e. it promotes the level of 'active oxygen' at the interface. However, the authors [482] concluded that Pt(IV), not Pt(11), is the active ingredient with regard to oxidation processes, even at low potentials, at platinum surfaces in aqueous media.

According to the model being postulated here the oxidised state of the species involved in the H_i peak is considered to be the hydrous oxide which mediates electrocatalytic reactions by becoming involved in a cyclic redox transition. The novel aspect of this theory is not the possible existence of a cyclic redox transition mechanism, as such mechanisms have already been postulated for oxide electrodes [219,278,280], but the fact that the mediator in the case of noble metal electrodes is a low level hydrous oxide generated in-situ at potentials quite cathodic to the value for compact monolayer oxide formation. This present view also emphasises the importance of the heteroegneous character, or active site approach, with regard to solid electrode behaviour. Single crystal surface behaviour was discussed in section (1.7) and the interpretation of many of the voltammetric features of these single crystals were shown to be quite controversial. It should be noted [483] that the potential values for some of the so-called "butterfly-peaks" for platinum single crystal surfaces coincide with those for hydrous oxide/adatom peaks for polycrystalline electrodes; yet hydrous oxide electrochemistry has been largely ignored by single crystal surface electrochemists to date.

It should be stressed that the importance of activated chemisorption is not disputed; however the fact that many species react in the $Pt^*/Pt(OH)_6^{2-}$ region highlights the importance of the hydroxy species in the electrocatalytic process. This theory also explains the origin of the oxygen atom that is frequently inserted, from the solvent, into organic molecules, e.g. methanol oxidation to CO_2 and water, upon oxidation. Surface oxide participation in these electroorganic oxidation reactions is also borne out by the work of Motoo and Shibata [267] who attributed the beneficial effect of certain types of adatoms, e.g. Ge, Sn, and Sb, to the ability of the latter to supply oxygen species at low potentials.

An interesting question here is why, if redox transitions are so important, other couples are not good electrocatalysts. The $MnO_2/MnO.OH$ system - which shows a clear transition at ca. 1.0 V(RHE) on the anodic sweep in base [484] - was examined here briefly and found to be a very poor electroorganic oxidation catalyst. Evidently the fact that both species involved in this couple are in a relatively high oxidation state (strongly binding the O or OH ligands) precludes activated chemisorption - an inner-sphere coordination mechanism is therefore not possible and high activity is not observed.

The dichromate and nitric acid work outlined here demonstrates another important aspect of incipient hydrous oxide formation, namely inhibition of cathodic processes at adatom sites. If the latter are oxidised then, despite the large driving overpotential, species such as dichromate and nitrate are unable to react as they apparently cannot displace OH^- or OH_2 groups at the active sites. Once such sites are reduced reaction can commence - although electrostatic repulsion [375] and competition with hydrogen for such sites can apparently cause problems in the case of platinum at low potentials. It may also be pointed out here that the type of behaviour shown here for dichromate was confirmed recently in this laboratory in experiments involving persulphate and iodate reduction on platinum and gold [485].

While no solution is afforded here to the deactivation problem, which is one of the main barriers to progress in methanol/air fuel cell developments, the present work provides the

basis of a better understanding of noble metal electrocatalysis in general, i.e. it provides a more solid basis on which further progress can take place.

References

1. J. O'M. Bockris and D.M. Drazic, in "Electrochemical Science", (Taylor and Francis, London, 1972).

2. W. Schottky and H. Rothe, *Hadb. Exp-Physk. Bd.*, 13 (1928) 145.

3. E. Lange, *Z. Electrochem.*, 55 (1951) 76; 56 (1952) 94.

4. W.J. Moore, in "Physical Chemistry", (Longman's, London, 1972) p. 206.

5. J. Willard Gibbs, Collected Work of ... in "Thermodynamics", (Yale University Press, 1906) Vol. 1, p. 429.

6. E.A. Guggenheim, *J. Phys. Chem.*, 33 (1929) 842.

7. D. C Grahame, *Chem. Rev.*, 41 (1947) 441.

8. R. Parsons, in "Adv. in Electrochem. and Electrochem. Eng.", (Interscience, New York, 1961) Vol. 1, Ch. 1.

9. P. Delahay, in "Double Layer and Electrode Kinetics", (Wiley Interscience, London, 1966) p. 17.

10. "Comprehensive Treatise of Electrochemistry", Eds. J.O'M. Bockris, B.E. Conway and E. Yeager, (Plenum Press, New York, 1980) Vol. 1.

11. J.A. V. Butler, *Proc. Roy. Soc. London*, A113 (1927) 594.

12. C. Lippmann, *Ann. Chim. Phys.*, 5 (1875) 494.

13. E. Gileadi, E. Kirowa-Eisner and J. Perciner, in "International Electrochemistry, an Experimental Approach", (Addison-Wesley, London, 1975) p. 27.

14. H. Von Helmholtz, *Wied. Ann.*, 7 (1879) 337.

15. A. Gouy, *J. Phys.*, 9 (1910) 457.

16. D.L. Chapman, *Phil. Mag.*, 25 (1913) 475.

17. O. Stern, *Z. Electrochem.*, 30 (1924) 508.

18. A.N. Frumkin, *Z. Physik.*, 35 (1926) 792.

19. W.V. Nikolaeva, A.N. Frumkin and S.A. Iofa, *Zh. Fiz. Khim.*, 26 (1952) 1326.

20. J.O'M. Bockris, M.A.V. Devanathan and K. Muller, *Pro. Roy. Soc. London*, A274 (1963) 55.

21. M.A.V. Devanathan and B.V.K.S.R.A. Tilak, *Chem. Rev.*, 65 (1965) 635.

22. R. Parsons, *J. Electrochem. Soc.*, 127 (1980) 176C.

23. A. Bewick and J. Robinson, *J. Electroanal. Chem.*, 60 (1975) 163; 71 (1976) 131.

24. C. Hinnnen, C. Nguyen Van Huong, A. Rousseau and J.D. Dalbera, *ibid.*, 95 (1978) 131; 106 (1980) 175.

25. W. Paik, M.A. Genshaw and J.O'M. Bockris, *J. Phys. Chem.*, 74 (1970) 4266.

26. J.O'M. Bockris, A. Damjanovic and W.E. O'Grady, *J. Collid. Interface Sci.*, 31 (1970) 387.

27. G.A. Parks and P.L. de Bruyn, *J. Phys. Chem.*, 66 (1962) 967.

28. S.M. Ahmed, in "Oxides and Oxide Films", Ed. J.W. Diggle, (Dekker, New York, 1972) Vol. 1, Ch. 4.

29. D.N. Furlong, D.E. Yates and T.W. Healy, in "Electrodes of Conductive Metallic Oxides", Ed. S. Trasatti, (Elsevier, Amsterdam, 1981) Part B, p. 367.

30. H. Gerischer, in "Adv. in Electrochem. and Electrochem. Eng.", Eds. Delahay and Tobias, (Interscience, New York, 1961) Vol. 1, p. 142.

31. H. Gerischer, in "Physical Chemistry, An Advanced Treatise", Vol 1XA, Eds. Eyring, Henderson and Jost, (Academic Press, New York, 1970) Ch. 5.

32. V.A. Myambin and Yu. V. Pleskov, in "Electrochemistry of Semiconductors", English translation by C.G.B. Garret from revised Russian edition, (Plenum Press, New York, 1967) p. 414.

33. R. Memming, *Electrochim. Acta*, 25 (1980) 77.

34. A. Heller and B. Miller, *ibid.*, 25 (1980) 29.

35. R.G. Egdell, J.B. Goodenough, A. Hammet and C.C. Naish, *J. Chem. Soc. Faraday Trans. I*, 79 (1983) 893.

36. G.A. Parks, *Chem. Rev.*, 65 (1965) 177.

37. S.M. Ahmed and D. Maksimov, *J. Collid. Interface Sci.*, 29 (1969) 97.

38. S.M. Ahmed, *Can J. Chem.*, 44 (1966) 1663.

39. S.M. Ahmed, *J. Phys. Chem.*, 73 (1969) 3546.

40. Y.G. Berube and P.L. de Bruyn, *J. Colloid. Interface Sci.*, 28 (1968) 92.

41. L. Blok and P.L. de Bruyn, *ibid.*, 32 (1970) 518, 527, 533.

42. S. Levine and A.L. Smith, *Disc. Faraday Soc.*, 52 (1971) 290.

43. R.J. Hunter and H.J.L. Wright, *J. Colloid. Interface Sci.*, 37 (1971) 564.

44. H.J.L. Wright and R.J. Hunter, *Aust. J. Chem.*, 26 (1973) 1183, 1191.

45. Th. F. Tadros and J. Lyklema, *J. Electroanal. Chem.*, 17 (1968) 267.

46. Th. F. Tadros and J. Lyklema, *ibid.*, 22 (1969) 1.

47. J. Lyklema, *ibid.*, 18 (1968) 341.

48. J. Lyklema, *Croatica Chemica Acta*, 43 (1971) 249.

49. J.W. Perram, *J. Chem. Soc. Faraday II*, 2 (1973) 993.

50. J.W. Perram, R.J. Hunter and H.J.L. Wright, *Chem. Phys. Lett.*, 23 (1973) 265.

51. J.W. Perram, R.J. Hunter and H.J.L. Wright, *Aust. J. Chem.*, 27 (1974) 461.

52. A. Daghetti, G. Lodi and S. Trasatti, *Materials Chem. and Phys.*, 8 (1983) 1.

53. W. Smit, C.L.M. Holten, H.N. Stein, J.J.M. de Goeig and H.M.J. Theelen, *J. Colloid. Interface Sci.*, 63 (1978) 120.

54. M.J. Dignam, *Can. J. Chem.*, 56 (1978) 595.

55. M.J. Dignam and R.K. Kalia, *Surf. Sci.*, 10 (1980) 154.

56. D.E. Yates, S. Levine and T.W. Healy, *J. Chem. Soc. Farday I*, 70 (1974) 1807.

57. J.A. Davis, A.P. James and J. O'Leckie, *J. Colloid, Interface Sci.*, 63 (1978) 480.

58. K.J. Vetter, *Z. Electrochem.*, 56 (1952) 797.

59. A.J. Bard and L.R. Faulkner, in "Electrochemical Methods", (Wiley, New York, 1980).

60. J.A.V. Butler, *Trans. Faraday Soc.*, 19 (1924) 729; 28 (1932) 379.

61. J.A.V. Butler, *Proc. Roy. Soc.*, A157 (1936) 423.

62. R.W. Gurney, *ibid.*, A134 (1931) 137.

63. R.W. Gurney and R.H. Fowler, *ibid.*, A136 (1932) 378.

64. A.N. Frumkin, *Z. Physik. Chem.*, A160 (1932) 116; A164 (1933) 121.

65. T. Erdey-Gruz and M. Volmer, *ibid.*, A150 (1930) 203.

66. J. Horiuti and M. Polanyi, *Acta Physicochem. U.R.S.S.*, 2 (1935) 505.

67. S. Levina and W. Sarinsky, *ibid.*, 6 (1937) 491; 7 (1937) 485.

68. J. Tafel, *Z. Physik. Chem.*, 50 (1905) 641.

69. J. O'M. Bockris and A.K.W. Reddy, in "Modern Electrochemistry", (Plenum Press, New York, 1970) Vol. 2.

70. R.A. Marcus, in "Trans. Symp. on Electrode Processes", Electrochem. Soc., (J. Wiley, New York, 1961) p. 239.

71. J.T. Hupp and M.J. Weaver, *J. Electroanal. Chem.*, 152 (1983) 1.

72. N. Sutin, *Prog. Inorg. Chem.*, 30 (1983) 441.

73. B.S. Brunschwig, J. Logan, M.D. Newton and N. Sutin, *J. Am. Chem. Soc.*, 102 (1980) 5978.

74. B.L. Tembe, H.L. Friedman and M.D. Newton, *J. Chem. Phys.*, 76 (1982) 1490.

75. R.A. Marcus, *Int. J. Chem. Kinet.*, 13 (1981) 865.

76. J.T. Hupp and M.J. Weaver, *J. Phys. Chem.*, 88 (1984) 1463.

77. M.D. Newton, *Int. J. Quantum Chem. Symp.*, 14 (1980) 363.

78. M.D. Weaver, in "Comp. Chem. Kinetics", Ed. R.G. Compton, (Elsevier, 1987) Vol. 27, Ch. 1.

80. F.G. Cottrell, *Z. Phys. Chem.*, 42 (1903) 385.

81. D.D. MacDonald, in "Transient Techniques in Electrochemistry", (Plenum Press, New York, 1977) Ch. 3.

82. P. Delahay, in "New Instrumental Methods in Electrochemistry", Ed. J.A. Bard, (Marcel Dekker, New York, 1970) Vol. 4, p. 129.

83. B. Davis, in "Integral Transforms and their Applications", (Springer-Verlag, New York, 1978).

84. L.A. Matheson and N. Nichols, *Trans. Electrochem. Soc.*, 73 (1938) 193.

85. F.G. Will and C.A. Knorr, *Z. Electrochem.*, 64 (1960) 258.

86. J.E.B. Randles, *Trans. Far. Soc.*, 44 (1948) 327.

87. A. Sevick, *Coll. Czech. Chem. Commun.*, 13 (1958) 347.

88. R.S. Nicholson, *Anal. Chem.*, 37 (1965) 1351.

89. R.S. Nicholson and I. Shain, *ibid.*, 36 (1964) 706.

90. H. Matsuda and Y. Ayabe, *Z. Electrochem.*, 59 (1955) 494.

91. L. Nadjo and J.M. Saveant, *J. Electroanal. Chem.*, 48 (1973) 113.

92. A.C. Testa and W.H. Reinmuth, *Anal. Chem.*, 33 (1961) 1320.

93. Z. Galus, in "Fundamentals of Electrochemical Analysis", E. Harwood Ltd., Chichester, 1976) p. 255-395.

94. I.M. Kolthaff and J.J. Lingane, in "Polarography", 2nd. ed., (Wiley-Interscience, New York, 1952).

95. D. Pletcher, *Chem. Soc. Rev.*, 4 (1975) 471.

96. D.H. Evans, *Accts. Chem. Res.*, 10 (1977) 313.

97. R.H. Wopshall and I. Shain, *Anal. Chem.*, 39 (1967) 1514.

98. R.H. Wopshall and I. Shain, *ibid.*, 39 (1967) 1527, 1535.

99. J.H. Sluyters and M. Sluyters-Rebach, *J. Electroanal Chem.*, 65 (1975) 831.

100. S. Srinivasin and Gileadi, *Electrochem. Acta*, 11 (1966) 321.

101. E. Laviron, *J. Electroanal. Chem.*, 52 (1974) 355.

102. E. Laviron, *ibid.*, 52 (1974) 19.

103. J. Robinson and D. Pletcher, Eds., Electrochemistry (Specialist Periodical Report), The Royal Society of Chemistry, London, 1984, Vol. 9, p. 101.

104. 1st and 2nd International Conferences on Non-traditional Approaches to the Study of Solid/Electrolyte Interfaces, *Surf. Sci.*, 101 (1980); *J. Electroanal. Chem.*, 150 (1983).

105. W. Van Benken and T. Kuwana, *Anal. Chem.*, 42 (1970) 1114.

106. R.W. Murray, W.R. Heinemann and G.W. O'Dom, *ibid.*, 39 (1967) 1666.

107. P.S. Hauge, *Surf. Sci.*, 96 (1980) 108.

108. N.H. Bashara and R.M.A. Azzan, Eds., *ibid.*, 56 (1976).

109. G.H. Brilmyer and A.J. Bard, *Anal. Chem.*, 52 (1980) 685.

110. R.E. Malpas and A.J. Bard, *ibid*, 52 (1980) 109.

111. A. Bewick and B.S. Pons, in "Adv. in Infrared and Raman Spec.", Eds. R.J.H. Clark and R.H. Hester, (Wiley Heydon, New York, 1985) Vol. 12, Ch. 1.

112. A. Bewick, K. Kunimatsu and B.S. Pons, *Electrochim. Acta*, 25 (1980) 465.

113. (a) B. Beden, A Bewick, M. Razaq and J. Weber, *J. Electroanal. Chem.*, 139 (1982) 203.
(b) S.G. Sun, T. Clavilier and A. Bewick, Ext Abstr. (38th ISE Meeting, Masstricht, 1987) Vol. 1, p. 35.

114. R.P. Van Duyne, in "Chemical and Biological Applications of Lasers", (Academic Press, 1979) Vol. 4, p. 101.

115. M. Fleischmann and I.R. Hill, in "Surface Enhanced Raman Scattering", Eds. R.K. Chang and T.E. Furtak, (Plenum Press, New York, 1982) p. 275.

116. S. Bruckenstein and R. Rao Gadde, *J. Am. Chem. Soc.*, 93 (1971) 793.

117. O. Walter and J. Heitbaum, *Ber. Bunsenges Phys. Chem.*, 88 (1984) 2.

118. S. Wilhelm, W. Vielstich, H.W. Buschmann and T. Iwasita, *J. Electroanal. Chem.*, 229 (1987) 377.

119. A. Benninghoven, *Surf. Sci.*, 35 (1973) 427; 53 (1975) 596.

120. M. Fleischmann, P. Graves, I.R. Hill, A. Oliver and J. Robinson, *J. Electroanal. Chem.*, 150 (1983) 33.

121. M. Fleischmann, A. Oliver and J. Robinson, *Electrochim. Acta*, 31 (1986) 889.

122. W.J. Albery, B.A. Coles and M.A. Couper, *J. Electroanal. Chem.*, 65 (1975) 901.

123. A. Otto, *Surf. Sci.*, 101 (1980) 99.

124. W.J. Anderson and W.N. Hansen, *J. Electroanal. Chem.*, 43 (1973) 329.

125. T.E. Furtak and K.L. Kleiwer, *Comments on Solid State Phys.*, 10 (1982) 103.

126. L.M. Abrantes and L.M. Peters, *J. Electroanal. Chem.*, 150 (1983) 593.

127. G. Bomchil and C.J. Rekel, *ibid.*, 101 (1979) 133.

128. W.E. O'Grady, *J. Electrochem. Soc.*, 127 (1980) 555.

129. A.W. Czonderna, Ed., "Methods of Surface Analysis", (Elsevier, Amsterdam, 1975).

130. D.M. Kolb and J. Schneider, *Electrochim. Acta*, 31 (1986) 929.

131. P.N. Ross and F.T. Wagner, *Adv. in Electrochem. and Electrochem. Eng.*, 13 (1985) 69.

132. 1st IBM workshop on STM, Oberlech, 1985, *IBM J. Res. Develop*, 30 (1986).

133. A. McDougall, in "Fuel Cells", Ed. C.A. McAuliffe, (The MacMillian Press, London, 1976).

134. c.f. ref. 133, p. 16.

135. M.W. Breiter, in "Electrochemical Process in Fuel Cells", (Springer-Verlag, Berlin, 1969).

136. c.f. ref. 133, Ch. 6.

137. B.D. McNicol, *J. Electroanal. Chem.*, 118 (1981) 71.

138. D.S. Cameron, G.A. Hards, B. Harrison and R.J. Potter *Platinum Metals Rev.*, 31 (1987) 173.

139. D. Pletcher, *J. Appl. Electrochem.*, 14 (1984) 403.

140. J.P. Randin, in "Comprehensive Treatise of Electrochemistry", Eds. J.O'M. Bockris, B.E. Conway, E. Yeager and R.E. White, (Plenum Press, New York, 1984), Vol. 4, p. 500.

141. G.P. Sakellaropoulos, *Adv. in Cat.*, 30 (1981) 217.

142. W.T. Grubb, *Nature*, 198 (1963) 883.

143. Southampton Electrochemistry Group, in "Instrumental Methods in Electrochemistry", (Ellis Horwood, England, 1985) Ch. 7.

144. A.D. Miller and S.H. Langer, *J. Electrochem. Soc.*, 120 (1973) 1695.

145. T. Meyer, in "Proceedings of the Symposium on Electrocatalysis", Electrochem. Soc. Meeting, 1982.

146. B.E. Conway and D.J. MacKinnon, *J. Electrochem. Soc.*, 116 (1969) 1665.

147. B.E. Conway, D.J. MacKinnon and B.V. Tilak, *Trans. Faraday Soc.*, 66 (1970) 1203.

148. E. Yeager, in "The Physics and Chemistry of Electrocatalysis", Electrochem. Soc. Meeting, San Francisco, 1983.

149. S. Trasatti, *J. Electroanal. Chem.*, 39 (1972) 163.

150. F.W. Brooman and A.T. Kuhn, *J. Electroanal. Chem.*, 49 (1974) 325.

151. K.F. Bonhoffer, *Z. Phys. Chem.*, A113 (1924) 99.

152. B.E. Conway and J.O'M. Bockris, *J. Chem. Phys.*, 26 (1957) 532.

153. E. Yeager, *J. Electrochem. Soc.*, 128 (1981) 160C.

154. G.C. Bond, in "Catalysis by Metals", (Academic Press, New York, 1962).

155. J.M. Thomas and W.J. Thomas, in "Introduction to the Principles of Heterogeneous Catalysis", (Academic Press, New York, 1967).

156. C.E. Heath and W.J. Sweeney, in "Fuel Cells", Ed. W. Mitchell, Jr. (Academic Press, New York, 1963) Ch. 3.

157. M. Temkin, *Zh. Fiz. Khim.*, 15 (1941) 296.

158. E. Gileadi and B.E. Conway, in "Modern Aspects of Electrochemistry", Eds. J.O'M. Bockris and B.E. Conway, Butterworth, London, 1964) Vol. 3, p. 347.

159. J. Horiuti and G. Okamoto, *Sci. Pap. Inst. Phys. Chem. Res. Tokyo*, 28 (1936) 231.

160. G.O. Okamoto, J. Horiuti and K. Hirota, *ibid.*, 29 (1936) 213.

161. J. Horiuti, in "Trans. of the Symposium on Electrode Processes", Ed. E. Yeager (Wiley, New York, 1961) p. 17.

162. M. Boudart, *J. Am. Chem. Soc.*, 72 (1952) 1531, 3556.

163. B.E. Conway and H.P. Dhar, *Croatica Chem. Acta*, 45 (1973) 109.

164. J.O'M. Bockris, E. Gileadi and K. Muller, *Electrochim. Acta*, 12 (1967) 1301.

165. N. Anastasijevic, A. Bewick and R.J. Nichols, I.S.E. Annual Meeting, Glasgow, 1988, abs. #16.

166. B.E. Conway H. Angerstein-Kozlowska and F.C. Ho, *J. Vac. Sci. Technol.*, 14 (1977) 351.

167. A. Bewick, K. Kunimasu, J. Robinson and J.R. Russell, *J. Electrochem. Chem.*, 119 (1981) 175.

168. A. Bewick and J.W. Russell, *J. Electroanal. Chem.*, 132 (1982) 329.

169. J.D.E. McIntyre and W.F. Peck, in "Electrocatalysis", Ed. M. Breiter, (Electrochem. Soc., Princeton, New Jersey, 1974) p. 212.

170. J.D.E. McIntyre and W.F. Peck, *Discuss. Faraday Soc.*, 56 (1973) 122.

171. G.C. Bond, *Discuss. Faraday Soc.*, 41 (1966) 200.

172. "Seminar on Hydrogen as an Energy Vector. Its Production, Use and Transportation", Directorate General for Research, Science and Education, Commission of the European Communities, Brussels - Luxemburg, 1978.

173. W.A. Titterington and J.F. Austin, Extended abstracts, Electrochem. Meeting, New York, (The Electrochem. Soc., Princeton, New Jersey, 1974) p. 576.

174. F. Galizziola, F. Tantardini and S. Trasatti, *J. Appl. Electrochem.*, 4 (1974) 57.

175. W. O'Grady, C. Iwakura, J. Huang and E. Yeager, in "Electrocatalysis", Ed. M.W. Breiter, (The Electrochem. Soc., Princeton, New Jersey, 1974) p. 286.

176. L.D. Burke, O.J. Murphy, J.F. O'Neill and S. Venkatesan, *J.C.S. Faraday 1*, 73 (1977) 1659.

177. J.O.'M. Bockris and A.K.M.S. Huq, *Proc. Roy. Soc.*, A237 (1956) 277.

178. J.P. Hoare, *J. Electrochem. Soc.*, 110 (1963) 1019.

179. N. Watanabe and M.A.V. Devanathan, *ibid.*, 111 (1964) 615.

180. W.R. Grove, *Phil. Mag.*, (a) 14 (1839) 127; (b) 21 (1842) 417.

181. G.N. Lewis, *J. Am. Chem. Soc.*, (a) 28 (1906) 158; (b) *idem.*, *Z. Physik. Chem. (Leipzip)*, 55 (1906) 534.

182. A. Damjanovic, M.A. Genshaw and J.O'M. Bockris, *J. Phys. Chem.*, 70 (1966) 3761.

183. R. Lorenz and H. Hauser, *Z. Anorg. Allgem. Chem.*, 51 (1906) 18.

184. H.G. Bain, *Trans. Am. Electrochem. Soc.*, 78 (1940) 173.

185. F.J. Brislee, *Trans. Faraday Soc.*, 1 (1905) 65.

186. J.P. Hoare, (a) in "The Electrochemistry of Oxygen", (Interscience, New York, 1968); (b) *idem.*, in "Advances in Electrochemistry and Electrochemical Engineering", Ed. Delahay, (Interscience, New York, 1967) Vol. 6, p. 201.

187. T.P. Hoar, *Proc. Roy. Soc.*, A142 (1933) 628.

188. J. Giner, *Z. Electrochem.*, 63 (1959) 386.

189. M.L.B. Rao, A. Damjanovic and J.O'M. Bockris, *J. Phys. Chem.*, 67 (1963) 2508.

190. J.P. Hoare, *J. Electrochem. Soc.*, 109 (1962) 858.

191. A.C.C. Tseung and S. Jasem, *Electrochim. Acta*, 22 (1977) 31.

192. A.J. Scarpelline and G.L. Fischer, *J. Electrochem. Soc.*, 129 (1982) 515, 522.

193. P.F. Garica, R.D. Shannon, P.E. Bierstedt and R.B. Flippen, *J. Electrochem. Soc.*, 127 (1980) 1974.

194. Y. Matsumura and E. Sato, *Electrochim. Acta*, 25 (1980) 585.

195. D.J. Schiffrin, in "Specialist Periodical Reports on Electrochemistry", Ed. D. Pletcher, (The Royal Soc. of Chem., London, 1983) Vol. 8.

196. J.P. Collman, P. Denisevich, Y. Konai, M. Marrocco, C. Koval and F. Anson, *J. Am. Soc.*, 102 (1980) 6027.

197. J.A.R. Van Veen, J.F. Van Baar and C.J. Kruese, *Ber. Bunsen. Phys. Chem.*, 85 (1981) 700.

198. J.O'M. Bockris and S. Srinivasan, "Fuel Cells: their Electrochemistry", (McGraw-Hill, 1969) p. 437.

199. A.J. Appleby, in "Modern Aspects of Electrochemistry", Eds. J.O'M. Bockris and B.E. Conway, (Plenum Press, New York, 1973) Vol. 9.

200. R. Woods, *J. Electroanal. Chem.*, 49 (1974) 217.

201. M.W. Breiter, *Electrochim. Acta*, 9 (1964) 441.

202. M. Bold and M. Breiter, *Z. Electrochem.*, 64 (1960) 897.

203. C.A. Knorr and F.G. Will, *Z. Electrochem.*, 64 (1960) 258, 270.

204. M.W. Breiter, *Z. Phys. Chem., Abs. B*, 52 (1967) 1.

205. J. Llopis and M. Vasquez, *Electrochim. Acta*, 11 (1966) 633.

206. L.D. Burke, F. MacCarthy and T. O'Meara, *J.C.S. Faraday 1*, 68 (1972) 1086.

207. P. Ruetschi and P. Delahay, *J. Chem. Phys.*, 23 (1955) 556.

208. D.J.G. Ives, in "Reference Electrodes, Theory and Practice", Eds. Ives and Jarvez (Academic Press, New York, 1961) p. 322.

209. L.D. Burke and E.J.M. O'Sullivan, *J. Electroanal. Chem.*, 129 (1981) 133.

210. D.L. Caldwell nad M.J. Hazelrigg, in "Modern Chlor-alkali Technology", Ed. M. O'Coulter, Ellis Horwood Ltd., Chichester, 1980) Vol. 1.

211. S. Saito, *ibid.*

212. H. Beer, *Chem. Ind.*, (1978) 491.

213. S. Trasatti and W.E. O'Grady, *Adv. Electrochem. and Electrochem. Eng.*, 12 (1981) 177.

214. G. Belanger and A.K. Vijh, in "Oxides and Oxide Films", Ed. A.K. Vijh, (Marcel Dekker, New York, 1977) Vol. 5, p. 1.

215. R. Woods, in "Electroanalytical Chemistry", Ed. A.J. Bard, (Marcel Dekker, New York, 1976) Vol. 9, p. 1.

216. S.D. James, *J. Electrochem. Soc.*, 116 (1969) 1681.

217. L.D. Burke and M.E.G. Lyons, in "Modern Aspects of Electrochemistry", No. 18, Ch. 4.

218. L.D. Burke and J.F. Healy, *J. Electroanal. Chem.*, 124 (1981) 327.

219. L.D. Burke and E.J.M. O'Sullivan, *J. Electroanal. Chem.*, 93 (1978) 11.

220. B.E. Conway and J. Mozota, *Electrochim. Acta*, 28 (1983) 9.

221. A.F. Wells, in "Structural Inorganic Chemistry", (Claredon Press, Oxford, 1984) p. 496.

222. R.G. Burns and V.M. Burns, in "Manganese Dioxide Symposium", Eds. B. Schumn, H.M. Joseph and A. Kozowa, (The I.C. MnO_2 Sample Office, Box 6116, Cleveland, OHIO 44101, U.S.A.) Vol. 2, p. 97.

223. K.S. Kang and J.L. Shay, *J. Electrochem. Soc.*, 130 (1983) 766.

224. (a) L.D. Burke and M.McRann, *J. Electroanal. Chem.*, 125 (1981) 127, 387.
(b) L.D. Burke, M.E. Lyons and D.P. Whelan, *J. Electroanal. Chem.*, 129 (1981) 133.

225. L.D. Burke and D.P. Whelan, *J. Electroanal. Chem.*, 162 (1984) 121; 124 (1981) 333.

226. H.A. Liebhafsky and E.J. Cairns, in "Fuel Cells and Fuel Batteries", (John Wiley and Sons, New York, 1968).

227. K.R. Williams, in "An Introduction to Fuel Cells", (Elsevier, Amsterdam, 1966).

228. W. Vielstich, in "Fuel Cells - Modern Processes for the Electrochemical Production of Energy", (translated by D.J.G. Ives, John Wiley and Sons, New York, 1970).

229. E. Justi and A. Winsel, in "Fuel Cells - their Electrochemistry", (McGraw-Hill, New York, 1969).

231. W. Mitchell, in "Fuel Cells", (Academic Press, New York, 1963).

232. D.R. Adams, P.Y. Cathou, R.E. Gaynor, R.D. Jackson, Jr., J.H. Kirsch, L.L. Leanlard, G.S. Lockwood, W.P. Warnock and R.E. Wilcox, in "Fuel Cells - Power for the Future", (Fuel Cell Research Associates, Cambridge, Massachusettes, 1960).

233. K.D. Snell and A.G. Keenan, *Electrochim. Acta*, 27 (1982) 1683.

234. G. Horanyi and G. Inzelt, *Acta Chim. Acad. Sci. Hung.*, 100 (1979) 229, 101.

235. W. Hauffe and J. Heitbaum, *Electrohim. Acta*, 23 (1978) 299.

236. H. Cnobloch and H. Kohlmuller, (27th I.S.E. Meeting, Zurich, 1976), Extended abs. #282.

237. D. Pletcher and V. Solis, *Electrochim. Acta*, 27 (1982) 775.

238. B. Beden, A. Bewick, K. Kunimatsu and C. Lamy, *J. Electroanl. Chem.*, 121 (1981) 343.

239. D. Takky, B. Beden, J.M. Leger and C. Lamy, *J. Electroanal. Chem.*, 145 (1983) 461.

240. J. Clavilier, R. Parsons, T. Durand, C. Lamy and J.M. Leger, *J. Electroanal. Chem.*, 124 (1981) 321.

241. E. Yeager, W. O'Grady, M. Woo and P. Hagans, *J. Electrochem. Soc.*, 125 (1978) 348.

242. D. Pletcher and V. Solis, *J. Electroanal. Chem.*, 131 (1981) 309.

243. A. Capon and R. Parsons, *J. Electroanal. Chem.*, (a) 44 (1973) 1; (b) 45 (1973) 205.

244. B. Beden, M.C. Morin, F. Hahn and C. Lamy, *J. Electroanal. Chem.*, 229 (1987) 353.

245. R. Parsons and T. VanderNoot, *J. Electroanal. Chem.*, 257 (1988) 9.

246. J.B. Goodenough, A. Hamnett, B.J. Kennedy and S.A. Weeks, *Electrochim. Acta*, 32 (1987) 1233.

247. A. Wieckowski, J. Sobrowski and A. Jablonska, *J. Electroanal. Chem.*, 55 (1974) 383.

248. B. Beden, I. Cetin and C. Lamy, (34th I.S.E. Meeting, Erlangen, F.R.G., 1983), Extended abs. #1007.

249. C. Lamy, *Electrochim. Acta*, 29 (1984) 1581.

250. C. Lamy, J.M. Leger, J. Clavilier and R. Parsons, *J. Electroanal. Chem.*, 150 (1983) 71.

251. S. Srinivasan, *J. Electroanal. Chem.*, 118 (1981) 51.

252. K. Machida and M. Enyo, *Bull. Chem. Soc. Jpn.*, 58 (1985) 2043.

253. M. Enyo, *J. Appl. Electrochem.*, 15 (1985) 907.

254. M. Beltowska-Brzezinska, *Electrochim. Acta*, 30 (1985) 1193.

255. R.R. Cadzic, M.L. Avramov-Ivic and A.V. Tripovic, *Electrochim. Acta*, 29 (1984) 1353.

256. K. Shimazu, D. Weisshaar and T. Kuwana, *J. Electroanal. Chem.*, 223 (1987) 223.

257. V.B. Hughes and R. Miles, *J. Electroanal. Chem.*, 145 (1983) 87.

258. E. Rach and J. Heitbaum, *Electrochim. Acta*, 32 (1987) 1173.

259. K. Gossner and E. Mizera, *J. Electroanal. Chem.*, 140 (1982) 35.

260. F. Kadirgan, B. Beden, J.M. Leger and C. Lamy, *J. Electroanl. Chem.*, 125 (1981) 89.

261. B. Beden, C. Lamy and J.M. Leger, *J. Electrochim. Acta*, 24 (1979) 1157.

262. R.W. Tsang, D.C. Johnson and G.R. Luecke, *J. Electrochem. Soc.*, 131 (1984) 2369.

263. R.R. Adzic, W.E. O'Grady and S. Srinivrsen, *J. Electrochem. Soc.*, 128 (1981) 1913.

264. F. Kadirgan, B. Beden and C. Lamy, *J. Electroanal. Chem.*, (a) 136 (1982) 119; (b) 136 (1982) 135.

265. M. Shibata and S. Motoo, *J. Electroanal. Chem.*, 209 (1986) 151.

266. G. Kokkinidis, *J. Electroanal. Chem.*, 201 (1986) 217.

267. S. Motoo and M. Shibata, *J. Electroanal. Chem.*, 139 (1982) 119.

268. I. Fonseca, L-C. Jaing and D. Pletcher, *J. Electrochem. Soc.*, 130 (1983) 2187.

269. R.W. Murray, *Accts. Chem. Res.*, 13 (1980) 153.

270. A. Merz and A.J. Bard, *J. Am. Chem. Soc.*, 100 (1978) 3222.

271. J.M. Leger, Ph.D. Thesis, University of Poitiers, October 1982.

272. J.B. Korr and L.L. Miller, *J. Electroanal. Chem.*, 101 (1979) 263.

273. I. Rubenstein and A.J. Bard, *J. Am. Chem. Soc.*, (a) 102 (1980) 6642; (b) 103 (1981) 97.

274. F. Beck, *J. Appl. Electrochem.*, 7 (1977) 239.

275. J.Y. Becker, J.B. Kerr, D. Pletcher and R. Rosas, *J. Electroanal. Chem.*, 117 (1981) 87, 101.

276. J.F. Evans, T. Kuwana, M.T. Henne and G.P. Royer, *J. Electroanal. Chem.*, 80 (1977) 409.

277. J.S. Clarke, R.E. Ehigamusoe and A.T. Kuhn, *J. Electroanal. Chem.*, 70 (1976) 333.

278. M. Fleishmann, K. Korinek and D. Pletcher, *J. Electroanal. Chem.*, 31 (1971) 39.

279. M. Fleishmann, K. Korinek and D. Pletcher, *J. Chem. Soc. Perkin Trans II*, (1972) 1396.

280. F. Beck and H. Schultz, *Electrochim. Acta*, 29 (1984) 1169.

281. B.V. Tilak, in "Proceedings of the Symposium on Electrocatalysis", (Electrochemical Soc. Meeting, 1982).

282. G.A. Somorjai, *Science*, 201 (1978) 489.

283. F.G. Will, *J. Electrochem. Soc.*, 112 (1965) 451.

284. J. Clavilier, R. Faure, G. Guinet and R. Durand, *J. Electroanal. Chem.*, 107 (1980) 205.

285. R. Faure, These de Doctorat, Institut National de Grenoble, Grenoble, 1982.

286. F.E. Woodard, C.L. Scortichini and C.N. Reilley, *J. Electroanal. Chem.*, 151 (1983) 109.

287. F.T. Wagner and P.N. Ross, Jr., *J. Electroanal. Chem.*, 150 (1983) 141.

288. D.W. Blakely and G.A. Somorjai, *Surf. Sci.*, 65 (1977) 419.

289. R.M. Ishikawa and A.T. Hubbard, *J. Electroanal. Chem.*, 69 (1976) 317.

290. A. Hubbard, R. Ishikawa and J. Katekaru, *J. Electroanal. Chem.*, 86 (1978) 271.

291. W.E. O'Grady, M.Y.C. Woo, P.L. Hagans and E. Yeager, *J. Vac. Sci. Technol.*, 14 (1977) 365.

292. E. Yeager, W.E. O'Grady, M.Y.C. Woo and P. Hagans, *J. Electrochem. Soc.*, 125 (1978) 396.

293. B. Love, K. Seto and J. Lipkowski, *Rev. Chem. Intermediates*, 8 (1987) 87 and references 11-21 therein.

294. J. Clavilier, *J. Electroanal. Chem.*, 107 (1980) 211.

295. D. Aberdam, R. Durand, R. Faure and F. El-Omar, *Surf. Sci.*, 171 (1983) 303.

296. N. Markovic, M. Hanson, G. McDougall and E. Yeager, The 1986 Meeting of the Electrochem. Soc., Boston, May 4-9th, 1986, abstract #505.

297. J. Clavilier, R. Durand, G. Guinet and R. Faure, *J. Electroanal. Chem.*, 127 (1981) 281.

298. J. Clavilier and D. Armand, *J. Electroanal. Chem.*, 199 (1986) 187.

299. D. Armand and J. Clavilier, *J. Electroanal. Chem.*, 225 (1987) 205.

300. P.N. Ross, Jr., *J. Electrochem. Soc.*, 126 (1979) 67.

301. P.N. Ross, Jr., *Surf. Sci.*, 102 (1981) 463.

302. C.L. Scortichini and C.N. Reilley, *J. ELectroanal. Chem.*, (a) 139 (1982) 233; (b) 139 (1982) 247; (c) 152 (1983) 255.

303. B. Love, K. Seto and J. Lipkowski, *J. Electroanal. Chem.*, 199 (1986) 219.

304. J. Clavilier, D. Armand, S.G. Sun and M. Petit, *J. Electroanal. Chem.*, 205 (1986) 267.

305. R.R. Adzic, A.V. Tripkovic and V.B. Vesovic, *J. Electroanal. Chem.*, 204 (1986) 329.

306. A.V. Tripkovic and R.R. Adzic, *J. Electroanal. Chem.*, 205 (1986) 335.

307. N.M. Markovic, N.S. Marinkovic and R.R. Adzic, *J. Electroanal. Chem.*, 241 (1988) 309.

308. D. Armand and J. Clavilier, *J. Electroanal. Chem.*, 233 (1987) 251.

309. A.T. Hubbard, J.L. Stickney, M.P. Soiaga, V.K.F. Chia, S.D. Rosasco, B.C. Sehardt, T. Solomun, D. Song, J.M. White and A. Wieckowski, *J. Electroanal. Chem.*, 168 (1984) 43.

310. J. Clavilier and S.G. Sun, *J. Electroanal. Chem.*, 119 (1986) 471.

311. C. Lamy, J.M. Leger and J. Clavilier, *J. Electroanal. Chem.*, 135 (1982) 321.

312. S. Motoo and N. Furuya, *J. Electroanal. Chem.*, 167 (1984) 309.

313. M. Hourai and A. Wieckowski, *J. Electroanal. Chem.*, 244 (1988) 147.

314. J. Clavilier, S. Armand and B.L. Wu, *J. Electroanal. Chem.*, 135 (1982) 159.

315. S. Motoo and N. Furuya, *J. Electroanal. Chem.*, 172 (1984) 339.

316. J.L. Gland, B.A. Sexton and G.B. Fisher, *Surf. Sci.*, 95 (1980) 587.

317. C.L. Scortichini, F.E. Woodard and C.N. Reilley, *J. Electroanal. Chem.*, 139 (1982) 265.

318. B.H. Loo and T.E. Furtak, *Electrochim. Acta*, 25 (1980) 505.

319. M. Nakamura and H. Kita, *J. Electroanal. Chem.*, 68 (1976) 49.

320. T.B Grimley and M. Torrini, *J. Phys. Chem.*, 6 (1973) 261.

321. T.L. Einstein and J.R. Schrieffer, *Phys. Rev. B.*, 7 (1973) 362.

322. R. Parsons, *J. Electroanal. Chem.*, 150 (1983) 51.

323. A. Hamelin, *J. Electroanal. Chem.*, (a) 144 (1983) 365; (b) 142 (1982) 299.

324. B.E. Conway, *Prog. Surf. Sci.*, 16 (1984) 1.

325. F.T. Wagner and P.N. Ross, Jr., *J. Electroanal. Chem.*, 250 (1988) 301.

326. K. Christmann, G. Erth and T. Pignet, *Surf. Sci.*, 54 (1976) 365.

327. R. McCabe and L. Schmidt, Proc. 7th Int. Vac. Congr. and 3rd Int. Conf. on Solid Surf., Vienna, 1977, p. 1201.

328. K. Christmann and G. Erth, *Surf. Sci.*, 60 (1976) 365.

329. A. Hamelin and J.P. Bellier, *J. Electroanal. Chem.*, 41 (1973) 179.

330. G. Valette, A. Hamelin and R. Parsons, *Z. Phys. Chem., N.F.*, 133 (1978) 71.

331. G. Fisher and J. Gland, *Surf. Sci.*, 94 (1980) 446.

332. G.N. Van Hung, C. Hinnen and J. Lecoeur, *J. Electroanal. Chem.*, 106 (1980) 185.

333. K. Al Jaff-Golge, D.M. Kolb and D. Scherson, *J. Electroanal. Chem.*, 200 (1988) 353.

334. E.K. Krauskopf, L.M. Rice and A. Wiekowski, *J. Electroanal. Chem.*, 244 (1988) 347.

335. J.D.E. McIntyre, W.F. Peck, Jr., J. Lipkowski and B. Love, COLL. 136, 194th National Meeting of ACS, August 30 - Sept. 4, 1987, New Orleans, L.A.

336. J. Wieckers, T. Twomey, D.M. Kolb and R.J. Behm, *J. Electroanal. Chem.*, 248 (1988) 451.

337. R.J. Behm, *Scan. Microsc. Suppl.*, 1 (1987) 61.

338. G. Doyen, D. Drakova, E. Kopatzki and R.J. Behm, *J. Vac. Sci. Technol.* A6 (1986) 327.

339. R.M. Cervino, W.E. Triaca and A.J. Arvia, *J. Electroanal. Chem.*, 182 (1985) 51.

340. A. Visintin, W.E. Triaca and A.J. Arvia, *J. Electroanal. Chem.*, 221 (1987) 239.

341. W.E. Triaca, T. Kessler, J.C. Canullo and A.J. Arvia, *J. Electrochem. Soc.*, 134 (1987) 1165.

342. A. Visintin, J.C. Canullo, W.E. Triaca and A.J. Arvia, *J. Electroanal. Chem.*, 239 (1988) 67.

343. A.C. Chialvo, W.E. Triaca and A.J. Arvia, *J. Electroanal. Chem.*, 171 (1984) 303.

344. C.L. Perdriel, A.J. Arvia and M. Ipohorski, *J. Electroanal. Chem.*, 215 (1986) 317.

345. E.R. Custidieno, S. Piovano, A.J. Arvia, A.C. Chialvo and M. Ipohorski, *J. ELectroanal. Chem.*, 221 (1987) 229.

346. A.J. Arvia, J.C. Canullo, E. Custidieno, C.L. Perdriel and W.E. Triaca, *Electrochim. Acta*, 31 (1986) 1359.

347. D.M. Kolb, *Ber. Bunsenges. Phys. Chem.*, 92 (1988) 1175.

348. L.D. Burke, in "Electrodes of Conductive Metallic Oxides", Part A, Ed. Trasatti (Elsevier Scientific Publishing Co.), p. 141.

349. C.M. Ferro, A.J. Calandra and A.J. Arvia, *J. Electroanal. Chem.*, 65 (1975) 963.

350. D.E. Icenhower, H.B. Urbach and J.H. Harrison, *J. Electrochem. Soc.*, 117 (1970) 1500.

351. L.D. Burke and V.J. Cunnane, *J. Electroanal. Chem.*, 210 (1986) 69.

352. M. Pourbaix, in "Atlas of Electrochemical Equilibria in Aqueous Solutions", (Pergamon Press, Oxford, 1966).

353. J.W. Schultze and M.M. Lohrengel, *Ber Bunsenges. Phys. Chem.*, 80 (1976) 552.

354. G. Gruneberg, *Electrochim. Acta*, 10 (1965) 339.

355. M.M. Lohrengel and J.W. Schultze, *Electrochim. Acta*, 21 (1976) 957.

356. J.J. MacDonald and B.E. Conway, *Proc. Roy. Soc.*, A269 (1962) 419.

357. A.I. Krasil'schikov, *Russ. J. Phys. Chem.*, 37 (1963) 273.

358. J.P. Hoare, *Electrochim. Acta*, 9 (1964) 1289.

359. R.S. Sirohi and M.A. Genshaw, *J. Electrochem. Soc.*, 116 (1969) 910.

360. D.W. Kirk, F.R. Foulkes and W.F. Graydon, *J. Electrochem. Soc.*, 127 (1980) 1069.

361. L.D. Burke, M.E. Lyons and D.P. Whelan, *J. Electroanal. Chem.*, 139 (1982) 131.

362. L.D. Burke and R.A. Scannell, in "Equilibrium Diagrams: Localised Corrosion", Eds. R.P. Frankenthal and J. Kruger, (The Electrochem. Soc., Pennington, New Jersey, 1984) p. 135-147.

363. M. Peucket, *J. Electroanal. Chem.*, 185 (1985) 379.

364. M. Peucket, F.P. Coenen and H.P. Bonzel, *Surf. Sci.*, 141 (1984) 515.

365. H. Angerstein-Kozlowska, B.E. Conway, B. Barnett and J. Mozota, *J. Electroanal. Chem.*, 100 (1979) 417.

366. G. Nguyen Van Huong, C. Hinnen and J. Lecoeur, *J. Electroanal. Chem.*, 106 (1980) 185.

367. J. Gonzales-Velasco and J. Heitbaum, *J. Electroanal. Chem.*, 54 (1974) 147.

368. H. Angerstein-Kozlowska, B.E. Conway, A. Hamelin and L. Stoicoviciu, *Electrochim. Acta*, 31 (1986) 1051.

369. H. Angerstein-Kozlowska, B.E. Conway, A. Hamelin and L. Stoicoviciu, *J. Electroanal. Chem.*, 228 (1987) 429.

370. D.A. Scherson and D.M. Kolb, *J. Electroanal. Chem.*, 176 (1984) 353.

371. H. Kita, H. Nakajima and H. Hayashi, *J. Electroanal. Chem.*, 190 (1985) 141.

372. L.D. Burke, M.I. Casey, V.J. Cunnane, O.J. Murphy and T.A.M. Twomey, *J. Electroanal. Chem.*, 189 (1985) 353.

373. L.D. Burke and G.P. Hopkins, *J. Appl. Electrochem.*, 14 (1984) 679.

374. H. Baltruschat, E. Rach and J. Heitbaum, *J. Electroanal. Chem.*, 194 (1985) 109.

375. G. Horanyi and E.M. Rizmayer, *J. Electroanal. Chem.*, 165 (1984) 279; 140 (1982) 347.

376. L.D. Burke and A. Moynihan, *Electrochim. Acta*, 15 (1970) 1437.

377. M. Betlowska-Brzezinska and J. Heitbaum, *J. Electroanal. Chem.*, 183 (1985) 167.

378. M. Enyo, *J. Electroanal. Chem.*, 186 (1985) 155.

379. S. Sibille, J. Moirou, J.-C. Marot and S. Deycard, *J. Electroanal. Chem.*, 88 (1978) 105.

380. R.M. Van Effen and D.H. Evans, *J. Electroanal. Chem.*, 107 (1980) 405; 103 (1979) 383.

381. E. Gonzalez-Herman, C. Alonso and J. Gonzalez-Velasco, *J. Electroanal. Chem.*, 223 (1987) 277.

382. E. Valles, E. Gomez, J.M. Feliu and A. Aldaz, *J. Electroanal. Chem.*, 190 (1985) 95.

383. C. Alonso and J. Roldan, *J. Electroanal. Chem.*, 248 (1988) 193.

384. P. Bindra and J. Roldan, *J. Electrochem. Soc.*, 132 (1985) 2581.

385. H. Kinza, *Z. Phys. Chem., (Leipzig)*, 225 (1974) 180.

386. J. Van der Plas and E. Barendrecht, *Electrochim. Acta*, 25 (1980) 1463.

387. C. Nishihara and H. Shindo, *J. Electroanal. Chem.*, 221 (1987) 245.

388. J. Desilvestro and M.J. Weaver, *J. Electroanal. Chem.*, 209 (1986) 377.

389. R. Luther and F. Pokorney, *Z. Anorg. Allg. Chem.*, 57 (1908) 290.

390. T.P. Dirske, *J. Electrochem. Soc.*, 106 (1959) 453.

391. N.A. Shumilova and G.V. Zhutaeva, in "Encyclopedia of Electrochemistry of the Elements", Ed. A.J. Bard (Dekker, New York, 1978), Vol. VIII, p. 1.

392. G.N. Lewis, *Z. Physik. Chem. (Leipzig)*, 55 (1906) 449.

393. A.J. de Bethune and N.A.S. Loud, in "Standard Aqueous Electrode Potentials and Temperature Coefficients", (C.A. Hampel, Skokie, Ill., 1964).

394. G.N. Lewis, *J. Amer. Chem. Soc.*, 28 (1906) 158.

395. C.P. Wales and J. Burbank, *J. Electrochem. Soc.*, 112 (1965) 13.

396. G.D. Briggs, M. Fleischmann, D.J. Lax and H.R. Thirsk, *Trans. Far. Soc.*, 64 (1968) 3120.

397. G. Poli, Z. Siedlecka and B. Rivolta, *Inst. Lomb. (Rand. Sci.)*, 97 (1963) 631.

398. N. Sato and Y. Shimizu, *Electrochim. Acta*, 18 (1973) 567.

399. A. Hickling and D. Taylor, *Disc. Far. Soc.*, 1 (1947) 277.

400. P. Jones, H.R. Thirsk and W.F.K. Wynne-Jones, *Trans. Far. Soc.*, 52 (1956) 1003.

401. T.P. Dirske, *J. Electrochem. Soc.*, 106 (1959) 920.

402. G.L. Vidovich, D.I. Leikis and B.N. Kabonov, *Dokl. Akad. Nauk. S.S.S.R.*, 124 (1959) 125.

403. T.P. Dirske and D.B. Devries, *J. Phys. Chem.*, 63 (1959) 278.

404. G.T. Croft, *J. Electrochem. Soc.*, 106 (1959) 278.

405. J.M.M. Droog, P.T. Alderliesten and G.A. Bootsma, *J. Electroanal. Chem.*, 99 (1979) 173.

406. T.G. Clarke, N.A. Hampson, J.B. Lee, J.R. Morley and I.B. Scanlon, *Ber. Bunsenges Phys. Chem.*, 73 (1969) 279.

407. P. Stonehart and F.P. Portante, *Electrochim. Acta*, 13 (1968) 1805.

408. J.M.M. Droog, *J. Electroanal. Chem.*, 115 (1980) 225.

409. R.S. Perkins, B.V. Tilak, B.E. Conway and H.A. Kozlowska, *Electrochim. Acta*, 17 (1972) 1447.

410. J.M.M. Droog and F. Huisman, *J. Electroanal. Chem.*, 115 (1980) 225.

411. N.A. Shumilova, G.V. Zhutaeva and M.P. Tarasevich, *Electrochim. Acta*, 11 (1966) 967.

412. G.V. Zhutaeva and N.A. Shumilova, *Electrokhim.*, 4 (1968) 99.

413. V.P. Loobmaa, V.E. Past and M.E. Khaga, *Electrokhim.*, 2 (1966) 927.

414. A. Hamelin, L. Doubova, D. Wagner and H. Schirmer, *J. Electroanal. Chem.*, 220 (1987) 155.

415. G. Valette, *J. Electroanal. Chem.*, 224 (1987) 285.

416. P. Bindra and J. Roldan, *J. Electrochem. Soc.*, 132 (1985) 2581.

417. H. Kita, H. Nakajima and K. Hayashi, *J. Electroanal. Chem.*, 190 (1985) 141.

418. B.R. Proud, D.D. McDonald and J.W. Tombinson, *Electrochim. Acta*, 25 (1980) 563.

419. R. Kotz and E. Yeager, *J. Electroanal. Chem.*, 111 (1980) 105.

420. J.A. MacMillan, *J. Inorg. Nucl. Chem.*, 13 (1960) 28.

421. G.V. Zhutaeva, N.A. Shumilova and V.I. Luk'yanycheva, *Electrokhim.*, 4 (1968) 196.

422. H.M. Villullas, G.I. Lacconi, A.S. Gioda and V.A. Macagno, *Electrochim. Acta*, 32 (1987) 1657.

423. S.T. Mayer and R.H. Muller, *J. Electrochem. Soc.*, 135 (1988) 2133.

424. M. Beltowska-Brzezinska, *Electrochim. Acta*, 30 (1985) 1193.

425. K.J. Laidler, in "Physical Chemistry with Biological Applications", (The Benjamin/Cummings Publishing Co., California, 1978) p. 429-457.

426. L.A. Larew and D.C. Johnson, *J. Electroanal. Chem.*, 262 (1989) 167.

427. A. Bewick, M. Fleischmann and M. Liler, *Electrochim. Acta*, 1 (1959) 83.

428. J.D.E. McIntyre and W.F. Peck, *J. Electrochem. Soc.*, 117 (1970) 747.

429. D. Britz and W.A. Brocke, *J. Electroanal. Chem.*, 58 (1975) 301.

430. L.D. Burke, J.K. Mulcahy and D.P. Whelan, *J. Electroanal. Chem.*, 163 (1984) 117.

431. V.E. Kazarinov and S.V. Dolidze, *Electrokhim*, 9 (1973) 1183.

432. J. Balej and O. Spalek, *Coll. Czech. Chem. Comm.*, 37 (1972) 499.

433. S. Shibata, *J. Electroanal. Chem.*, 89 (1978) 37.

434. B.E. Conway, H. Angerstein-Kozlowska, *Acc. Chem. Res.*, 14 (1981) 49.

435. H. Angerstein-Kozlowska, B.E. Conway and W.B.A. Sharp, *J. Electroanal. Chem.*, 43 (1973) 9.

436. P.N. Ross, Jr., *J. Electroanal. Chem.*, 76 (1977) 139.

437. V.S. Bagotzky and M.R. Tarasevich, *J. Electroanal. Chem.*, 101 (1979) 1.

438. A.J. Appleby, *J. Electrochem. Soc.*, 120 (1973) 1205.

439. K.J. Vetter and V. Berndt, *Z. Electrochem.*, 62 (1958) 378.

440. H. Angerstein-Kozlowska, B.E. Conway, B. Barnett and J. Mozota, *J. Electroanal. Chem.*, 28 (1983) 1.

441. L.D. Burke and M.B.C. Roche, *J. Electroanal. Chem.*, 159 (1983) 89.

442. W. Visscher and M.A.V. Devanathan, *J. Electrochem. Soc.*, 8 (1964) 127.

443. K.J. Vetter and J.W. Schultze, *J. ELectroanal. Chem.*, 34 (1972) 131.

444. K.J. Vetter and J.W. Schultze, *ibid*, 34 (1972) 141.

445. J.W. Schultze, *Z. Phys. Chem.*, 73 (1970) 29.

446. J.L. Ord and F.C. Ho, *J. Electrochem. Soc.*, 118 (1971) 46.

447. L.B. Harris and A. Damjanovic, *ibid*, 122 (1975) 593.

448. A. Damjanovic, A.R. Ward, B. Ulrick and M. O'Jea, *ibid*, 122 (1975) 471.

449. V.I. Biriss and A. Damjanovic, *J. Electrochem. Soc.*, 130 (1983) 1688.

450. T. Biegler and R. Woods, *J. Electroanal. Chem.*, 20 (1973) 1969.

451. T. Biegler, D.A.J. Rand and R. Woods, *J. Electroanal. Chem.*, 29 (1971) 269.

452. W. Visscher and M. Blijlevens, *J. Electroanal. Chem.*, 47 (1973) 363.

453. A.T. Kuhn and T.H. Randle, *J. Chem. Soc. Faraday 1*, 81 (1985) 403.

454. D. Gilroy, *J. Electroanal. Chem.*, 71 (1976) 257.

455. D. Gilroy, *ibid*, 83 (1977) 329.

456. M. Fleischmann and H.R. Thirsk, is "Adv. in Electrochem. and Electrochem. Eng.", Eds. P. Delahay and C.W. Tobias, (Interscience, New York, 1963) Vol. 3, p. 123.

457. S.D. James, *J. Electrochem. Soc.*, 116 (1969) 1681.

458. S. Shibata, *J. Electroanal. Chem.*, 89 (1978) 37.

459. S. Altmann and H.R. Busch, *Trans. Faraday Soc.*, 45 (1949) 720.

460. G.C. Allen, P.M. Tucker, A. Capon and R. Parsons, *J. Electroanal. Chem.*, 50 (1974) 335.

461. L.D. Burke and M.B.C. Roche, *J. Electroanal. Chem.*, 137 (1982) 175.

462. L.D. Burke and M.B.C. Roche, *J. Electrochem. Soc.*, 129 (1982) 2641.

463. L.D. Burke and M.B.C. Roche, *J. Electroanal. Chem.*, 164 (1984) 315.

464. S.L. Chang, in "Energy Conversion", (Prentice-Hall, Englewood Cliffs, New Jersey, 1963).

465. B.E. Conway, H. Angerstein-Kozlowska and W.B.A. Sharp, *J. Chem. Soc. Faraday Trans. 1*, 74 (1978) 1373.

466. A. Bewick and A.M. Tukford, *Sym. Faraday Soc.*, 4 (1970) 114.

467. B.E. Conway and H. Angerstein-Kozlowska, *Acc. Chem. Res.*, 14 (1981) 49.

468. M. Fujihira and T. Kuwana, *Electrochim. Acta*, 20 (1975) 565.

469. J.P. Hoare, *Electrochim. Acta*, 27 (1982) 1751.

470. S. Juanto, B. Beden, F. Hahn, J.M. Leger and C. Lamy, *J. Electroanal. Chem.*, 237 (1987) 119.

471. S.G. Sun, J. Clavilier and A. Bewick, *J. Electroanal. Chem.*, 240 (1988) 147.

472. V.S. Bagotsky and Yu. B. Vassilyev, *Electrochim. Acta*, 12 (1967) 1323.

473. J. Clavilier, *J. Electroanal. Chem.*, 236 (1987) 87.

474. H.A. Liebhafsky and E.J. Cairns, in "Fuel Cells and Fuel Batteries", (John Wiley and Sons, New York, 1968), p. 412.

475. K. Venkateswara Rao and C.B. Roy, *Ind. J. Chem.*, 19A (1980) 840.

476. G. Horanyi, P. Konig and I. Teles, *Acta Chim. (Budapest)*, 72 (1972) 165.

477. L.D. Burke and K.J. O'Dwyer, *Electrochim. Acta*, accepted.

478. G. Kokkinidis and D. Sazou, *J. Electroanal. Chem.*, 237 (1987) 137.

479. H.L. Li, D.H. Robertson and J.Q. Chambers, *J. Electrochem. Soc.*, 135 (1988) 1153.

480. S.G. Roscoe and B.E. Conway, *J. Electroanal. Chem.*, 249 (1988) 217.

481. G. Horanyi and K. Torkos, *J. Electroanal. Chem.*, 140 (1982) 329.

482. J.B. Goodenough, A. Hamnett, B.J. Kennedy, R. Manoharan and S.A. Weeks, *J. Electroanal. Chem.*, 240 (1988) 133.

483. L.D. Burke, Ext. Absts. of the Spring Meeting (Atlanta), The Electrochem. Soc., (Pennington, New Jersey, 1988), Vol. 88-1, p. 690.

484. L.D. Burke and M.J.G. Ahern, *J. Electroanal. Chem.*, 183 (1985) 183.

485. L.D. Burke, J.F. O'Sullivan, K.J. O'Dwyer, R.A. Scannell, M.J.G. Ahern and M.M. McCarthy, *J. Electrochem. Soc.*, submitted.

486. H. Ebert, R. Parsons, G. Ritzoulis and T. VanderNoot, *J. Electroanal. Chem.*, 264 (1989) 181.

PUBLICATIONS

1. Electrooxidation of Formaldehyde at Silver Anodes - Role of Submonolayer Hydroxy Complexes in Noble Metal Electrocatalysis. L.D. Burke and W.A. O'Leary. J. Electrochem. Soc., 135 (1988) 1965-1970.

2. Electrooxidation of Formaldehyde at Silver Anodes - Role of Submonolayer Hydroxy Complexes in Noble Metal Electrocatalysis. L.D. Burke and W.A. O'Leary. Ext. Absts., Vol. 87-1, Philadelphia Meeting, Electrochem. Soc., 1988, p. 767.

3. The Role of Hydrous Oxide in the ELectrochemical Behaviour of Platinum. L.D. Burke, M.B.C. Roche and W.A. O'Leary. J. Appl. Electrochem., 18 (1988) 781-790.

4. Mediation of Interfacial Reactions by Low Levels of In-situ Generated Hydroxy Species. L.D. Burke, K.J. O'Dwyer and W.A. O'Leary, Ext. Absts., Bologna Meeting, I.S.E., 1988, p. 83-85.

5. Incipient Hydrous Oxides - the Missing Link in Noble Metal Electrocatalysis. L.D. Burke, J.F. Healy, K.J. O'Dwyer and W.A. O'Leary. J. Electrochem. Soc., 136 (1989) 1015-1021.

6. The Importance of Superficial (Adatom) Surface Oxidation in the Electrocatalytic Behaviour of Noble Metals in Aqueous Media. L.D. Burke and W.A. O'Leary. J. Appl. Electrochem., (in press).

7. A Study of Isopropanol Oxidation at Platinised Platinum Electrodes in Acid Solution. L.D. Burke and W.A. O'Leary. Proc. Roy. Irish Acad., (in press).

8. The Importance of Metastable, Hydrated Adatom and Hydroxy Species in the Electrochemical Behaviour of Noble Metal Electrode Systems - with Particular Reference to Pt. L.D. Burke and W.A. O'Leary. J. Electrochem. Soc., (submitted).

9. The Hydrous Oxide Mediator Mechanism for Electrocatalysis at the Metal/Aqueous Solution Interface. L.D. Burke, K.J. O'Dwyer, W.A. O'Leary and T.G. Ryan. The 40th Meeting, I.S.E., Kyoto, Japan, 1989, (accepted for presentation).

10. The Possiblity of an Electronic Criterion of Stereochemistry of Bis (Chelate) Copper (II) Complexes. A. O'Leary, S. Tyagi and B.J. Hathaway. Inorganica Chemica Acta, 76 (1983) L89.